NASA/CR—1999–209426

A Comparison of Single-Cycle Versus Multiple-Cycle Proof Testing Strategies

R.C. McClung, G.G. Chell, and H.R. Millwater
Southwest Research Institute, San Antonio, Texas

D.A. Russell and G.E. Orient
Rocketdyne Division, Rockwell International Corporation, Canoga Park, California

Prepared for Marshall Space Flight Center
under Contract NAS8–37451

July 1999

The NASA STI Program Office...in Profile

Since its founding, NASA has been dedicated to the advancement of aeronautics and space science. The NASA Scientific and Technical Information (STI) Program Office plays a key part in helping NASA maintain this important role.

The NASA STI Program Office is operated by Langley Research Center, the lead center for NASA's scientific and technical information. The NASA STI Program Office provides access to the NASA STI Database, the largest collection of aeronautical and space science STI in the world. The Program Office is also NASA's institutional mechanism for disseminating the results of its research and development activities. These results are published by NASA in the NASA STI Report Series, which includes the following report types:

- TECHNICAL PUBLICATION. Reports of completed research or a major significant phase of research that present the results of NASA programs and include extensive data or theoretical analysis. Includes compilations of significant scientific and technical data and information deemed to be of continuing reference value. NASA's counterpart of peer-reviewed formal professional papers but has less stringent limitations on manuscript length and extent of graphic presentations.

- TECHNICAL MEMORANDUM. Scientific and technical findings that are preliminary or of specialized interest, e.g., quick release reports, working papers, and bibliographies that contain minimal annotation. Does not contain extensive analysis.

- CONTRACTOR REPORT. Scientific and technical findings by NASA-sponsored contractors and grantees.

- CONFERENCE PUBLICATION. Collected papers from scientific and technical conferences, symposia, seminars, or other meetings sponsored or cosponsored by NASA.

- SPECIAL PUBLICATION. Scientific, technical, or historical information from NASA programs, projects, and mission, often concerned with subjects having substantial public interest.

- TECHNICAL TRANSLATION. English-language translations of foreign scientific and technical material pertinent to NASA's mission.

Specialized services that complement the STI Program Office's diverse offerings include creating custom thesauri, building customized databases, organizing and publishing research results...even providing videos.

For more information about the NASA STI Program Office, see the following:

- Access the NASA STI Program Home Page at ***http://www.sti.nasa.gov***

- E-mail your question via the Internet to help@sti.nasa.gov

- Fax your question to the NASA Access Help Desk at (301) 621-0134

- Telephone the NASA Access Help Desk at (301) 621-0390

- Write to:
  NASA Access Help Desk
  NASA Center for AeroSpace Information
  800 Elkridge Landing Road
  Linthicum Heights, MD 21090-2934

NASA/CR—1999-209426

A Comparison of Single-Cycle Versus Multiple-Cycle Proof Testing Strategies

R.C. McClung, G.G. Chell, and H.R. Millwater
Southwest Research Institute, San Antonio, Texas

D.A. Russell and G.E. Orient
Rocketdyne Division, Rockwell International Corporation, Canoga Park, California

Prepared for Marshall Space Flight Center
under Contract NAS8-37451

National Aeronautics and
Space Administration

Marshall Space Flight Center • MSFC, Alabama 35812

July 1999

Acknowledgments

The continuing encouragement and support of the NASA Marshall Space Flight Center technical staff is gratefully acknowledged. In particular, Gwyn C. Faile, Henry M. Lee, and Rod Stallworth maintained a cordial and cooperative relationship with the program team that was essential to the success of the research.

A number of our colleagues at Southwest Research Institute made important contributions to the program. Vic Aaron, Tom Masden, and Jack FitzGerald are thanked for their invaluable assistance in conducting the crack growth experiments. V.P. Swaminathan led the fractographic investigations, and Jim Spencer performed the crack length measurements from the fracture surfaces. John Hanley was task leader for the acoustic emission studies. Tim Grant helped with the development of improved J solutions. Janet Buckingham performed some of the statistical analysis. Luz H. Escobedo provided extensive assistance with preparation of this report. Stephen J. Hudak, Jr., is especially thanked for his advice and support throughout the entire research effort.

Available from:

NASA Center for AeroSpace Information
800 Elkridge Landing Road
Linthicum Heights, MD 21090–2934
(301) 621–0390

National Technical Information Service
5285 Port Royal Road
Springfield, VA 22161
(703) 487–4650

TABLE OF CONTENTS

Page

LIST OF TABLES v

LIST OF FIGURES vi

DEFINITION OF SYMBOLS xi

NONSTANDARD ABBREVIATIONS xiii

EXECUTIVE SUMMARY xv

1. INTRODUCTION 1
   - 1.1 General Background to the MCPT Problem 1
   - 1.2 Review of Key Background Information from Phase I 3
     - 1.2.1 Rocketdyne Experience with MCPT 4
     - 1.2.2 Distributions of Initial Flaw Sizes and Shapes 4
     - 1.2.3 *J*-Integral Solutions for Semi-Elliptical Surface Flaws 4
     - 1.2.4 Fracture Mechanics Properties of Inconel 718 5
     - 1.2.5 First-Generation Analytical Model for MCPT 6
     - 1.2.6 Phase I Conclusions 6
   - 1.3 Work Scope for Phase II Investigations 7

2. ANALYTICAL DEVELOPMENT 8
   - 2.1 Improved *J*-Integral Solutions for Surface Flaws 8
   - 2.2 *J*-Integral Solutions for Cracks at Notches 15
     - 2.2.1 Finite Element Results 15
     - 2.2.2 Simple *J*-Estimation Technique 21
   - 2.3 Elastic-Plastic Fatigue Crack Growth Analysis 27
   - 2.4 Tear-Fatigue Theory 29

3. EXPERIMENTAL CHARACTERIZATION AND VALIDATION 34
   - 3.1 Updated J-Resistance Curves 34
   - 3.2 Relationship Between J-Resistance Curves and Fatigue Crack Growth 37
   - 3.3 Characterizing the Onset of Stable Tearing 41
   - 3.4 Elastic-Plastic Fatigue Crack Growth Experiments 42
   - 3.5 Experimental Simulation of Multiple Cycle Proof Testing 47
   - 3.6 Effect of Proof Testing on Subsequent Fatigue Crack Growth Rates 55
   - 3.7 Fractographic Observations 56
     - 3.7.1. Crack Growth Mechanisms 56
     - 3.7.2. Crack Shapes 64
   - 3.8 Acoustic Emission Investigations 69

TABLE OF CONTENTS (CONT.)

Page

4. PROBABILISTIC ANALYSIS 78
   4.1 The MCPT Question 78
   4.2 Probabilistic Formulation 80
   4.3 An Example Problem 81
   4.4 Parameter Studies 91
   4.5 Cracks at Notches 104
   4.6 Memory vs. Loss-of-Memory in Tear-Fatigue Theory 105

5. DISCUSSION 111
   5.1 Other Proof Testing Issues 111
      5.1.1. Hold Times and Time-Dependent Fracture Behavior 111
      5.1.2. Cyclic Hardening and Softening 113
      5.1.3. Weldments 114
   5.2 The Generality of the Results 115

6. SUMMARY AND CONCLUSIONS 117

7. ENGINEERING GUIDELINES 121
   7.1 General Background 121
   7.2 Introduction to Flow Chart Format and Decision Process 122
   7.3 Engineering Guidelines: Detailed Description 126

8. REFERENCES 140

APPENDIX A. Further Documentation of Improved *J* Solutions for Surface Flaws A.1
   Finite Element Solutions A.1
   Reference Stress Estimates A.4
   Comparisons of Reference Stress and Finite Element Results A.14
   Discussion: Accuracy of J Solutions A.24
   Acknowledgements A.25
   References A.25

LIST OF TABLES

Page

Table 2.1. Numerical values of the shape factors for $K_t = 4.29$ 22
Table 2.2. Numerical values of the shape factors for $K_t = 6.43$ 22
Table 2.3. Numerical values of the shape factors for $K_t = 8.57$ 22
Table 3.1. Summary of test conditions for specimens examined fractographically 57
Table A1. Summary of geometries and constitutive laws for finite element J solutions . . A.2
Table A2. Summary of reference stress parameters calculated from finite element solutions..A.9
Table A3. Ratio of predicted to published h_1 for different ξ/c values A.15

LIST OF FIGURES

Page

Figure 1.1. Single-cycle proof test logic represented in terms of residual strength and residual fatigue life 2

Figure 2.1. Geometric construction for limit load solution of surface-cracked plate, illustrating effective plate width 12

Figure 2.2. Comparison of reference stress J predictions (solid line) with Wang (top) and Dodds (bottom) finite element results 14

Figure 2.3. Schematic showing geometrical relationship between notch depth (D), notch root radius (r_o), crack depth (d), notch plus crack depth (a), and half plate width (b) 17

Figure 2.4. Linear elastic solutions for cracks at double edge notches in plates with K_t = 4.29 18

Figure 2.5. Linear elastic solutions for cracks at double edge notches in plates with K_t = 6.43 19

Figure 2.6. Linear elastic solutions for cracks at double edge notches in plates with K_t = 8.57 20

Figure 2.7. Asymptotic behavior of $h_1(a/b, n)$ for K_t = 4.29 as d/r_0 increases ($d=r_0/2$ corresponds to a/b = 0.3622) 23

Figure 2.8. Asymptotic behavior of $h_1(a/b, n)$ for K_t = 6.43 as d/r_0 increases ($d=r_0/2$ corresponds to a/b = 0.32425) 24

Figure 2.9. Asymptotic behavior of $h_1(a/b, n)$ for K_t = 8.57 as d/r_0 increases ($d=r_0/2$ corresponds to a/b = 0.3129) 25

Figure 2.10. Schematic representation of tear-fatigue theory 31

Figure 3.1. Crack growth resistance curves for Inconel 718 36

Figure 3.2. Fatigue crack growth data for Inconel 718 with superimposed resistance curve data 38

Figure 3.3. Resistance curves for Inconel 718 with superimposed FCG curve 39

LIST OF FIGURES (CONT.)

Page

Figure 3.4. Typical load-displacement records from zero-max loading (top) and zero-max displacement (bottom) tests 44

Figure 3.5. Elastic-plastic fatigue crack growth data superimposed on scatterbands from SSY FCG data 45

Figure 3.6. Load vs. crack mouth opening displacement history for test S26 showing failure on the second cycle at the terminal maximum load 48

Figure 3.7. Load vs. crack mouth opening displacement history for test S27 49

Figure 3.8. Load vs. crack mouth opening displacement history for test S20 showing failure on the fifth cycle at the terminal maximum load 52

Figure 3.9. Load vs. load line displacement history for simulated proof test followed by simulated service cycling 54

Figure 3.10. Fracture surface of specimen SD-3 at 300x (top) and 3000x (bottom) showing quasi-cleavage fracture features and fatigue striations 58

Figure 3.11. Fracture surface of specimen S-25 at 300x (top) and 3000x (bottom) showing transgranular fatigue striations 59

Figure 3.12. Fracture surface of specimen S-11 at 300x (top) and 2000x (bottom) showing tear ridges and ductile dimples at precipitate particles 61

Figure 3.13. Fracture surface of specimen SCR-8 at 300x (top) and 3000x (bottom) showing tear ridges and ductile dimples at precipitate particles 62

Figure 3.14. Fracture surface of specimen S-13 at 300x (top) and 3000x (bottom) showing tear ridges and few ductile dimples 63

Figure 3.15. Fracture surface of multiple cycle crack growth specimen (zero-max displacement, five cycles) 65

Figure 3.16. Crack growth as a function of angular position for selected multiple cycle crack growth specimens 66

Figure 3.17. Crack growth as a function of angular position for selected single-cycle crack growth specimens 67

LIST OF FIGURES (CONT.)

Page

Figure 3.18. CMOD and load history of specimen S19 70

Figure 3.19. CMOD vs. load for specimen S19 72

Figure 3.20. CMOD vs. AE count rate for specimen S19 73

Figure 3.21. CMOD vs. AE event rate for specimen S19 74

Figure 3.22. AE activity and CMOD history for specimen S27 76

Figure 4.1. Schematic representation of calculation of P[(Ns ≤ Ns')] 82

Figure 4.2. Schematic representation of calculation of P[(Ns ≤ Ns') ∩ (Np > Np')] . . 83

Figure 4.3 Distribution of initial crack depths and corresponding exponential distribution. 85

Figure 4.4. PDF of crack depth before and after proof testing for a sample problem 87

Figure 4.5. CDF of crack depth before and after proof testing for a sample problem 87

Figure 4.6. Service cycles to failure as a function of initial crack depth for a sample problem 89

Figure 4.7. Probability of failure as a function of service cycles for a sample problem 89

Figure 4.8. Probability of failure in service as a function of number of proof cycles for a sample problem 90

Figure 4.9. CDF of in-service failure probability after different numbers of proof cycles (N), conditional on proof test success, for proof factor of 1.1 (top) and 1.3 (bottom) 92

Figure 4.10. CDF of in-service failure probability after different numbers of proof cycles (N), conditional on proof test success, for low tearing resistance (top) and high tearing resistance (bottom) 93

Figure 4.11. CDF of in-service failure probability after different numbers of proof cycles (N), conditional on proof test success (a) CT R-curve and 1.3 proof factor (b) upper bound R-curve and 1.1 proof factor 94

LIST OF FIGURES (CONT.)

Page

Figure 4.12. CDF of in-service failure probability after different numbers of proof cycles, conditional on proof test success (a) $a/c = 0.1$ (b) $a/c = 0.2$ (c) $a/c = 0.5$ 96

Figure 4.13. Probability of failure in service as a function of number of proof cycles for $a/c = 0.5$ example 98

Figure 4.14. Cumulative distribution functions (top) and probability density functions (bottom) for three exponential distributions of initial crack depth 100

Figure 4.15. CDF of in-service failure probability after different numbers of proof cycles, conditional on proof test success (a) exponential distribution with mean value $a = 0.01$ in. (b) exponential distribution with mean value $a = 0.08$ in. 101

Figure 4.16. Cumulative distribution functions (top) and probability density functions (bottom) for three Weibull distributions of initial crack depth 102

Figure 4.17. CDF of in-service failure probability after different numbers of proof cycles, conditional on proof test success (a) Weibull distribution with shape parameter $\beta = 0.5$ (b) Weibull distribution with shape parameter $\beta = 2.0$ 103

Figure 4.18. CDF of in-service failure probability after different numbers of proof cycles; notched geometry, 100 ksi proof stress, $a_i = \exp[.05]$ 106

Figure 4.19. Total, elastic, and plastic J values for cracks emanating from double edge notches with 100 ksi nominal stress 107

Figure 4.20. CDF of in-service failure probability after different numbers of proof cycles; notched geometry, 50 ksi proof stress, $a_i = \exp[.05]$ 107

Figure 4.21. Computed in-service failure probability for different numbers of proof cycles and different assumptions about material memory following the proof overload 110

Figure 7.1. Flow chart for Engineering Guidelines 123

LIST OF FIGURES (CONT.)

Page

Figure A1. Geometric nomenclature for semi-elliptical surface crack in finite plate . . A.3

Figure A2. Variation in extracted h_1 with applied stress from Wang (1988) analyses A.5

Figure A3. Variation in extracted h_1 with applied stress from Dodds (1992) analyses A.6

Figure A4. Comparison of h_1 values from various authors A.7

Figure A5. Normalized representative plate width ξ/(b-c) as function of a/t A.11

Figure A6. Normalized representative plate width ξ/t as function of a/t A.12

Figure A7. Normalized representative plate width ξ/c as function of a/t A.13

Figure A8. Comparison of reference stress J predictions with Wang (1988) finite element results A.16

Figure A9. Comparison of reference stress J predictions with Dodds (1992) finite element results A.17

Figure A10. Comparison of reference stress J predictions with Wang (1991) finite element results A.18

Figure A11. Comparison of reference stress J predictions with Kirk (1992) finite element results in terms of normalized applied stress A.19

Figure A12. Comparison of reference stress J predictions with Kirk (1992) finite element results in terms of normalized applied strain A.20

Figure A13. Comparison of reference stress h_1 predictions with Yagawa (1993) finite element results A.21

DEFINITION OF SYMBOLS

a	crack depth
a'	area-equivalent crack depth for semi-elliptical crack (= $\pi a/4$)
a_f	final crack size
a_i	initial crack size
b	half-width of a (cracked) plate
c	half surface crack length, or half of the remaining ligament for double edge cracked plate
C	crack growth law constant
C_2	constant in crack-tip plastic zone size equation
d	length of crack growing from notch root
D	notch depth
da/dN	crack growth rate per cycle
$(da/dN)_f$	fatigue crack growth rate
d_e	effective length of crack at notch root (including plastic zone correction)
E	Young's modulus
E'	$E/(1-\nu^2)$, effective modulus in plane strain
f	collapse function or yield function (= σ_L/σ_{ys})
F	geometric term in expression for K_1
h	half-height of a (cracked) plate
H	crack growth function giving number of service cycles for an initial flaw size
h_1	non-dimensional factor in fully plastic J_p term
J	J-integral
J^*	an advanced path-area integral used in nonlinear fracture mechanics
J_{app}	applied value of J
J_e	elastic component of J
J_i	some suitable measure of J for the initiation of tearing
J_{Ic}	J at crack initiation, measure of toughness
J_{mat}	crack-growth resistance value of J for ductile tearing under monotonic loading
J_{max}	J at maximum load in fatigue cycle
J_{min}	minimum value of J
J_p	plastic component of J
J_{total}	total J, generally the sum of elastic and plastic components
K or K_I	stress intensity factor
K_{Ic}	fracture toughness
K_{max}	K_I at maximum load in fatigue cycle
K_{min}	K_I at minimum load in fatigue cycle
K_t	stress concentration factor (based on gross section stress)
m	exponent in fatigue crack growth law
n	strain-hardening exponent in Ramberg-Osgood constitutive equation
N	number of load cycles (sometimes number of proof cycles)
N_f	residual fatigue life
N_i	residual fatigue life corresponding to a_i
Np	number of proof cycles (Np' is a specific value)
Ns	number of service cycles (Ns' is a specific value)
P	applied load

P_{o_*}	characteristic yield load
P_*^*	optimized yield load
Q	hydrostatic crack tip stress parameter
R	ratio of minimum to maximum load in fatigue cycle
r_o	notch root radius
r_y	radius of crack-tip plastic zone
S_T	nominal applied (gross section) stress in notched body
t	thickness of a specimen or component
T^*	an advanced path-area integral used in nonlinear fracture mechanics
U	effective stress range ratio
V	structural parameter in optimized reference stress method
α	constant in Ramberg-Osgood constitutive equation
β	shape parameter of a Weibull distribution
$\Delta\epsilon$	cyclic change in strain, or strain range
$\Delta\sigma$	cyclic change in stress, or stress range
Δa	change in crack length due to crack growth
Δa_t	total crack extension due to ductile tearing
ΔJ	cyclic change in J
ΔJ_{eff}	effective value of ΔJ (corrected for crack closure)
ΔK	cyclic change in stress intensity factor
ΔK_ϵ	range of the strain intensity factor
ΔK_{eff}	effective value of ΔK (corrected for crack closure)
δ_t	crack tip opening displacement
ν	Poisson's ratio
ξ	geometric term in effective plate width expression
π	usual meaning
σ or σ_∞	applied nominal stress
σ_0	stress constant in Ramberg-Osgood constitutive equation
σ_{flow}	flow stress
σ_L	plastic limit stress
σ_{max}	stress at maximum load in cycle
σ_{min}	stress at minimum load in cycle
σ_{open}	crack opening stress
σ_p	proof stress
σ_r	residual strength
σ_{ref}	reference stress
σ_s	service stress
σ_{ult}	ultimate strength
σ_{ys}	yield stress
ϕ	factor in effective crack depth (plastice zone correction) expression
ϕ^*	optimized value of ϕ
ε_0	strain constant in Ramberg-Osgood constitutive equation
ε_{ref}	reference strain
ε^p_{ref}	reference plastic strain

NONSTANDARD ABBREVIATIONS

AE	Acoustic Emission
ASTM	American Society for Testing and Materials
CDF	Cumulative Distribution Function
CEGB	Central Electricity Generating Board
CMOD	Crack Mouth Opening Displacement
CT	Compact Tension (specimen)
DECP	Double Edge Cracked Plate
EDM	Electro-Discharge Machining
EDS	Energy Dispersive Spectography
EPFCG	Elastic-Plastic Fatigue Crack Growth
EPRI	Electric Power Research Institute
FAD	Failure Assessment Diagram
FCG	Fatigue Crack Growth
FE	Finite Element
HRR	Hutchinson-Rice-Rosengren
MCPT	Multiple Cycle Proof Testing
NDE	Nondestructive Evaluation
PDF	Probability Distribution Function
PTP	Proof Test Philosophy
RSECP	Restrained Single Edge Cracked Plate (specimen)
RSM	Reference Stress Method
SCPT	Single Cycle Proof Testing
SEM	Scanning Electron Microscope
SSME	Space Shuttle Main Engine
SSY	Small-Scale Yielding
STA	Solution Treated and Aged
SwRI	Southwest Research Institute

EXECUTIVE SUMMARY

Single-cycle and multiple-cycle proof testing (SCPT and MCPT) strategies for reusable aerospace propulsion system components are critically evaluated and compared from a rigorous elastic-plastic fracture mechanics perspective within a probabilistic framework.

Previous research on MCPT included documentation of Rocketdyne experience with MCPT, distributions of initial flaw sizes and shapes in selected SSME hardware and test coupons, development of *J*-integral solutions for surface flaws, characterization of the fracture mechanics properties of Inconel 718, and development of a first-generation analytical model for MCPT. The results of these previous studies are briefly reviewed.

New *J*-integral estimation methods based on the reference stress approach are derived and validated for semi-elliptical surface cracks and for cracks at notches. A limited number of new elastic-plastic finite element *J*-integral solutions were developed to support the derivation and validation of the simple estimation methods, which have broader generality.

An engineering methodology based on the *J*-integral is developed to characterize crack growth rates during elastic-plastic fatigue crack growth (FCG) and the tear-fatigue interaction near instability. The FCG methodology employs the correlating parameter ΔJ_{eff}, which incorporates the effects of fatigue crack closure. These methodologies are integrated to develop an improved deterministic analytical model for crack growth and failure during MCPT.

Surface crack growth experiments were conducted with Inconel 718 to characterize tearing resistance, FCG under small-scale yielding and elastic-plastic conditions, and crack growth during simulated MCPT. Fractography and acoustic emission studies provide additional insight into fracture behavior. The test results provide validation of the engineering methodologies for elastic-plastic FCG and tear-fatigue, and the analytical model for crack growth during MCPT.

The relative merits of SCPT and MCPT for ductile materials are directly compared using a probabilistic analysis linked with an elastic-plastic crack growth computer code. The conditional probability of failure in service is computed for a population of components that have survived a previous proof test, based on an assumed distribution of initial crack depths in the proof-tested hardware. Parameter studies investigate the influence of proof factor, tearing resistance, crack shape, initial crack depth distribution, and notches on the MCPT versus SCPT comparison.

Both analytical and experimental studies clearly show that MCPT can be effective in removing some of the largest flaws from the population that would not have been removed by conventional SCPT at the same proof loads. Hence, MCPT can be an effective means of identifying and removing defective hardware that could go undetected by conventional SCPT. MCPT can also cause additional subcritical crack growth to occur in components that do not fail during the proof test. Therefore, in general, a cracked component that survives MCPT has a slightly shorter remaining service life than if the component had been subjected to a SCPT at the same load. However, this service life difference is negligibly small in most cases.

In general, the probabilistic studies show that for ductile materials, when MCPT is consistently applied to a fleet of components containing a distribution of initial flaws, the overall fleet reliability will be higher for a population of components that have been subjected to MCPT than for a population of components that have been subjected to SCPT at the same proof load. This benefit generally increases with increasing numbers of proof cycles, although the incremental benefit of additional proof cycles decreases with increasing numbers of cycles.

MCPT can be inferior to SCPT under certain conditions: when the probability of failure due to any proof loading is itself negligibly small; when the crack driving force decreases with increasing crack size; and when cracks are located at severely stressed notch roots and the crack lengths of concern are comparable to the plastic notch field or smaller.

MCPT can be preferable to SCPT only when viewed from the perspective of component reliability; i.e., a *probabilistic* assessment of structural integrity. From a purely deterministic standpoint, the potential advantages of MCPT cannot be recognized or documented. In particular, if proof testing is being used for the specific purpose of establishing a guaranteed maximum size for any flaw remaining in the component following the proof test, then MCPT offers no additional benefit. MCPT does not increase or decrease this guaranteed maximum flaw size relative to SCPT. The potential advantage of MCPT over SCPT is that the inferred frequency of flaws that are slightly smaller than this critical maximum flaw size may be decreased, thereby improving component reliability from a probabilistic perspective.

The parameter studies conducted under the current contract indicate that for wide ranges of variation in many of the important factors, the overall performance of MCPT in comparison to SCPT is relatively consistent. MCPT appears to be either beneficial or benign in comparison to SCPT, and any benefit generally continues to increase with increasing numbers of proof cycles. In situations where component failure risk is relatively high, MCPT can be a useful means of obtaining additional reliability. In situations where component failure risk is relatively low, MCPT itself offers no additional benefit. However, if multiple proof cycles are desirable or required for other (non-fracture mechanics) reasons, then these multiple cycles will not generally cause any significant deterioration of fleet reliability.

The specific benefit or detriment associated with MCPT depends on a large number of different factors, including proof loads, material fracture properties, and crack and component geometries. Therefore, it is not possible to provide a simple set of universal formulas or graphs that can be used to select the mathematically optimum proof test protocol and quantify the incremental benefit of that protocol. Individual fracture mechanics analyses of critical component locations are recommended to perform this evaluation for specific proof testing problems. These analyses would be facilitated by the availability of a general-purpose computer code for elastic-plastic crack growth analysis with simple probabilistic capabilities.

Within this limitation, a series of practical engineering guidelines are proposed to help select the optimum proof test protocol in a given application. The guidelines are given in the form of an annotated flow chart that provides detailed, step-by-step guidance to evaluate the relative suitability of SCPT vs. MCPT for a given proof testing application.

1. INTRODUCTION

1.1 General Background to the MCPT Problem

Although proof testing is generally not the preferred method of crack detection, it has proven useful as a supplement to conventional nondestructive evaluation (NDE) methods, particularly when NDE is compromised by geometric complexities of the component or structure. The objective of proof testing is to screen out gross manufacturing or material deficiencies and therefore provide additional quality assurance of delivered hardware. It is in this spirit that Rocketdyne has utilized proof testing on components of the Space Shuttle Main Engine (SSME).

Since 1952, Rocketdyne has selectively implemented a modified version of conventional single-cycle proof testing (SCPT) involving multiple proof cycles. This multiple-cycle proof testing (MCPT) was originally motivated by component failures on the Nalar program at pressures significantly less than the initial hydrostatic proof. Failures were experienced as low as 46% of proof pressure. The current procedure for MCPT on the SSME consists of the application of five proof cycles at a minimum pressure of 1.2 times the maximum operating pressure, each with a minimum hold time of 30 seconds. Since the inception of MCPT, Rocketdyne proof testing has shown that component failures can occur on the second, third, fourth, or fifth cycles at significantly lower pressures than applied on the first cycle [1]. These failures generally initiated from undetected flaws in the component, typically in thin sections where the defects were large compared to the thickness. In several cases these hardware deficiencies, revealed only after having passed the first proof pressure cycle, were judged to have presented a significant risk of component failure or malfunction in service. Literature searches located several additional manuscripts also describing component failure during multiple proof cycles, including experience in both aerospace pressure vessel [2,3] and gas transmission line pipe [4] applications. This direct hardware experience illustrates a potential deficiency in the conventional single cycle test, demonstrates the potential benefit arising from MCPT, and poses a challenge to determine optimum strategies for proof testing.

The primary justification for five-cycle proof testing has been the successful record of performance of Rocketdyne engines and the lack of service failures of pressurized components whenever this procedure has been implemented. There has not been, however, a well-established theoretical basis either to demonstrate clearly the superiority of MCPT (in comparison to conventional SCPT) or to specify the optimum proof pressures, temperature, and numbers of cycles to achieve maximum component reliability. The current practice is based heavily on engineering experience rather than analytical models. The purpose of the research described in this report has been to develop such an analytical model for MCPT which enables proof testing strategies to be evaluated on a rational basis.

Analytical models for conventional single cycle proof testing of brittle materials have been relatively well-established for many years [5]. See Figure 1.1, which illustrates standard proof testing logic in terms of both the residual strength σ_r and the residual fatigue life N_f of some

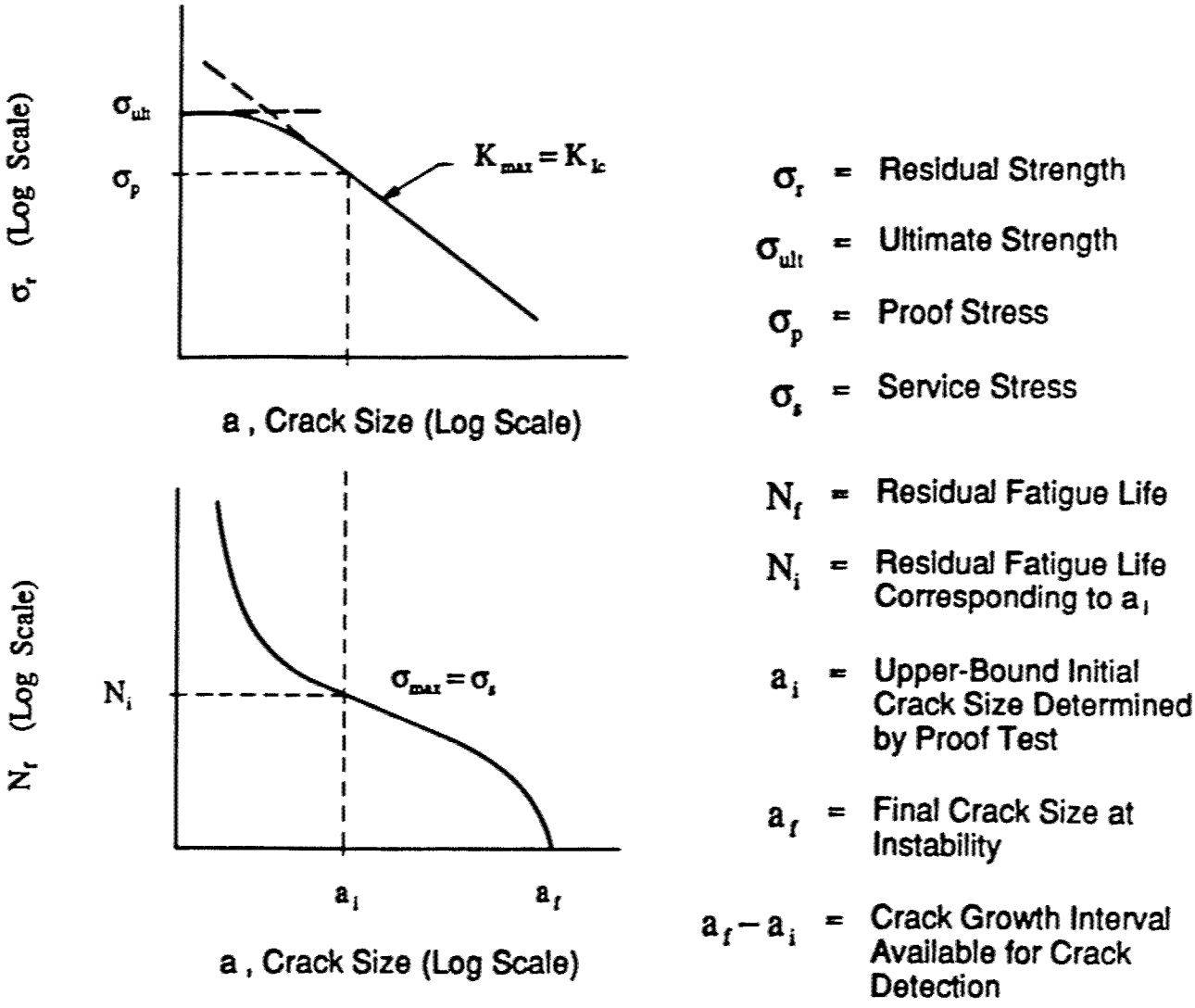

Figure 1.1. Single-cycle proof test logic represented in terms of residual strength and residual fatigue life

structural component. Since brittle materials exhibit a well-defined instability point given by $K_{max} = K_{Ic}$, the successful application of σ_p guarantees that any flaw still present is less than some size a_i. Taking a_i as the initial crack size in a fracture mechanics based fatigue crack growth analysis defines a corresponding minimum residual fatigue life N_f. Rigorous characterization of this fracture process typically requires only determination of the applied stress intensity factor K_{max} and the inherent fracture toughness of the material, K_{Ic}.

The application of additional proof cycles to a brittle material system is of no benefit, since stable crack growth does not occur during loading. Stable crack growth can occur during proof testing of a ductile material system, however, and this phenomenon suggests possible advantages—and disadvantages—of a multiple cycle proof testing strategy. The potential advantage of MCPT is that a flaw which is not large enough to cause failure during the first proof cycle may nevertheless be revealed by growing sufficiently to cause failure during a subsequent proof cycle. The potential disadvantage is that stable crack growth may occur without failure during all proof cycles, so that the remaining service life of the component is actually decreased by the proof testing process.

The current research starts with the assumption that damage growth and failure during MCPT can be described as fracture mechanics events. This assumption implies that defects are crack-like during the first proof cycle and enables us to draw upon a broad base of elastic-plastic fracture mechanics technology. The goals of the research are to characterize the extent of subcritical flaw growth during SCPT and MCPT of reusable propulsion system components, to characterize flaws which are removed from the population during SCPT and MCPT, and to move towards the identification of an optimum MCPT strategy.

1.2 Review of Key Background Information from Phase I

Results from the first two years of work under this contract were summarized in a major technical report subsequently published by NASA as Contractor Report 4318 [6]. Full documentation of these early results will not be repeated in the current Final Report. For convenience, however, the key investigations and key results from those first two years will be briefly summarized in the paragraphs that follow. The new investigations and new results presented in detail in the current Final Report naturally build on the earlier work, leading to a final set of program conclusions. In some cases, the new results and conclusions are based on the early investigations in their original form; in other cases the new material is an extension or updating of the older material; and in still other cases the new approaches or results have superseded their counterparts from the first two years.

For convenience, the first two years of work summarized in Contractor Report 4318 will be denoted as "Phase I" throughout this Final Report. The work conducted after the Contractor Report was submitted to NASA, leading up to the preparation of this Final Report, will be denoted as "Phase II."

1.2.1 Rocketdyne Experience with MCPT

The specific details of Rocketdyne experience with multiple-cycle proof testing were collected and summarized. This study focused on observed proof failures on a subsequent proof cycle, after the component had successfully endured one or more proof cycles at the same proof load. Where details were found identifying the defect size, the defect depths were generally an appreciable fraction of the component thickness, and the defect lengths were many times the thickness. Many of the failures occurred in relatively thin sections. MCPT failures were not isolated to a particular material or material system, but were observed to occur in a broad range of materials. Inconel 718 was the most common material.

1.2.2 Distributions of Initial Flaw Sizes and Shapes

Data relative to initial defect sizes and shapes for SSME hardware or fabrication processes were collected at Rocketdyne. The data sources included material test coupons, selected SSME hardware, and available multi-cycle proof failure information. Although some of the defect shapes were irregular, it was found useful to idealize all of the defects as semi-elliptical surface cracks and to determine the equivalent depth and surface length for each flaw. Statistical distributions were then defined to model the depth and aspect ratio of the defects. The predominant defect shape was found to be roughly semi-circular. The lognormal distribution was chosen to describe crack depth, based on conventional statistical tests of the available data.

1.2.3 *J*-Integral Solutions for Semi-Elliptical Surface Flaws

A fracture mechanics description of the SSME MCPT process must be elastic-plastic, rather than linear elastic, in nature. The material of greatest interest, IN-718, has a relatively high initiation toughness, so brittle fracture does not readily occur. Furthermore, the flaws of interest in SSME components are physically small, so the crack driving force is not significant unless the applied stresses are large. When the applied stresses are large, as is frequently the case, linear elasticity is typically not satisfied. In particular, since the crack depths of probable interest are large compared to the section thickness, stresses in the net section may approach or surpass the yield strength of the material.

The *J*-integral was chosen as the characteristic fracture mechanics parameter for the current study in view of its widespread use in elastic-plastic fracture analysis. Use of *J* also makes available the well-developed stability and failure assessment schemes presented in the EPRI elastic-plastic fracture handbook [7]. This approach to crack growth analysis requires two key inputs: an expression for the applied *J* and a description of the material *J*-resistance curve, both corresponding to the particular specimen and crack geometry of interest.

No closed form solutions were available in the literature to estimate the applied value of *J*, J_{app} for a semi-circular surface crack in a finite thickness plate. A limited number of finite element results for specific crack and specimen geometries and materials had been published, but these had not yet led to generalized analytical expressions. A new *J* estimation method was

derived based on the reference stress approach developed by Ainsworth and colleagues at the Central Electricity Generating Board (CEGB) of the United Kingdom [8]. The reference stress technique requires only three basic pieces of information, all of which are readily available in this case: (1) a solution for the linear elastic stress intensity factor K; (2) a description of the elastic-plastic constitutive response; and (3) an estimate of the limit load for the cracked member, assuming an elastic-perfectly plastic material. An additional modification to the reference stress solution was then implemented based on the J estimates developed by Dowling [9] for semi-circular flaws in infinite bodies. Comparisons of this modified J estimation scheme with the available finite element results for semi-ellipitical surface flaws showed good agreement.

1.2.4 Fracture Mechanics Properties of Inconel 718

All experimental investigations were performed on IN-718 heat-treated to the STA-1 condition (designed for optimum resistance to hydrogen embrittlement). Tensile tests determined that the average 0.2% yield strength was 161.2 ksi, ultimate tensile strength 205.5 ksi, elongation 22.2%, and reduction in area 33.3%. The elastic modulus was $29.69(10)^3$ ksi.

A J-resistance curve for surface-flawed IN-718 was generated experimentally. The specimens had a rectangular cross-section 1.25 inches in width and were either 0.2 or 0.5 inches thick. Semi-circular surface cracks were initiated by electro-discharge machining and fatigue pre-cracking. Initial crack depths after pre-cracking ranged from $a/t = 0.36$ to 0.73. Loads were applied in uniaxial tension. Tests were conducted in both load control and crack mouth opening displacement control. No significant changes in crack shape were observed during stable crack growth.

The resistance curve was constructed from the experimental data by directly measuring initial crack depth a and crack extension Δa and by estimating J in one of two ways. The first method used the modified reference stress estimation scheme described earlier. An independent second method was based on an "equivalent energy" approach. These two estimation techniques gave results which usually agreed within 10 percent. The apparent toughness of the surface-cracked configuration was significantly higher than the toughness observed for thick compact tension (CT) specimens.

Fatigue crack growth (FCG) tests were conducted on through-thickness cracked panels to determine both baseline FCG rate data and information regarding fatigue range marking. Two tests were run on 0.2-in. thick specimens and one on a 0.5-in. thick specimen to provide data over a wide range of growth rates. Visual examination of the fracture surfaces revealed significant differences in the fracture surface morphology at high and low growth rates, verifying that range marking could be used successfully to delineate the crack front fractographically. A series of crack shape study experiments were then conducted on surface-flawed 0.2-in. thick specimens under small-scale yielding conditions. The crack shape was found to remain nearly constant around $a/2c = 0.5$ as the crack grew from $a/t = 0.3$ to 0.9.

1.2.5 First-Generation Analytical Model for MCPT

A comprehensive survey of the available literature suggested that it was not yet possible to predict with certainty how crack growth would be influenced by multiple proof cycles. A variety of different behaviors had been reported experimentally, and several different analytical approaches had been proposed. However, it was found useful to assemble a simple first-generation model for crack extension during simulated MCPT. This analytical model was designed to demonstrate the potential effects of many different variables on ductile crack growth during SCPT and MCPT and to make a preliminary evaluation of the possible differences between SCPT and MCPT. The model was a simple numerical tool to explore "what-if" scenarios and to plan further critical experiments.

The simple model was based on the Electric Power Research Institute (EPRI)-elastic-plastic fracture analysis scheme and considered only crack advance due to ductile tearing. Stable (or unstable) crack growth was evaluated by comparison of J_{app} and J-resistance curves. The capability to model different values of system compliance, ranging from pure load control to pure displacement control, was included. Analysis of crack growth on subsequent proof cycles after the first was addressed by regarding each reload cycle as the first loading cycle in a new test. The initial crack length for this new test was taken as the predicted final crack length from the end of the previous proof cycle. This caused a translation of the J-resistance curve along the Δa axis, although the shape of the resistance curve was assumed to be unchanged by the unload-reload cycle. This approach was thought to give an upper bound estimate of crack advance in nearly all cases.

The model was exercised to investigate the effects of crack geometry, applied load, number of proof cycles, resistance curve shape, system compliance, and other variables on crack growth during MCPT. However, the key issue in evaluating SCPT vs. MCPT is not how a single flaw behaves, but rather how a proof test protocol influences a distribution of defect sizes which may be present in a population of components. Therefore, Monte Carlo simulation was used to evaluate the effects of SCPT and MCPT on crack size distributions before vs. after various proof test procedures.

1.2.6 Phase I Conclusions

The changes in the crack size distribution during MCPT were shown to depend on the interactions between the number of proof cycles applied, the nature of the resistance curve, the initial crack size distribution, the component boundary conditions, and the magnitude of the applied load or displacement. Therefore, the relative advantages and disadvantages of single-cycle versus multiple-cycle proof testing appeared to be specific to individual component geometry, material, and loading.

However, a number of important issues were not resolved by the Phase I investigations. In particular, no direct experimental evaluations of the Phase I analytical model were carried out in Phase I. Other major remaining issues included the potential contributions of fatigue crack

growth mechanisms, the relationship between ductile tearing and fatigue, possible changes in the behavior of very deep cracks, and the full significance of local control mode (load vs. displacement). Finally, it was not yet clear how best to quantify the differences between MCPT and SCPT with respect to the practical implications for hardware reliability. In other words, what is the best numerical way to ask and answer the MCPT vs. SCPT question?

1.3 Work Scope for Phase II Investigations

The Phase II investigations were designed to resolve these outstanding issues in search of a more definitive answer to the MCPT question. The effort involved close coordination between experimental and analytical investigations. Critical experiments were used to develop clearer understandings of fundamental fracture mechanics issues and to evaluate or validate the original and subsequent improved analytical models. Analytical development activities included the development of new or improved J solutions and the development of practical fracture mechanics approaches to characterize crack growth, including improved models for crack growth during MCPT. Finally, a series of probabilistic analyses employed these improved MCPT models to evaluate the implications of SCPT and MCPT for predicted fleet reliability, leading to a series of conclusions about the selection of the optimum proof test strategies.

The remainder of this Final Report is a careful documentation of the Phase II investigations, results, and conclusions. The **Analytical Development** chapter summarizes improved J solutions for surface cracks, new finite element solutions and simple estimates of J for cracks growing from notches, an engineering methodology to characterize elastic-plastic fatigue crack growth, and a new second-generation model for MCPT based on tear-fatigue theory. The **Experimental Characterization and Validation** chapter first presents updated J-resistance curves and shows the relationship between the J-R curves and FCG curves. Then critical experiments are documented which characterize elastic-plastic FCG and tear-fatigue behavior, along with the effect of proof testing on subsequent FCG rates. Fractographic observations and the results of acoustic emission studies are also summarized. In the **Probabilistic Analysis** chapter, the SCPT vs. MCPT question is posed and answered from a more rigorous quantitative standpoint with respect to fleet reliability. The results of extensive parameter studies are presented to show the effects of important proof testing variables on the probability of hardware failure in service. A **Discussion** chapter provides some broader perspective and briefly addresses a variety of other secondary MCPT issues outside the scope of this contract. Finally, the **Summary and Conclusions** and **Engineering Guidelines** chapters summarize the important results of the study and their practical implications for the specification of optimum proof test protocols. The guidelines are organized as an annotated flow chart that provides detailed, step-by-step guidance to evaluate the relative suitability of SCPT vs. MCPT for a given proof testing application.

2. ANALYTICAL DEVELOPMENT

In Phase I, analytical development work included the development of J solutions for semi-elliptical surface cracks, the implementation of the EPRI J scheme for the analysis of ductile tearing, and the development of a simple analytical model for MCPT based on ductile tearing considerations.

Significant new analytical development activities were conducted in Phase II. An improved reference stress J estimate was developed for the semi-elliptical surface crack, drawing from newly available finite element J solutions. Phase I observations about the significance of local control mode led to increased interest in cracks growing from notches, so new J solutions were generated for this important geometry. A limited set of elastic-plastic finite element solutions were produced first, providing a basis for the derivation and verification of a simple J estimation method. An engineering methodology was developed to treat fatigue crack growth under elastic-plastic cycling. Finally, an improved analytical model for crack growth during MCPT was developed based on tear-fatigue theory. All of these analytical activities and associated results are documented in some detail in the remainder of the chapter.

2.1 Improved J-Integral Solutions for Surface Flaws

The approach developed in Phase I to estimate J for the important semi-elliptical surface crack geometry was based on a reference stress formulation [8] and the only set of finite element solutions [10] for that geometry available at that time. The reference stress formulation was modified by adapting an earlier solution by Dowling [9] for a surface crack in a semi-infinite body in order to improve agreement with the FE results.

In the years immediately following the completion of Phase I, several additional sets of finite element J-integral solutions for the surface crack became available [11-14], including a wider variety of geometries and constitutive relationships. The Phase I solution did not always show good agreement with the new FE results. Therefore, in the Phase II effort, these new numerical results were used to develop an improved reference stress estimate of J with greater generality. A more complete description of this analytical effort is given in Appendix A. For convenience, a shorter synopsis of the method and results is provided here.

Following the EPRI handbook [7] approach, a general form for J in a Ramberg-Osgood material can be written according to

$$J_{total} = \frac{K^2}{E'}\left\{1 + \frac{F^2}{C_2}\left(\frac{n-1}{n+1}\right)\left[\frac{(\sigma_{-}/\sigma_0)^2}{1+(\sigma_{-}/\sigma_0)^2}\right]\right\} + \alpha\,\sigma_0\,e_0\,th_1\left(\frac{\sigma_{-}}{\sigma_0}\right)^{n+1} \qquad (2.1)$$

The first term in Eqn. 2.1 represents the elastic component of J, J_e, and the bracketed factor is an effective crack length correction similar to the EPRI handbook suggestion for evaluating first order plastic effects with F defined as a geometry-dependent term in the elastic K expression:

$$K = F \sigma_{\infty} \sqrt{\pi a} \tag{2.2}$$

The coefficient C_2 is set equal to 2 for plane stress and 6 for plane strain based on arguments about the size of the crack-tip plastic zone. The effective elastic modulus E' is set equal to E for plane stress and $E/(1 - \nu^2)$ for plane strain.

The second term in Eqn. 2.1 represents the plastic component of J, J_p, and is defined in terms of the Ramberg-Osgood (constitutive) constants ϵ_o and σ_o, which satisfy the stress-strain law of the general form

$$\frac{\epsilon}{\epsilon_o} = \frac{\sigma}{\sigma_o} + \alpha \left(\frac{\sigma}{\sigma_o} \right)^n \tag{2.3}$$

Here ϵ is the uniaxial strain corresponding to the stress, σ, and $\epsilon_o = \sigma_o/E$. The applied (uniform uniaxial) stress σ_∞, and the non-dimensional factor h_1 depends on geometry and strain hardening exponent but not on the magnitude of the applied stress. It is this h_1 which is tabulated in the elastic-plastic fracture handbooks, and it is this h_1 (or its equivalent) which any simple estimation technique must compute accurately.

The basic form of the Ainsworth reference stress expression for the plastic component is

$$J_p = K^2 \frac{\varepsilon^p_{ref}}{\sigma_{ref}} \tag{2.4}$$

where the reference stress σ_{ref} is computed as

$$\sigma_{ref} = \sigma_{\infty} \frac{\sigma_{ys}}{\sigma_L} \tag{2.5}$$

Here σ_L is the plastic limit stress for a cracked body for a rigid plastic material of yield stress σ_{ys}. Note that σ_{ys} is also the plastic limit stress for an elastic-perfectly plastic uncracked body. For convenience, a collapse function f is defined as the ratio of the two plastic limit loads:

$$f = \frac{\sigma_L}{\sigma_{ys}} \tag{2.6}$$

Note that f is always bounded by 0 and 1, and so the reference stress will always be equal to or (in general) greater than the applied stress. Note also that f is a function of geometry and the type of applied load (tensile, pressure, bending) but not a function of the magnitude of the load or constitutive law. The reference strain plastic ε^{p}_{ref} is calculated from the constitutive relationship as the uniaxial plastic strain corresponding to a uniaxial stress σ_{ref}.

In order to compare the reference stress estimates more directly with the FE J solutions, Eqn. 2.6 was expanded and an effective crack length term added to give the general form,

$$J_{total} = \frac{K^2}{E}\left\{1 + \frac{F^2}{C_2}\left(\frac{n-1}{n+1}\right)\left[\frac{(\sigma_{-}/\sigma_0)^2}{1+(\sigma_{-}/\sigma_0)^2}\right]\right\} + \frac{K^2}{E}\left\{\left(\frac{\varepsilon_{ref}E}{\sigma_{ref}}\right) - 1\right\} \qquad (2.7)$$

where ε_{ref} is the total (elastic plus plastic) reference strain. For simplicity and slight conservatism, plane stress was assumed in this particular formulation. Expanding the second (plastic J) term for a Ramberg-Osgood material, it is possible to derive the general form,

$$J_p = \alpha\,\sigma_0\,\varepsilon_0\,t\left\{\frac{F^2\pi(a/t)}{f^{(n-1)}}\right\}\left(\frac{\sigma_{-}}{\sigma_0}\right)^{n+1} \qquad (2.8)$$

Note that the term in the curly brackets in Eqn. 2.8 is equivalent to h_1 in Eqn. 2.1. In order to estimate h_1 using the reference stress approach, then, (and hence to estimate total J) only F and f must be determined. Since F can be extracted directly from the K solution, the challenge is focused on f, and ultimately on the proper form for the plastic limit stress σ_L, as the only significant remaining unknown.

Unfortunately, "exact" theoretical solutions do not exist for f as they do for K. Various bounding theorems can be used to estimate f, but different approaches can yield different expressions for the limit stress. Furthermore, it is not intuitively obvious for the surface cracked geometry whether the relevant limit stress should characterize the overall plastic deformation of the cracked structure (a global limit stress) or the plastic deformation local to a point on the defect (a local limit stress). Miller [15] and Chell [16] concluded from their studies that global limit stresses gave better agreement with FE results than local limit stresses. In general, as Chell has noted [16], the optimum choice of the collapse function f does not necessarily represent the true plastic yield load of the structure. Instead, it can represent an empirical yield load which will produce good agreement between the reference stress procedure and elastic-plastic FE computations of the J-integral.

The simplest choice of yield function f for the surface flaw is that based on the reduction in load bearing area due to the presence of the defect. This gives the global yield function,

$$f = 1 - \frac{\pi\, a\, c}{4\, b\, t} \tag{2.9}$$

Here a is the maximum depth and $2c$ the surface length of a semi-elliptical surface crack in a plate of thickness t, width $2b$, and height $2h$. This was the form used in the Phase I estimate. A potential disadvantage of this form, as will be shown later, is that f appears to be over estimated for wide plates (large b/c ratios). As b/c goes to infinity, this simple net section area criterion implies that the effect of the defect—no matter how deep—is vanishingly small. The limit stress is then merely that of a defect-free plate, and $f = 1$.

An alternative approach is to define some effective plate dimension (in the width direction) that characterizes collapse. One such construction is shown in Fig. 2.1, where the effective width is given as $(2\xi + 2c)$. The limit stress is defined when stresses in this enclosed region are at yield. The remaining problem now is to select the proper value of ξ. Remembering that the optimum choice of a limit load can be driven by optimum agreement with FE solutions, it is possible to work backwards from available numerical solutions to evaluate different means of defining ξ.

The limit or yield function for the geometrical construction of Fig. 2.1 can be written as

$$f = \frac{\xi + c\left(1 - \dfrac{a'}{t}\right)}{\xi + c} \tag{2.10}$$

Here the actual semi-elliptical cracked area has been represented by the equivalent rectangular area a' x $2c$, where $a' = \pi a/4$.

There are several possible ways that ξ might be related to the plate geometry. If the form of h_1 in Eqn. 2.8 and the nominal net section area criterion (Eqn. 2.9) are correct, then $\xi = (b\text{-}c)$ and the non-dimensional quantity $\xi/(b\text{-}c)$ will be equal to 1. Alternatively, it is possible that ξ is related to the plate thickness t, so that the ratio ξ/t will be approximately constant. Another characteristic dimension of the cracked geometry is the crack width $2c$, so the nondimensional ratio ξ/c may be significant.

Yield functions f were computed for the five sets of recently published FE solutions, and then ξ values were calculated by inversion of Eqn. 2.10. In general, ξ was found to be considerably smaller than the remaining plate width $(b\text{-}c)$, especially for large b/c ratios. Therefore, the nominal net section area criterion (Eqn. 2.9) often gave limit load estimates much too high and reference stress J estimates too low. This was precisely the finding in Phase I. The Phase I approach attempted to solve this problem by calibrating the reference stress formulation

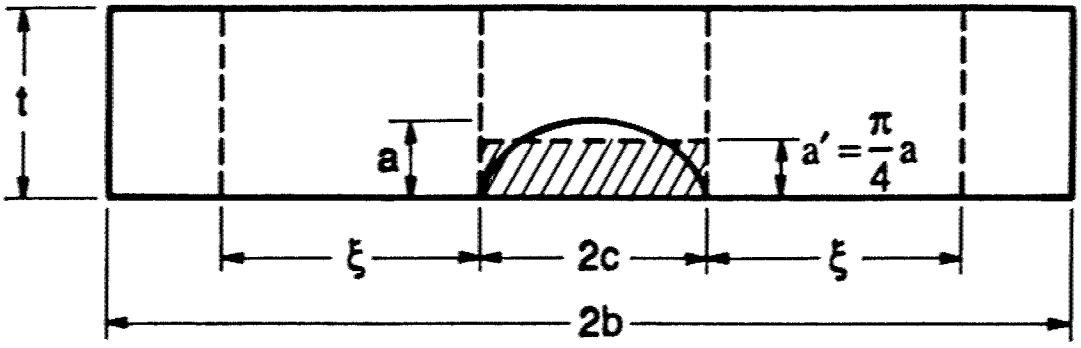

Figure 2.1. Geometric construction for limit load solution of surface-cracked plate, illustrating effective plate width

to a solution for a surface crack in a semi-infinite plate. While this approach gave good agreement with the earlier Wang FE results, it did not agree well with all of the more recent FE results. Furthermore, it is not clear that the specific calibration factor used in Phase I for a semi-circular crack in an infinite plate is necessarily applicable to all crack shapes and component geometries, and alternative calibration factors were not generally available. These limitations prompted the Phase II investigations into alternative reference stress formulations.

The parameter ξ was also found to be poorly correlated with the plate thickness t. However, a better correlation was exhibited between ξ and the crack half-width c. The ratio ξ/c was approximately bounded by 1 and 3 for most of the geometries considered.

Comparisons of predicted and published FE h_1 values for several different choices of ξ/c found that a value of $\xi/c = 1.75$ gave remarkably good estimates of J for a wide range of crack shapes and sizes and strain hardening behavior. This selection gave predictions of the plastic J term (as represented by the plastic factor h_1) which were usually within ±15 percent of the published FE results, never more than 20 percent low, and only occasionally excessively conservative. Some of the larger disagreements may have been due to inaccuracies in the FE solutions, as discussed later. In any event, the accuracy of the total J estimate will often be much better than the accuracy of the plastic J estimate. If a more universally conservative fracture assessment is desired for all crack shapes, then a smaller ξ/c value, perhaps 1.0, may be appropriate (at the expense of greater conservatism for the deepest cracks).

Excellent agreement (±12 percent) was observed between the reference stress predictions of total J and the FE results of Wang [10] and Dodds [13] for different crack shapes, crack depths, and strain hardening exponents, as shown in Fig. 2.2. All these analyses were based on the standard Ramberg-Osgood constitutive model. Reference stress estimates of additional results due to Wang [11] based on a more complex stress-strain law (fully elastic below the yield stress, fully power law above the yield stress) were slightly more conservative, perhaps due to the sharp knee in the stress-strain relationship.

Comparisons of the reference stress estimates of total J with the Kirk [12] finite element results based on a bilinear stress-strain law (with a sharp corner at the elastic-plastic transition) found that the reference stress estimates were somewhat conservative at applied stresses very near the yield stress, but generally did a good job of following the very severe upturn in J with increasing load.

Comparisons of the reference stress estimates of h_1 for $\xi/c = 1.75$ with the calculations of Yagawa *et al.*, indicated general agreement for most geometries but significant disagreement in a few cases. Reference stress and FE results for the plastic J term agreed within ±20 percent in almost two-thirds of the cases considered, and reference stress estimates were never more than 20 percent low. Some apparent dependence of prediction quality on both a/c and a/t was observed. However, Yagawa *et al.*, had systematically compared their elastic predictions of K with the benchmark Newman-Raju finite element results [17] for the same configurations, and found significant disagreement in some cases. These cases corresponded to the same geometries

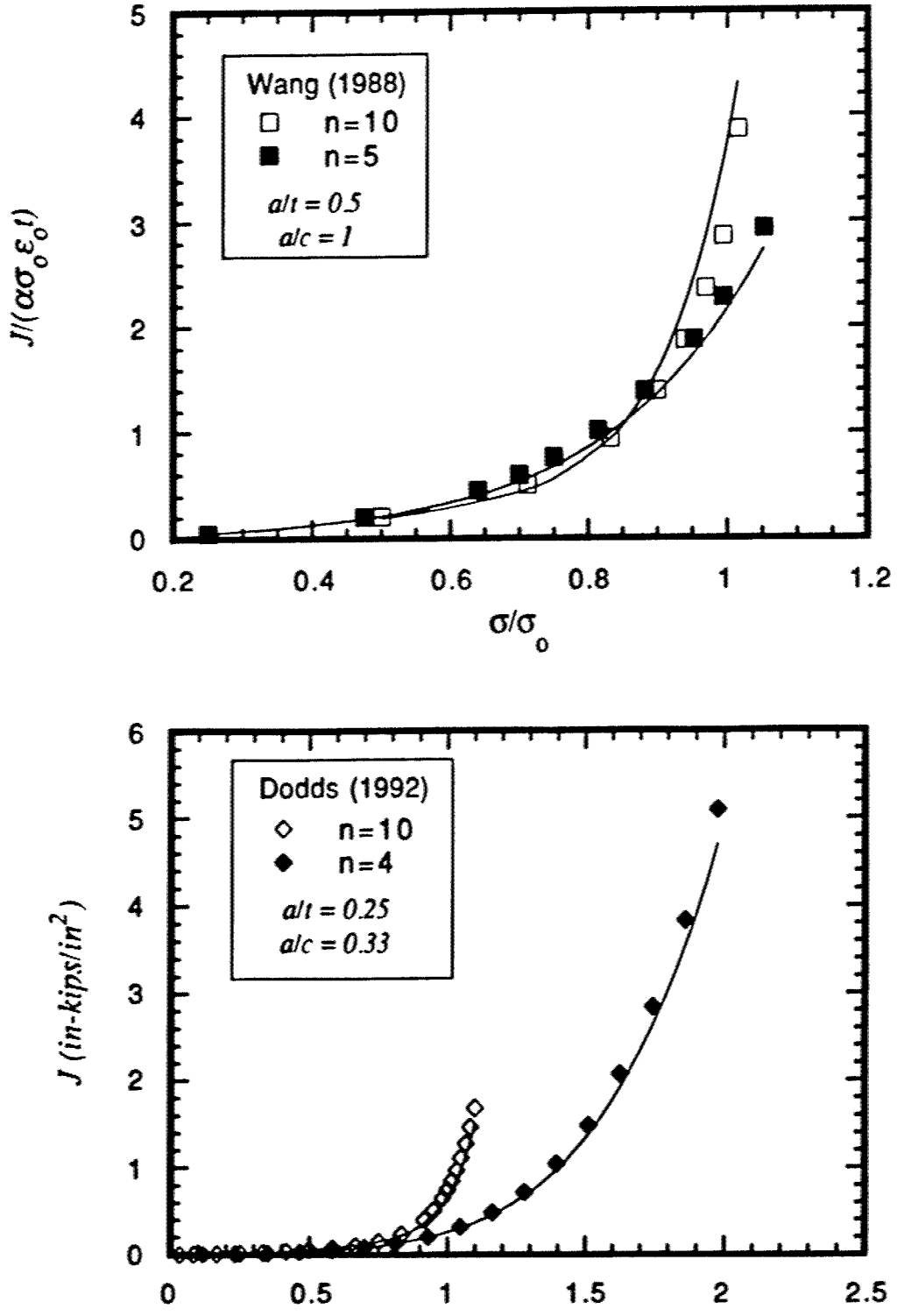

Figure 2.2. Comparison of reference stress J predictions (solid line) with Wang (top) and Dodds (bottom) finite element results

where the reference stress J estimates most disagreed with Yagawa, indicating that some of the Yagawa results may be in error.

More detailed comparisons of the simple estimation technique with the various FE results are given in Appendix A.

The search for improved J solution techniques is continuing under other contract efforts [18] at SwRI as new finite element J solutions become available and new insights into the reference stress approach are gained. However, the technique described above, which was used throughout the Phase II effort on the current contract, appears to be a reasonably accurate and robust approach for members loaded in uniform uniaxial tension.

2.2 *J*-Integral Solutions for Cracks at Notches

The behavior of cracks at notches during MCPT was a topic of particular interest due to the observations in the Phase I studies about the effects of local control mode on crack growth. Notched geometries are one form of intermediate control mode; although the remote boundary conditions may be driven in load control, the local elastic-plastic deformation at the notch root generates a local response which exhibits some characteristics of displacement or strain control.

However, J solutions are not readily available for cracks at notches. Only a very limited number of solutions for a very limited range of geometries and loading conditions are available in the literature. Therefore, it was necessary to generate a new series of J solutions that could be used in later parameter studies of MCPT behavior. First, a series of finite element analyses were performed on a selected notch geometry in order to obtain elastic and fully plastic J solutions. Next, a simple estimation technique with greater generality was derived and validated against these FE calculations. The estimation technique was required for the parameter studies because it was not practical to perform the full FE analysis for each crack size and notch geometry in the parameter studies.

2.2.1 Finite Element Results

J solutions were computed for cracks emanating from notches using the elastic-plastic finite element method. Preliminary linear elastic runs were made to verify the finite element model used in the computations would provide good accuracy. The stress intensity factors for cracks were calculated, and these solutions were compared with the expected values for very short cracks (which experience an approximately uniform local stress of $K_t S_T$, where K_t is the stress concentration factor, and S_T the nominally applied stress) and relatively long cracks (which should behave as cracks of depth $a = D + d$ subjected to a gross section stress, S_T, where D is the depth of the notch and d the actual crack depth measured from the root of the notch).

Three double edge notch geometries under plane stress tensile loading were considered in the investigation, corresponding to K_t values of 4.29, 6.43, and 8.57 where

$$K_t = \frac{\textit{stress at notch}}{\textit{gross section stress}} \tag{2.11}$$

Corresponding values of D/r_o were 2.41, 6.2, and 11.6. Here, b is half the width of the plate and r_o is the radius of the semi-circular notch tip. The relationships between d, a, r_o, D, and b, are shown schematically in Fig. 2.3. The notches extended 30% across the section (D = 0.3b = 1.5 inch, where b = 5 inch) and had root radii of 0.622 inch, 0.2425 inch and 0.129 inch.

The linear elastic results for a gross section stress S_T = 120 ksi are shown in Figures 2.4 through 2.6, where it can be seen that the computed results are in excellent agreement with the limiting short and long crack solutions.

Having verified the accuracy of the finite element mesh for the three notch geometries, the fully plastic component of J, J_p, was then calculated for various crack depths and strain hardening exponents, n, assuming a Ramberg-Osgood stress-strain law (Eqn. 2.3) with a characteristic yield stress σ_o = 60 ksi and Young's Modulus E = 30,000 ksi. The constant α = 100 was chosen to have a very high value in order to induce high levels of plasticity at relatively low stress levels. Values of n = 1, 3, 5, 10 and 15 were used in the analysis, and for each value the applied load, P, was incremented in the computations until $J_e/J < 0.0005$ (where J_e is the elastic component of J), which ensured that the fully plastic solution had been reached. Following the EPRI handbook of elastic-plastic J solutions [7] for the double edge cracked plates (DECP), J_p was expressed in the form

$$J_p = \left(J - J_e\right) = \alpha \sigma_o \epsilon_o c h_1\left(\frac{a}{b}, n, \frac{D}{r_o}\right) \left\{\frac{P}{P_o}\right\}^{n+1} \tag{2.12}$$

so that the EPRI J solutions would be recovered at relatively large d values ($d > 0.5r_o$) when the notch plus crack could be represented to a good approximation as a crack of effective depth, a = D_o+d subjected to the nominal stress. In the equation, P is the applied load, P_o is a characteristic yield load per unit breadth of plate given by

$$P_o = \frac{4}{\sqrt{3}} c \sigma_o \tag{2.13}$$

$c = b - a$, and $h_1(a/b,n, D/r_o)$ is a function whose values were derived from Mr. Orient's FE results. At large d values, h_1 $(a/b, n, D/r_o)$ should become independent of D/r_o, and the h_1 values tabulated in the EPRI handbook for the double edge cracked plate should be recovered.

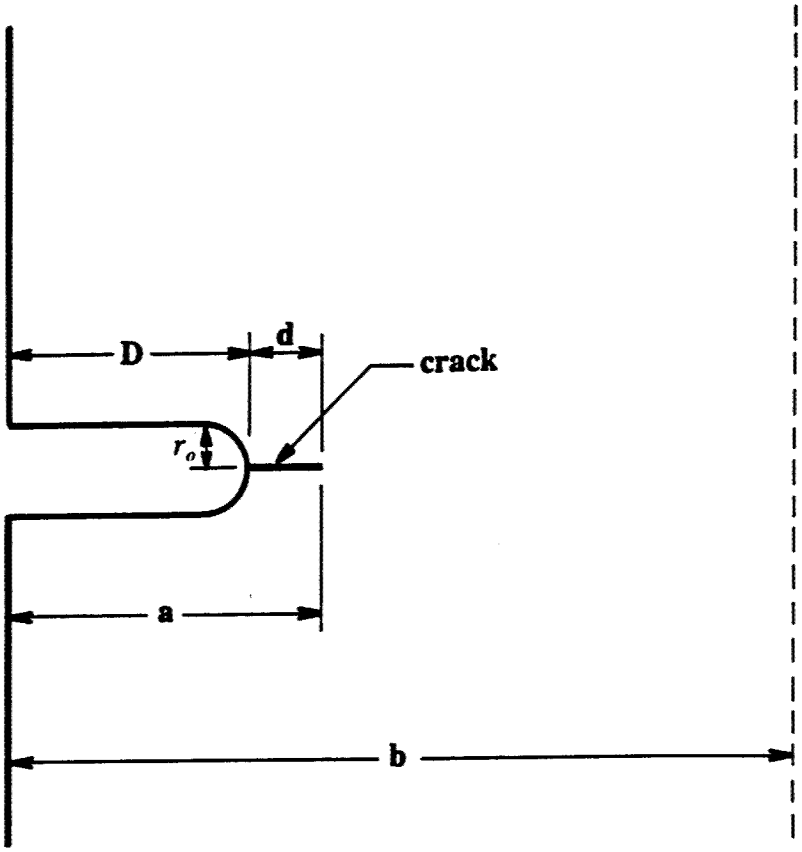

Figure 2.3. Schematic showing geometrical relationship between notch depth (D), notch root radius (r_o), crack depth (d), notch plus crack depth (a), and half plate width (b)

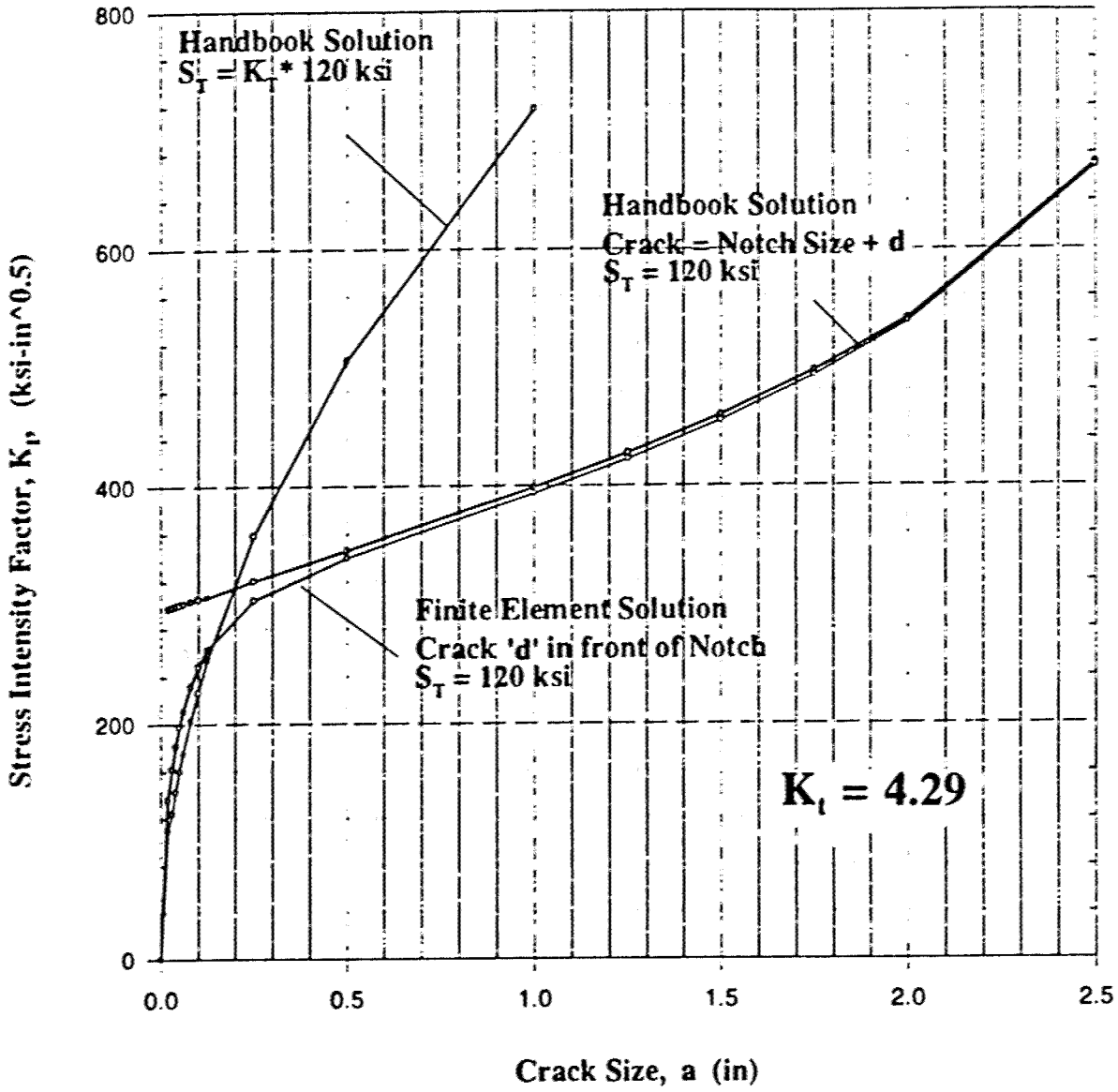

Figure 2.4. Linear elastic solutions for cracks at double edge notches in plates with K_t= 4.29

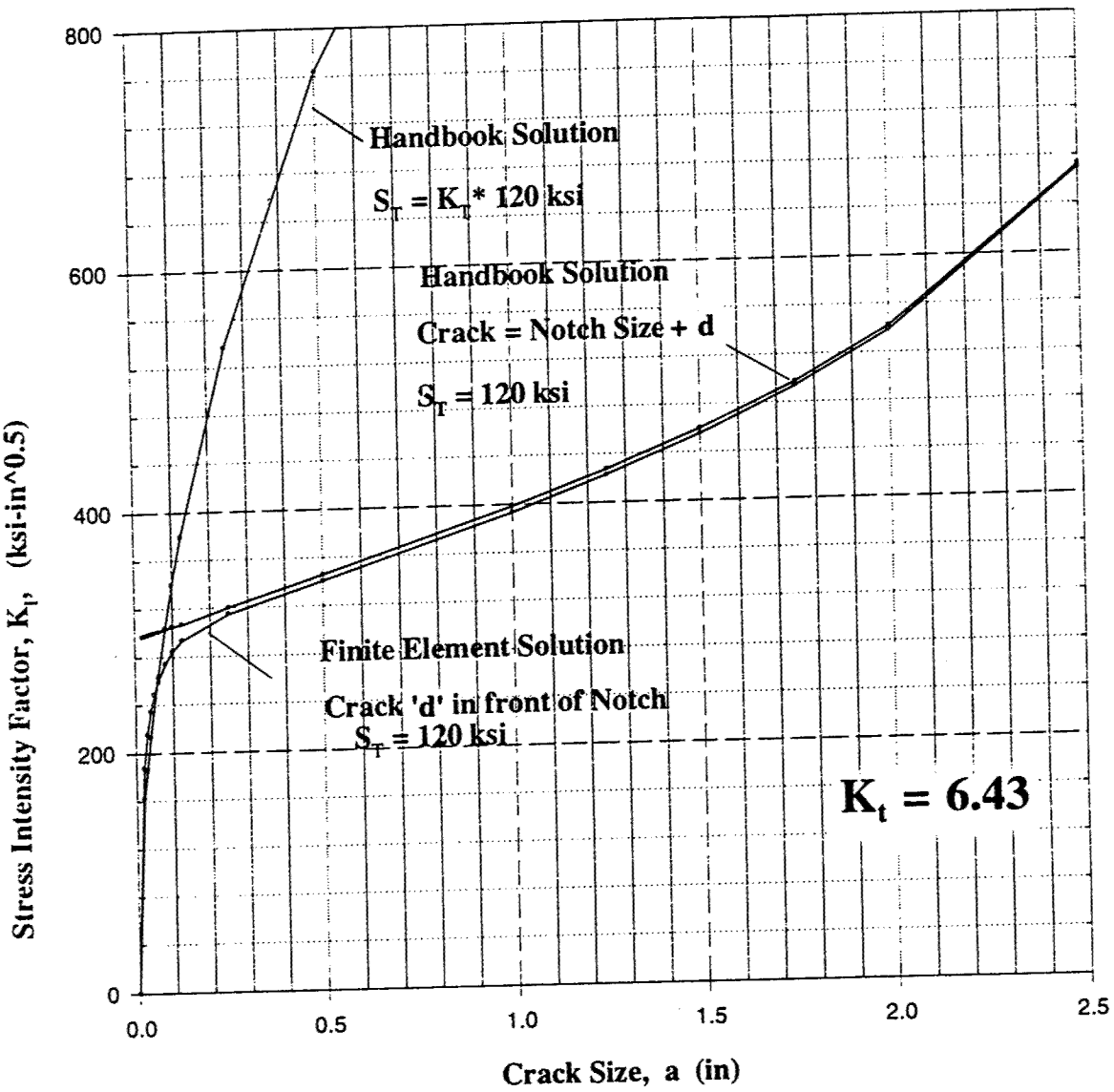

Figure 2.5. Linear elastic solutions for cracks at double edge notches in plates with $K_t = 6.43$

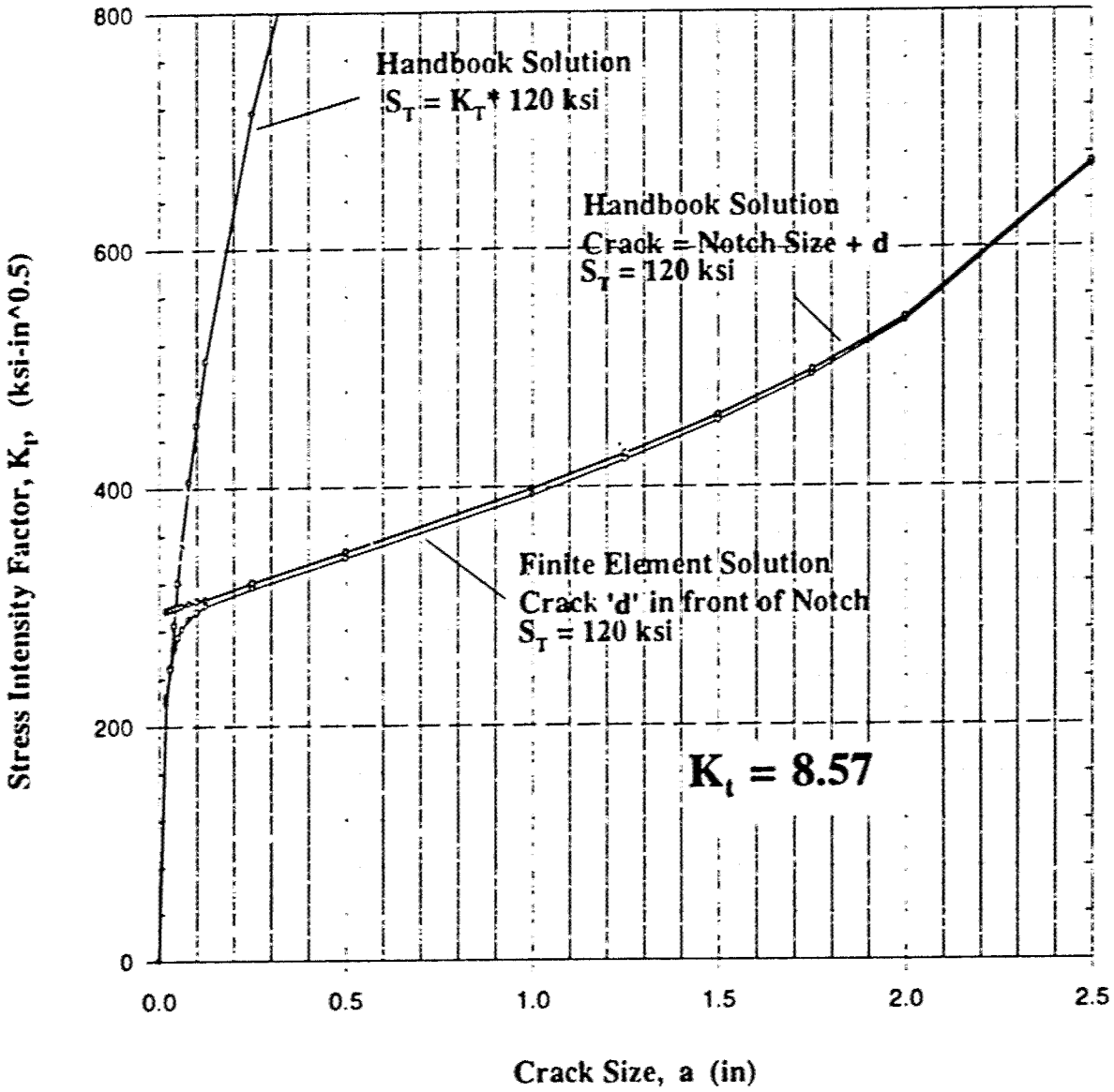

Figure 2.6. Linear elastic solutions for cracks at double edge notches in plates with $K_t = 8.57$

The computed values for the function $h_1(a/b,n,D/r_o)$ for various a/b values are shown in Tables 2.1 through 2.3 for the cases where K_t=4.29, 6.43, and 8.57, respectively. The same results are shown in graphical form in Figures 2.7 through 2.9, where the asymptotic behavior of the solutions at relatively large d/r_o can be observed ($d = r_o/2$ corresponds to a/b = 0.3622 in Fig. 2.7, 0.32425 in Fig. 2.8, and 0.3129 in Fig. 2.9). Also shown in the figures are the $h_1(a/b,n,D/r_o)$ values given in the EPRI handbook. It can be seen that the results for the deepest crack obtained in the present study agree reasonably well with the EPRI solutions, showing that, as in the linear elastic case, the effect of the notch is limited to crack depths, d, which are less than about half the root radius, r_o, of the notch.

2.2.2 Simple *J*-Estimation Technique

A simple *J*-estimation technique with greater generality was developed and validated against these FE calculations. These development and validation exercises were performed under another NASA-Marshall contract on elastic-plastic fatigue crack growth (EPFCG) [18] in order to fulfill the statement of work of that contract, and so details of the analysis are provided elsewhere [19]. For convenience, since the resulting *J*-estimation method was employed in the current program, a brief summary of the method is provided here.

The proposed *J* estimation scheme for cracks at notches combines the scheme adopted by EPRI and used in the elastic-plastic handbooks, with the reference stress method (RSM). In the proposed scheme, hereafter referred to as the modified RSM, first order plasticity effects are included in *J* via a first order plastically corrected value for the linear elastic solution, J_e given by

$$J_e(d_e) = J_e(d + \phi r_y) \tag{2.14}$$

where

$$J_e = \frac{K_I^2}{E} \tag{2.15}$$

and K_I is the stress intensity factor. The effective depth, $d_e = d + \phi r_y$, includes a plastic zone correction determined by the terms ϕ and r_y which are defined as

$$\phi = \frac{1}{1 + \left(\frac{P}{P_o}\right)^2} \tag{2.16}$$

$$r_y = \frac{1}{C_2\pi}\left[\frac{n-1}{n+1}\right]\left(\frac{K_I}{\sigma_o}\right)^2 \tag{2.17}$$

Table 2.1. Numerical values of the shape factors for $K_t = 4.29$

a/b	n=3	n=5	n=10	n=15
0.315	0.929	1.072	1.203	1.210
0.326	1.203	1.327	1.350	1.223
0.337	1.345	1.425	1.304	1.157
0.347	1.416	1.440	1.257	1.100
0.358	1.449	1.419	1.215	1.050
0.369	1.459	1.398	1.175	1.006
0.380	1.457	1.378	1.139	0.966

Table 2.2. Numerical values of the shape factors for $K_t = 6.43$

a/b	n=3	n=5	n=10	n=15
0.315	1.290	1.416	1.376	1.261
0.326	1.426	1.453	1.319	1.190
0.337	1.444	1.428	1.270	1.130
0.347	1.442	1.407	1.229	1.079
0.358	1.440	1.389	1.191	1.034
0.369	1.438	1.372	1.155	0.994
0.380	1.436	1.356	1.124	0.958

Table 2.3. Numerical values of the shape factors for $K_t = 8.57$

a/b	n=3	n=5	n=10	n=15
0.304	0.952	1.115	1.265	1.283
0.315	1.417	1.457	1.351	1.241
0.326	1.434	1.432	1.302	1.178
0.337	1.432	1.413	1.260	1.124
0.347	1.431	1.397	1.221	1.076
0.358	1.430	1.381	1.185	1.029
0.369	1.429	1.366	1.150	0.986
0.380	1.428	1.350	1.117	0.947

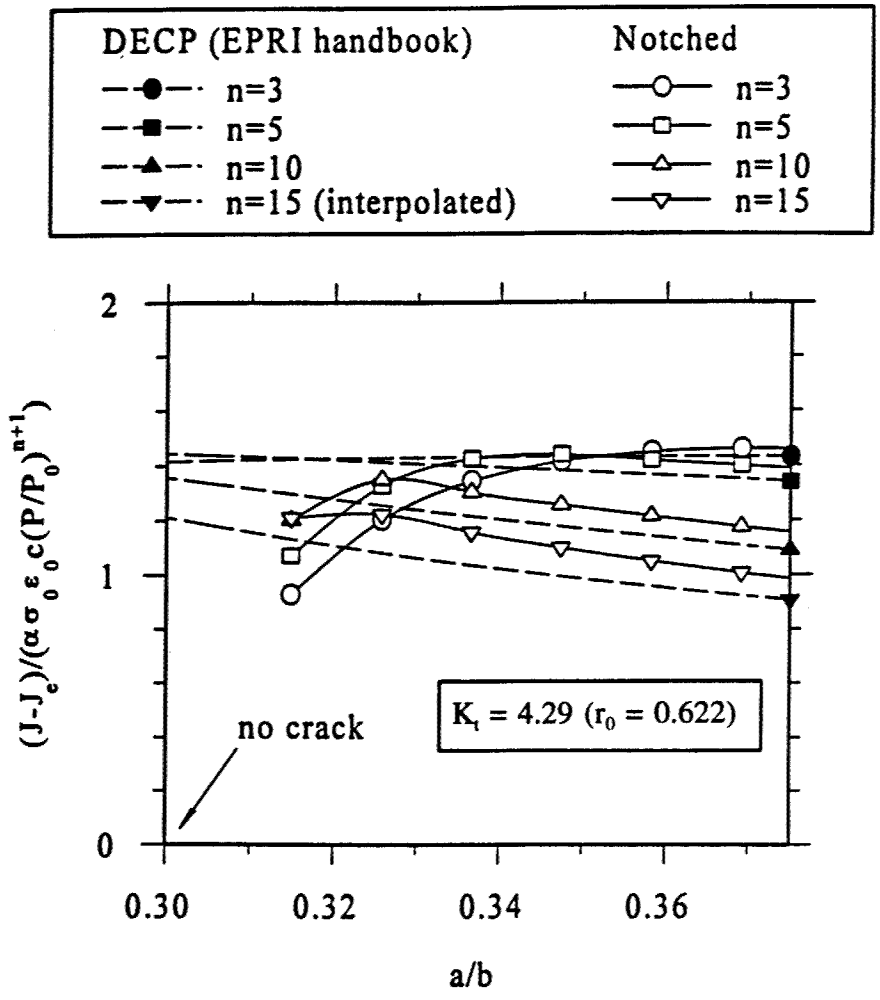

Figure 2.7. Asymptotic behavior of $h_1(a/b, n)$ for $K_t = 4.29$ as d/r_0 increases ($d=r_0/2$ corresponds to $a/b = 0.3622$)

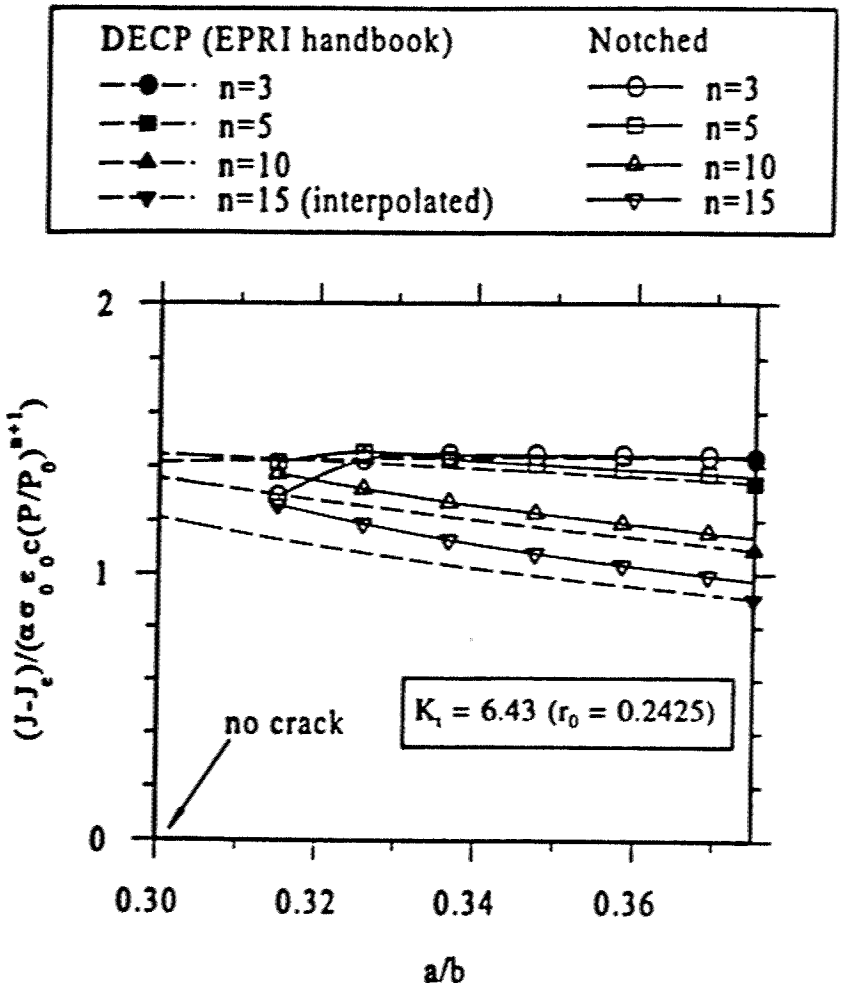

Figure 2.8. Asymptotic behavior of $h_1(a/b, n)$ for $K_t = 6.43$ as d/r_0 increases ($d=r_0/2$ corresponds to $a/b = 0.32425$)

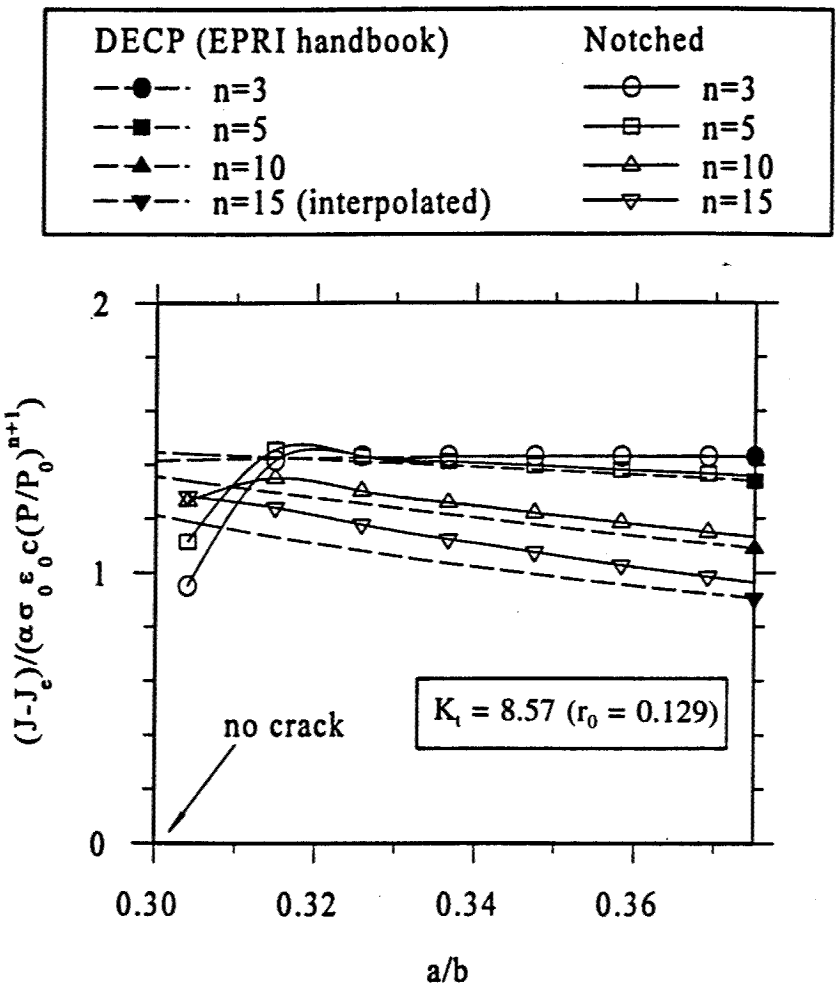

Figure 2.9. Asymptotic behavior of $h_1(a/b, n)$ for K_t = 8.57 as d/r_0 increases ($d=r_0/2$ corresponds to a/b = 0.3129)

Here again C_2 equals 2 for plane stress, and 6 for plane strain. This ensures that the correct linear elastic limit is recovered by the scheme.

The fully plastic contribution to J, J_p, is evaluated using the RSM. For the purposes of validating the approach, the optimized RSM is employed. In this method, a yield load, P_o^*, and structural parameter, $V(a/b,D/r_o)$, are derived from the finite element solutions for J_p. The values of P_o^* and $V(a/b,D/r_o)$ are chosen so as to optimize the fit of the RSM estimate of J_p to the finite element solutions for a range of n values. This approach ensures that the correct fully plastic limit is recovered by the scheme.

Note that in general, the values of P_o^* and $V(a/b,D/r_o)$ are not known a priori in the absence of appropriate finite element solutions for J_p. P_o^* is often approximated by P_o, and $V(a/b,D/r_o)$ is assumed to have the value of unity. Using the optimized approach provides an accurate representation of the fully plastic solution, enabling the accuracy of the modified RSM to be explicitly investigated in the important elastic-plastic regime which interpolates between linear elastic and fully plastic behavior.

The optimized RSM expression for J_p is therefore

$$J_p = J_e(d)\ V(a/b,D/r_o) \left[\frac{E\epsilon_{ref}^p}{\sigma_{ref}}\right] \tag{2.18}$$

where ϵ_{ref}^p is the plastic component of the reference strain which, for Ramberg-Osgood materials, is given by

$$\epsilon_{ref}^p = \alpha \left(\frac{P}{P_o^*}\right)^n \tag{2.19}$$

and

$$\sigma_{ref} = \frac{P}{P_o^*}\ \sigma_o \tag{2.20}$$

The optimized yield load, P_o^*, was also employed to compute the linear elastic term $J_e(d_o)$ in Eqn. 2.14 by first computing an optimized value of ϕ^* via Eqn. 2.16 with an appropriate substitution for P_o^*.

This estimation technique was extensively validated by comparison with available finite element results, including a total of 10 EPRI J solutions [20] and 88 J solutions generated in this program (as described earlier). Agreement was excellent in nearly all cases. Further details are available in Reference [19].

2.3 Elastic-Plastic Fatigue Crack Growth Analysis

The customary approach to analysis of crack growth under monotonic loading employs the maximum value of the stress intensity factor, K, or the J-integral. However, crack growth during multiple cycle proof testing can occur due not only to monotonic modes such as ductile tearing, but also due to cyclic modes such as fatigue crack growth (FCG).

When small-scale yielding is satisfied, the range of the stress intensity factor (ΔK) is well-established as the parameter of choice to solve practical FCG problems. In the elastic-plastic regime, however, ΔK is clearly invalid, and an alternative parameter must be employed [21]. Proposed choices in this case include relatively simple parameters such as the range of the strain intensity factor (ΔK_ε), the crack-tip opening displacement (δ_t), and the J-integral (ΔJ); and more sophisticated path-area integrals [22] such as J^* and T^*.

The selection of the optimum parameter must be guided equally by at least three considerations. The first is that the parameter must represent with sufficient accuracy the actual driving force for crack extension or the actual crack growth mechanism: the parameter must be *physically meaningful* and *theoretically valid.* The second is that the parameter must be easily and accurately calculated or estimated for a variety of actual materials, loads, and crack configurations: it must be *practical.* The third is that the parameter must have demonstrated success in the actual correlation of FCG rate data under different conditions: it must be *useful.*

At the present time and based on these criteria, ΔJ appears to be the parameter of choice for characterization of EPFCG. J is now widely recognized as an appropriate and physically meaningful parameter to characterize elastic-plastic crack growth under monotonic loading, and early objections about the use of J for cyclic loading have been answered satisfactorily [23-25]. The large number of J solutions and J-estimation schemes developed for elastic-plastic fracture problems are readily available to characterize the crack driving force in FCG quickly and accurately for many different geometries and materials. And finally, ΔJ has been used successfully by dozens of researchers and engineers during the past twenty years to correlate actual FCG data and predict actual fatigue lives.

Lamba and others [23-25] have pointed out that the correct estimate of ΔJ comprises the monotonic J expression with single values of σ and ε replaced by their ranges, $\Delta\sigma$ and $\Delta\varepsilon$ (*not* independent calculations of J_{max} and J_{min}). The cyclic analog of Eqn. 2.1, then, is

$$\Delta J = \frac{\Delta K^2}{E'}\left\{1 + \frac{F^2}{C_2}\left(\frac{n-1}{n+1}\right)\left[\frac{\left(\sigma_-^{max}/\sigma_0\right)^2}{1+\left(\sigma_-^{max}/\sigma_0\right)^2}\right]\right\} + 4\alpha\,\sigma_0 e_0 a h_1 \left(\frac{\Delta\sigma_-}{2\sigma_0}\right)^{n+1} \quad (2.21)$$

Here the plastic term includes the "doubling" of the monotonic stress-strain curve to approximate correctly the effects of reversed deformation. Further changes in the constitutive relationship due to cyclic hardening or softening are addressed through changes in the Ramberg-Osgood constants, as discussed later. Alternative formulations based on the reference stress approach can easily be written for non-Ramberg-Osgood materials.

However, many authors have concluded that the proper form of ΔJ for correlation of EPFCG data must include corrections for plasticity-induced crack closure [21]. This closure correction is particularly important because crack opening stresses under EPFCG conditions can be significantly different from typical small-scale yielding (SSY) behavior. Based on energy arguments [21], the correct form of the closure-corrected ΔJ_{eff} expression appears to be given approximately by

$$\Delta J_{eff} = \frac{(U\Delta K)^2}{E'}\left\{1 + \frac{F^2}{C_2}\left(\frac{n-1}{n+1}\right)\left[\frac{\left(\sigma_-^{max}/\sigma_0\right)^2}{1+\left(\sigma_-^{max}/\sigma_0\right)^2}\right]\right\} + 4\alpha\,\sigma_0 e_0 a h_1 U \left(\frac{\Delta\sigma_-}{2\sigma_0}\right)^{n+1} \quad (2.22)$$

where U is the effective stress range ratio,

$$U = \frac{\sigma_{max} - \sigma_{open}}{\sigma_{max} - \sigma_{min}} \quad (2.23)$$

Here σ_{open} is the nominal stress at which the crack first becomes fully open during the load-increasing half of the cycle. Note that in the derivation of Eqn. 2.22, U was applied to the stress range and the elastic strain range, but not to the plastic strain range. Kubo et al. [26] have shown from their finite element analyses of growing cracks under cyclic loading that ΔJ_{eff} approximately satisfies path-independence.

The effective stress range ratio U was estimated as a function of σ_{max}/σ_0 and the stress ratio $R = \sigma_{min}/\sigma_{max}$ from finite element analyses of crack closure in a low hardening material under intermediate and large scale yielding conditions [27]. Alternatively, U can be estimated from a set of simple equations developed by Newman [28] based on his modified-Dugdale closure model. Although the Newman equations were originally developed for SSY conditions, their extension into the EPFCG regime with a suitable choice of σ_0 has been demonstrated [21].

Adequate predictions of crack growth rates due to FCG mechanisms follow from an accurate characterization of ΔJ_{eff} and a simple Paris equation crack growth relationship

$$\frac{da}{dN} = C\left(\Delta J_{eff}\right)^m \tag{2.24}$$

Exceptions to this philosophy are those applications in which alternative crack growth mechanisms come into play, such as ductile tearing or creep-fatigue.

A more comprehensive engineering methodology for elastic-plastic fatigue crack growth is under development in another contract effort [18, 29-30].

2.4 Tear-Fatigue Theory

The fundamental problem in developing an analytical model of multiple-cycle proof testing is understanding and quantitatively describing crack growth during large load-unload-reload cycles, when deformation is elastic-plastic and both fatigue and ductile tearing crack extension mechanisms may be active. As noted in the Interim Report from Phase I [6], a variety of analytical theories and experimental data have been published to support different fracture mechanics approaches to related load-unload-reload problems. These different approaches are not always consistent, and some experimental data appear to conflict with some theories.

A simple analytical model was proposed in the Phase I Report as an aid to further analytical and experimental investigations in the context of the MCPT contract. This model was based on the *J*-resistance curve and so directly addressed only ductile tearing contributions to crack extension. The effects of multiple cycles were included by updating the origin (initial crack length) of the resistance curve to the final crack length from the previous cycle. This was recognized as a bounding criterion; the other bound was to do no updating and hence to predict no growth on any subsequent cycle to the same maximum load.

Around the same time that the SwRI/Rocketdyne team was beginning the Phase I effort, technical staff at the former Central Electricity Generating Board (CEGB) in the UK were engaged in detailed studies of related load-unload-reload crack growth phenomena which were motivated by their power plant applications. They developed an analytical theory and a corresponding computational framework to describe these phenomena, which they described as "tear-fatigue" [31, 32], and conducted detailed experimental validations. One of the principal investigators in these studies, Dr. Graham Chell, subsequently joined the SwRI technical staff. Upon critical review, the tear-fatigue concepts were found to be generally consistent with the Phase I and early Phase II experimental results and with the evolving analytical approach in Phase II. Furthermore, the tear-fatigue approach appears to provide a suitable quantitative framework within which to describe MCPT effects in aerospace propulsion systems.

The tear-fatigue model describes crack growth as the linear summation of growth due to fatigue and ductile fracture,

$$da/dN = (da/dN)_f + (da/dN)_t \tag{2.25}$$

where $(da/dN)_f$ is the crack growth rate given by a relationship describing the fatigue contribution to crack extension, such as the Paris Law, and $(da/dN)_t$ is the crack growth in each load cycle due to ductile tearing, as expressed by a J-resistance curve construction. In this model, it is assumed that fatigue and ductile fracture mechanisms do not interact. For ductile tearing to occur during cyclic loading, it is necessary for the value of the J integral calculated at maximum load, J_{max}, to increase with each cycle.

Equation 2.25 can be further expanded to give the crack growth rate equation

$$da/dN = (da/dN)_f + \left[\left(dJ_{max}/dN\right)/\left(dJ_{mat}/d\Delta a_t\right)\right] \tag{2.26}$$

Here J_{mat} is the crack growth resistance value of J characterizing ductile tearing as measured under monotonic loading, and Δa_t is the total crack extension due to ductile tearing. The term (dJ_{max}/dN) describes the increase in J_{max} in each cycle due to an increase in crack length caused by the fatigue and tearing mechanisms. These equations were originally assumed to apply only for $J_{max} > J_i$, where J_i is some suitable measure of J for the initiation of tearing. As will be shown later, the customary value of J_{Ic} may be a poor choice for J_i under some conditions.

This model is interpreted geometrically in Fig. 2.10. Here the ductile crack growth relationship is expressed in terms of the interaction between the J-applied and J-resistance curves in J vs. total a space. The J-resistance curve originates from the true initial crack length for a "virgin" precracked specimen. As noted above, on subsequent cycles the effective origin of the tearing resistance curve is advanced by an increment equal to the fatigue crack growth contribution, $(da/dN)_f$. The two individual components of crack growth are shown more clearly in the idealized inset diagram. Note in this construction that dJ_{max}/dN includes the slight increase in J_{max} due to the additional tearing $d\Delta a_t$.

Several minor extensions of this model appear to be required to address the full range of possible MCPT problems. First of all, although the original tear-fatigue model was expressed in terms of ΔJ, subsequent work concentrated on assumed FCG calculations based on the linear elastic stress intensity factor, ΔK. For generality, the model was modified to express the crack driving force in terms of the appropriate elastic-plastic parameter, ΔJ_{eff} [21], including crack closure effects. For many load-unload-reload proof test applications with a minimum applied stress of zero, the fully plastic component of ΔJ_{eff} will be essentially zero (since the effective cyclic yield strength for reversed loading is twice the normal monotonic value), even if the maximum load or stress exceeds the yield condition. However, the intermediate-scale plasticity term in ΔJ_{eff} (the effective crack length term, which is a first-order plasticity correction) may not

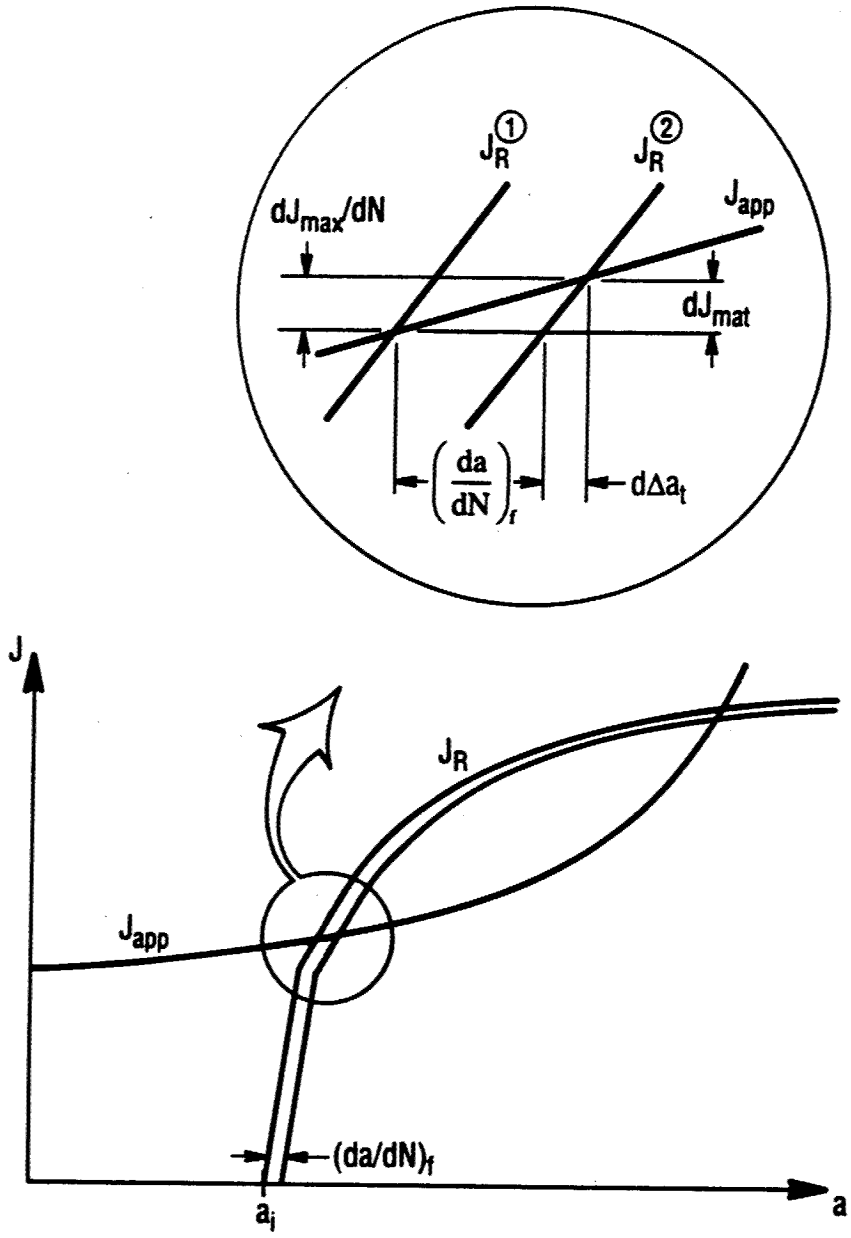

Figure 2.10. Schematic representation of tear-fatigue theory

be negligible. And if constraint conditions impose locally compressive loading (i.e., a negative stress ratio), the fully plastic ΔJ_{eff} term may make some meaningful contributions. Furthermore, the general J (rather than K) framework for the fatigue calculation facilitates other modifications which involve the relationship between the fatigue and tearing resistance curves.

Two minor modifications to the model appear useful to preserve consistency between the treatment of tearing and fatigue under conditions when fatigue precedes tearing, the two contributions are of comparable magnitude, and the crack advance per cycle is comparatively large in comparison to the section thickness or remaining ligament. The first modification addresses the first occurrence of ductile tearing following previous fatigue cycling. Traditional applications of tear-fatigue theory assumes that no tearing occurs until J_{max} exceeds some value J_i, which is commonly taken as J_{Ic} or some similar standard measure of initiation toughness. However, since these typical values of J_i are associated with some finite value of Δa_i on the J-resistance curve, the first exceedance of J_i will cause a sudden jump in the crack length by Δa_i. When Δa_i is a small number in comparison to the local geometry (crack size, section depth, remaining ligament, etc.) this artificial jump is of no consequence, but when the local geometric scale is small (and hence Δa_i is relatively large), the jump can be problematic.

This artificial jump can be avoided in one of two ways. The computationally simplest way is to employ the entire J-resistance curve as a description of ductile crack advance (ignoring, for the moment, the differentiation between crack tip blunting and ductile tearing) and to set J_i (and therefore Δa_i) as an artificially very small number. The problem can also be addressed from the standpoint of fatigue crack growth analysis by updating on each cycle the contribution to fatigue crack advance due to the largest elastic-plastic cycle (from the original $J = 0$ to the current $J = J_{max}$) as J_{max} increases cycle-by-cycle. This approach effectively performs updated rainflow cycle counting on the entire cyclic J history. This approach also requires translating the J-resistance curve in accordance with the crack advance due to fatigue crack growth. These two approaches (employing the entire J resistance curve with an artificially low J_i value, or employing a more complex FCG analysis with a more realistic J_i value) give essentially the same result when the FCG curve and blunting line portion of the J-R curve are approximately coincidental (see Section 3.2).

One potentially significant difference between the analysis of fatigue crack growth resistance and tearing resistance in this regime still remains. The classical engineering approach to tearing resistance curve analysis compares the applied and resistance J curves at the updated or final crack length $(a + \Delta a)$, as shown in Fig. 2.10. In other words, $J_{max} = J_{max}(a + \Delta a)$, and the final calculated Δa value is also a function of the change in the resistance curve between $J_{max}(a)$ and $J_{max}(a + \Delta a)$. In contrast, the traditional approach to FCG analysis calculates the cyclic crack growth increment on the basis of the current crack length and does not consider the influence of this growth increment on the subsequent change in resistance to fatigue crack growth: $J_{max} = J_{max}(a)$. Again, this difference is insignificant when the incremental Δa is very small in comparison to the total a, or when the change in J_{max} with Δa is negligible, and so no adjustment is needed for the great majority of FCG analyses. However, when Δa is relatively large and the applied J_{max} begins to increase significantly with further Δa (as may often occur

near instability, especially in thin-walled small components), another small modification may be appropriate. A simple first-order correction to the crack length appears adequate. This first-order correction involves first simply predicting an initial guess for $\Delta a^{(1)}$ on the basis of the crack length at the beginning of the cycle: $J_{max}^{(1)} = J_{max}(a^{(n)})$. Then an updated value of J_{max} based on the new crack length $(a^{(n)} + \Delta a^{(1)})$ is computed, and this new value of $J_{max}^{(2)}$ is used to make an updated prediction for $\Delta a^{(2)}$. The final predicted value of the crack length is then $a^{(n+1)} = a^{(n)} + \Delta a^{(2)}$. The additional accuracy introduced by further iteration is insufficient to warrant the effort.

3. EXPERIMENTAL CHARACTERIZATION AND VALIDATION

In Phase I, experimental characterization work included the generation of a *J*-resistance curve for surface-flawed IN-718 (employing the Phase I reference stress estimates for *J*), generation of baseline fatigue crack growth properties under small-scale yielding conditions, and SSY FCG crack shape studies based on range marking and post-test fractography.

Significant new experimental characterization and validation activities were conducted in Phase II. An updated form of the *J*-resistance curve was developed, based on the Phase I test results, a few additional surface crack *J*-R experiments, and the improved reference stress *J* estimation methods. The relationship between the *J*-resistance curve and the fatigue crack growth curve was explored. A number of additional crack growth tests were conducted to guide and verify methodology development, with a primary focus on the effects of various cyclic histories (different control conditions and load ratios) and crack depths. Specialized tests examined simulated MCPT load histories as well as fatigue cycling following a proof overload. Fractographic studies were conducted to evaluate crack growth micromechanisms and crack shape development during elastic-plastic loading. The suitability of acoustic emission to detect crack growth during MCPT was briefly evaluated. All of these experimental activities and associated results are documented in some detail in the remainder of the chapter. Further information about specimen geometry and material properties was provided in the Phase I report [6].

3.1 Updated J-Resistance Curves

Updated Analysis Methods. As noted in the Introduction, a *J*-resistance curve had been generated earlier in the program for semi-circular surface cracks in finite-sized plates of Inconel 718. This Phase I *J*-R curve was based on the Phase I reference stress *J* estimation techniques and the surface-crack experiments also conducted during Phase I of the program. As noted in the Analytical Development section, improved reference stress estimates of *J* for the semi-elliptical surface crack in a finite-sized flat plate were developed in Phase II of the program. Using these new reference stress *J* estimates, all of the original crack growth experiments that had been used to construct the Phase I surface crack resistance curve were re-analyzed to generate a Phase II resistance curve. The Ramberg-Osgood constants (Eqn. 2.3) used in these *J* calculations were $\varepsilon_0 = 0.006$, $\sigma_0 = 179.8$ ksi, $n = 15.8$, and $\alpha = 1$.

New Surface Crack Experiments. The surface crack experiments conducted in Phase I were limited to initial crack depths in the general range of $a/t = 0.36$ to 0.73, with most crack depths about $a/t = 0.6$. A critical question posed early in the Phase II investigations was whether significantly deeper cracks might exhibit different tearing behavior, and if so, whether this might be an important factor in MCPT failures. In order to investigate these questions, two additional surface crack tearing resistance experiments were conducted in Phase II. These tests involved the application of single displacement-controlled cycles to specimens with surface flaw depths in the range from $a/t = 0.8$ to 0.9. The tearing resistance data obtained from these deep crack tests were found to be similar to the previous data from less deep cracks.

The updated tearing resistance data for surface-cracked IN-718, including both of the new experiments, and the new analysis of both old and new experiments, are shown in Fig. 3.1. Also shown on this figure are the original resistance curve data from compact tension specimens.

Effect of Specimen Thickness on Tearing Resistance. The Phase I analysis of the surface crack resistance curve had suggested that crack growth resistance in the thicker (t = 0.5) surface crack specimen was similar to crack growth resistance in the thinner (t = 0.2 in.) surface crack specimen. The Phase II analysis of the surface crack resistance curves indicated that the new J formulas gave generally similar results to the old J formulas for the thinner specimens, so that the J-R curve did not change significantly. However, the new calculated J values for the thicker specimens were slightly lower than the values calculated in Phase II, so that the 0.2 in. and 0.5 in. data no longer appear to belong to the same population. Although firm conclusions should not be derived from only four data points, it appears that the crack growth resistance for the thick surface crack specimens is lower than for the thin surface crack specimens, but still higher than for the CT configuration.

The decrease in apparent crack growth resistance for the thicker specimens is qualitatively consistent with an expected increase in constraint due to the thicker geometry. The thick surface crack geometry can be thought of as an intermediate case between the thick CT specimens and the thin surface crack specimens. Note that constraint is affected by a variety of factors, including specimen thickness, specimen configuration, and applied stress as a fraction of the yield stress. Constraint generally increases with increasing thickness, tendencies towards bending rather than tensile configurations, and decreasing applied stress. The thick surface crack specimens compared to the thinner specimens also experienced slightly lower maximum applied stresses (σ_{max} = 120-150 ksi for thick specimens, 150-180 ksi for thin specimens, compare σ_{ys} = 165 ksi).

Current thinking in the international fracture mechanics community is that these apparent changes in crack growth resistance may in fact be only apparent effects and not real effects. The argument is that a single parameter (J) description is insufficient to describe the changes in the driving force for crack extension that are caused by changes in constraint. In other words, constraint actually influences the applied driving force, not the resistance. The approach currently receiving the most attention as a means of correcting this claimed deficiency is a two-parameter characterization of the driving force based on J and a factor Q, which is derived from the higher order terms in the crack-tip stress field expression and which essentially describes the hydrostatic stress components via comparison with the benchmark Hutchinson-Rice-Rosengren (HRR) stress fields. Unfortunately, practical applications of J-Q theory are still largely in their infancy at this writing. Most investigations to date have focused on two-dimensional geometries rather than surface cracks, and elastic-plastic crack extension involving cleavage rather than stable ductile tearing. Therefore, at the present time, these constraint effects must be characterized in terms of apparent changes in the resistance curve.

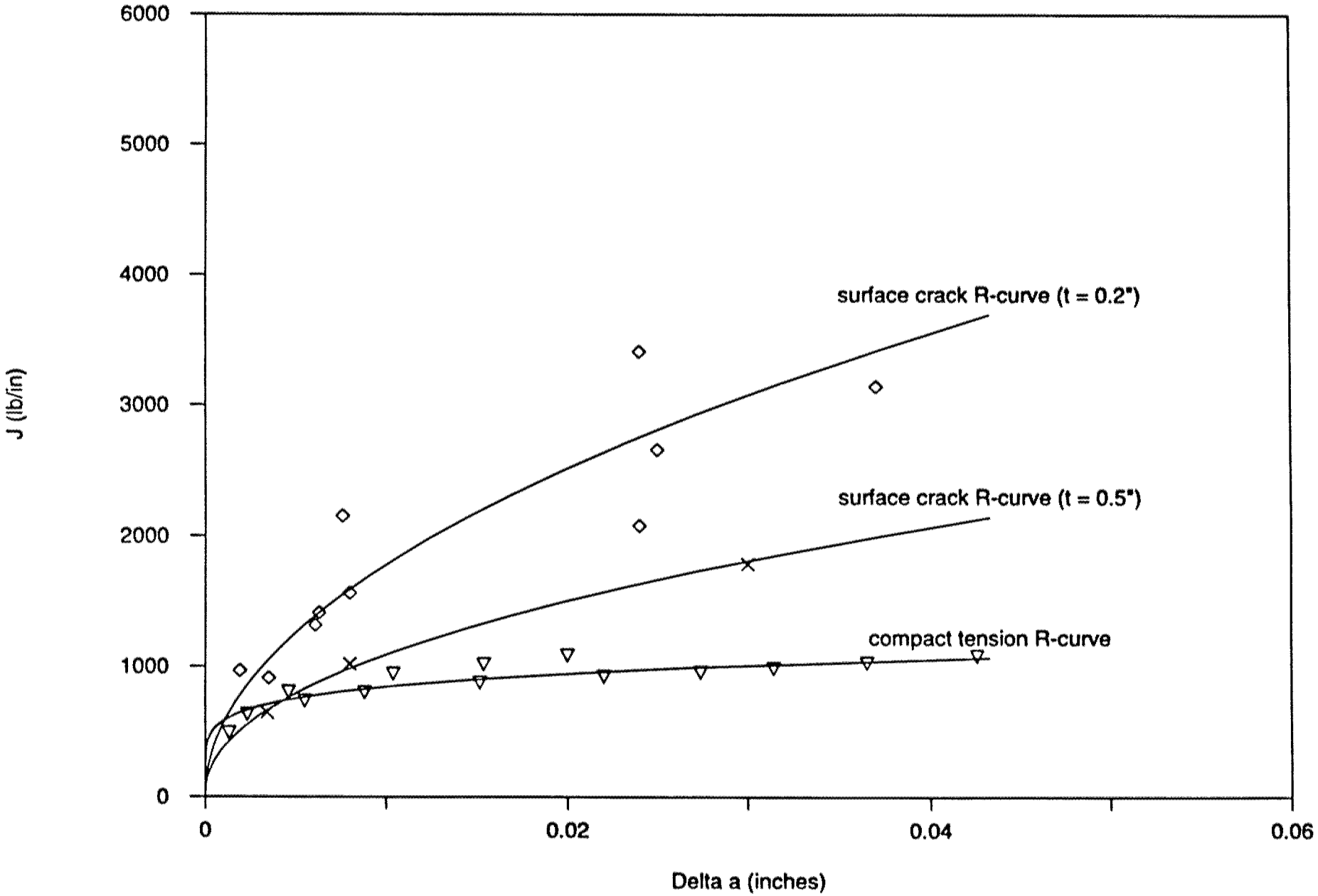

Figure 3.1. Crack growth resistance curves for Inconel 718

3.2 Relationship Between J-Resistance Curves and Fatigue Crack Growth

As noted previously in the Analytical Development section, crack growth behavior during multiple cycle proof testing can conceivably occur by several different mechanisms, including (1) rupture mechanisms such as ductile tearing; (2) true fatigue mechanisms, such as those associated with striation formation; and (3) interactions between rupture and fatigue.

As a first step in studying the relationship between crack growth during fatigue (*da/dN*) and ductile tearing (R-curve) experiments, data from the Phase I fatigue crack growth tests on Inconel 718 were compared with the *J*-resistance data summarized in the previous section. The FCG data, which belong to the small scale yielding regime and hence were originally correlated with ΔK, were re-expressed in terms of the more general elastic-plastic parameter ΔJ according to the usual relationship $J = K^2/E$. An estimate of the crack closure level was made by noting that the original FCG tests satisfied plane strain conditions, for which $\sigma_{open}/\sigma_{max} = 0.2$ has been shown to be a reasonable approximation at $R = 0$ [33]. The FCG data were then expressed as *da/dN* vs. ΔJ_{eff} values, and the central tendency line (in log-log space) was identified via least-squares regression.

Data from the *J*-resistance curves were superimposed on the FCG plot by recognizing that for one "cycle" of monotonic loading with no previous history, $J_{max} = \Delta J_{eff}$ and $\Delta a = da/dN$. Both types of R-curve data were included in this exercise: CT specimens with through-cracks and plate specimens with surface cracks. For simplicity, only the surface crack data from the thinner specimens are included in these comparisons.

The FCG and R-curve data are shown together in Fig. 3.2 on the traditional log-log FCG graph. Note that the R-curve data are entirely consistent with the latter stages of FCG. The form of these data is similar to the usual upturn in *da/dN*-ΔK data near instability (e.g., near K_{Ic} or plastic collapse). This upturn occurs at a lower value for the CT specimen, where constraint is higher. The upturn occurs at a considerably higher value for the surface cracked plates, where deep flaws and high stresses cause a reduction in constraint, and many of the R-curve data points are shown to lie within the FCG data scatter band. The FCG band must be extrapolated beyond the region of the FCG data to pass through the region of the R-curve data, of course, but previous experience with ΔJ indicates that this should be a reliable extrapolation. Dowling, for example, found that the linear Paris law form of the ΔJ - *da/dN* relationship was consistent over five orders of magnitude in crack growth rates [34].

The relationship between FCG and R-curve data is shown from a different perspective in Fig. 3.3, which superimposes the FCG scatter band on the traditional *J*-resistance curve data. Note that the FCG curve corresponds almost exactly to the "blunting line" portion of the R-curve, but that as additional ductile tearing begins to occur at higher *J* values, the R-curve line begins to deviate from the baseline FCG curve.

This apparent coincidence of the R-curve blunting line and the high growth rate portion of the FCG curve is not necessarily surprising in view of the crack growth mechanisms involved.

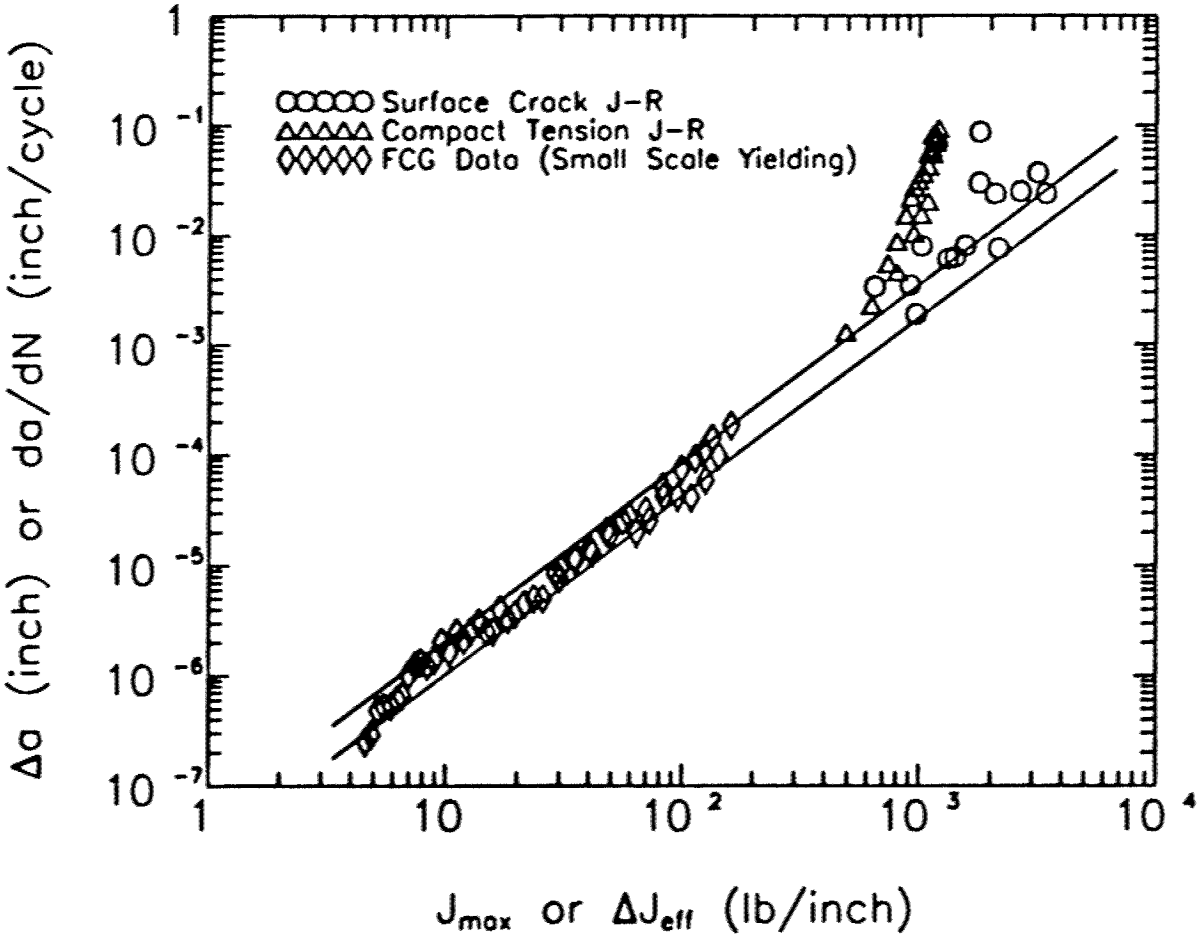

Figure 3.2. Fatigue crack growth data for Inconel 718 with superimposed resistance curve data

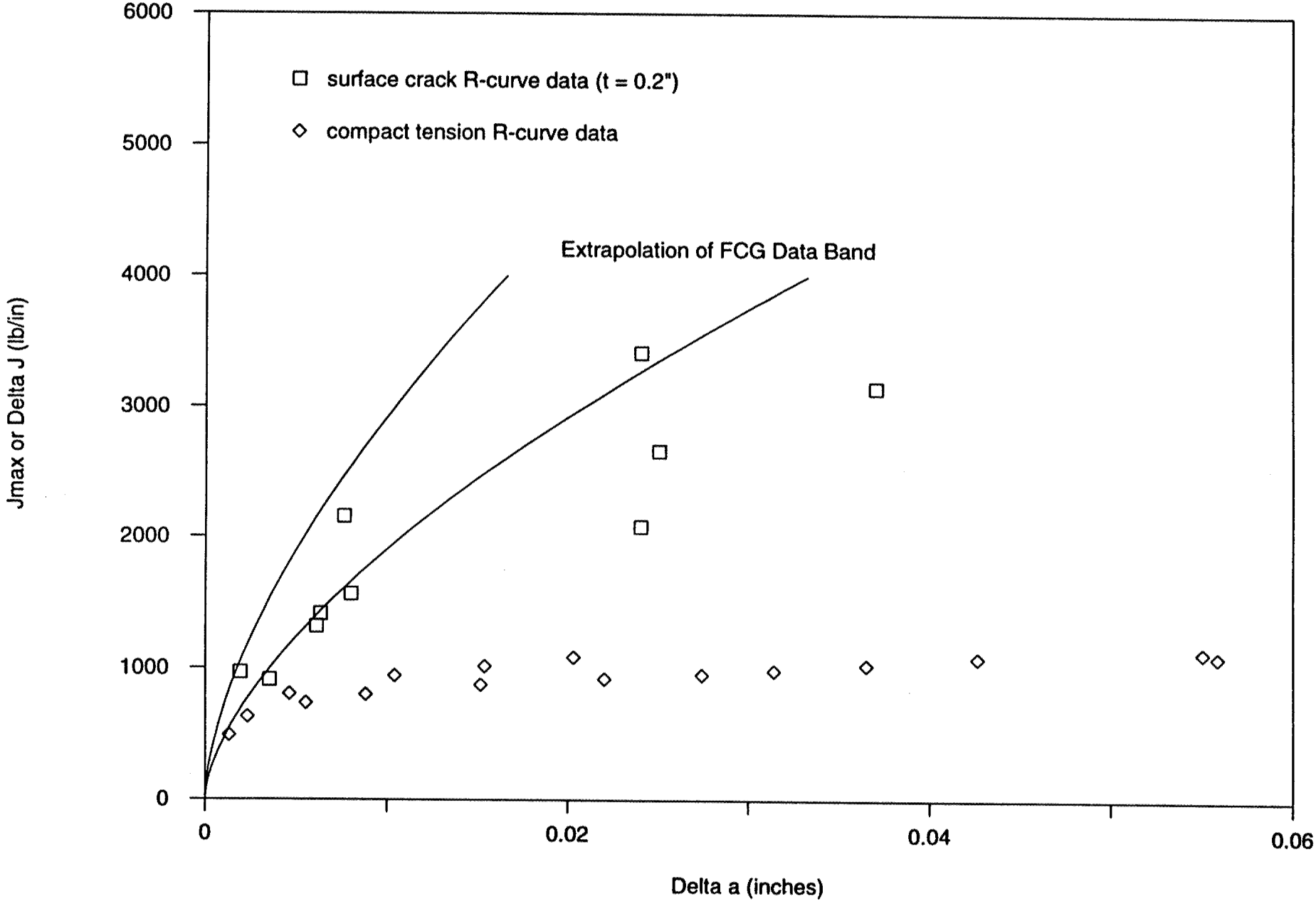

Figure 3.3. Resistance curves for Inconel 718 with superimposed FCG curve

The so-called "blunting" line of the R-curve, as its name implies, is thought to describe the crack extension during initial loading that occurs due to crack tip blunting alone, before the initiation of ductile tearing (or brittle cleavage) [35]. On the other hand, the mechanism of Stage II crack growth during low cycle fatigue is widely believed to be a progressive plastic blunting process [36]. The broadening of slip zones at the crack tip and the associated blunting of the crack tip during the tensile loading excursion in low cycle fatigue define the extent of crack advance during that particular cycle, before the application of reversed loading (locally compressive) causes a reversal of slip directions and a crushing/folding of the new crack surfaces. The point to be made is that the basic mechanism of crack extension is apparently the same in both the "low cycle fatigue crack growth" process and the blunting portion of the "ductile fracture" process. The material at the crack tip is largely unaware of whether initial blunting will be followed by further loading to tearing or by unloading. The primary difference in the two processes is the more complex residual stress/deformation field that develops in the vicinity of the fatigue crack tip due to previous load/unload and crack growth histories. Consideration of crack closure effects, as we have done above, represents a first-order compensation for this difference.

Wilhem and Ratwani [37] previously suggested a similar relationship between fatigue and fracture data as described by the linear elastic stress intensity factor (ΔK and K_R), based on their empirical observations of crack growth in 2024-T3 aluminum. They proposed a "full range resistance curve" that was a continuous, monotonically increasing function of crack extension and that was composed of both fatigue (da vs. K_{max}) and fracture (Δa vs. K_R) data. Their primary goal was apparently to reconcile thickness effects in fatigue crack growth rate data by relating them to thickness effects on the R-curve. Wilhem and Ratwani went on to suggest that there may not be a smooth transition between fatigue resistance and fracture resistance portions of the curve, based on their supposition that the crack tip plastic zone in fatigue was different in size from that developed during static (monotonic) loading. Actually, however, the size of the "forward" plastic zone has been shown to be essentially the same under monotonic and cyclic loading [38]. Any apparent discontinuities between fatigue and fracture data may instead be due to uncompensated differences in crack closure behavior.

This line of thinking is consistent with the ideas of Kobayashi *et al.* [39], who suggested that the Paris Law (striation mechanism) portion of the fatigue crack growth curve was parallel to the blunting line. The difference between the two lines was attributed to plasticity-induced crack closure. The specific data generated by Kobayashi *et al.* to evaluate these ideas are somewhat difficult to interpret, however, due in part to the wide range of stress ratios ($R = -1.5$ to $+0.5$) and applied loads (elastic to elastic-plastic) considered. Crack closure levels (which were not measured) are certain to change considerably with both stress ratio and applied load, and the CT geometry employed was not an ideal choice for load histories with large compressive excursions. The present investigations were simplified by considering only a single stress ratio for all tests ($R = 0$).

The available data are too limited to draw definitive conclusions about the relationship between the FCG curve and the tearing resistance curve. In the current research program, we

have studied only a single material, and only about twenty surface crack tests have been performed, all with the same crack shape and specimen width. The fatigue crack growth curve is extrapolated from lower values of the cyclic driving force and therefore somewhat uncertain, and we have not explicitly addressed the normal ±2× scatter in fatigue crack growth rates (the curve shown represents the mean value). It does appear possible that the fatigue curve serves as an approximate upper bound to the tearing resistance curve, and the two may be effectively equivalent for lower constraint and smaller crack growth increments. For higher constraint and larger crack growth increments, it seems clear that the onset of stable tearing will cause a divergence of the two curves.

3.3 Characterizing the Onset of Stable Tearing

Also shown in Fig. 3.1 is a power law representation of the surface crack tearing resistance curve for 0.2-in. thick specimens with the general form (units are inches and lb/in)

$$da = 3.16(10)^{-9}\left(J_{max}\right)^2 \tag{3.1}$$

As noted in the Phase I Report, there is no single theoretically correct mathematical form of the resistance curve. Several different empirical forms have been proposed [40]. The power law form was chosen here because it seemed to correspond well to the individual data points, and because it was consistent with the general power law form of the fatigue crack growth curve. The general form of the FCG curve, for comparison, was

$$\frac{da}{dN} = 3.50(10)^{-8}\left(\Delta J_{eff}\right)^{1.62} \tag{3.2}$$

An appropriate value for J_i, the critical value at which ductile tearing initiates, can be chosen as the intersection of the fatigue crack growth curve and the tearing resistance curve, which is essentially the point at which the two curves diverge for increasing crack extension. For the t = 0.2-in. surface crack data shown, this value was J_i = 557 in.-lbs/in.^{2}.

Note that conventional definitions for J_i, such as the J_{Ic} value based on the ASTM Standard Test Method E 1737, are not appropriate for this application. The current E 1737 methodology defines J_{Ic} as the intersection of a constructed offset line parallel to a hypothetical blunting line of slope $2\sigma_{flow}$, where the offset is 0.2 mm (0.008 in.). This definition would lead to a J_{Ic} value greater than 2000. in.-lbs/in.^{2} for the given surface crack data, which would cause serious errors in calculation of crack growth for some intermediate J_{max} values by the customary tear-fatigue approach. Note that the Δa value corresponding to this J_{Ic} value is on the order of 0.01, which is a significant fraction of the crack depth for some MCPT applications. Of course, the strict ASTM validity restrictions on J_{Ic} would also rule out its use for this surface crack configuration, since the plane strain constraint limitations are not satisfied for the low constraint, high stress surface crack tests.

It is also interesting that the point at which the power law representation of the CT resistance curve intersects the fatigue crack growth curve is about 586. in.-lbs/in.^{2}, which is close to the intersection point of the fatigue curve with the surface crack resistance curve. Despite extensive research in the area by many fracture mechanics experts around the world during the past few years, the effects of constraint on apparent ductile tearing resistance are still not understood well. It is not clear if we should expect a higher J_i value for lower constraint, a higher tearing modulus value (the slope of the tearing resistance curve above J_i), or both.

3.4 Elastic-Plastic Fatigue Crack Growth Experiments

Further experiments were conducted to investigate fatigue crack growth under elastic-plastic loading conditions. The cyclic histories were varied to explore the effects of different loading regimes and different control conditions.

Specimens were 0.2-in thick with semi-circular surface cracks. Initial flaws were introduced by electro-discharge machining (EDM) followed by fatigue pre-cracking at relatively low applied stresses. The specimens were heat tinted following the precrack and then again (under less severe conditions, resulting in a lighter tint) following the completion of the test in order to aid identification of the fracture surfaces. Most tests were conducted at fixed rates of crack mouth displacement in order to provide greater experimental control, but some tests were conducted in load control, and some tests employed a manual form of displacement control in which decisions about displacement reversals were actually based on observations of applied load.

Careful monitoring of the load and crack mouth opening displacement (CMOD) information (including on-line computer data acquisition) made it possible to accurately estimate the changing crack depth by noting the change in elastic specimen compliance and comparing these values with analytical estimates. Inspection of final crack surfaces showed that the crack shape remained relatively constant during this large growth, although crack growth immediately at the specimen surface is typically retarded and some slight "canoeing" is observed. A photograph of a typical fracture surface is shown in Section 3.7.2 on fractography of crack shapes.

In the first series of elastic-plastic fatigue crack growth tests, initial crack depths were approximately a/t = 0.6 (a = 0.12-in.). Final crack depths were typically around a/t = 0.75 - 0.85, or about 0.04-in. of crack growth in the depth direction.

The extent of unloading was observed to have a large effect on crack growth during subsequent loading cycles. Tests in which extensive crack growth on the first cycle was followed by unload-reload cycles between zero load and the previous maximum load or displacement (so-called zero-max loading) resulted in essentially no crack growth during a small number of subsequent cycles. Other tests in which crack growth on the first cycle was followed by unloading to zero crack mouth displacement (which corresponds to a large compressive stress) and repeated reloadings between zero displacement and the previous maximum displacement (so-called zero-max displacement) resulted in substantial crack growth on essentially all subsequent cycles. Load vs. crack mouth opening displacement histories for these two types of tests are

shown in Fig. 3.4. The observed crack growth is obviously consistent with the amount of energy (area inside the hysteresis loops) associated with each cycle type.

Additional fatigue crack growth tests were conducted on specimens with deeper initial surface cracks (a/t = 0.75 to 0.82). These tests were conducted in load control at a stress ratio of R = 0 (minimum stress is zero) with slightly smaller maximum stresses (σ_{max} = 135 to 145 ksi) than the previous tests (in which σ_{max} typically exceeded the nominal yield stress of 160 ksi at some point during the test). The smaller maximum stresses were chosen to minimize the loss of constraint caused by general yielding of the specimen. Cycling was continued in these tests until failure (specimen separation) occurred or was imminent, which typically required about 380 cycles.

All of these tests were analyzed with the elastic-plastic fatigue crack growth methodology described in Section 2 on Analytical Development. Delta J effective was estimated with a revised version of the modified reference stress approach that accounted for crack closure. The crack depth, a, for each cycle of interest was estimated from compliance (load vs. elastic crack mouth displacement) information.

The resulting crack growth data from the elastic-plastic fatigue crack growth tests are shown in Fig. 3.5. The scatterband on this figure is based on previous SSY FCG data, and it shows that this approach to describing elastic-plastic fatigue crack growth using ΔJ_{eff} is generally consistent with the existing FCG data base. The scatter in crack growth rate appears to be larger, but there are several logical explanations for this apparent scatter. First of all, since the crack depths are calculated indirectly from approximate compliance relationships, they are subject to more uncertainty, and this will affect the values of both da/dN and J. Of greater significance, the analysis assumed as constant several quantities, such as crack closure and the stress-strain relationship, that were actually changing during portions of these tests.

Consider, for example, the V-shaped set of data in the middle of Figure 3.5 taken from a zero-max displacement test. The first loading cycle is represented by the upper right data point, and the data continue chronologically in a clockwise direction. Crack closure levels may require several cycles to reach stable levels at the beginning of the test. Before stability is reached, the opening stresses will be somewhat lower (and gradually increasing). This means that the actual ΔJ_{eff} values for the first few data points may be slightly larger than indicated, which would move these points to the right, over towards the middle of the scatterband. During the last half of this test, when the data as plotted show a clear increase in da/dN with little apparent change in ΔJ_{eff}, it is likely that the cyclic stress-strain relationship is changing. Inconel 718 in the STA-1 condition is known to cyclically soften, the flow stress decreasing from 180 ksi down to around 160 ksi and the strain hardening exponent decreasing from 15.8 down to around 6.2. Significant cyclic softening is likely in this particular test, in view of the large number of elastic-plastic cycles, and this would cause a significant (and gradual) increase in ΔJ_{eff} by up to a factor of 2x. While it is not possible to predict these transient changes exactly, it is clear that our straightforward approach may be underestimating ΔJ_{eff} towards the end of the test, and that the actual data points may again move to the right, over towards the middle of the scatterband.

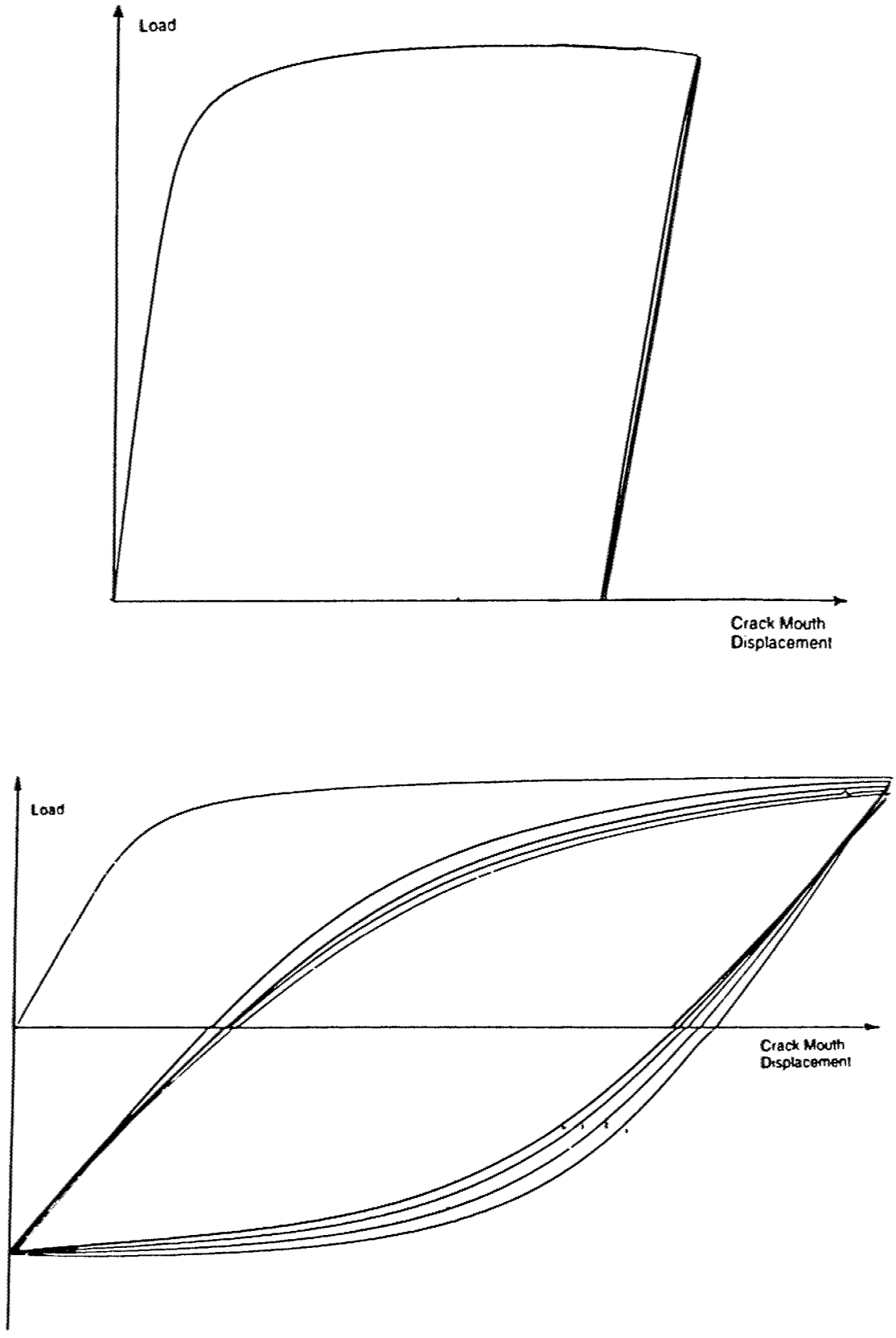

Figure 3.4. Typical load-displacement records from zero-max loading (top) and zero-max displacement (bottom) tests

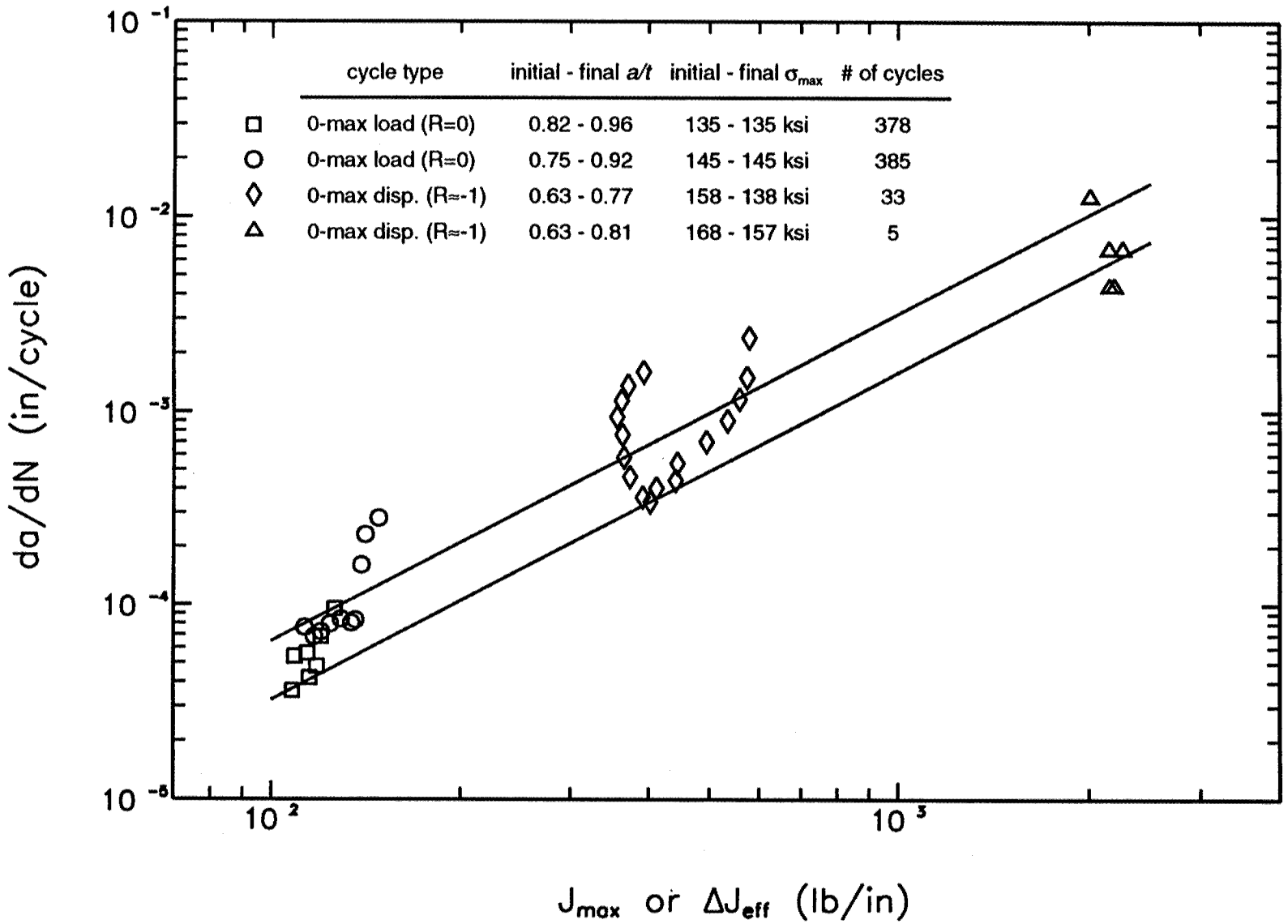

Figure 3.5. Elastic-plastic fatigue crack growth data superimposed on scatterbands from SSY FCG data

Other reasons for apparent scatter are also worthy of note. The first (top) point in the two zero-max displacement tests corresponds to the first loading cycle, where J_{max} has been computed in the usual resistance curve manner. It is likely that this first cycle included some significant ductile tearing, and so it is reasonable that the resulting crack growth would be slightly greater than predicted by a purely FCG approach. The last (top) three data points in the 145 ksi zero-max loading experiment, which all lie above the scatterband, correspond to the last three cycles before separation of the specimen into two halves. Here, again, there are likely other crack growth mechanisms coming into play as instability is approached (including possible ductile tearing) that would be expected to increase the crack growth rate at the same nominal crack driving force. The 135 ksi zero-max load test and both zero-max displacement tests were suspended before final fracture occurred.

The ΔJ_{eff} estimates based on Eqn. (2.21) comprise distinct elastic and plastic components, plus an effective crack length (ΔJ_z) correction to the elastic term. It is interesting to note how the crack growth experiments represented in Figure 3.5 span the full range of elastic to plastic conditions. The plastic component of ΔJ_{eff} for the two zero-max displacement tests is much larger than the elastic components (as reflected by the significant hysteresis in the load-CMOD traces). But the plastic component of J_{eff} for the two zero-max load tests is essentially zero. In other words, these cycles are nearly totally elastic, despite following on the heels of a very plastic initial cycle and despite the maximum nominal (gross) stress in the cycle being greater than the yield stress. This maximum stress does influence the calculated driving force in two ways, by changing closure behavior and by increasing the small contribution of the effective crack length correction. Furthermore, there is a gradual ratchetting process taking place during the fatigue cycling by which the irreversible crack opening displacement (the CMOD at zero load) is slowly increasing over the course of many cycles, and this may have implications for predicting final fracture in such a test. In spite of these complications, crack growth was successfully correlated in these tests using essentially a closure-corrected ΔK-based approach.

The Phase I analysis focused on the potential use of J-resistance curve approaches to describing crack growth on all cycles, and it is useful to reflect briefly on how those approaches handle this multiple cycle crack growth data. The central idea of that preliminary R-curve model was that each cycle could be treated as an independent R-curve test on a virgin specimen, neglecting previous load histories but taking the initial crack size for the next cycle as the final crack size from the previous cycle. This approach clearly fails to predict the observed crack growth (or lack thereof) in the zero-max load tests. The predictions of that model for zero-max load-control tests were for crack growth to be greater on the second proof cycle than on the first, and subsequently to increase further on each cycle. The new approach based on elastic-plastic fatigue crack growth is successful in describing the observed crack growth (Figure 3.5).

On the other hand, that same preliminary R-curve model appears to work quite well for the zero-max displacement tests. In these tests, the complete reversal of the local displacement fields (the nature of the global displacement fields is unknown) apparently causes a complete "resetting" of the crack tip. The original R-curve model predicted that in a displacement-controlled configuration, the stresses would slowly decrease on each cycle and the crack growth

rates would also decrease on each cycle. Both phenomena were observed to occur (except for the increase in *da/dN* during the last half of one test, which has been discussed previously). Estimates of J_{max} for these tests based on conventional R-curve approaches give values that are similar to the calculated ΔJ_{eff} values, and so would give similar predictions for crack growth on each cycle.

3.5 Experimental Simulation of Multiple Cycle Proof Testing

Three surface crack experiments were performed to investigate crack growth under simulated MCPT histories. These experiments also provided data to evaluate the tear-fatigue relationships presented earlier in the Analytical Development section.

The initial crack depth on the first two specimens was slightly larger than previously tested, between a/t = 0.8 and 0.9, with an aspect ratio around a/c = 0.9. The tests were conducted in pure load control, at maximum stresses that were expected to cause measurable crack growth but not to cause gross yielding of the entire uncracked section area. Because the remaining ligament to the back face was so small, severe plastic deformation was certain to occur in that region. Multiple load cycles were applied with a hold time at maximum load of 30 seconds. The loading half of the cycle was completed in 10 seconds, while the unloading half was completed in 5 seconds.

The fundamental goal in these two tests was to find a maximum stress level at which appreciable crack growth would occur on more than one cycle. In other words, the intent was to generate crack growth during several consecutive cycles of a pure zero-max load control test. In previous experiments, we had typically either seen fracture on the first cycle of a load control test, or some crack growth on the first cycle followed by negligible crack growth per cycle on subsequent loading cycles.

In short, we were successful in causing crack growth during more than one cycle of these zero-max load tests. The specific load (P) vs. crack mouth opening displacement histories for the two tests are shown in Figures 3.6 and 3.7. In both tests, the initial maximum stress was about 140 ksi, or a load of about 35 kips (note that the yield stress for this IN-718 is about 160 ksi). At least two identical cycles were conducted at that stress level. If no additional increase in the CMOD was observed on the second cycle (which suggests no additional crack growth), then the maximum stress was slightly increased, and at least two cycles were conducted at that new maximum stress. If some CMOD increase was observed on the second cycle at a given maximum stress, then cycling continued at the same maximum stress (and with the same hold times) until the CMOD increase per cycle became negligible or until the specimen fractured.

On the first test (specimen S26, Fig. 3.6), the initial maximum stress was 140 ksi. On the first cycle, some additional CMOD accumulated during the hold time, but the second cycle P-CMOD trace was essentially elastic with no further CMOD increase during the hold time. The maximum stress was increased to 143 ksi for the third cycle, and more extensive CMOD increase occurred during the hold time. On the second cycle at 143 ksi (the fourth cycle overall), how-

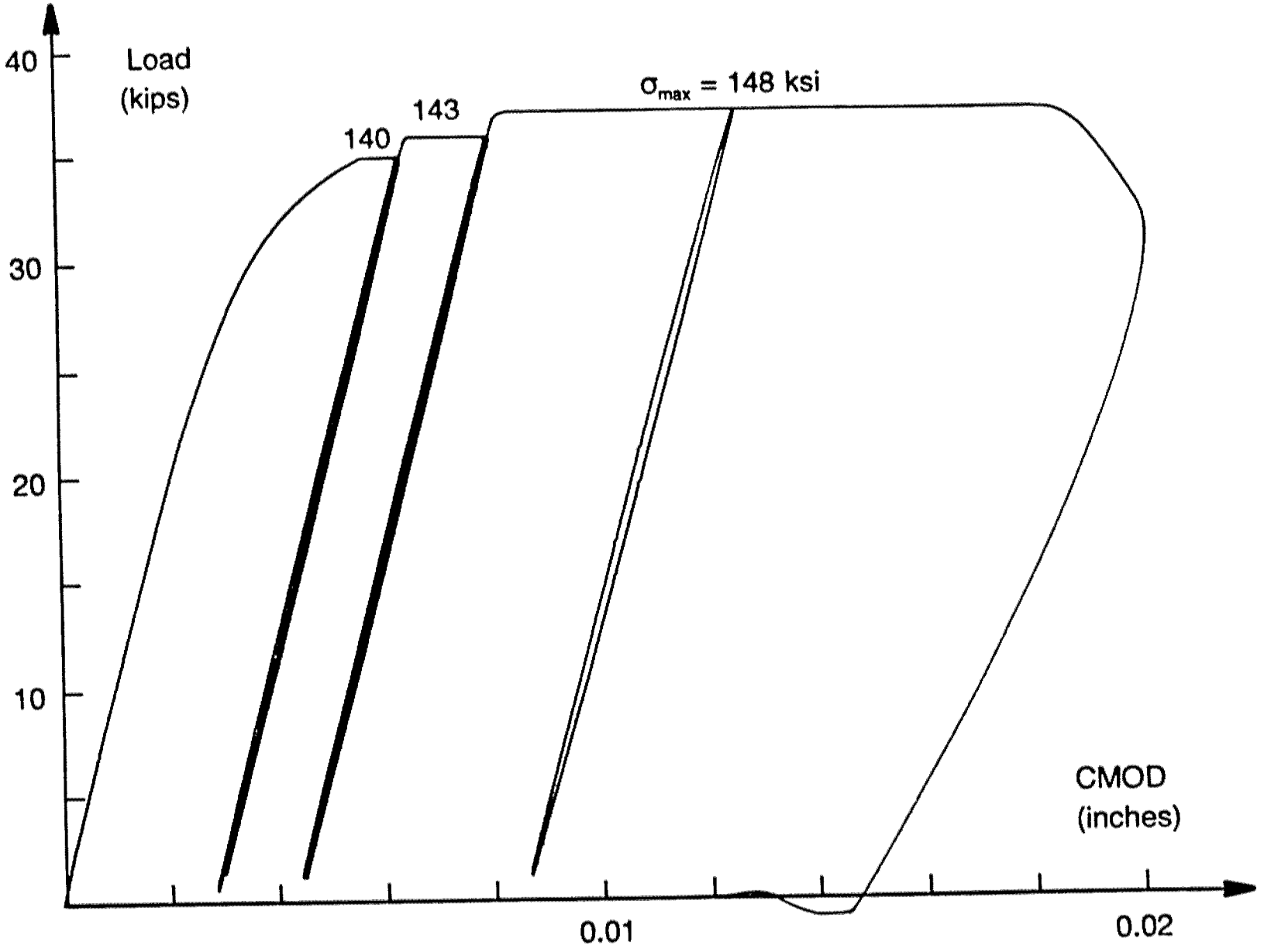

Figure 3.6. Load vs. crack mouth opening displacement history for test S26 showing failure on the second cycle at the terminal maximum load

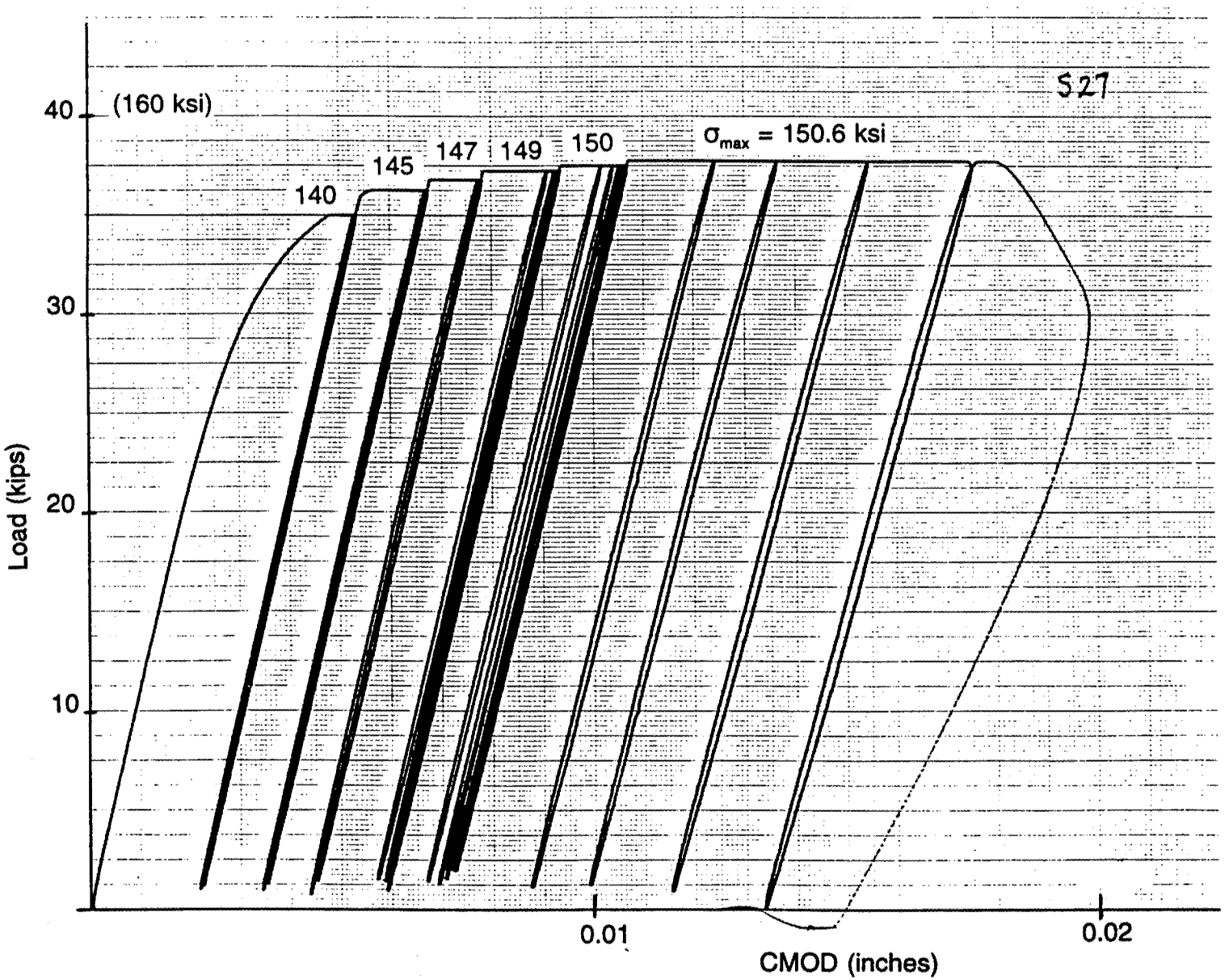

Figure 3.7. Load vs. crack mouth opening displacement history for test S27

ever, the CMOD did not increase further. For the fifth cycle, the maximum stress was again increased to about 148 ksi. Much more extensive CMOD increase occurred during the 30-sec. hold time. The rate of CMOD increase increased slightly during the first 5 or 10 seconds and then gradually decreased, so that by the end of the 30 seconds the rate of CMOD increase had almost decreased to zero. On the second cycle at 148 ksi (the sixth cycle overall), the CMOD increased very slowly during the first few seconds of the hold time, and then gradually increased faster and faster. After about 25 seconds of the hold time, the specimen fractured completely and the load dropped (the CMOD trace is meaningless beyond this point because the clip gauge breaks away from the specimen surface). Also note the appreciable hysteresis in the load/unload trace prior to the last cycle.

The second test (S27, Fig. 3.7) was slightly more complicated, because smaller load steps were employed in an attempt to get more than two cycles at the final stress before fracture. A second goal was to unload immediately before final fracture seemed imminent in order to see if anything different happened on the next (failure) cycle. At the first three maximum stress levels (140, 145, and 147 ksi), some CMOD increase was observed (as before) during the hold time on the first cycle and no CMOD increase during the hold time on the second cycle. At the fourth and fifth maximum stress levels (about 149 and 150 ksi), a little growth was observed during the second cycles (mostly towards the end of the hold time), so additional cycles were conducted at the same stress level. The CMOD increase per cycle decreased to nearly zero on successive cycles, however, so after 1-3 additional cycles the maximum stress was increased again. The final maximum stress was 150.6 ksi. CMOD growth was fairly slow and steady during the hold times of the first two cycles, with slightly less growth on the second cycle than on the first. After a few seconds of hold time on the third cycle, the CMOD began to increase more and more rapidly, so the specimen was unloaded after only 15 seconds in order to prevent fracture. On the fourth cycle at 150.6 ksi, the CMOD again began to increase rapidly during the hold time, and the specimen was unloaded after about 7 seconds. On the fifth cycle (the 20th cycle overall), the specimen fractured in less than 1 second after reaching maximum load.

During each of the cycles at the final maximum stress in both tests, the elastic compliance (measured on the forward loading portion of the P-CMOD trace) increases (the stiffness decreases) slightly but measurably, indicating that crack growth was occurring on each individual cycle.

The gradually stepping up of the load is not thought to be particularly significant to the overall fracture process. This stepping up was done primarily because it was not possible to predict in advance what an appropriate failure stress would be (before the specimen is broken open, the true initial crack depth is not known). If we had known *a priori* to load to 148 ksi on the very first cycle on specimen S26, we probably would have seen subcritical crack growth on the first two cycles and then failed sometime during the third cycle.

The load stepping process does provide some interesting information, however. Note that it is possible to be very close to the "failure stress" (within a few percent) and still see no significant crack growth on subsequent loading cycles. Another way of looking at this is that if

the applied stress is not very close to the "failure stress," subsequent loading cycles will not do additional damage to the specimen.

An additional MCPT experiment was conducted to evaluate the generality of the tear-fatigue crack growth theory. This test, like the previous two such critical tests, was conducted with large amplitude zero-max load control cycling until failure occurred. In the first two tests, the initial crack depth was quite large (a/t = 0.8 to 0.9) and the maximum nominal applied stress was less than yield (σ_{max} around 150 ksi, compare σ_{ys} = 165 ksi) so that some elastic constraint was maintained on the remaining ligament. In this latest test, the initial crack depth was chosen somewhat shallower (a/t = 0.6) and the maximum nominal applied stress was above yield (final σ_{max} = 169 ksi), so relatively little elastic constraint was maintained. The goal was to determine if the same sort of fracture behavior was observed under these conditions (as would be predicted by the tear-fatigue theory), or if the behavior observed previously was somehow unique to the very deepest flaws with lower applied stresses.

In short, the new test (S20) exhibited very similar behavior to the previous two such tests. This is apparently a further confirmation of the tear-fatigue model. The load vs. crack mouth opening displacement history from the test is shown in Fig. 3.8. Note that in this test, as in the two previous, the initial load excursions employed smaller maximum stresses. This was done primarily because the depth of the initial crack was not known until after the test; the depth could only be estimated from the surface length. If the crack depth was significantly underestimated, then the specimen could easily be broken on the very first cycle by going to a maximum stress too great.

This practice of going up to the terminal maximum stress in small steps was also useful to show, however, that multiple cycling at smaller maximum loads (i.e., J_{max} values significantly less than some critical value for tearing) does not produce significant additional crack growth. The test protocol was to select a maximum stress and conduct at least two cycles at that σ_{max}, each with a 30-second hold time. Some increase in CMOD, probably corresponding to increases in crack depth, always occurred on the first cycle to some new maximum stress, because J_{max} was increasing to a new maximum. In general, however, the second or any subsequent cycle to the same maximum load did not produce significant additional CMOD increase (or crack growth). If some additional CMOD increase occurred on the second cycle, then a third cycle to the same σ_{max} was conducted, and so on. When an additional cycle produced no significant crack growth (which was usually the case), then the maximum stress was increased slightly for the next cycle and the same process was repeated.* In test S20, significant CMOD increases occurred on

---

* The excursions at lower maximum stresses are thought to be relatively inconsequential for crack growth in comparison to later cycles at the highest maximum stress, since J_{max} increases so sharply with increasing maximum stress (in this case, a 5 percent increase in maximum stress from 160 to 169 ksi produces nearly a 40 percent increase in J_{max}). Fatigue contributions to crack growth under these conditions are always small, and are relatively insignificant until we are very close to instability.

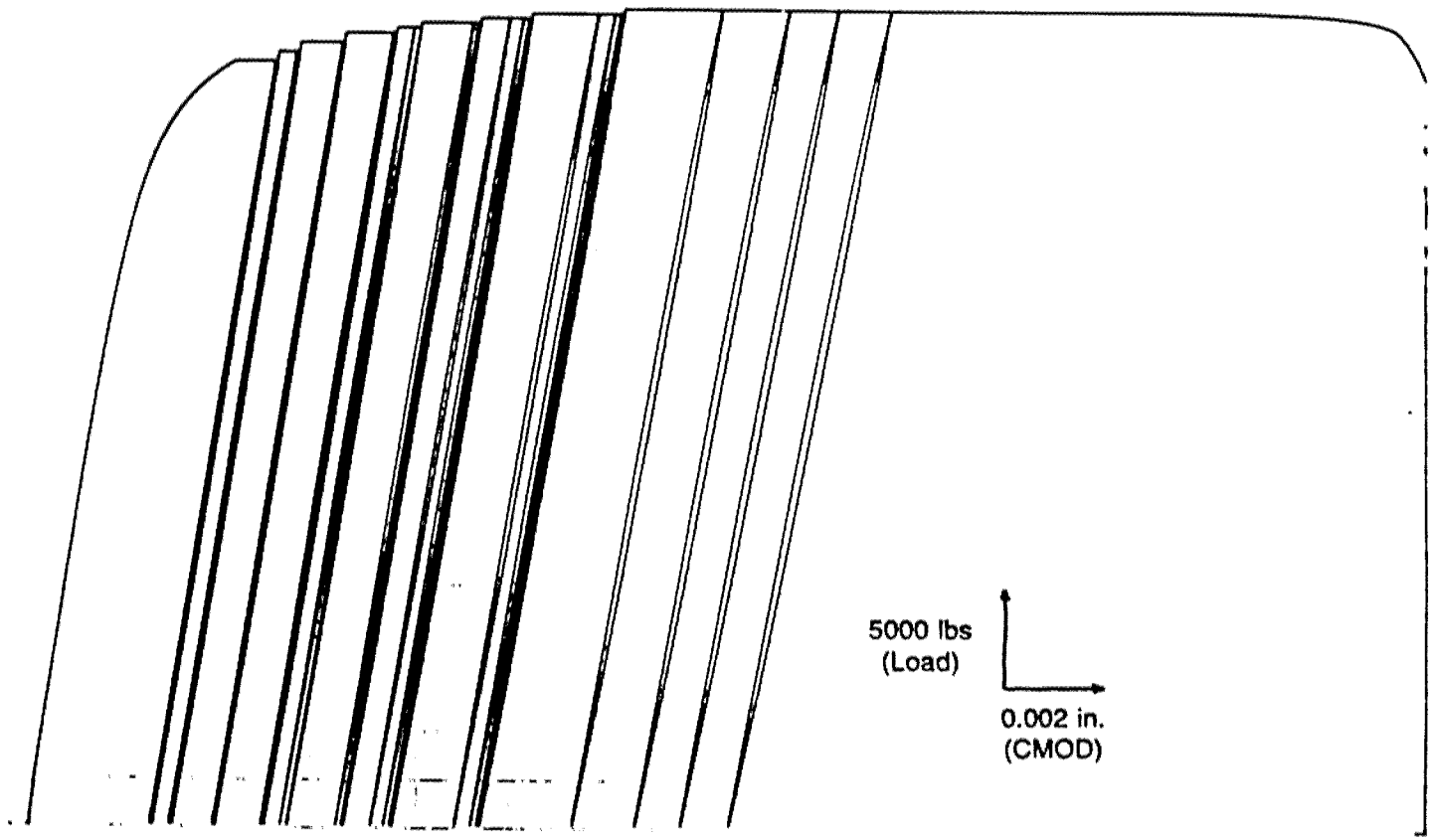

Figure 3.8. Load vs. crack mouth opening displacement history for test S20 showing failure on the fifth cycle at the terminal maximum load

subsequent cycles only at the terminal σ_{max}, 169 ksi. Failure occurred after 29 seconds (of a 30-second hold time!) on the fifth cycle at 169 ksi.

Quantitative Verification of Tear-Fatigue Theory. This experimentally observed behavior provides a clear qualitative verification of the tear-fatigue theory described in Section 2 on Analytical Development. It is also useful to evaluate the tear-fatigue formulation on a more rigorous quantitative basis. The actual initial flaw size and shape, and the actual maximum stress value during the failure cycles, are known after the test has been completed. Based on these values, it is possible to predict the number of simulated proof cycles to failure. As discussed earlier, this simple calculation assumes that negligible crack growth occurs during previous simulated proof cycles at lower stresses.

A computer code was developed to model crack growth during simulated MCPT cycling. This computer code, which was originally derived from a similar code developed in Phase I, implemented the elastic-plastic fatigue crack growth and tear-fatigue models described in Section 2, and was ultimately used to perform the probabilistic studies described in Section 4.

The predicted number of proof cycles to failure was approximately 13 cycles for S26, 2 cycles for S27, and 6 cycles for S20. This compares to actual experimental numbers of 2 cycles for S26, 5 cycles for S27, and 5 cycles for S20. This agreement is excellent, especially considering the extreme sensitivity of the predicted numbers to minor variations in crack size/shape or maximum stress. For example, specimen S20 was predicted to fail on the 6th cycle at 167 ksi. Changing the maximum stress to 168 ksi predicted failure on the first cycle, while changing to 166 ksi predicted 20 cycles. Keeping a 167 ksi maximum stress but changing the initial crack depth from 0.123 to 0.120 predicted 20 cycles. Even a small change in the crack aspect ratio from 0.984 to 1.0 changes the prediction from 6 cycles to 10 cycles. Given the inherent uncertainties associated with the J-resistance curve, estimation of J_{max}, and measurement of the exact crack size and shape, the predictions are shown to be very good.

A few additional experimental investigations into the tear-fatigue phenomenon have been conducted under the broader "Proof Test Philosophy" (PTP) contract [41] in conjunction with the validation of the general failure assessment diagram (FAD) approach to proof test analysis. The FAD approach is a convenient diagrammatic representation of the J-based approach employed in the current contract. These tear-fatigue investigations are being documented in more detail in reports under the PTP contract. However, since the results are highly relevant to the MCPT contract effort, the highlights are briefly reviewed here. All of these tests were conducted with the same Inconel 718 material studied in the current contract.

In these tests, conducted with restrained single edge cracked plate (RSECP) specimens, two specimens were tested under simulated service cyclic loads, and two received a proof overload before cyclic loading. The load vs. load line displacement history from one of the proof overload tests is shown in Fig. 3.9. Note that the simulated proof overload was conducted in displacement control to insure stability, while the ensuing simulated service cycling was conducted in load control to permit tear-fatigue behavior as instability was approached. The

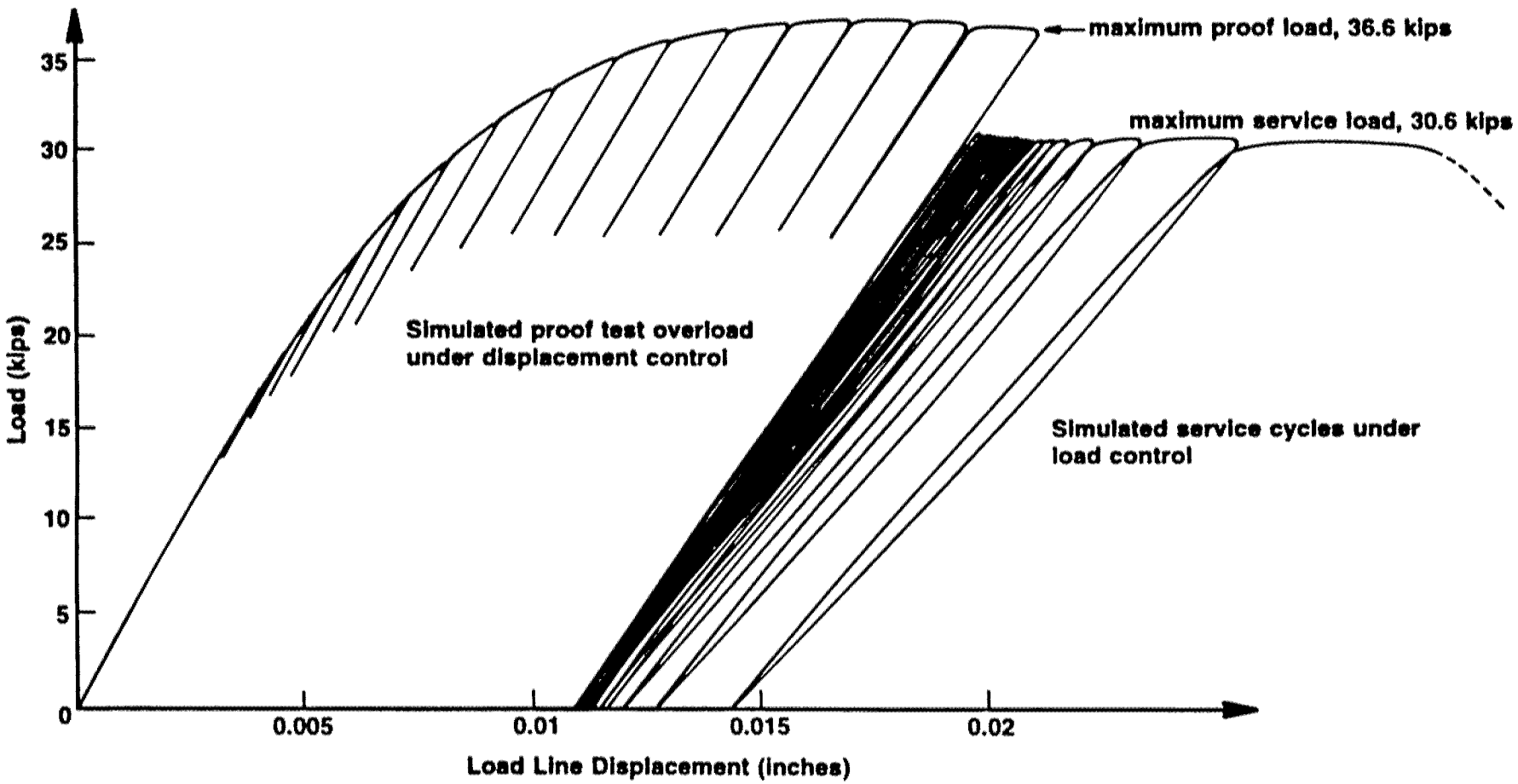

Figure 3.9. Load vs. load line displacement history for simulated proof test followed by simulated service cycling

proof overload appeared to retard the subsequent cyclic crack growth rate. This "retardation" is not the fatigue load interaction effect commonly associated with occasional overloads in spectrum histories, but instead can mainly be attributed to the suppression in ductile tearing by the overload. Even though the applied J value at the maximum load in the first fatigue cycle exceeded the initiation value, no additional tearing was observed during fatigue cycling until numerous cycles had been applied and the crack had grown due to fatigue mechanisms. In contrast, subsequent calculations indicated that in the absence of the proof loading, those specimens would have been expected to fail upon first application of the service cycle maximum load. This behavior is consistent with the standard tear-fatigue algorithms.

3.6 Effect of Proof Testing on Subsequent Fatigue Crack Growth Rates

Two crack growth experiments were performed to explore the potential effect of proof testing on subsequent fatigue crack growth rates in surface-flawed IN-718. Two specimens were precracked to nominally identical initial crack shapes and sizes (a/c = 1.0, a/t = 0.6). One specimen was subjected to a single "proof cycle" with a maximum nominal stress of 164 ksi, followed by unloading to zero load. This proof cycle caused significant crack tip deformation and limited crack growth (a = 0.0025", compared to an initial crack size of a = 0.124"). The same specimen was then subjected to fatigue cycling at a stress ratio of R = 0 and a maximum nominal stress of 136 ksi. Note that these stress levels approximately preserve the proof factor of 1.2 used by Rocketdyne in their multiple-cycle proof test specification. The second, nominally identical specimen did not experience a proof cycle but was subjected to the same fatigue history.

The total fatigue lives of the two specimens were 1555 cycles to failure for the "proof tested" specimen and 1406 cycles to failure for the unproofed specimen. While this might appear at first glance to indicate some "retardation" of crack growth in the proof tested specimen, it should be noted that the two life values are quite close in comparison to the normal scatter observed in fatigue crack growth lives for identical specimens subjected to identical load histories. We choose to interpret these two tests as indicating that the proof cycle has no significant effect on crack growth rates during the subsequent fatigue cycling.

It is not possible, of course, to reach a definitive conclusion based on such a small number of tests. This conclusion is consistent, however, with expectations based on conventional wisdom about overload effects in fatigue crack growth. That conventional wisdom suggests that overloads must be considerably larger than 1.2× (perhaps 1.5× or even greater) before causing significant retardation. Furthermore, the mechanisms that cause retardation are most significant only when the crack tip plasticity is well-contained and the specimen is nominally elastic. These conditions are certainly not met for the large crack sizes and large applied stresses being considered in the present experimental program.

These conclusions are also consistent with the observations of a previous Rocketdyne study of overload retardation in Inconel 718 and other SSME materials [42]. This study found that for R = 0.1 loading at room temperature, overload retardations were entirely negligible for overloads less than 60 percent.

We draw the conclusion, then, based on accepted theory and a limited number of confirming experiments, that proof testing of large surface flaws in IN-718 at proof stresses that are capable of producing measurable crack growth during the proof cycle has a negligible influence on the subsequent fatigue crack growth rates. It appears that other factors are more significant for variations in crack growth and hence for remaining structural life.

3.7 Fractographic Observations

3.7.1. Crack Growth Mechanisms

The analytical approach proposed to address MCPT problems is based on a single elastic-plastic fatigue crack growth relationship employing ΔJ_{eff} that can be applied from the small scale yielding regime up into the elastic-plastic and fully plastic regime. At this high end, the elastic-plastic FCG relationship is postulated to interface smoothly with a ductile crack extension relationship employing the J-resistance curve. Empirical observations of crack growth data also indicated a possible relationship between the blunting portion of monotonic crack advance and the elastic-plastic regime of the FCG curve.

A brief series of fractographic studies were performed on five different crack growth specimens in order to investigate the micromechanisms of crack advance under different conditions and to determine if the proposed analytical approach appeared to be consistent with the range of observed material responses. The five specimens had experienced five different types of load histories: SSY fatigue crack growth, zero-max load control fatigue cycling with maximum stress near yield, zero-max displacement control fatigue cycling with both severe and moderate plasticity, and a single monotonic load excursion. Table 3.1 provides a convenient overview of the test conditions for each specimen. These fractographic investigations were led by SwRI Staff Engineer V. P. Swaminathan, who assisted in the preparation of this portion of the report.

Specimen SD-3 was used to generate baseline fatigue crack growth information in the traditional SSY range under constant amplitude load cycling with a simple through-crack (center-crack) configuration. Fractography showed that crack propagation was by the usual transgranular cyclic growth mechanism. Scanning electron microscope (SEM) investigations under low magnifications (<300X) showed quasi-cleavage fracture features, as seen in Fig. 3.10 (top). Under higher magnifications (3000X), clear fatigue striations were predominant, as shown in Fig. 3.11 (bottom). Striation spacing increased with crack length. Even at the higher ΔK values, the fracture surface revealed predominantly striations with very limited ductile tearing.

Specimen S-25 was used to study crack growth under zero-max load control cycling with a high maximum stress. The crack configuration was a semi-circular surface crack with an original precrack depth of about $a/t = 0.75$. The specimen separated into two pieces after 385

Table 3.1. Summary of test conditions for specimens examined fractographically

Specimen	Test Type	Maximum Stress (cf. σ_{ys} = 160 ksi)	ΔJ_{eff} or J_{max}
SD-3	SSY FCG	~ 56 ksi	35-140 lb./in.
S-25	SSY FCG with high σ_{max}	~ 145 ksi	110-150 lb./in.
S-11	severe EPFCG	168-157 ksi	~2000 lb./in.
SCR-8	monotonic	176 ksi	~2900 lb./in.
S-13	moderate EPFCG	158-138 ksi	350-600 lb./in.

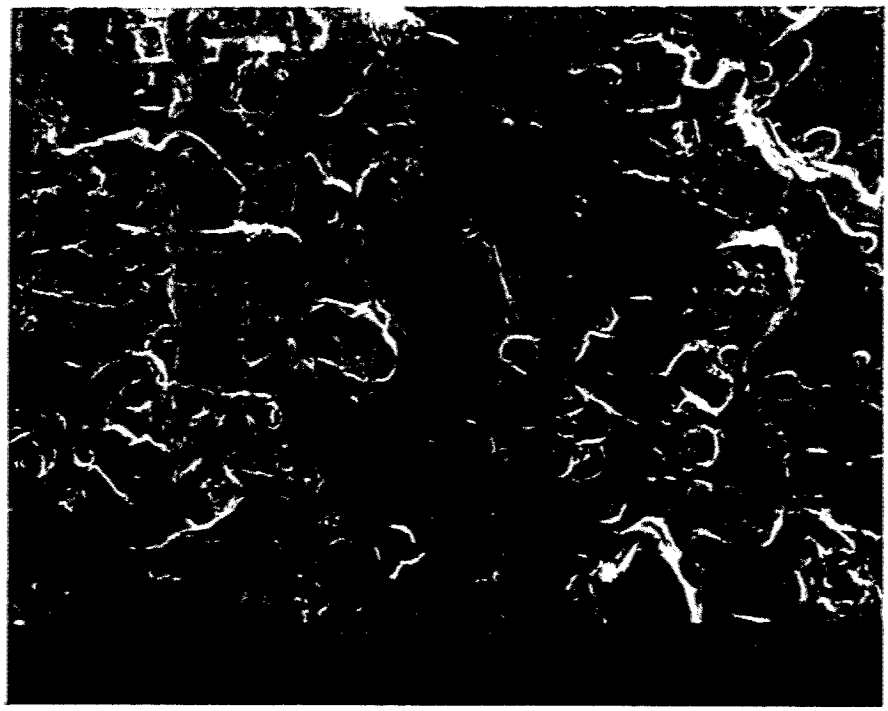

58074

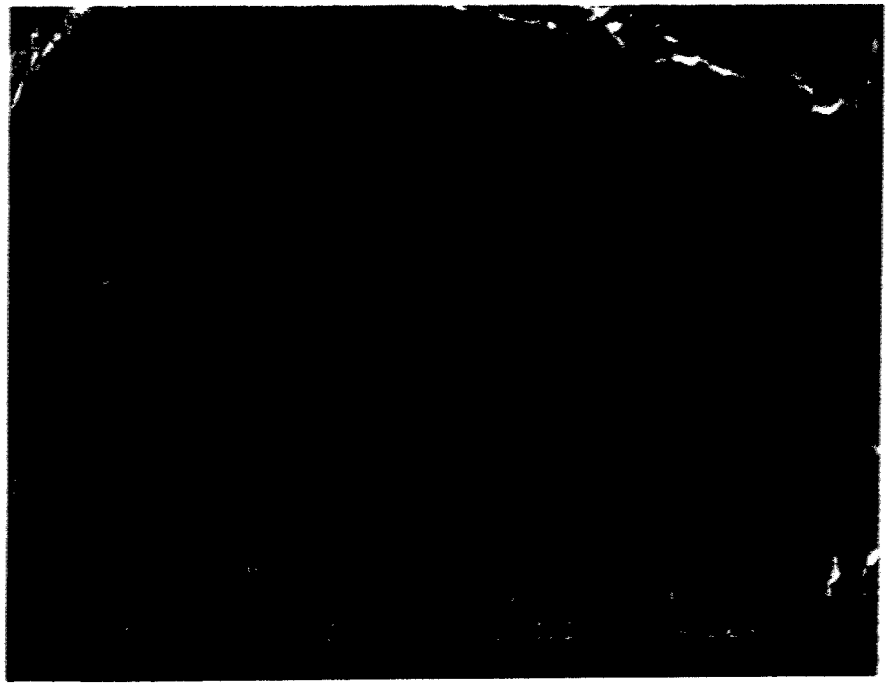

58076

Figure 3.10. Fracture surface of specimen SD-3 at 300x (top) and 3000x (bottom) showing quasi-cleavage fracture features and fatigue striations

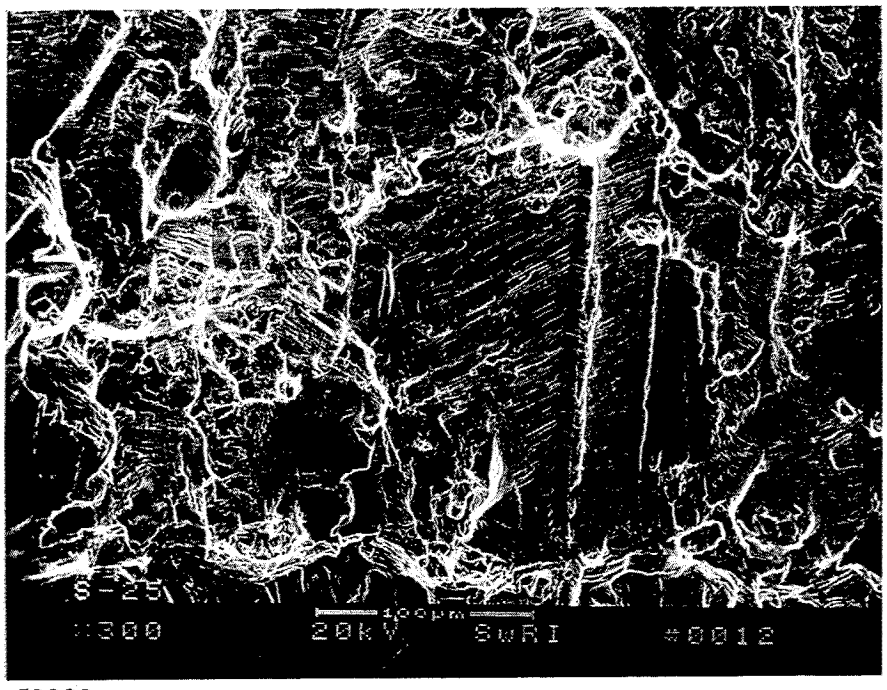

59282

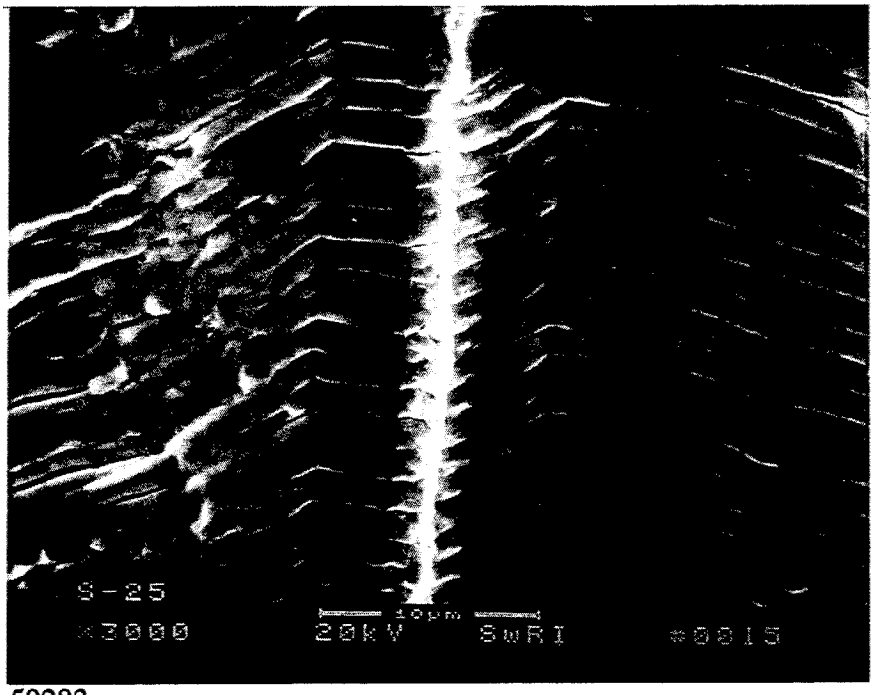

59283

Figure 3.11. Fracture surface of specimen S-25 at 300x (top) and 3000x (bottom) showing transgranular fatigue striations

load cycles. The fractographic features on this specimen were primarily transgranular fatigue striations. See Fig. 3.11. However, in comparison to the fractographic features of SD-3, this specimen had relatively larger striation spacing at similar magnifications, which is in keeping with a slightly higher crack growth rate. These striations were approximately the same distance apart as the independently computed average crack growth per cycle, with the striation spacing increasing significantly very close to final fracture. Occasional breaks in striations parallel to the direction of crack propagation and connecting to the adjoining striations indicated locally larger plastic deformations at the crack tip of this specimen. The fraction of ductile tearing increased at larger crack lengths.

Specimen S-11 was used to study crack growth under zero-max displacement control cycling with a large maximum stress (168 ksi on first cycle, gradually decreasing to 157 ksi on last cycle) and a high compressive minimum stress (about -150 ksi). Five cycles were used to grow this semi-circular surface crack from an initial depth of a/t = 0.63 to a final depth of a/t = 0.81. The fracture mode on this specimen was predominantly ductile dimple and tear ridges, as illustrated in Fig. 3.12. No striations were observed on the fracture surface. The ductile dimples seemed to initiate at precipitate particles. These particles (for example, Fig. 3.12 - bottom) were identified by energy dispersive spectrographic (EDS) analysis in the SEM to be a columbium- (niobium-) rich intermetallic phase containing Ti.

Specimen SCR-8 experienced only a single (monotonic) loading excursion under crack mouth displacement control, during which the semi-circular surface crack grew from an initial depth of a/t = 0.525 to a final depth of a/t = 0.645. The fractographic features of this specimen, as seen in Fig. 3.13, were similar to those of S-11: predominantly ductile fracture mode with dimples and tear ridges. Again, the niobium-rich precipitate particles were found in the dimples, indicating that the dimple fracture initiated at these particles. Under high magnifications in the SEM, fine slip lines perpendicular to the crack growth direction were also observed. These resemble fine striations, but are not associated with a striation growth mechanism.

Specimen S-13 was used to study crack growth under zero-max displacement control cycling with a moderately high maximum stress (158 ksi on first cycle, gradually decreasing to 138 ksi on last cycle) and a moderately high compressive minimum stress (ranging from -145 ksi to -132 ksi). The applied ΔJ_{eff} values were intermediate between the LEFM specimens SD-3 and S-25 and the highly plastic specimens S-11 and SCR-8. Thirty-three cycles were used to grow this crack from an initial depth of a/t = 0.63 to a final depth of a/t = 0.77. Estimated da/dN values ranged from about $3(10)^{-4}$ to $2(10)^{-3}$ in./cycle.

The fractographic features on S-13, shown in Fig. 3.14, indicated a predominantly ductile fracture mode with tear ridges. Fewer ductile dimples were observed in comparison to Specimens S-11 (5 cycles, ΔJ_{eff} = 2000 lb./in.) and SCR-8 (1 cycle, J_{max} = 2900 lb./in.). This may be attributable to the severe deformation of the fracture surfaces experienced during the high compressive loads; numerous fractographic features appeared to have been "squashed." It is interesting to note, however, that specimen S-11 experienced even higher compressive loads, but

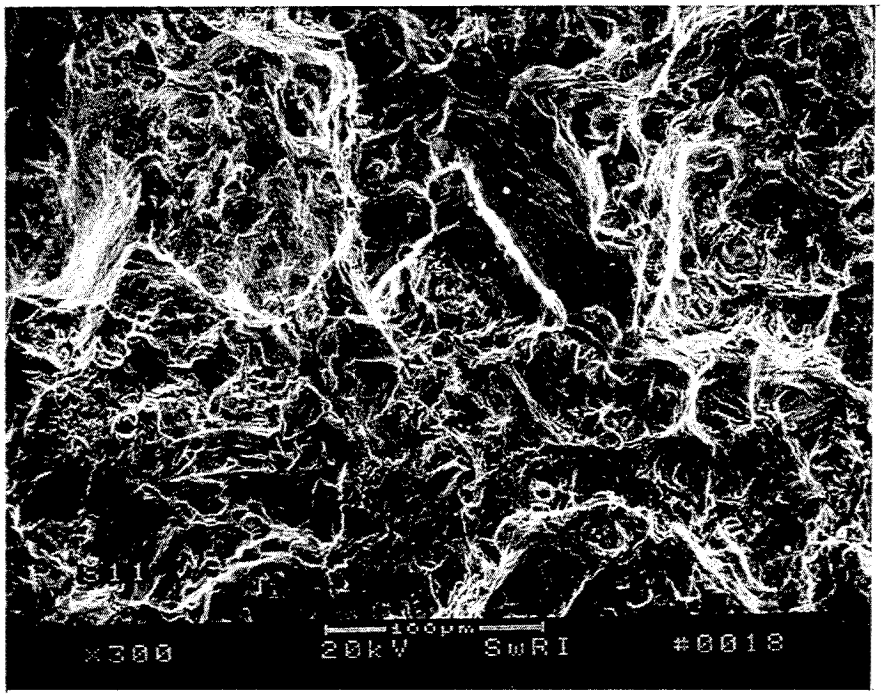

58117

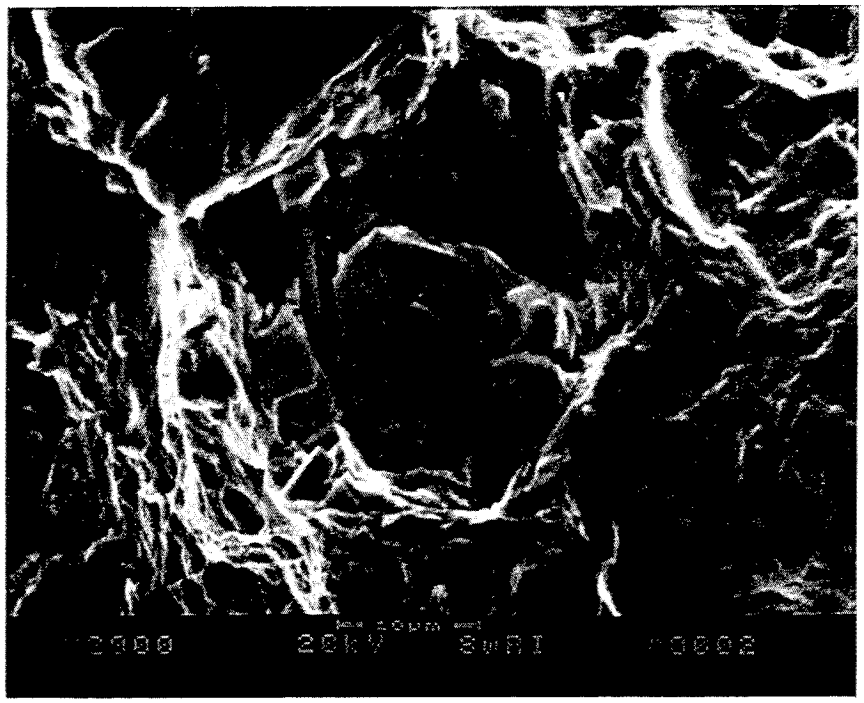

58032

Figure 3.12. Fracture surface of specimen S-11 at 300x (top) and 2000x (bottom) showing tear ridges and ductile dimples at precipitate particles

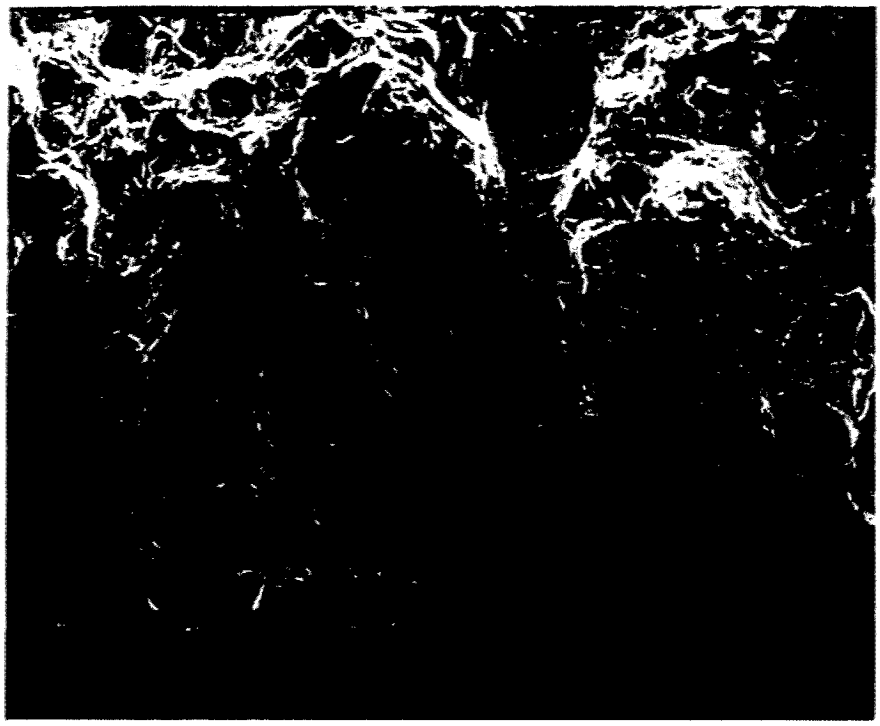

58106

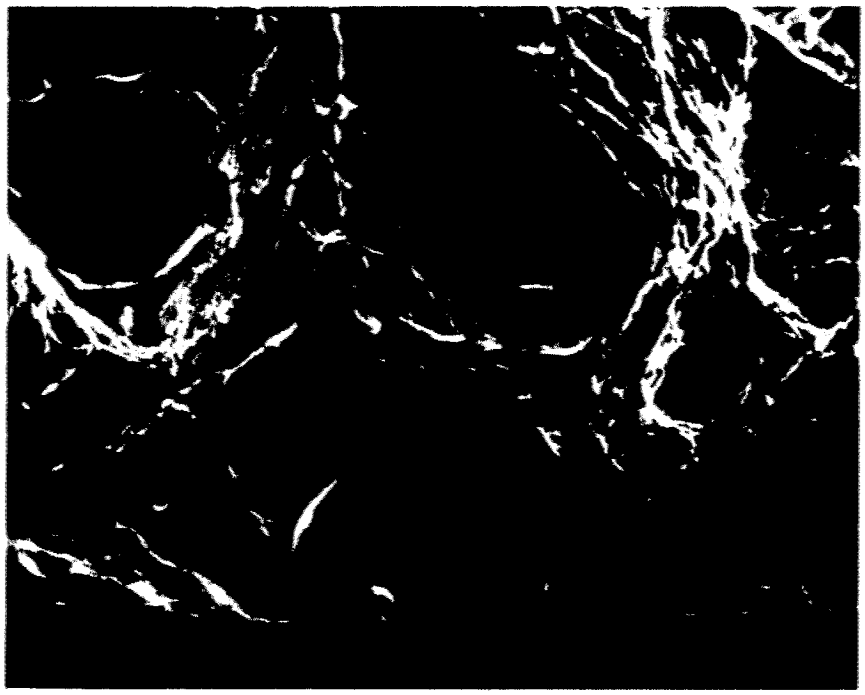

58107

Figure 3.13. Fracture surface of specimen SCR-8 at 300x (top) and 3000x (bottom) showing tear ridges and ductile dimples at precipitate particles

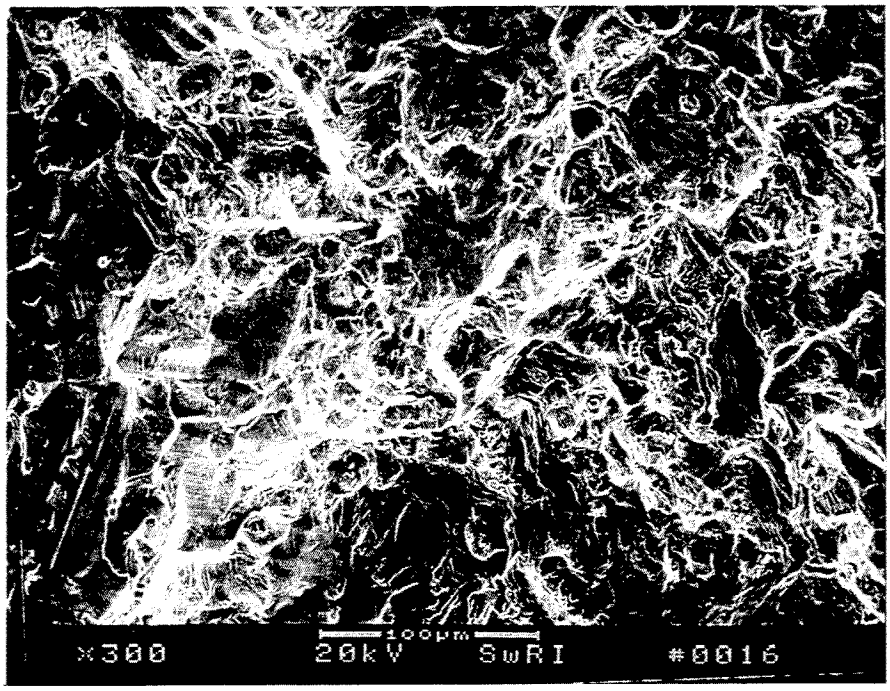

60359

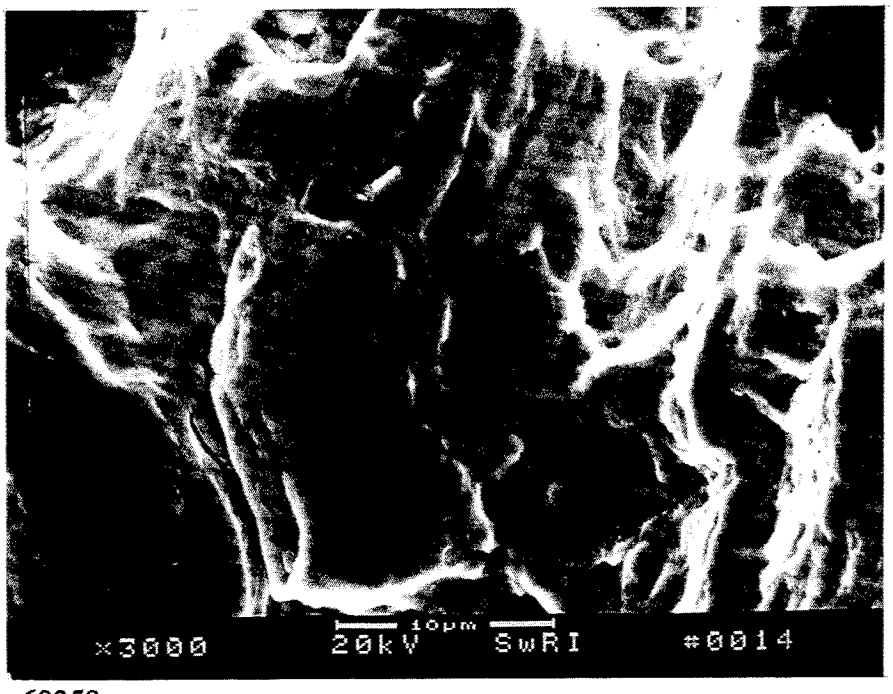

60358

Figure 3.14. Fracture surface of specimen S-13 at 300x (top) and 3000x (bottom) showing tear ridges and few ductile dimples

did not appear to show nearly as much crushing of fracture features (and did show more extensive dimpling). The increased compressive deformation of S-13 may indicate higher crack closure levels in this specimen compared to S-11, which would have been expected to some degree. It is possible that the apparent decrease in dimpling observed in S-13 is significant, and could indicate a slight change in crack advance mechanism. Note that the maximum loads in S-11 were somewhat higher than those in S-13. No apparent fatigue striations were observed on the fracture surface of S-13, in contrast to specimen S-25 at slightly lower applied ΔJ_{eff} (110 to 150 lb./in.). It is possible that striations were formed and then rubbed out by the compressive deformation.

In summary, it appears that the fracture surfaces of IN-718 go through a gradual transition from striations at lower applied J or ΔJ values to ductile tear ridges and (possibly) increasingly to ductile dimpling at higher applied J or ΔJ values. These do not appear to be abrupt transitions, and the gradual increases in crack growth rate appear consistent with the gradual changes in fracture surfaces. The fracture surfaces of the "ductile tearing" specimen, SCR-8, and the 5 cycle MCPT specimen, S-11, share a similarity that is consistent with the relationship between the R-curve and low cycle fatigue crack growth that was previously postulated from empirical observations of crack growth data. The fracture surfaces of the SSY FCG specimen, SD-3, and the high stress load cycling specimen, S-25, share a similarity that confirms the extension of the SSY growth rate curve up into the elastic-plastic regime. It appears reasonable, therefore, to use an elastic-plastic fatigue crack growth approach to model crack advance under cyclic loading well into the plastic range, even when the fracture mode is gradually changing.

3.7.2. Crack Shapes

All specimens were fatigued to complete fracture at the end of the test after the original and final crack shapes had been delineated with fatigue marker bands or heat tinting. This made it possible to characterize the initial and final crack shapes and determine the extent of crack growth at several angular orientations around the perimeter of the crack. An example of a fracture surface from one of the multiple cycle crack growth tests is shown in Fig. 3.15. Visible and designated on this photograph are the initial EDM flaw, the low ΔK fatigue precrack, the region of crack growth during the multiple cycle test, and the final low ΔK fatigue fracture surface.

The total amount of crack growth during four multiple cycle tests is shown in Fig. 3.16 as a function of angular position around the perimeter. Similar crack growth data are presented in Fig. 3.17 for selected single cycle (resistance curve) tests. The total final crack lengths would be obtained by adding these values to the size of the original fatigue precrack (not shown here). These precrack lengths varied little around the perimeter, typically remaining within a few mils of the ideal theoretical semi-elliptical shape (aspect ratios varied from $a/2c$ = 0.88 to 1.03, with an average value around 0.97). Any significant variations in the crack extension around the perimeter, therefore, are due to the single cycle or multiple cycle crack growth process itself.

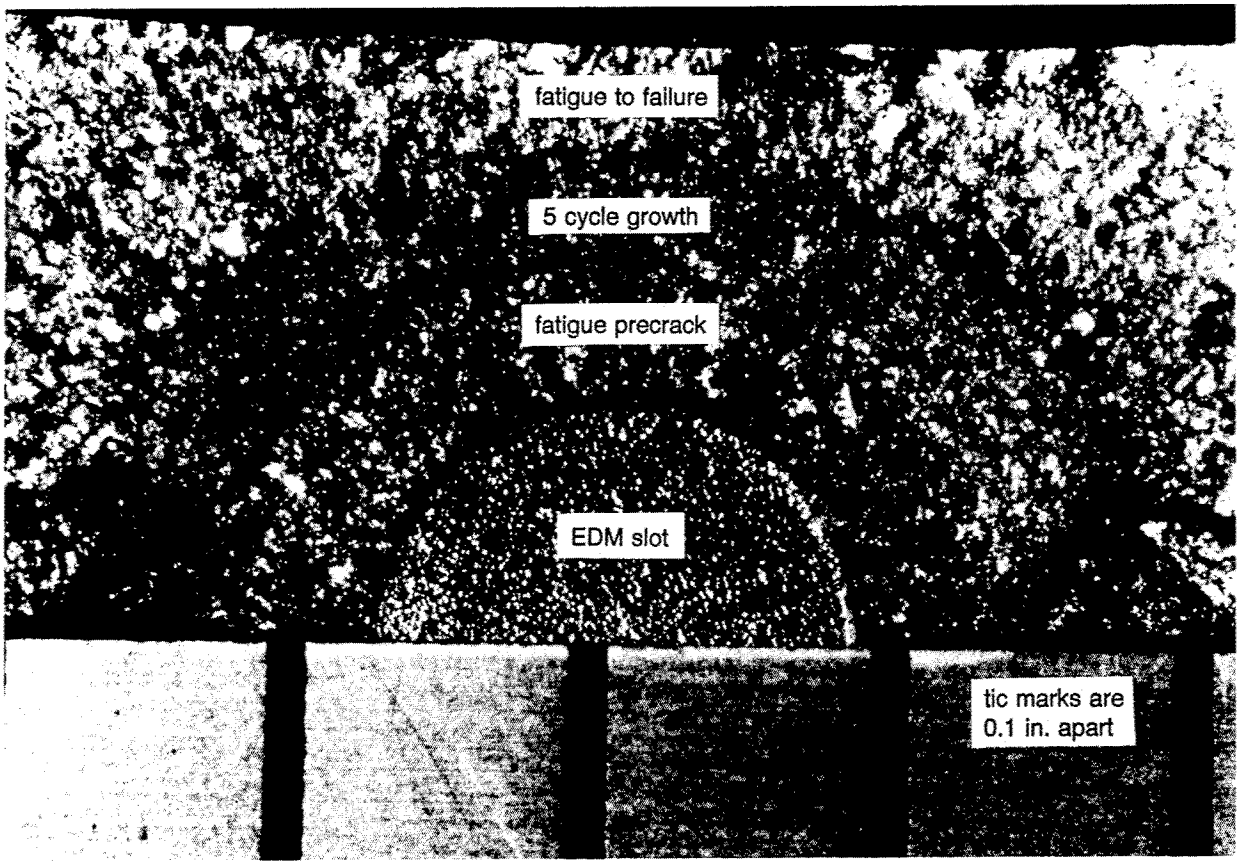

Figure 3.15. Fracture surface of multiple cycle crack growth specimen (zero-max displacement, five cycles)

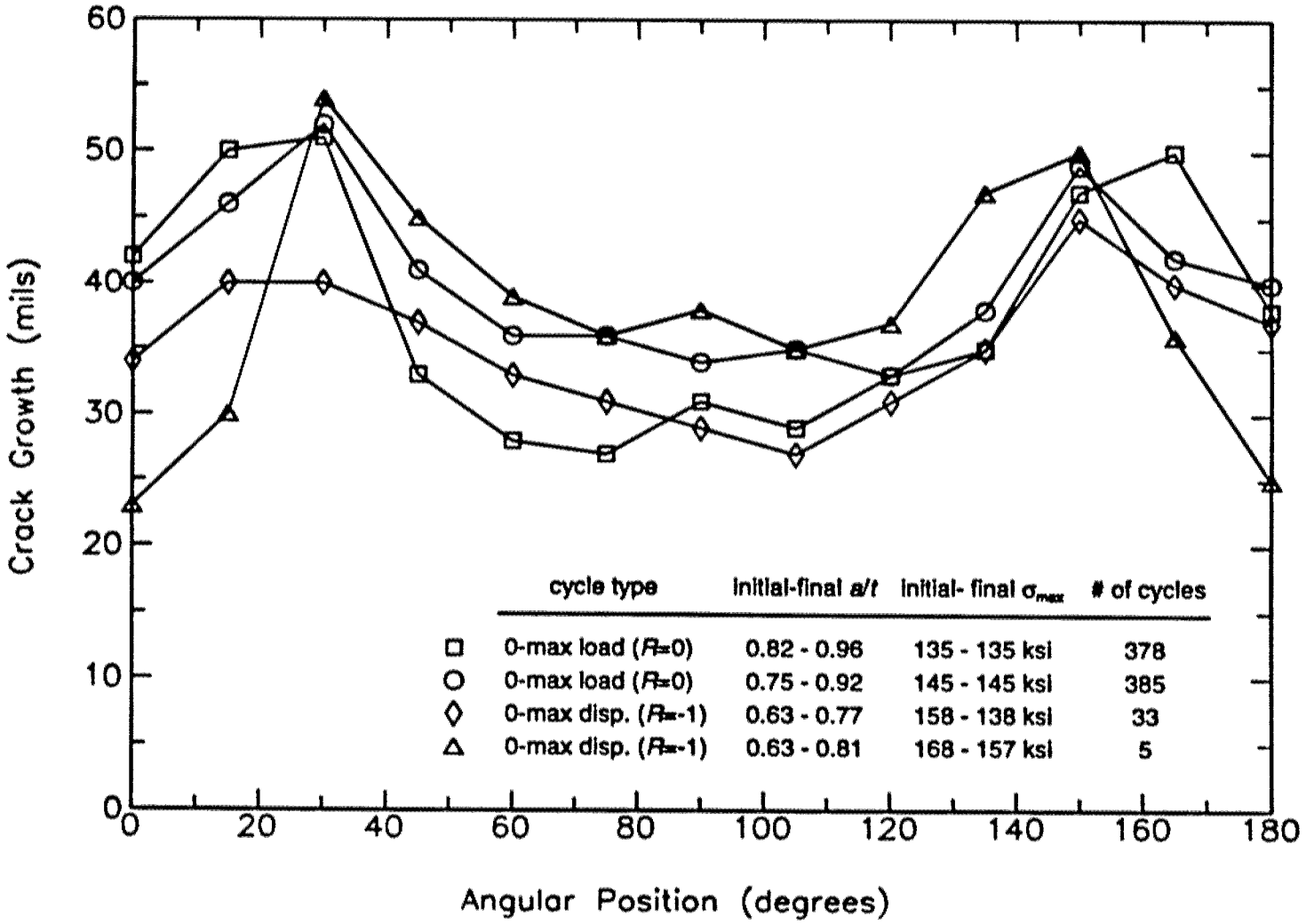

Figure 3.16. Crack growth as a function of angular position for selected multiple cycle crack growth specimens

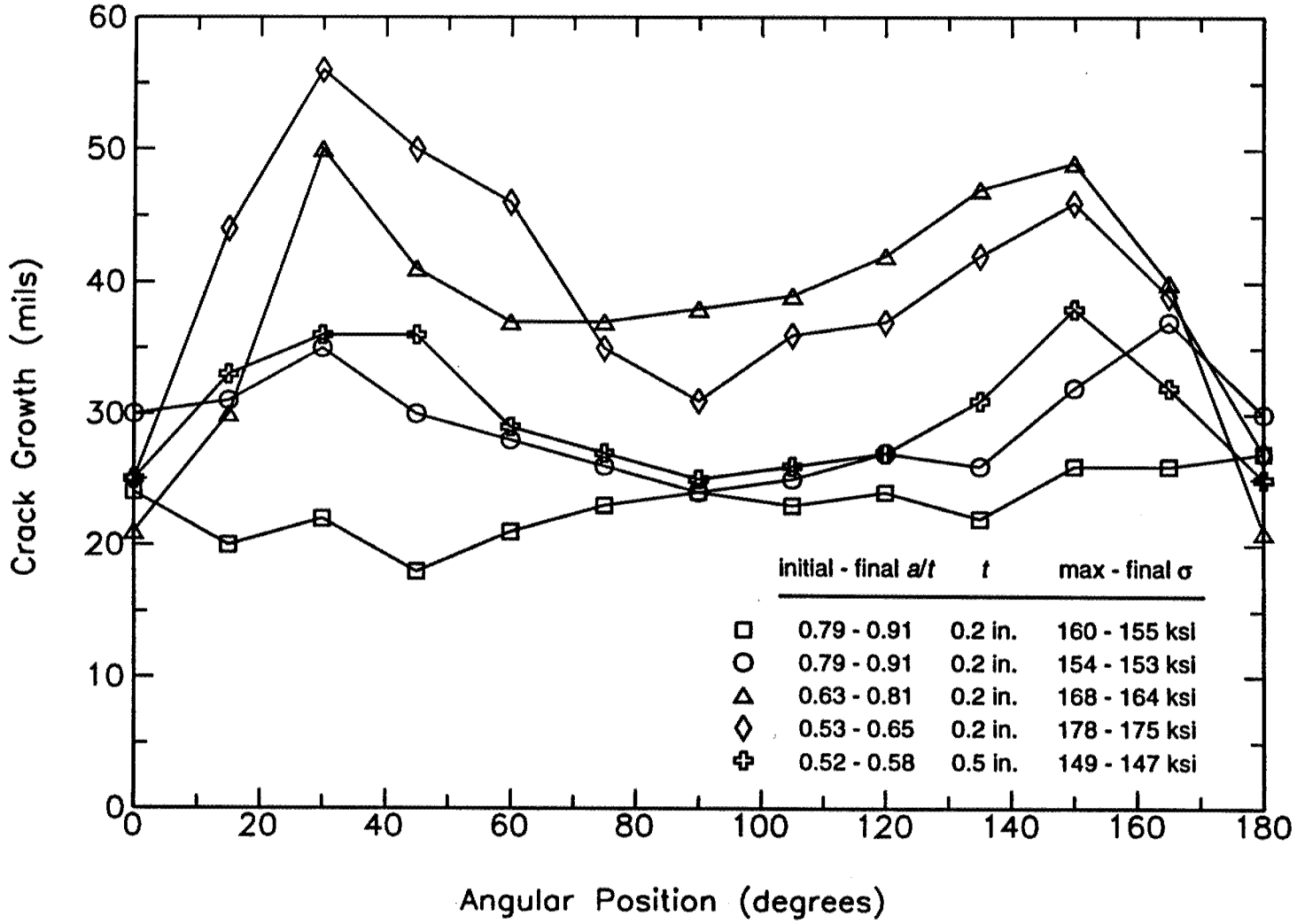

Figure 3.17. Crack growth as a function of angular position for selected single-cycle crack growth specimens

There is a distinct maximum in the crack extension at an angular position around 30 degrees from the front surface of the crack in those specimens experiencing substantial crack growth. Some of these specimens also exhibited a clear retardation of growth at the specimen surface itself; the specimen shown in Fig. 3.15 was the most extreme case observed. Specimens that experienced only small increments of crack growth, including other tests not shown here, generally experienced crack extension that was more uniform around the perimeter.

These results are consistent with the three-dimensional elastic-plastic finite element calculations of applied J at higher maximum stresses for semi-circular (a/c = 1) surface cracks as a function of angular position published by Wang and Parks [10]. They found a similar maximum in J at about 30 degrees for applied stresses near yield and a sharp decrease in J approaching the front surface. Similar numerical results for deep semi-circular surface cracks have recently been published by Yagawa *et al.* [14], who show that the specific angular variation of J changes with both crack depth and crack aspect ratio. Bauschke, *et al.* [43] reported a comparable angular dependence for surface crack growth in their experiments with Al 7075-T7351 for a/c = 0.4 - 1.1 and a/t = 0.3 - 0.75 at loads near the yield load, although they typically measured more retardation at the surface and much larger differences between the maximum growth and the growth at the position 90 degrees from the surface for smaller a/c values.

It is particularly interesting that the zero-max loading multiple cycle tests produced a similar crack shape to the zero-max displacement and the single cycle tests, even though the zero-max cycles were nominally elastic. In contrast, small scale yielding fatigue crack growth tests with lower (elastic) maximum stresses produced crack shapes that were much more regular, even for very deep cracks that had experienced substantial growth. This may indicate that the development of the crack shape is influenced by J_{max} in ways that are not fully reflected by our simple, one-dimensional cycle-by-cycle computation of ΔJ.

The crack growth data and analyses summarized in Figs. 3.1 and 3.5 were based on crack growth measurements at the deepest point of the crack (90 degree position), although it is clear from Figs. 3.15 - 3.17 that this is not always the position of greatest extension. Nevertheless, this original choice of the 90 degree position is thought to be an appropriate one for engineering applications. The reference stress J estimates used are based on the K solution at this 90 degree position. The global limit load solution employed in the reference stress estimate is not tied to any particular crack front location, but failure of this geometry in this material occurs primarily by extension of the crack at the 90 degree position to the back surface, followed quickly by final fracture of the resulting through crack. And this seems to be the key issue from an engineering standpoint. The slightly greater crack extension at the 30 degree position, while certainly interesting from a fracture mechanics research standpoint, does not appear in these particular tests to exert any direct influence on tendencies for final fracture, which occurs as the 90 degree position of the crack approaches the back face. The complex crack shape does exert some influence on the resulting applied J at the 90 degree position, but this is a more indirect effect that might be neglected in an engineering approach to predicting crack growth or fracture. Of

course, other applications in which the crack shape changes were more severe might require a more rigorous treatment of these effects.

It should be possible to use a three-dimensional finite element calculation of variations in applied J around the perimeter to predict the experimentally observed variability in crack extension around the perimeter. This could be accomplished using the resistance curve construction of Fig. 3.3 or the fatigue crack growth curve of Fig. 3.2, although there may also be some variations in material resistance to crack extension around the perimeter (e.g., due to changes in stress state) that would complicate such a prediction. Since the K-solution does not exhibit a similar maximum at some intermediate position around the crack perimeter, it is not immediately evident how the reference stress approach might be used to estimate these angular variations in applied J.

3.8 Acoustic Emission Investigations

The acoustic emission (AE) technique can provide valuable supplemental information during the course of proof testing, particularly for tough, ductile materials where stable crack growth can occur on loading. Acoustic emission may be defined as transient elastic waves generated by the rapid release of energy from localized sources within a material. These localized sources may be associated with severe deformation, with localized fracture events, or even with the rubbing of mating crack surfaces. The resulting sound waves typically occur in short bursts or groups of bursts at very high frequencies (above 100 kHz) and of very low intensity.

Acoustic emission could potentially provide the capability to detect otherwise undetectable subcritical crack growth during proof testing, and hence could perhaps eliminate one of the major potential disadvantages of MCPT. Therefore, a limited series of AE investigations were conducted in conjunction with the experimental studies of crack growth during MCPT. The actual AE monitoring and subsequent analysis was performed by John Hanley of the SwRI Nondestructive Evaluation Science and Technology Division, who assisted in the preparation of this portion of the report.

Acoustic emission was monitored during mechanical testing on specimen S19, which had a nominal cross-section of 0.2 × 1.25 in. and a semi-circular fatigue precrack about 0.12 in. deep. The specimen was subjected to a complex series of load and displacement excursions for the particular purpose of recording the AE from various phenomena. Figure 3.18 shows crack mouth opening displacement and load versus time in seconds. The CMOD was first extended to 15, 17.5 and 20 mils from 0 to 900 seconds, interrupted only by brief elastic unloadings to zero load. The specimen was then taken into compression to a large compressive load and then returned to the original CMOD for two cycles from 900 to 1500 seconds. The CMOD was then extended monotonically to 23 mils and fatigue cycled at zero-max load for 2100 seconds at approximately 0.25 Hz. The CMOD was finally extended to 27.5 mils and the specimen was fatigue cycled at zero-max load at approximately 0.1 Hz until failure. The clip gauge was disconnected at about 2600 seconds so that it would not be damaged when the specimen failed.

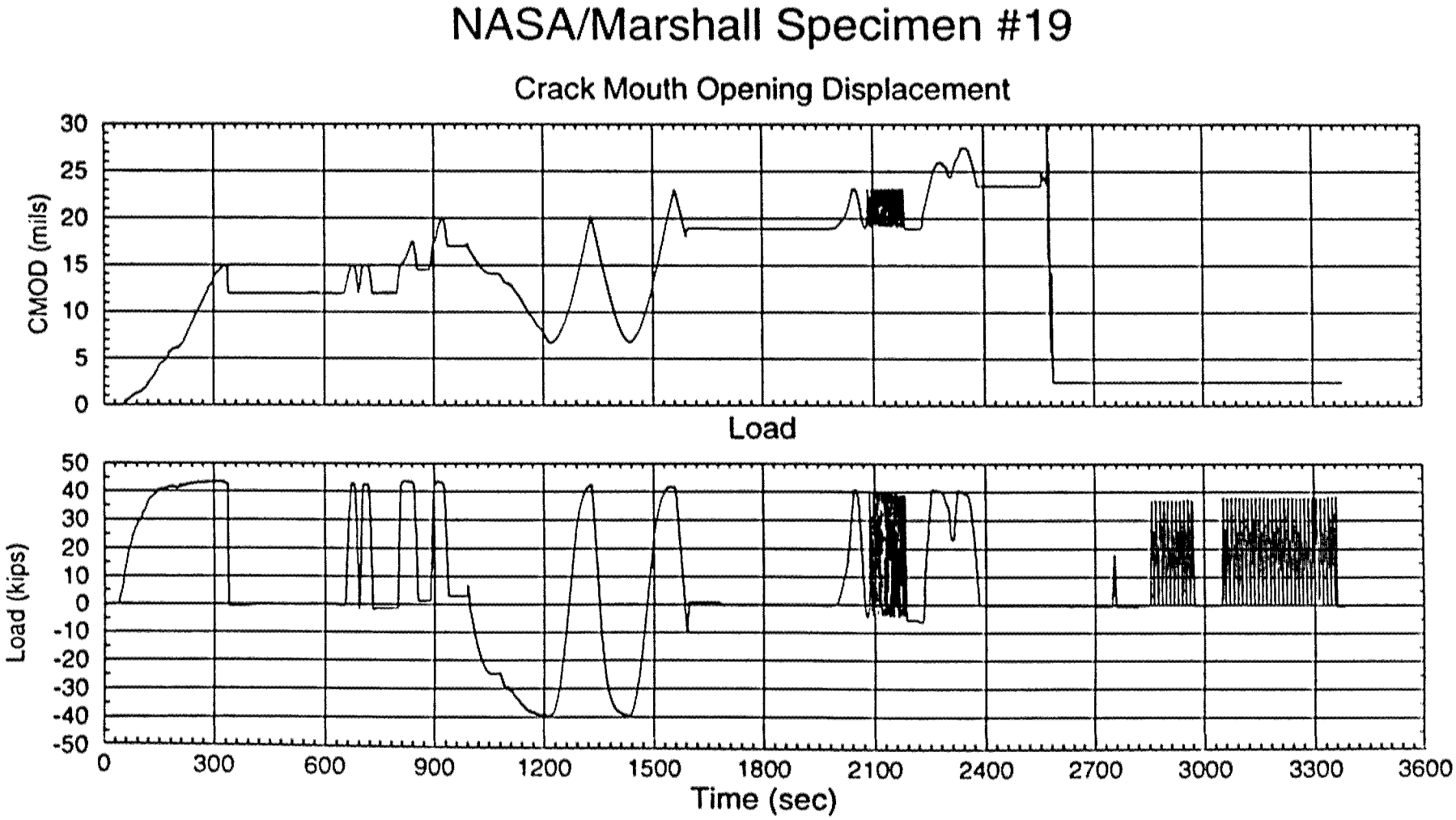

Figure 3.18. CMOD and load history of specimen S19

A Physical Acoustics (PAC) U-30 AE sensor was coupled to the specimen with vacuum grease and fastened with a C-clamp. A PAC 1220A preamp with 60 dB gain was used to amplify the AE signals collected by a PAC 3000/3004 AE system. The system records clock time and AE parameters such as amplitude, energy, duration, counts, and rise time for every event. Frequency content can also be derived from counts and duration. An event is recorded whenever the voltage level of AE exceeds a preset threshold. Voltages proportional to CMOD and load were also recorded for every event so that CMOD-load variations could be correlated with AE.

For AE characterization, the load excursions were classified into three categories:

1) CMOD increase (along the "backbone" of the load-displacement curve)
2) Crack rubbing during decreasing load (below the backbone)
3) Crack rubbing during increasing load (below the backbone)

The CMOD versus load plot in Fig. 3.19 shows where these AE events occurred during the testing (excluding those events recorded during prolonged zero-max fatigue cycling). Figure 3.19 also gives a clearer indication of the test history. Note that load is directly proportional to applied stress; the nominal applied stress (in ksi) is 4.0× the applied load (in kips). CMOD increase produced slightly more events than either of the crack rubbing categories. The AE parameters did not, by themselves, indicate from which of the three categories a lone event may have come.

Potential correlations were explored between different mechanical test parameters related to fracture mechanics "events" and a wide range of AE parameters in both the time and frequency domains. The strongest correlations found were between event rate and count rate versus CMOD during CMOD increase, as shown in Figs. 3.20 and 3.21. Both of these plots show monotonically increasing curves. Similar relationships have been reported in the literature. However, the same correlations were not apparent from any rubbing phenomena during the test, including fatigue cycling.

The crack almost certainly experienced stable tearing during the "CMOD increasing" portions of the history, and so it is likely that the AE events recorded then were generated by the crack advancing through the material. There should have also been some measurable crack advance during the two large unload-reload cycles (with severe compressive peaks), and it is possible that the AE events recorded in the upper one-third of those loading cycles were also generated by crack growth. The crack closure level for these large cycles (i.e., the load at which the crack first becomes fully open during loading or first becomes partially closed during unloading) was probably in the vicinity of zero load. Possible evidence for this statement is provided by the large number of events that began around zero load during the unloading half of these large cycles, events that may have been caused by rubbing of crack surfaces now in contact. If the crack opened during reloading at around the same load level or even slightly higher, then it would have been fully open by the time the AE events were recorded between +15 and +40 kips. In other words, the "rubbing up" or "rubbing down" events detected at large

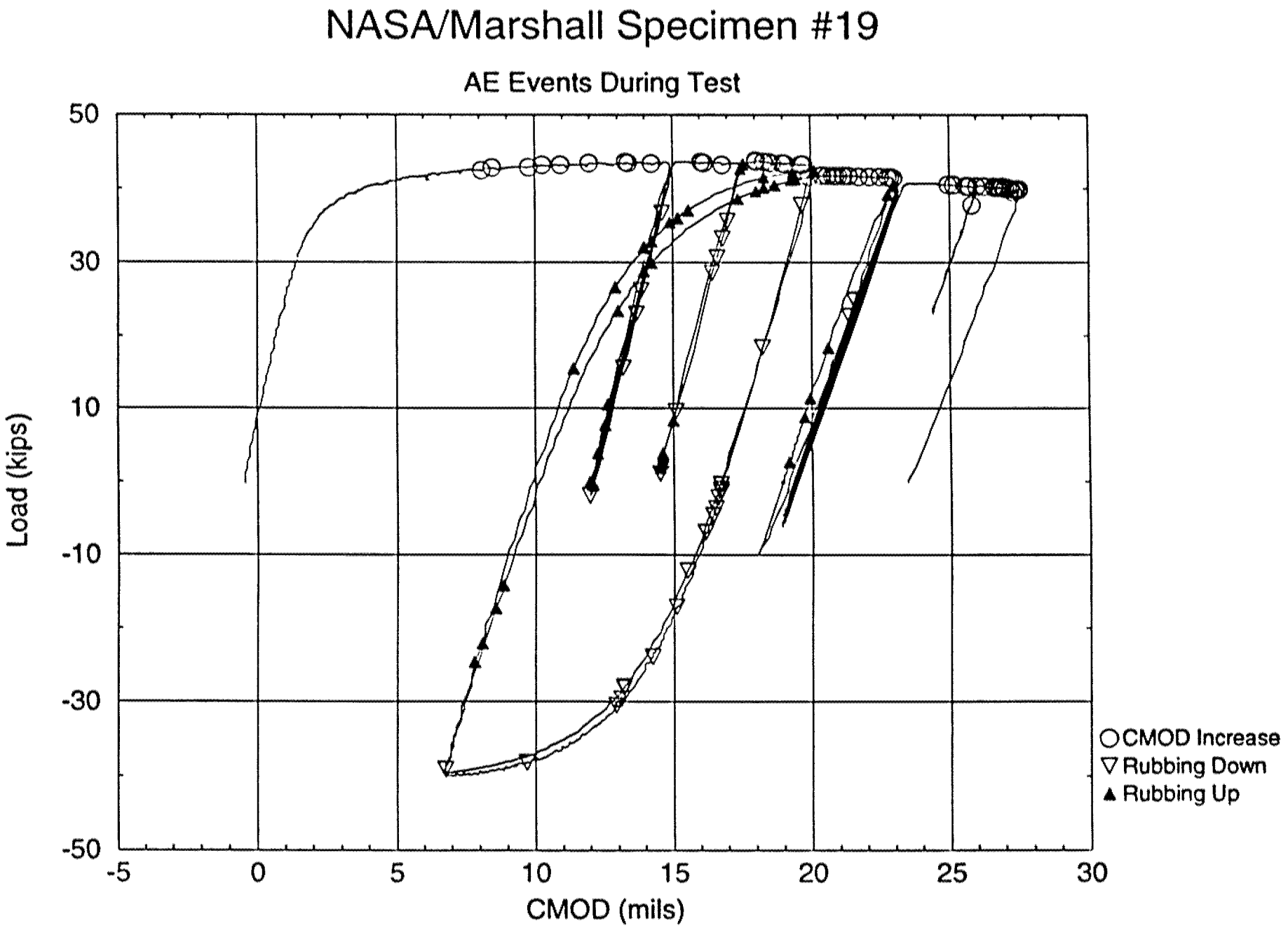

Figure 3.19. CMOD vs. load for specimen S19

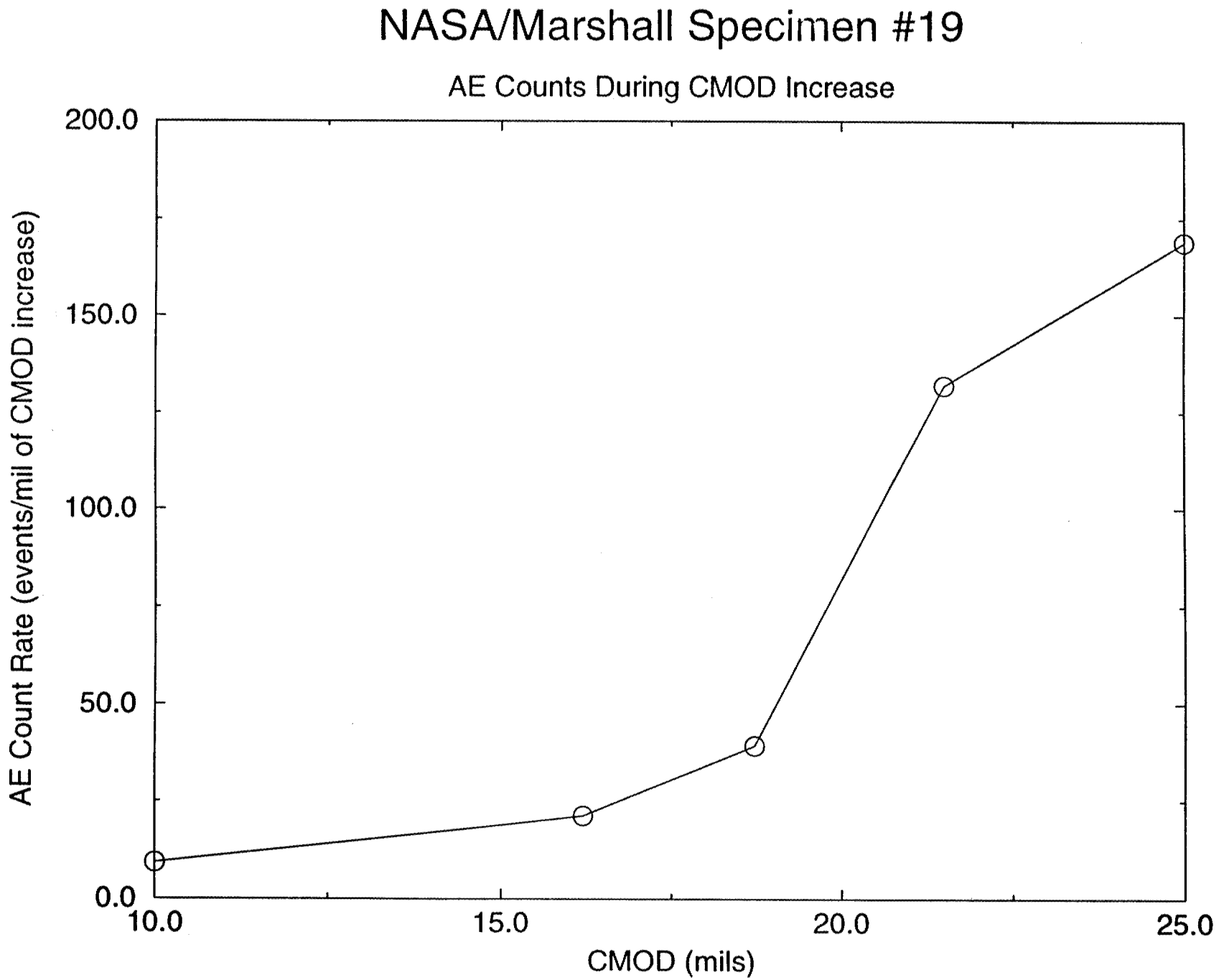

Figure 3.20. CMOD vs. AE count rate for specimen S19

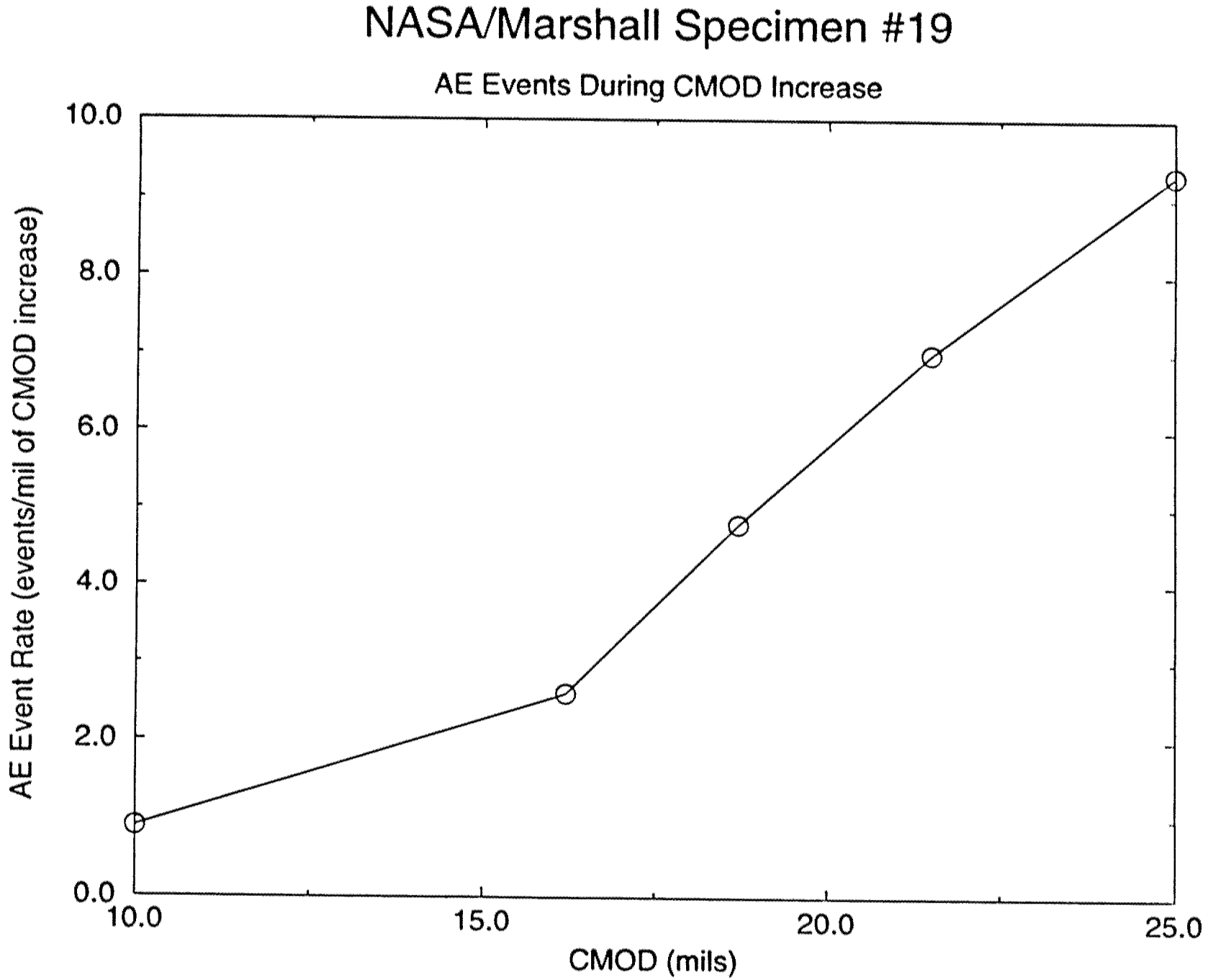

Figure 3.21. CMOD vs. AE event rate for specimen S19

positive loads probably did not originate from actual crack surface rubbing, but perhaps from some crack tip event.

It is also possible that these AE events (and those recorded during CMOD increase) were generated by near-tip deformation rather than actual crack extension. On the other hand, the absence of AE events during the first 8 mils of CMOD increase, when crack tip deformation was becoming severe but crack extension via tearing had not yet initiated, may indicate that these AE events are actually indicative of crack advance processes. There were a few AE events, not shown on Fig. 3.19, recorded during the initial loading process, but most of these occurred when the applied load was less than 10 kips and therefore probably reflect initial crack opening or other "start-up" events. No AE events were recorded between CMOD = 1.5 and 8 mils, when pre-tearing crack tip deformation would have been particularly intense.

It is not clear if the AE information could be linked to quantitative estimates of crack size or crack growth. Other cracked configurations (specimens or structures) may respond with different monotonic relationships (Figs. 3.20 and 3.21), since geometry and material characteristics have much influence on the AE signal. Further testing would be required to better assess the feasibility of measuring damage with AE.

Acoustic emission monitoring was also conducted during the test of specimen S27. Due to scheduling conflicts, the hydraulic isolation system could not be installed to reduce the level of background acoustic activity. Nevertheless, we decided that it would be useful to "listen" during the test in order to determine if important events could still be detected. This may be significant to application of AE in a "production" environment, where complete acoustic isolation of major background noise may not be feasible.

As expected, the increased level of background noise made it more difficult to detect AE activity generated by crack extension. Nevertheless, by adjusting the threshold settings and conducting further post-processing of the signals, some useful information could be detected. One view of the AE history is given in Figure 3.22, which shows the AE amplitude of those events with more than 10 counts, along with the corresponding CMOD vs. time history (a numerical scale is not shown for the CMOD values). Note the extensive AE activity during the first loading cycle, when the crack first experiences severe plastic deformation and begins to extend. AE activity during the following cycles, even when the load is increased slightly, is limited and scattered, and does not seem to follow any definite pattern. If the working environment was quieter, of course, more meaningful patterns of activity might have been detected, but we cannot say for sure. It is likely that very little crack extension occurred during these intermediate cycles, so the absence of detected AE activity may be appropriate.

The important observation, however, is the definite increase in AE activity on the last few cycles before final fracture (especially during the next-to-last cycle, conducted at around the 42-minute mark). In retrospect, this was probably a signal that crack growth or crack tip damage was beginning to increase significantly and that failure was imminent. If CMOD information was unavailable (as would be the case in an actual proof test), this AE signal could serve as a

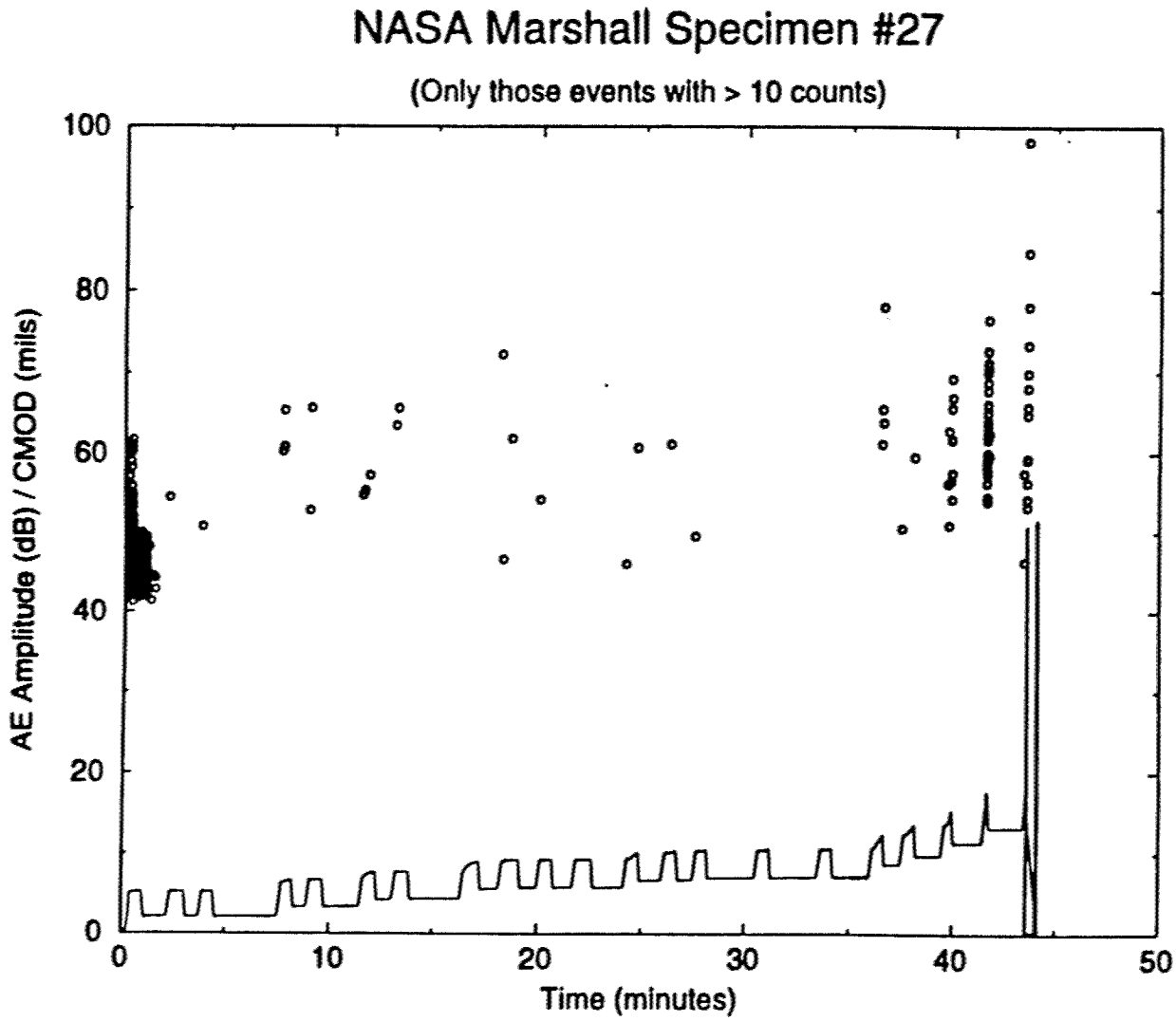

Figure 3.22. AE activity and CMOD history for specimen S27

warning that substantial flaw growth had occurred and that the part may have been seriously damaged, even though actual "failure" may not have occurred.

The limited information available from this particular AE monitoring suggests that AE activity due to the presence of a significant flaw may be most likely to occur on the very first loading cycle, when the crack first deforms plastically and begins to extend, or on loading cycles very near to failure. While other cycles may also generate AE activity that may help to identify the presence of a crack, in practice these signals may be harder to identify as clear indications of a flawed component. Of course, these are all preliminary conclusions, and much more rigorous testing and evaluation would be required to validate the procedure for specific hardware systems.

Isolation and filtering of background noise could still be a problem for the practical application of AE in a production environment. Source location algorithms, which employ multiple AE transducers and signal processing involving triangulation based on time-of-flight concepts to identify the probable location of the AE source, could be useful as one means of separating meaningful AE signals from background noise.

4. PROBABILISTIC ANALYSIS

In Phase I, defect size data from actual SSME hardware or fabrication processes were collected and analyzed to determine a representative distribution for initial crack size. This distribution and the first-generation analytical model for MCPT were employed to perform simple Monte Carlo analyses of the changes in crack size distributions predicted for various proof test protocols.

Extensive probabilistic analyses were conducted in Phase II. These new analyses, which were based on the improved second-generation analytical model for MCPT, and which employed more rigorous probabilistic methods, completely supersede the Phase I probabilistic analyses. The defect size information collected in Phase I was re-analyzed to obtain a more probable distribution of initial crack depths. A simple probabilistic method was derived to compute the conditional probability of failure in service for a population of components that have survived a previous proof test, based on an assumed distribution of initial crack depths. The method was used to perform a series of parameter studies that investigated the effects of proof factor, tearing resistance, constitutive relationship, crack shape, initial crack depth distribution, and notches on the MCPT vs. SCPT comparison. The potential impact of the memory assumption in the tear-fatigue model on this comparison was also evaluated. The probabilistic parameter studies provided a rational basis to draw conclusions about the relative merits of MCPT and SCPT.

4.1 The MCPT Question

It is useful to review briefly the fundamental problem which has motivated this entire research investigation. Engineering hardware may contain crack-like defects of various sizes. Larger defects obviously pose a greater and more immediate risk to hardware integrity in service. One means of screening hardware to identify components containing dangerously large flaws is to subject the hardware to a "proof test": a controlled overload of the component to a maximum load which is generally greater than the maximum load expected in service. Flaws which are larger than some critical size (which can be defined from fracture mechanics analysis) will cause the component to fail during the proof test, thereby preventing a seriously defective component from entering service.

However, the component may also contain flaws which are smaller than the critical size. If the component material behaves in a brittle manner, then these smaller flaws will not be significantly affected by the proof test; i.e., they will not grow to a larger size. However, if the component material behaves in a ductile manner, then these smaller flaws could grow during the proof test without causing failure of the component. These small flaws could therefore remain undetected by the proof test, and their size could even be increased. If the flaws were extremely small, then their existence and their limited growth during the proof test are probably of little consequence to the in-service reliability of the component. However, it is possible that a relatively large flaw which is still too small to cause failure during the proof test will grow significantly during the proof test, thereby damaging the component and seriously increasing the probability of early in-service failure.

These arguments are true for any proof testing approach to components made from ductile materials, regardless of the number of proof cycles. However, the introduction of multiple proof cycles further complicates the issue. Additional proof cycles could, on the one hand, cause the failure of additional components containing relatively large flaws which were not large enough to fail during the first cycle, but which grew to criticality during subsequent proof cycles. On the other hand, additional proof cycles could cause additional subcritical crack growth (i.e., crack growth that does not cause failure during the proof test) which could leave the component more damaged than after the first proof cycle. This additional damage might be negligible, or considerable.

The challenge is to select the appropriate proof testing protocol which maximizes the relative benefit of removing defective components from the population, while minimizing the relative detriment of causing additional damage to components which pass the proof test. But this challenge can not be satisfactorily addressed by considering only individual components with individual cracks. If the individual crack was big enough to cause failure during a particular proof test, then that particular proof test was the right thing to do. But if the individual crack was not big enough to cause failure during the proof test, then that particular proof test was the wrong thing to do, because the proof test may have caused some additional (arguably unnecessary!) damage to the component.

The desirability of a particular proof test protocol must be assessed, instead, on the basis of how it impacts a population of components containing a population of defects of different sizes. Taking into account the probability that a defect of a given initial size exists in the component, and employing a fracture mechanics analysis to determine how much a crack of a given size will grow during the proof test (or if it will fail during the proof test), it is possible to construct the probable distribution of crack sizes at the end of the proof test. This exercise was carried out in Phase I, based on the initial crack size distribution and analytical MCPT crack growth model available at that time.

However, determining the final crack size distribution, and comparing it with the initial crack size distribution, will not (in general) be sufficient to determine if a particular proof testing protocol was good or bad. In general, the proof test will remove some large flaws from the population, while increasing the size of the smaller flaws, and hence possibly increasing the probability of finding flaws of some intermediate size. What is needed is some way of weighing and comparing the relative good and bad of these two changes in the flaw size distribution.

The natural approach, consistent with the logical construction behind Figure 1.1 in the Introduction, is to consider how the changes in the *distribution of crack size* will impact the *distribution of component life* once the component is put into service. Components with larger flaws will have a relatively shorter service life, while components with smaller flaws will have a relatively longer service life. Again, a simple probabilistic analysis can be carried out in which the crack size distribution at the beginning of the service life can be linked to a fracture mechanics calculation of the remaining life for each initial crack size, in order to determine the probability of failure in service after a given number of service cycles. A proof test protocol that

decreases the total probability of failure in service after an appropriate number of service cycles is a good protocol. All other things being equal, if proof test protocol A yields a lower in-service failure probability than proof test protocol B, then it can be concluded that protocol A is better than protocol B. From a fracture mechanics standpoint, therefore, this in-service reliability calculation provides a rational basis to compare and ultimately to optimize proof testing protocols.

4.2 Probabilistic Formulation

In the following paragraphs, a simple probabilistic formulation is outlined that facilitates this weighted comparison of different proof test protocols on the basis of in-service failure probability.

The probability of failure in Ns' service cycles given no failure in Np' proof cycles can be computed using conditional probability. The conditional probability equation for two events A and B (the probability of A given B) is defined as the intersection of A and B divided by the probability of B. In mathematical notation

$$P[A|B] = \frac{P[A \cap B]}{P[B]} \tag{4.1}$$

In the MCPT problem, event A corresponds to failure within Ns' service cycles and event B is survival after Np' proof test cycles. In equation form,

$$P[Ns \leq Ns' \mid Np > Np'] = \frac{P[(Ns \leq Ns') \cap (Np > Np')]}{P[Np > Np']} \tag{4.2}$$

where Ns' and Np' are specified deterministic values where a solution is desired. For example, to determine the probability of failure after 50 service cycles given no failure in 5 proof cycles, $Ns' = 50$ and $Np' = 5$.

In general, computing $P[Np > Np']$ and $P[(Ns \leq Ns') \cap (Np > Np')]$ is a difficult procedure and requires a time-consuming method such as Monte Carlo simulation or an advanced method such as Advanced Mean Value. The calculation is required at numerous values and combinations of Ns' and Np' so an efficient method is desirable.

For simplicity, only a single random variable (the initial crack size, a_i) is being considered at the present time. Therefore, the probability equation can be solved using a much simpler technique. The problem is reformulated in terms of the initial crack size, and the probability can then be determined from the initial crack size probability density function.

Mathematically, this can be represented as,

$$P[Ns \leq Ns'] = P[H(a_i) \leq Ns'] = P[a_i \leq H^{-1}(Ns')] = P[a_i \leq a_i'] \qquad (4.3)$$

where a_i is the initial crack size random variable, $Ns = H(a_i)$ denotes the crack growth, H^{-1} is the inverse crack growth function, and $a_i' = H^{-1}(Ns')$ is the initial crack size that causes failure on the Ns' service cycle.

$P[a_i \leq a_i']$ can be determined analytically since the probability density function and cumulative distribution function of a_i are both known. Therefore, the task is to find the initial crack size, a_i', that corresponds to failure on the Ns' service cycle. Note that this particular procedure cannot be used for more than one random variable because *combinations* of random variable values can cause failure on the Ns' cycle; thus, it is not possible to determine a single a_i, or any other random variable value, that can represent the failure condition. Monte Carlo or advanced methods would be required in this case.

Rather than developing a new crack growth code to solve the inverse problem, even if possible, the a_i' that corresponds to Ns' can be computed using any existing crack growth code and a search procedure. A simple bisection root finding method is sufficient. A similar procedure is performed for $P[Np > Np']$. The probability calculation procedure is shown in Figure 4.1.

Computing the intersection of two events is a system reliability problem which can be difficult to solve. But again, because only one random variable is being considered, the solution is much simpler than in the general case. Because $P[(Ns \leq Ns')]$ and $P[(Np > Np')]$ can both be represented in terms of the initial crack size distribution a_i, the intersection can be computed algebraically. An example is shown in Figure 4.2.

The above methodology can be repeated for different values of Ns' and Np'. The solution is quick, requiring only several minutes of cpu time on an HP workstation for the MCPT crack growth code employed in these studies.

4.3 An Example Problem

The MCPT crack growth computer code originally developed in Phase I was extensively modified to perform probabilistic analyses of fleet reliability. The first major step was to modify the deterministic crack growth algorithms to follow the analytical approaches described earlier in Section 2 on Analytical Development. These new algorithms included the improved reference stress J solutions for semi-elliptical surface cracks, the general elastic-plastic fatigue crack growth methodology, and tear-fatigue theory, including the minor modifications required to address typical reusable aerospace propulsion system applications. The code was also modified to permit analysis of proof testing at one stress level, followed by service cycling at another stress level.

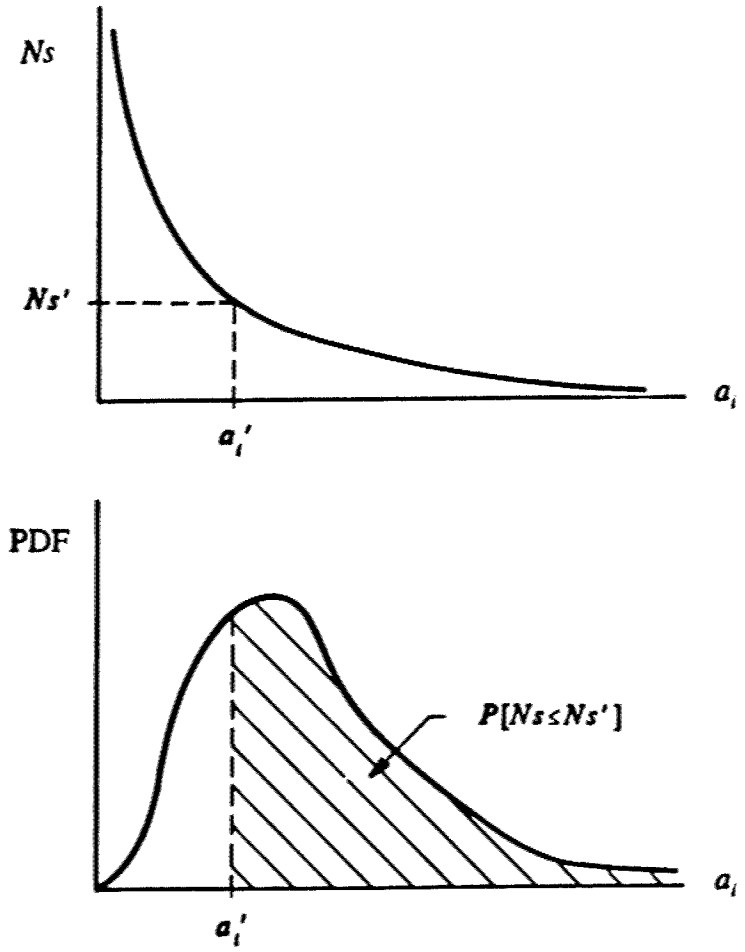

Figure 4.1. Schematic representation of calculation of $P[(Ns \leq Ns')]$

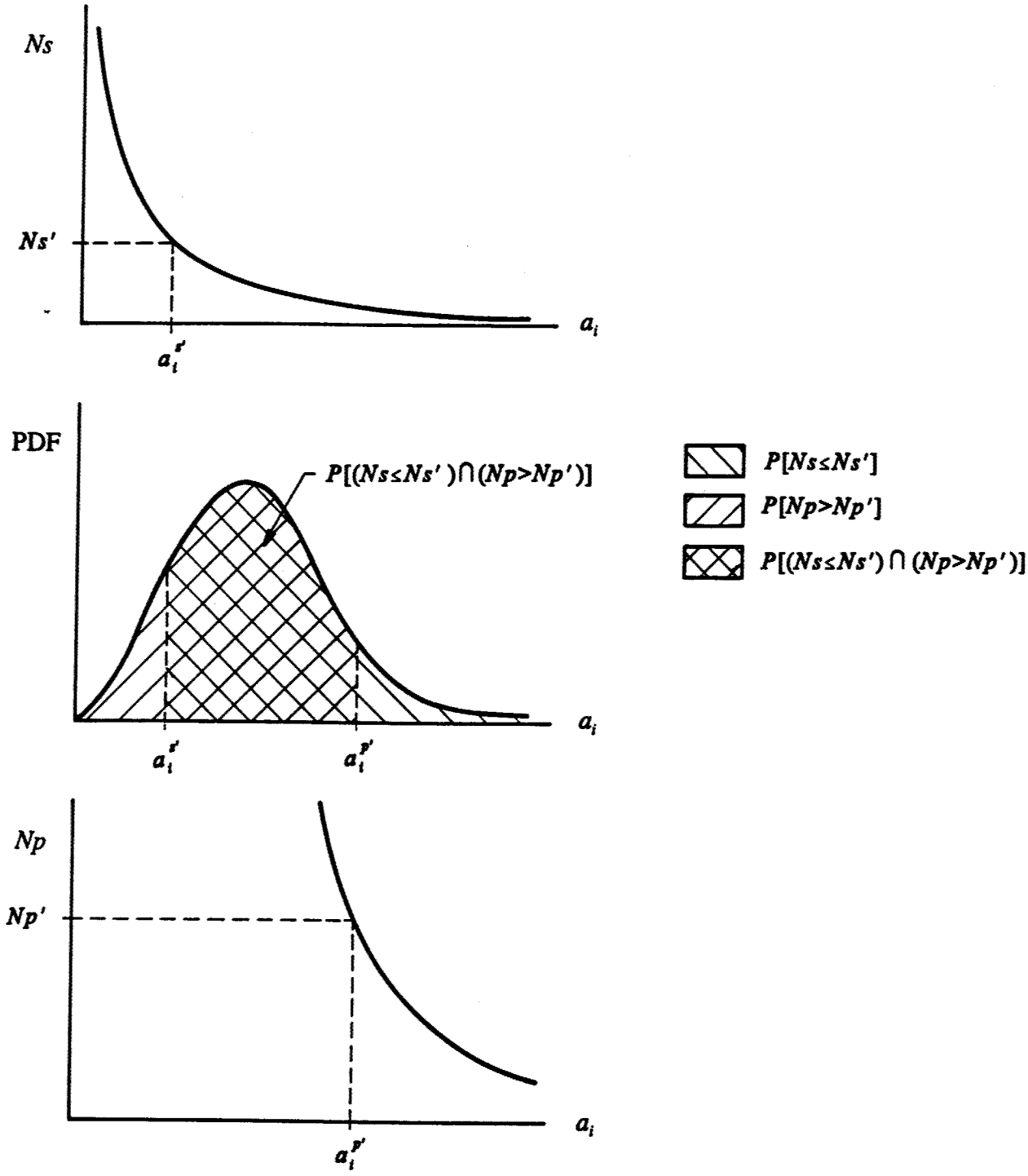

Figure 4.2. Schematic representation of calculation of $P[(Ns \leq Ns') \cap (Np > Np')]$

Analysis of crack growth during proof testing or service cycling followed the same approach. Failure during proof or service cycling was defined as either catastrophic rupture (burst) or full penetration of a crack (leak). The updated deterministic MCPT code was then linked to appropriate probabilistic analysis routines, which were taken from the general purpose NESSUS computer code originally developed at SwRI under long-term NASA funding [44].

In order to illustrate this type of analysis and the types of results which it generates, one particular sample MCPT problem was solved and illustrated with a series of graphs.

Initial Crack Depth Distribution. In this problem, each component was assumed to contain a single defect from a given distribution of initial defect depths. In Phase I, a distribution of initial crack sizes was developed from a study of SSME hardware and fabrication processes. The data sources included material test coupons, selected SSME hardware, and available multi-cycle proof failure information. A particular lognormal distribution was selected as the most accurate statistical description of the collected crack depth data.

While this lognormal form did exhibit the closest agreement with the available data based on rigorous statistical tests, further study led to the conclusion that the lognormal was not the most realistic representation of actual initial flaw size distributions in engine hardware. The lognormal probability distribution function (PDF) goes to zero for very small crack sizes. This is consistent with the collected data, because very few very small cracks were detected, measured, and recorded. However, in reality, many very small flaws were likely present but either not detected (due to the lower probability of detection for small flaws) or not recorded based on judgements about their relative significance. Therefore, a more realistic initial crack depth distribution would likely follow a monotonically increasing frequency with decreasing size. This conclusion is, in fact, very consistent with other studies of initial flaw distributions in the literature. For example, Becher and Pedersen [45], Bruckner and Munz [46], and Lidiard and Williams [47] all selected exponential distributions. Therefore, the collected crack depth data from Phase I were used to generate an exponential distribution. The collected data and the resulting exponential distribution are shown together in Figure 4.3. The mean value of this exponential distribution was 0.0212 inches.

Note that although the probabilistic analysis conservatively assumes that every component has an initial flaw, the form of the exponential distribution implies that the majority of these cracks will be negligibly small. The analysis conducted here did not evaluate the more complicated problem in which each component may itself contain a distribution of initial flaws.

Crack Shape. Each defect was assumed to have an aspect ratio of $a/c = 0.1$. The actual population of defect shapes was found to have a mean value around $a/c = 1.0$, but many actual MCPT failures are associated with much smaller a/c ratios, so this was thought to be a good choice for demonstration purposes.

In this example problem, and in later parameter studies where different initial values of a/c were considered, the crack aspect ratio was assumed to be fixed as the crack grew under

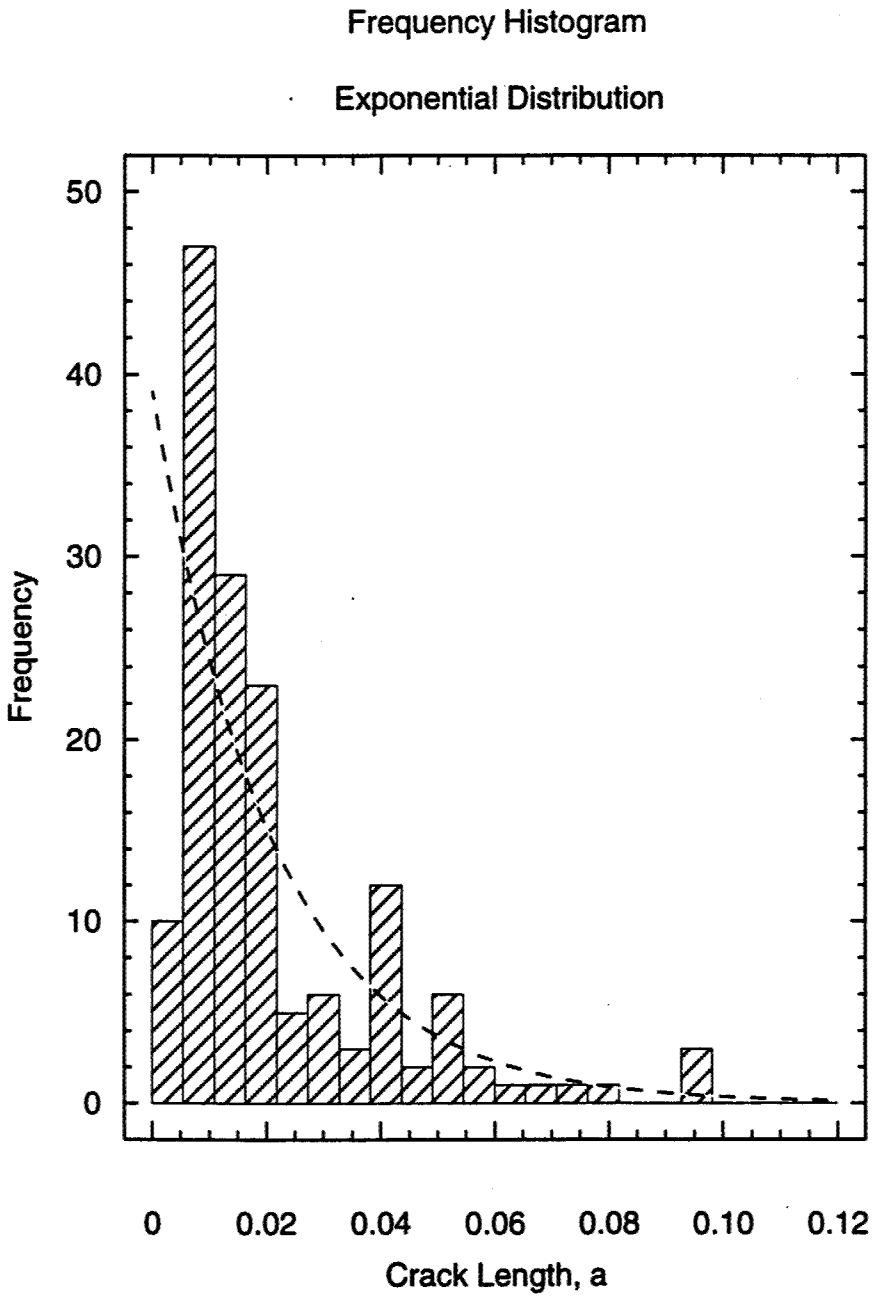

Figure 4.3 Distribution of initial crack depths and corresponding exponential distribution.

either monotonic or cyclic loading (in other words, all crack growth was one-degree-of-freedom). This was a necessary simplification to facilitate rapid probabilistic fatigue crack growth calculations, and to accommodate fundamental uncertainties about complex crack growth around the perimeter during monotonic loading (see Section 3.7.2). However, this simplification should not have a significant influence on the failure probability calculations. Although very small flaws with large aspect ratios would most certainly experience large changes in aspect ratio as the cracks grew during fatigue, these small flaws would exhibit such large propagation lives that failure probabilities during early service cycling would be negligible. The flaws which might fail during the proof test, or during the first few hundred service cycles, would have already been so large that any changes in their aspect ratio would be minor.

Material and Loading Parameters. The material was assumed to be IN-718 with monotonic Ramberg-Osgood properties (see Section 3.1). Tearing resistance was assumed to be characterized by the surface crack *J*-R curve for thin plate specimens which was determined experimentally (see again Section 3.1). The component thickness in this analysis was assumed to be 0.1 in. The proof stress was fixed at 150 ksi, with a proof factor of 1.2, so that the maximum stress in service was 125 ksi. In-service cycling was assumed to occur at a stress ratio of $R = 0$. Proof testing was simulated for 1 cycle, 5 cycle, and 20 cycle protocols.

Results of the Example Problem. The PDFs of initial and (calculated) final crack depths after N proof cycles is shown in Figure 4.4 (the $N = 0$ data correspond to the initial distribution before proof testing). Proof testing caused a significant decrease in the probability that a large crack remains in the component, primarily because components with large cracks failed during the proof test. The probability of having a remaining large crack continued to decrease with larger numbers of proof cycles. However, note that the largest possible flaw size remaining in the component (the upper limit on the final crack size distribution) after a single proof cycle did not change (either increase or decrease) with additional proof cycles.

The analysis procedure assumed that if a component fails during the proof test, it will be replaced with a new component, drawn from the same initial population, which is also subjected to a proof test. Therefore, at the end of the proof test, the total number of components (and therefore the total number of cracks) are the same as before the proof test. However, the cracks that remain are more likely to be small cracks. This is reflected in the PDFs, which indicate a higher probability that a small crack exists in the component following proof testing.

The same data is expressed in an alternative form in the cumulative distribution function (CDF) of crack size as a function of N proof cycles, Figure 4.5. This figure shows more clearly that as the number of proof cycles increases, there is a steadily increasing cumulative probability that the remaining crack will be small, and therefore a steadily decreasing cumulative probability that the remaining crack will be large.

Following proof testing, the maximum simulated stress was decreased to 125 ksi, and cycling proceeded at this level until the component fails in service. The final crack size at the end of the proof test was taken to be the crack size at the beginning of the service cycling.

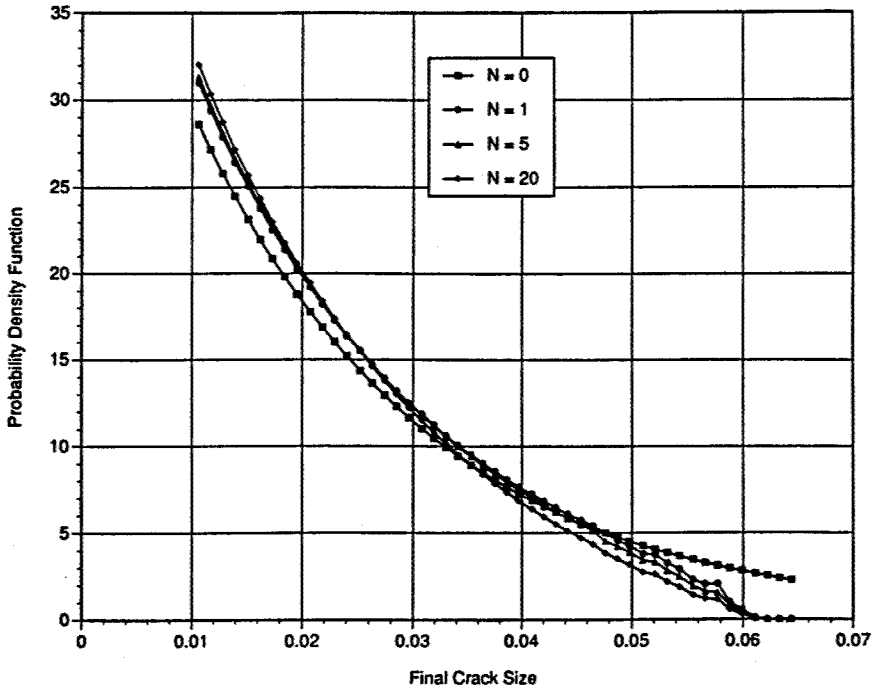

Figure 4.4. PDF of crack depth before and after proof testing for a sample problem

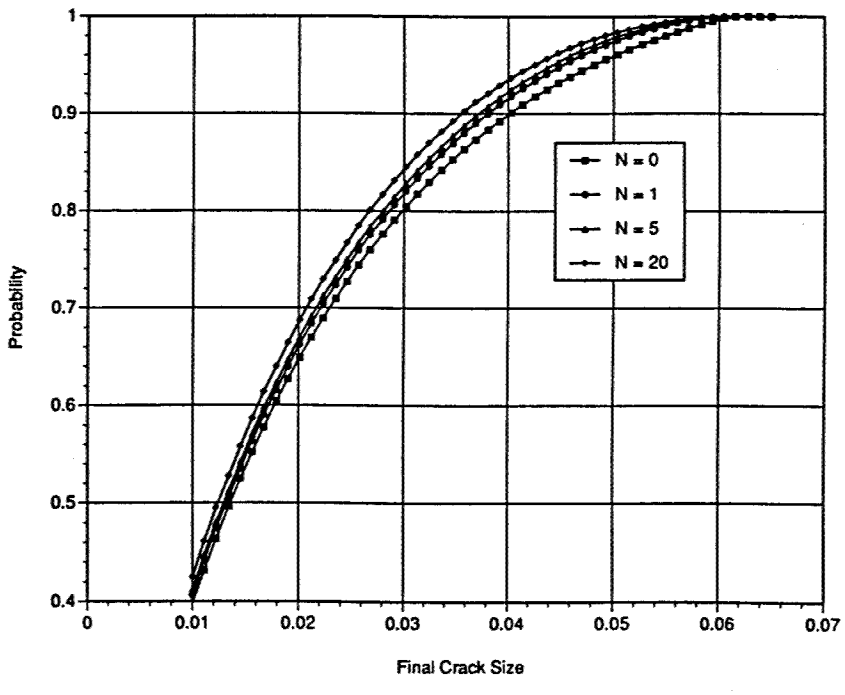

Figure 4.5. CDF of crack depth before and after proof testing for a sample problem

The number of service cycles to failure was calculated as a function of the initial crack size *before* proof testing, and the results of this deterministic computation are shown in Figure 4.6 for different proof test protocols. Naturally, if the initial crack size is larger, the remaining service life will be shorter. This figure, which essentially describes the behavior of a single component which does not fail during the proof test, illustrates an important result. As the number of proof cycles increases, the remaining life in service for that particular (nonfailing) component decreases. This is because an increasing number of proof cycles causes an increasing amount of crack growth during the proof test, assuming the same initial flaw size before the proof test. In short, if a component does not fail during the proof test, then any existing defects have been made larger by subjecting the component to a larger number of proof cycles. Therefore, it is not generally possible to justify multiple cycle proof testing by considering only individual components that survive the proof test.

However, the true test of MCPT vs. single-cycle proof testing (or vs. no proof testing at all) is the effect of proof testing on the total population of components. Although proof testing may have made some (nonfailed) components slightly worse, proof testing has also removed some components with large flaws from the population. Figure 4.4 indicated that increasing numbers of proof cycles removed more large flaws from the population. The question is how those two different effects (some components worse, some components with large flaws screened) interact to influence the overall probability that the component will fail in service.

This question is answered, at least for this particular problem, by Figure 4.7. Here is shown the probability of failure in service as a function of service cycles, given that the component survived the proof test. Naturally, as the number of service cycles increases, the probability of failure in service increases. For this particular problem, an increasing number of proof cycles is shown to lead to a steadily decreasing probability of in-service failure at all life levels. In other words, for this particular problem, MCPT is better than SCPT if the fleet of components is considered. On the average, for this particular problem, if a large number of proof cycles are conducted, more good is done by removing more large flaws from the population than harm is done by growing small flaws to larger sizes.

These calculations also indicate that the incremental benefit of additional proof cycles steadily decreases with increasing numbers of proof cycles. See Figure 4.8, which shows how the probability of failure changes with number of proof cycles. The first proof cycle provides most of the improvement in service reliability. Additional proof cycles provide some further decrease in failure probability, but the difference becomes smaller and smaller for larger numbers of proof cycles.

This numerical model makes it possible to perform a wide range of parameter studies. As changes are made in the assumptions or input values relative to initial flaw distribution, tearing resistance, constitutive properties, flaw shape, J vs. a relationship, etc., the probabilistic model will indicate when MCPT is preferable and when it is not preferable.

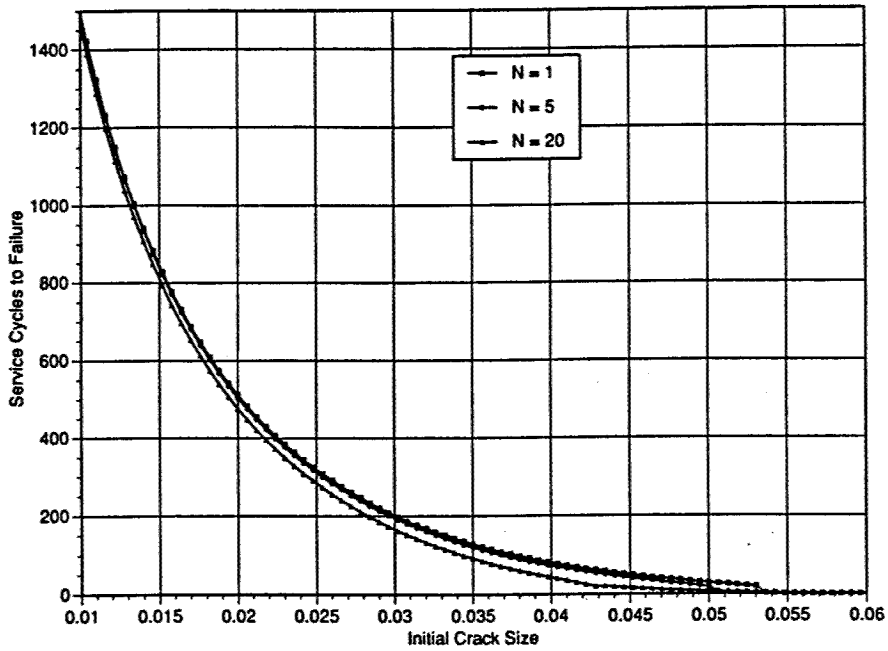

Figure 4.6. Service cycles to failure as a function of initial crack depth for a sample problem

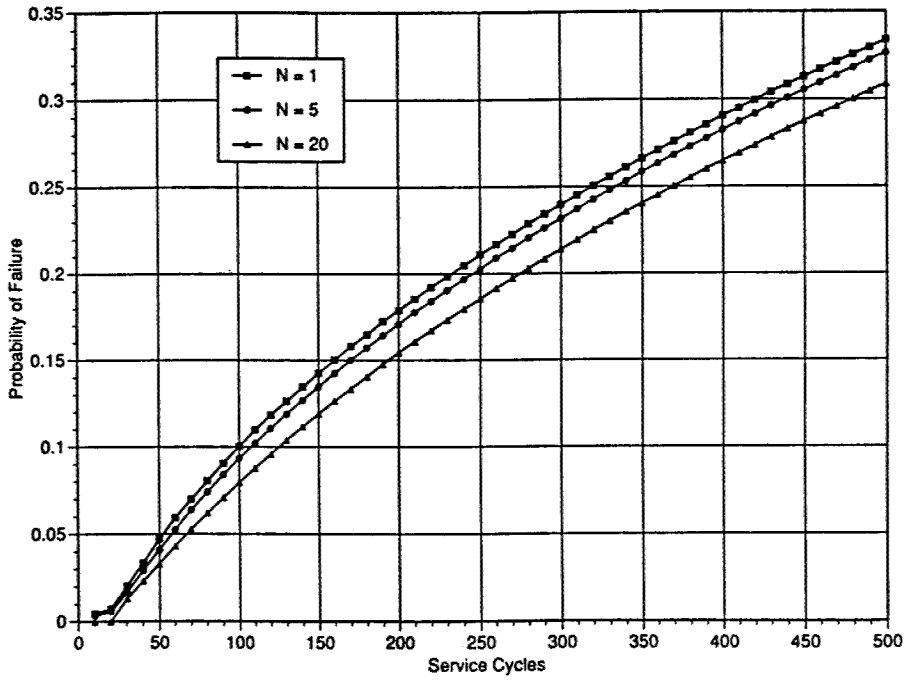

Figure 4.7. Probability of failure as a function of service cycles for a sample problem

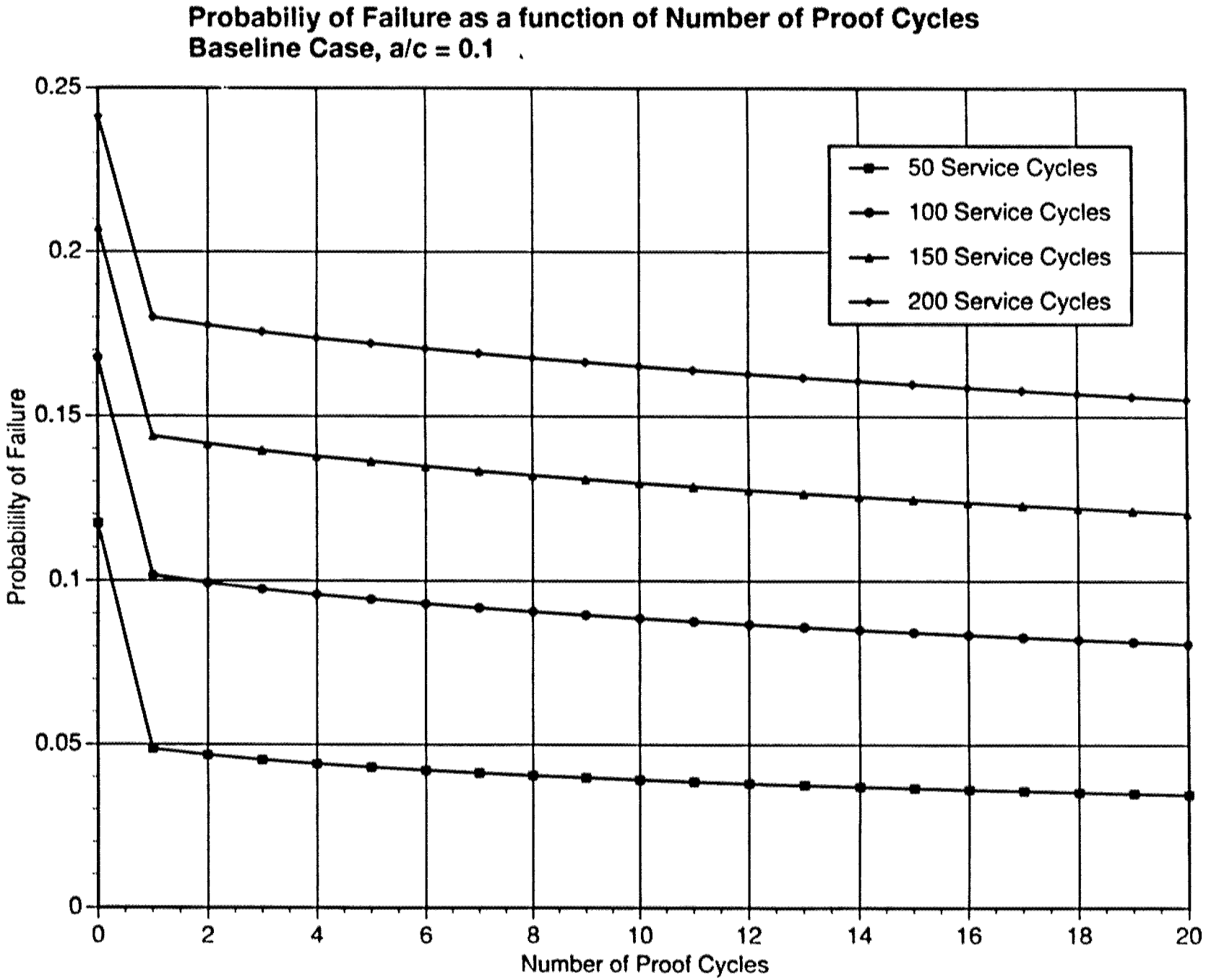

Figure 4.8. Probability of failure in service as a function of number of proof cycles for a sample problem

It must be emphasized that in the example problem above, and in all the parameter studies below, the absolute values of "probability of failure" in service are entirely artificial and should not be interpreted as representing actual probabilities of failure for actual hardware. The numbers are artificially high due to the assumption that every simulated component contains a "worst-case" defect with shape $a/c = 0.1$, and that every component is stressed uniformly to a severe level. These assumptions were useful to insure that the probabilistic studies were focused on applications in which proof test failure was an important issue. However, *relative* comparisons of failure probability between different analyses may be of some value.

4.4 Parameter Studies

A series of parameter studies were conducted in which one parameter at a time was systematically varied, typically considering one "high" and one "low" value of the chosen parameter while keeping all other parameters at standard, moderate values. For example, proof factors of 1.1 and 1.3 were considered while keeping the R curve, initial crack size distribution, crack shape, and stress-strain relationship fixed. Each of those other parameters was also exercised in turn. In the following paragraphs, the trends observed from these parameter studies are summarized. All possible combinations of different parameters could not be evaluated, however, and so the complete generality of all observations cannot be guaranteed.

Effect of Proof Factor. When the proof factor (proof load/service load) is smaller, the first proof cycle produces a smaller improvement in in-service reliability, but subsequent cycles appear to offer some significant additional improvement. When the proof factor is larger, the first cycle has a larger impact on the in-service reliability, and subsequent cycles offer relatively less further improvement. See Figure 4.9, which compares the CDF of in-service failure probability following 0, 1, 5, and 20 proof cycles for proof factors of 1.1 and 1.3.

Effect of Tearing Resistance. Material resistance to stable tearing, as characterized by the J-resistance curve, appears to have a similar effect. When tearing resistance is relatively low, the first proof cycle increases in-service reliability significantly, and subsequent cycles lead to little further improvement. When tearing resistance is relatively high, the first cycle is relatively less effective and the succeeding cycles more effective (but still less effective than the first cycle on a per-cycle basis). These trends are illustrated by Figure 4.10, which compares CDFs for the compact tension specimen R-curve (relatively low tearing resistance) and an approximate upper bound resistance curve derived from the fatigue crack growth curve (see Figure 3.3 in Section 3).

Combined Effect of Proof Factor and Toughness. A study of simultaneous changes in both the proof factor and material toughness suggests that the net effect of the two parameter variations is not significantly different from the effect of either parameter variation independently. Figure 4.11(a) shows the results for a low toughness resistance curve and a large proof factor, while Figure 4.11(b) shows the results for a high toughness resistance curve and a small proof factor.

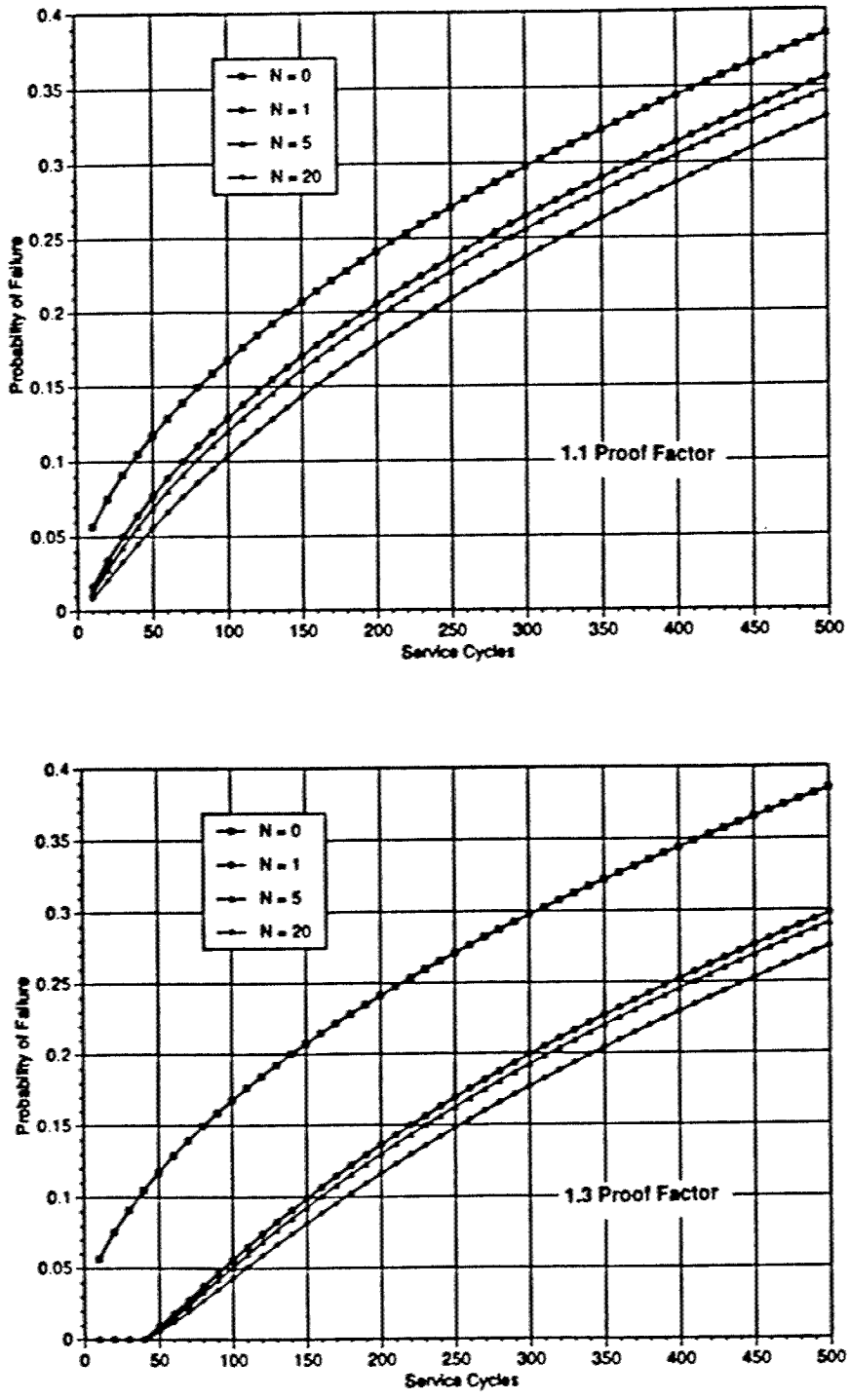

Figure 4.9 CDF of in-service failure probability after different numbers of proof cycles (N), conditional on proof test success, for proof factor of 1.1 (top) and 1.3 (bottom)

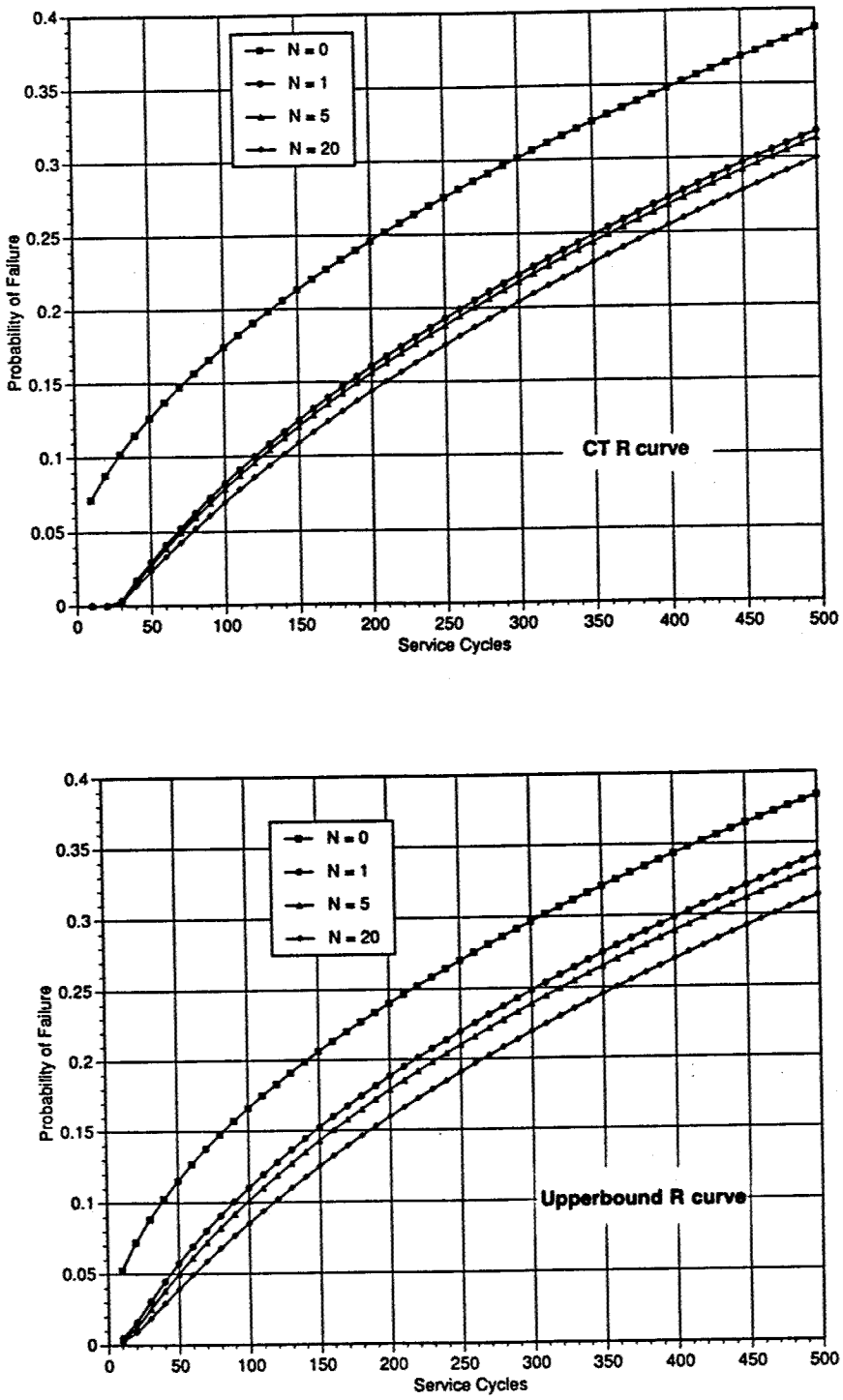

Figure 4.10. CDF of in-service failure probability after different numbers of proof cycles (N), conditional on proof test success, for low tearing resistance (top) and high tearing resistance (bottom)

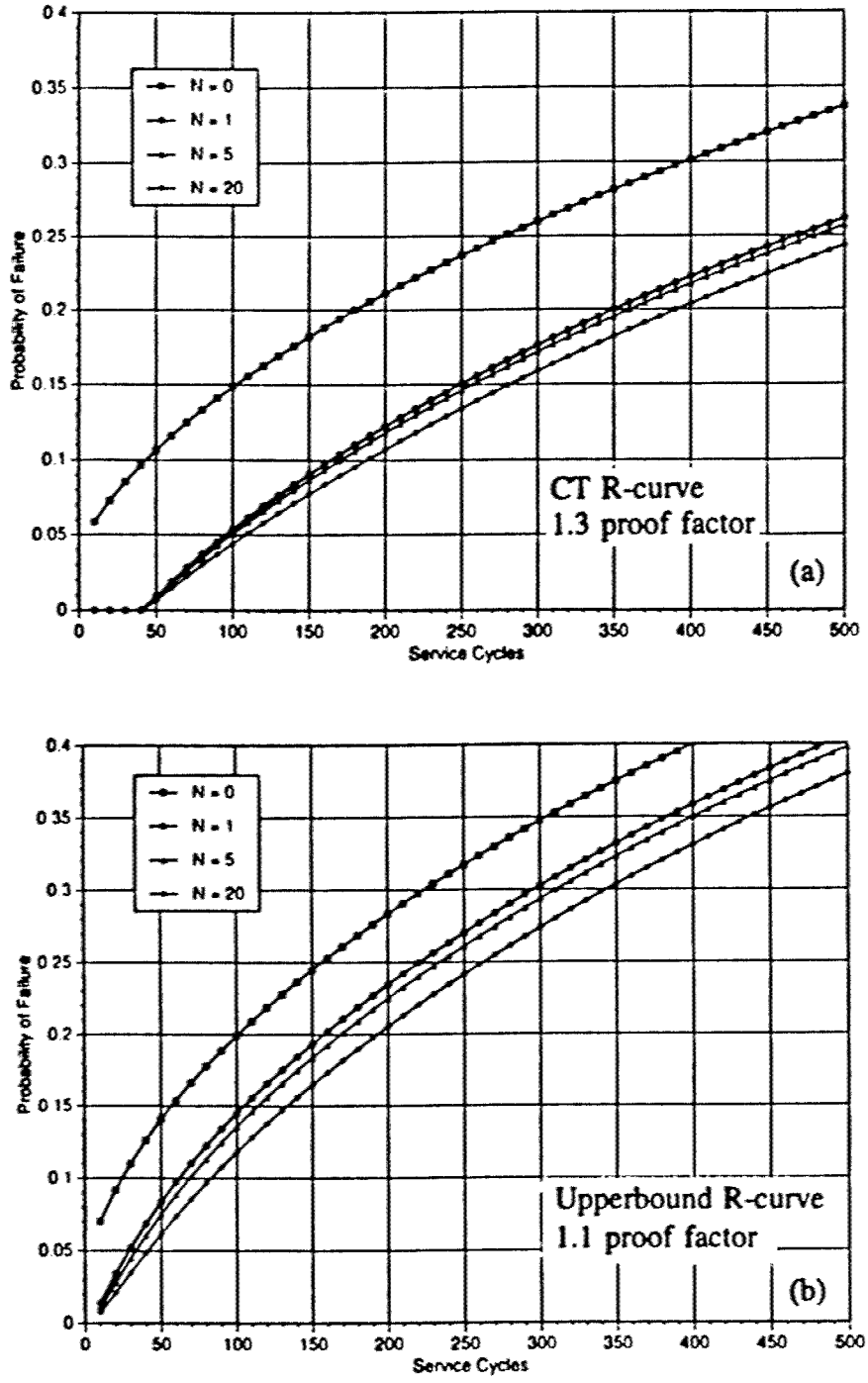

Figure 4.11. CDF of in-service failure probability after different numbers of proof cycles (N), conditional on proof test success
(a) CT R-curve and 1.3 proof factor
(b) upper bound R-curve and 1.1 proof factor

Effect of Material Stress-Strain Curve. A significant change in the material stress-strain curve alone does not appear to have much of an effect on proof test efficacy, for the parameter combinations considered in this study.

Effect of Crack Shape. Most analyses of MCPT behavior conducted in the recent history of the program have focused on long, shallow flaws (aspect ratio typically $a/c = 0.1$). These are the flaw geometries which have been shown by analysis and experience to be most likely to fail during proof testing, especially multiple cycle proof testing. Rocketdyne experience, as documented in Table 1 of the Phase I report, is that pre-existing defects which could be identified after a multiple cycle proof testing failure typically exhibited high aspect ratios. Experimental and analytical studies conducted in the current program have shown that for high toughness materials such as Inconel 718, small aspect ratio flaws are not likely to fail unless applied stresses are extremely high (greater than yield) or the cracks are extremely large. High aspect ratio flaws, for which the crack driving force is considerably higher at the same crack depth, are more likely to fail at more reasonable applied stresses.

However, the majority of defects in actual hardware will have relatively smaller aspect ratios. A study of actual material defects from Rocketdyne experience (selected SSME hardware, available MCPT proof failure information, and material test coupons) found that the predominant crack shape was roughly semicircular ($a/c = 1$). This study was also reported in the Phase I report. Therefore, the behavior of these more typical defects during MCPT is also important.

To address this issue, MCPT parameter studies were conducted in which a/c was varied while all other variables were held constant. Results are shown in Figure 4.12 for a/c values of 0.1, 0.2, and 0.5. For larger values of a/c, the probabilities of failure are much lower for all scenarios (no proof test, or different numbers of proof cycles). Proof testing of any type (single cycle or multiple cycle) is also of relatively less benefit, and multiple cycle testing offers relatively little advantage over single cycle testing. In fact, for $a/c = 0.5$, some probabilities of failure in service were actually found to be marginally higher for larger numbers of proof cycles. However, it must be emphasized that the differences were extremely small, and that the total probabilities of failure are significantly lower (an order of magnitude) than the baseline case considered in Section 4.3. See Figure 4.13, which shows the probability of failure in service as a function of number of proof cycles for the $a/c = 0.5$ case.

Effect of Crack Size Distribution. Nearly all MCPT parameter studies to date have been based on a particular crack size distribution which was derived from analysis of the Rocketdyne flaw data cited earlier. As noted earlier, a particular exponential distribution has been employed in the Phase II analysis. Of course, the actual distribution of defects in a given population of components will certainly differ from this single prototypical distribution, and in general the actual distribution will not be known. The key question for MCPT analysis is how different initial defect distributions may impact the suitability of different MCPT protocols. In order to investigate this question further, a number of MCPT analyses were conducted in which different initial crack depth distributions were assumed. For the purposes of this study, all other variables (including crack aspect ratio, $a/c = 0.1$) were held constant at baseline values.

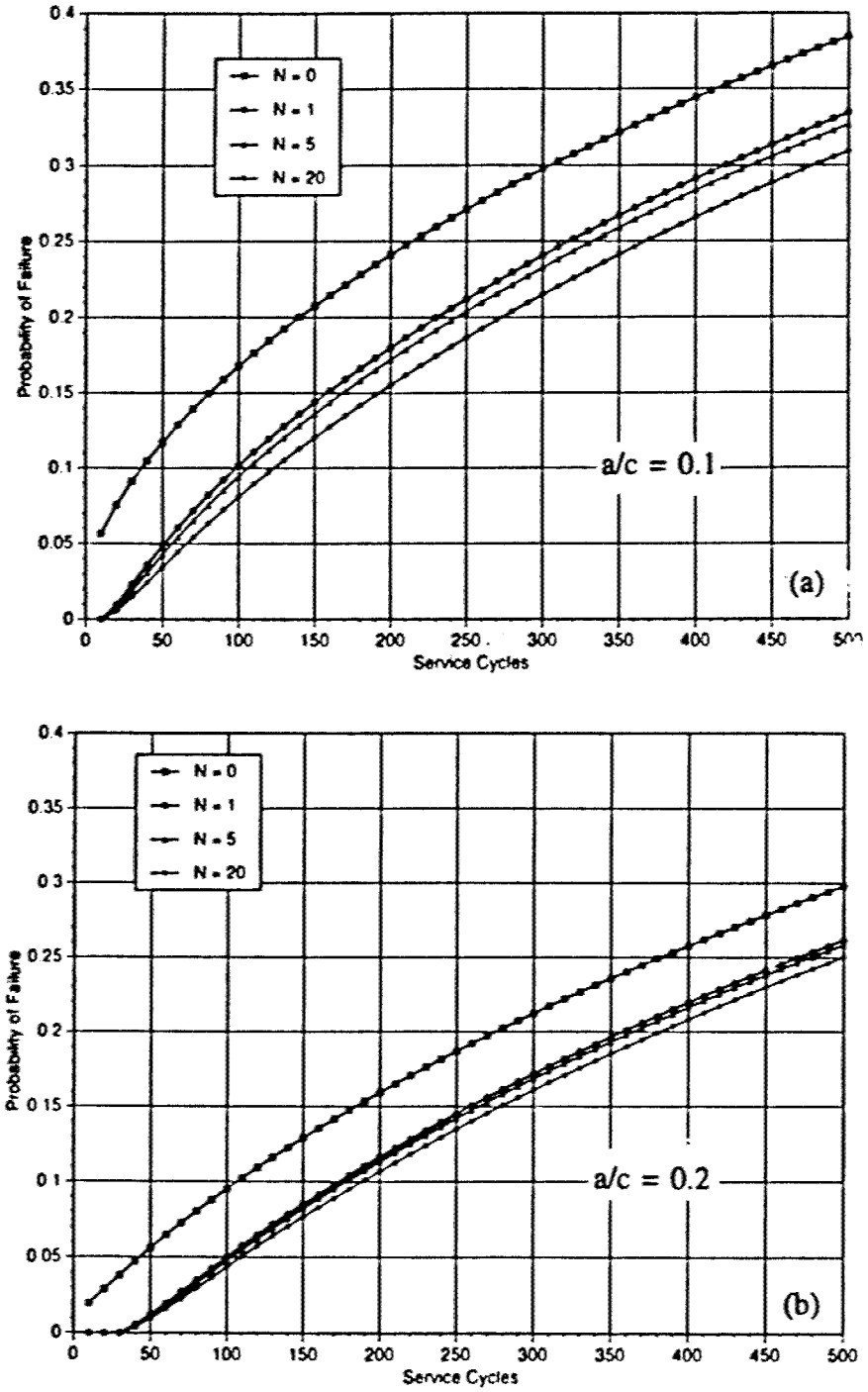

Figure 4.12. CDF of in-service failure probability after different numbers of proof cycles, conditional on proof test success

(a) $a/c = 0.1$

(b) $a/c = 0.2$

(c) $a/c = 0.5$

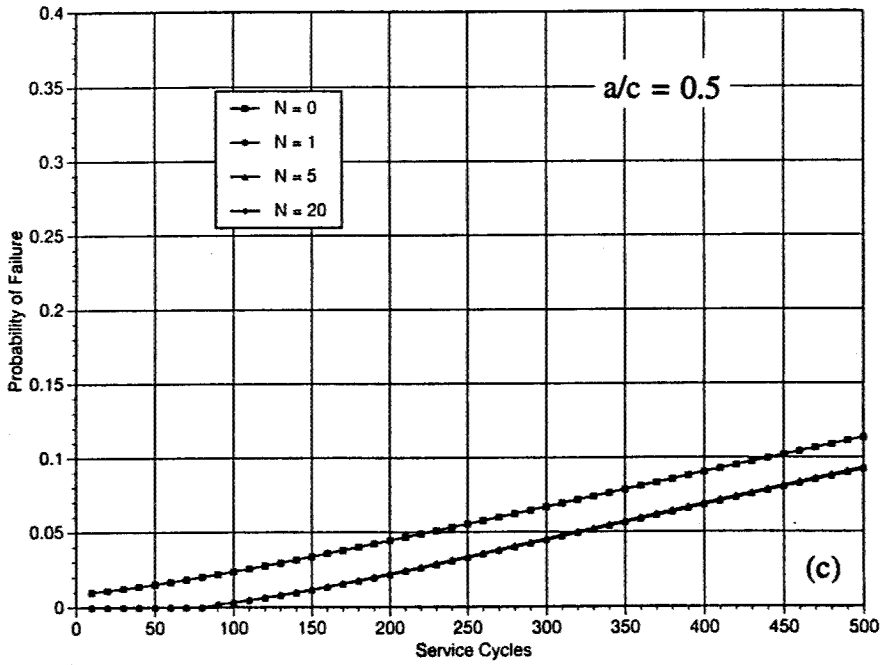

Figure 4.12. CDF of in-service failure probability after different numbers of proof cycles, conditional on proof test success (Cont.)
(a) $a/c = 0.1$
(b) $a/c = 0.2$
(c) $a/c = 0.5$

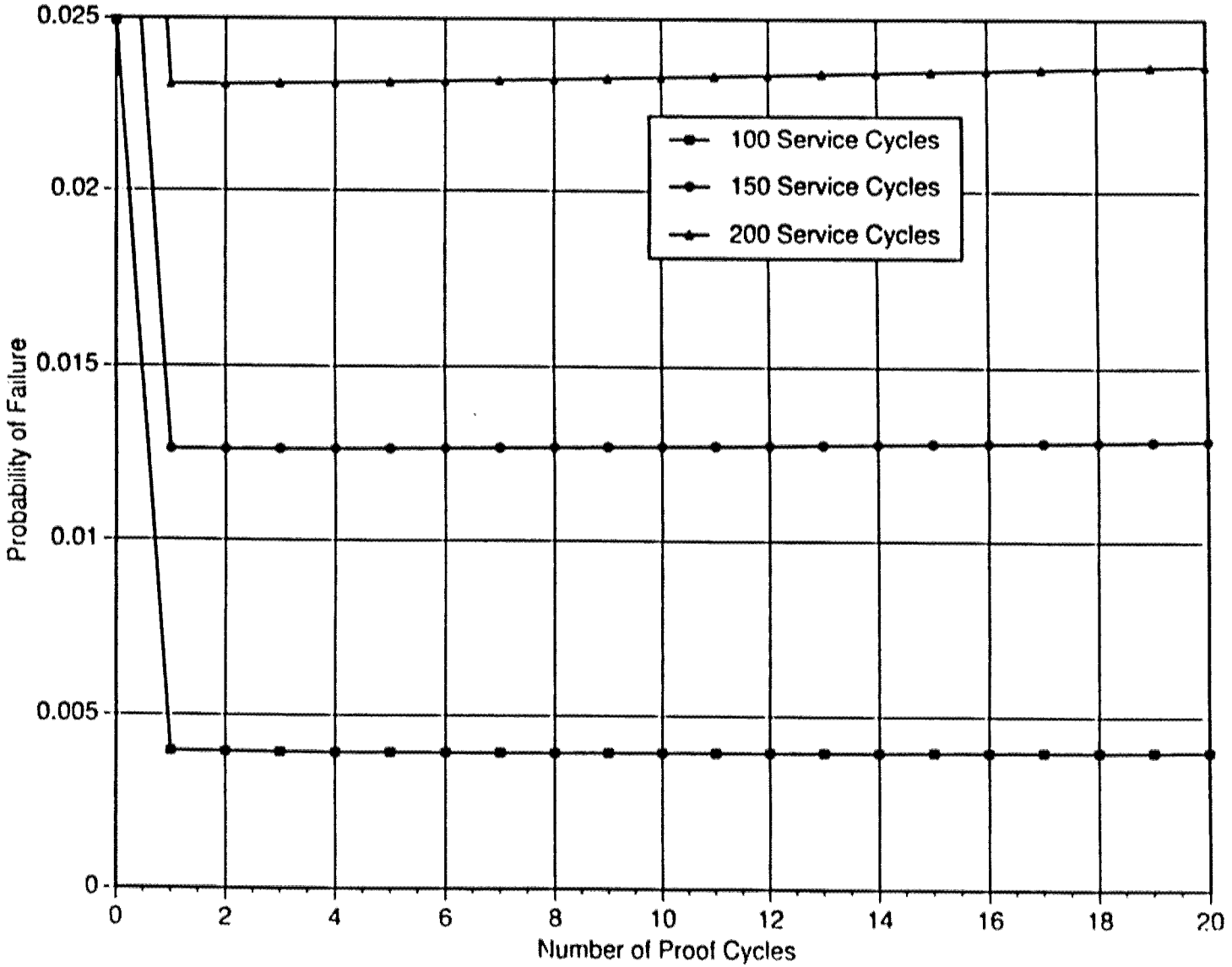

Figure 4.13. Probability of failure in service as a function of number of proof cycles for $a/c = 0.5$ example

One set of analyses considered three different exponential distributions for initial crack depth (before any proof testing). The baseline distribution has a mean value very nearly equal to $a = 0.02$ in. Alternative exponential distributions with mean values of $a = 0.01$ and $a = 0.08$ were also employed as inputs to the MCPT analysis. The cumulative distribution functions (CDFs) and probability density functions (PDFs) for these three exponential forms are shown in Figure 4.14.

Resulting calculations of in-service reliability are shown in Figure 4.15 for the two new distributions (compare Figure 4.12(a) for the baseline distribution). When nearly all cracks are extremely small, Figure 4.15(a), proof testing is of very little value in improving the reliability in service. Closer inspection of the data reveals that 5 cycle proof testing yields slightly lower probabilities of failure than single cycle testing, and 20 cycle proof testing slightly higher probabilities of failure than single cycle testing, but these differences are so small as to be negligible. When flaws are extremely small, proof testing has essentially no impact --good or bad--on reliability in service. When many cracks are large, Figure 4.15(b) (note change in scale), proof testing is shown to have a large impact on in-service reliability, as would be expected. Of greater interest, multiple cycle testing appears to offer some significant additional benefit beyond single cycle testing, and this relative benefit appears to increase with larger numbers of proof cycles.

A second set of analyses of crack size distribution effects employed three different Weibull distributions. The Weibull distribution is a more general mathematical function than the exponential distribution and is characterized by both a "scale parameter" and a "shape parameter." The shape parameter, β, describes the fundamental form of the distribution. When $\beta = 1$, the Weibull distribution is the same as an exponential distribution. In this brief study, distributions with $\beta = 0.5$, 1, and 2 were considered. The $\beta = 1$ distribution was chosen identical to the original baseline exponential distribution, so only two new initial crack size distributions were analyzed. The CDFs and PDFs for these three Weibull distributions are shown in Figure 4.16. Note that the three Weibulls were constructed in such a way that the cumulative probability of occurrence was identically equal to 0.95 at $a = 0.06$ in. for all three distributions. In other words, 95% of all cracks were smaller than 0.06 in. deep for all three distributions.

The computed values of in-service failure probability from the usual MCPT probabilistic analysis for the two new runs are shown in Figure 4.17 (again compare Figure 4.12(a) for the results from the baseline $\beta = 1$ case). Although total failure probabilities differ dramatically for the three input distributions, proof testing has a strikingly similar effect on failure probability in all three cases. A single proof cycle decreases failure probabilities about 0.05, and additional proof cycles decrease the failure probability by incrementally smaller values. This is an encouraging result, if it is in fact general, because it suggests that the relative merits of SCPT and MCPT are not strongly influenced by specific assumptions made about the form of the initial crack size distribution.

In general, these parameter studies showed that when MCPT is consistently applied to a fleet of components containing a distribution of initial flaws, the overall fleet reliability will be

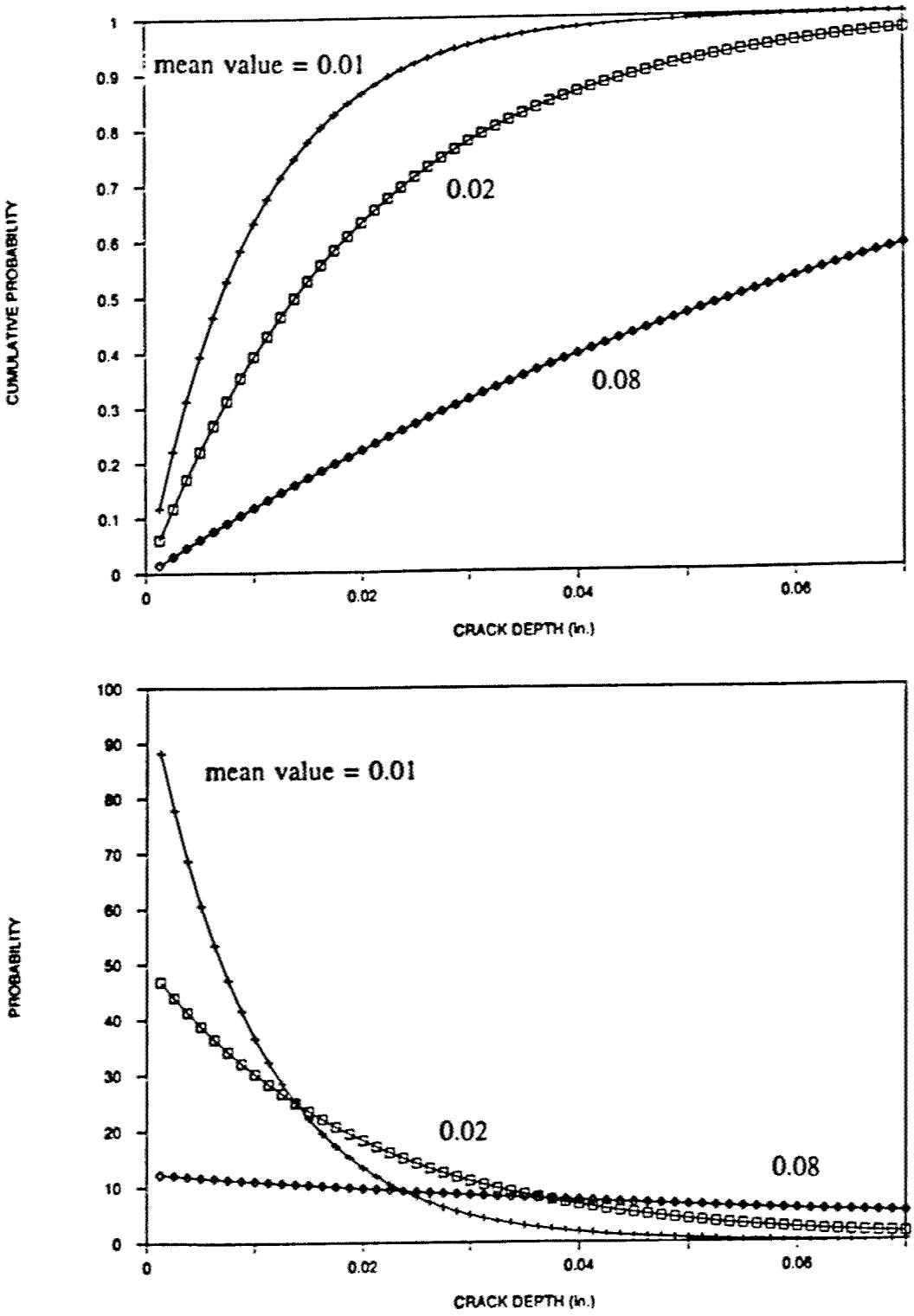

Figure 4.14. Cumulative distribution functions (top) and probability density functions (bottom) for three exponential distributions of initial crack depth

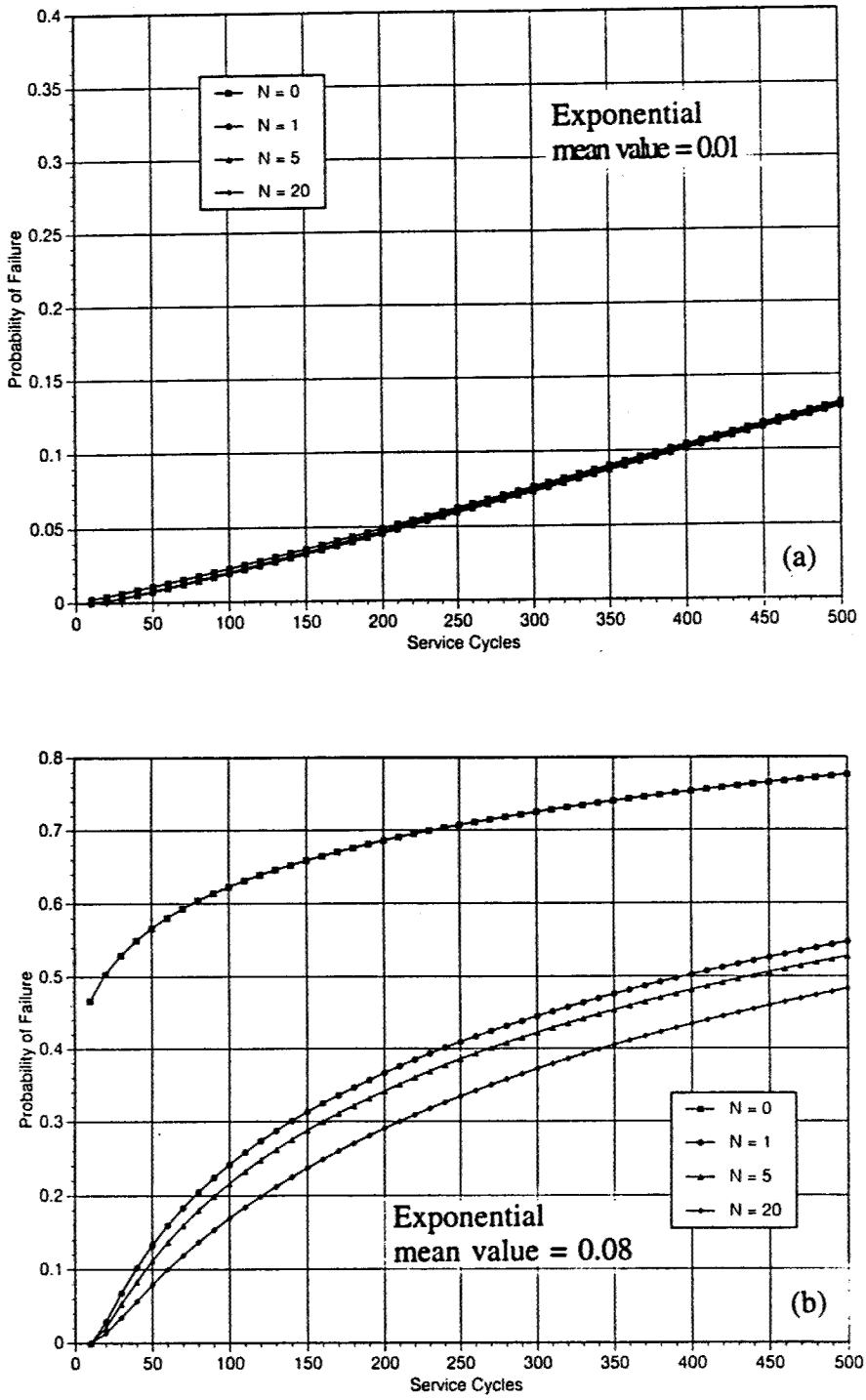

Figure 4.15. CDF of in-service failure probability after different numbers of proof cycles, conditional on proof test success

(a) exponential distribution with mean value a = 0.01 in.

(b) exponential distribution with mean value a = 0.08 in.

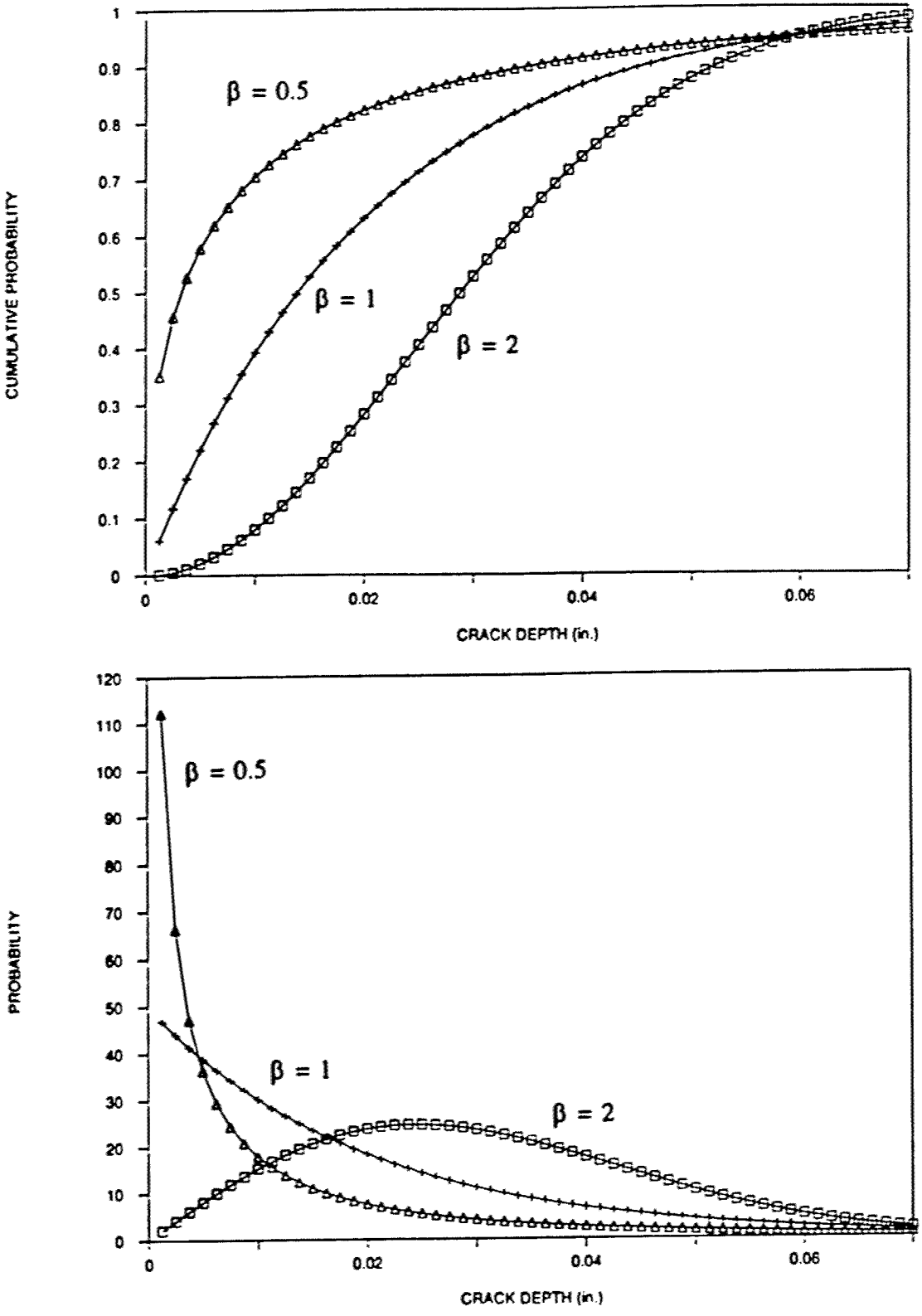

Figure 4.16. Cumulative distribution functions (top) and probability density functions (bottom) for three Weibull distributions of initial crack depth

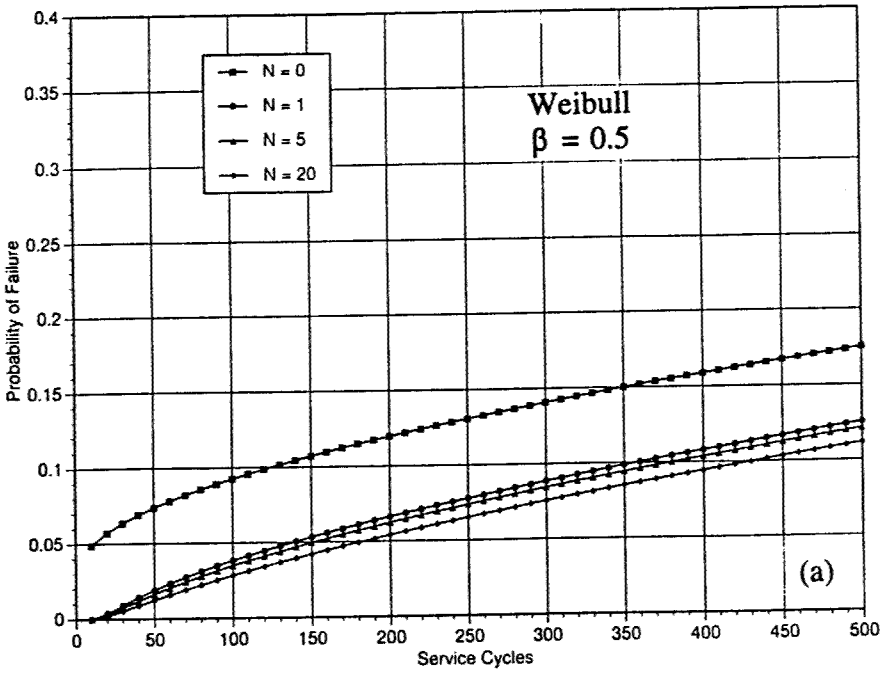

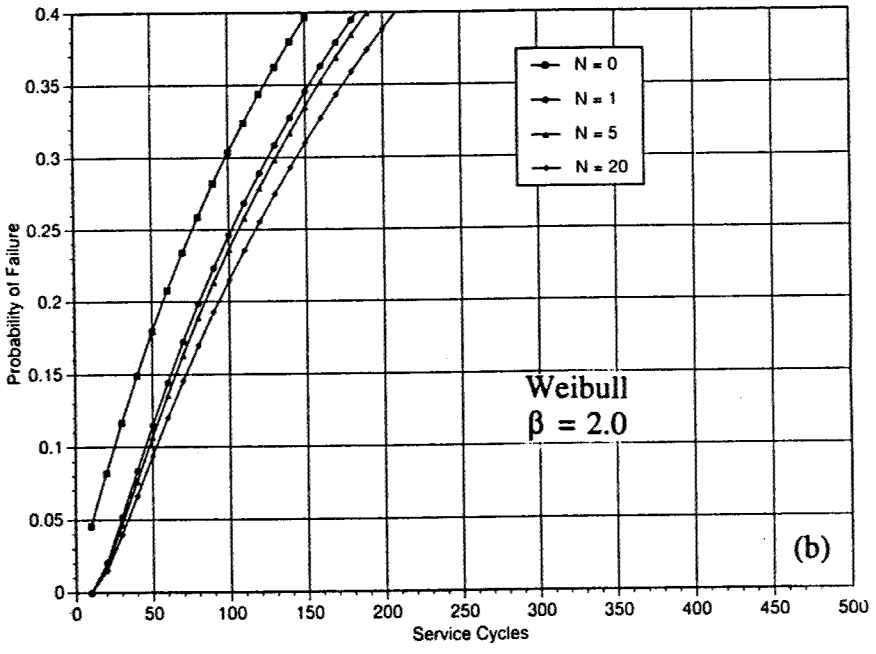

Figure 4.17. CDF of in-service failure probability after different numbers of proof cycles, conditional on proof test success
(a) Weibull distribution with shape parameter $\beta = 0.5$
(b) Weibull distribution with shape parameter $\beta = 2.0$

higher for a population of components that have been subjected to MCPT than for a population of components that have been subjected to SCPT at the same proof load. From the standpoint of in-service reliability, more good is done by removing a few additional large flaws from the population than harm is done by incremental growth of many small flaws in the population. This benefit generally increases with increasing numbers of proof cycles, although the incremental benefit of additional proof cycles decreases with increasing numbers of cycles. In some cases, the improvement produced by the subsequent cycles is negligible for all practical purposes.

On the other hand, the parameter studies indicated that from the standpoint of in-service fleet reliability, MCPT can be inferior to SCPT, albeit negligibly so, when the probability of failure due to any proof loading is itself negligibly small. This situation may arise, for example, when the proof loads are relatively small, the possible crack sizes are relatively small, and the material is relatively tough, so that the driving force for crack extension is substantially lower than the material toughness. In this situation, the potential benefit to be gained by removing additional large flaws from the population is negligibly small. Therefore, the additional subcritical crack growth caused by the additional proof cycles will reduce net in-service reliability. However, in most cases, this decrease in reliability will also be negligibly small. Therefore, while MCPT is of no additional benefit in this situation compared to SCPT, it can be regarded as being of no additional detriment, either.

4.5 Cracks at Notches

An elastic-plastic J estimation computer software module for a crack at a hole was incorporated into the probabilistic MCPT/NESSUS computer code. This module was based on a new J estimation technique developed under the EPFCG contract, and documented in Section 2.2. The computer code was then used to study the relative influence of different numbers of proof cycles on in-service reliability following a successful proof test. In this report, some sample results are shown in order to illustrate the observed trends.

The J solutions were based on a double edge notched plate, with small through-cracks growing out of the notch roots. This was a convenient geometry for the generation of FE J solutions, against which the simple estimates could be validated, and the general results are expected to be typical of a variety of similar notched configurations. A schematic of the notch geometry was shown previously in Figure 2.3. These studies focused on a notch with $D/R = 2.41$ and stress concentration factor, $K_t = 4.29$. The exponential distribution of initial crack depths used in previous studies (see Section 4.3) was implemented here as the initial distribution of crack size, d, measured from the root of the notch. The half-width of the notched plate, b, was chosen as 1 in., and the notch depth, D, was fixed at 0.3 in.

Several different loads and resistance curves were explored, along with some variations in the mean value of the initial crack size distribution. The proof factor was 1.2 in all analyses discussed here. The stress-strain relationship was the same set of Inconel 718 monotonic Ramberg-Osgood properties used in the previous parameter studies.

As anticipated, the notches brought about some differences in some of the SCPT vs. MCPT comparisons. These differences are clearest in one of the extreme cases examined. Figure 4.18 shows the usual comparison of failure probability in service vs. number of service cycles following different numbers of proof cycles. In this case, the nominal proof stress was 100 ksi, so extreme yielding occurred at the root of the notch (remember $K_t = 4.29$). A resistance curve with a low tearing modulus (the CT R-curve) was employed. The mean value of the exponential distribution of initial crack depth was increased from $d = 0.02$ in. to $d = 0.05$ in. Figure 4.18 indicates that, in this case, a larger number of proof cycles (1 to 5 to 20) leads to a higher probability of failure in service. In the extreme case of 20 proof cycles, in-service reliability after about 200 service cycles is actually worse than without any proof test.

The calculated elastic, plastic, and total values of the J-integral under these same conditions (100 ksi) are presented in Figure 4.19. Ductile fracture is driven by the total J value, while fatigue crack growth under zero-max cycling is driven by ΔJ, which is approximately equal to the elastic J under these conditions. As a reference point, the critical crack size for ductile fracture with the CT R-curve is about $d = 0.17$ in. at 100 ksi. Note that the total J value is relatively large and increases only slightly with crack length for cracks which are relatively close to the notch root (esp. for $d < 0.15$ in.). This trend is, to some degree, a reflection of the intermediate control condition in the notch vicinity, where local deformation introduces a form of secondary loading somewhat akin to displacement control. This shape of the J-a curve means that, for cracks in this size range, it is possible for the crack to grow substantially without significantly increasing the chance that it will fail. Therefore, additional proof cycling is more likely to cause additional damage to the structure without failing additional defective structures.

When the cracks are larger compared to the notch field, these notch effects on the crack tip driving force become less important. The studies of J solutions for cracks at notches (Section 2.2) found that the notch field had effectively no influence on J for cracks that were larger than 30 to 50 percent of the notch root radius. The J solution for these longer cracks growing from a notch root was the same as the J solution for a crack of the same total length (the sum of the notch depth and crack length) in an unnotched body. Therefore, the notch effect on MCPT behavior would be negligible.

At a lower applied stress (50 ksi proof stress), keeping all other variables constant, increasing numbers of proof cycles still lead to an increase in in-service failure probability, but on a much-diminished scale. See Figure 4.20. Note that here all of the failure probabilities are extremely small numbers, and the differences between different numbers of proof cycles are minimal. One might conclude in this situation that, although additional proof cycles are more damaging, the effect is entirely negligible.

4.6 Memory vs. Loss-of-Memory in Tear-Fatigue Theory

The tear-fatigue model employed in the current MCPT/NESSUS computer code effectively describes crack growth during concurrent fatigue cycling and ductile tearing. The model has

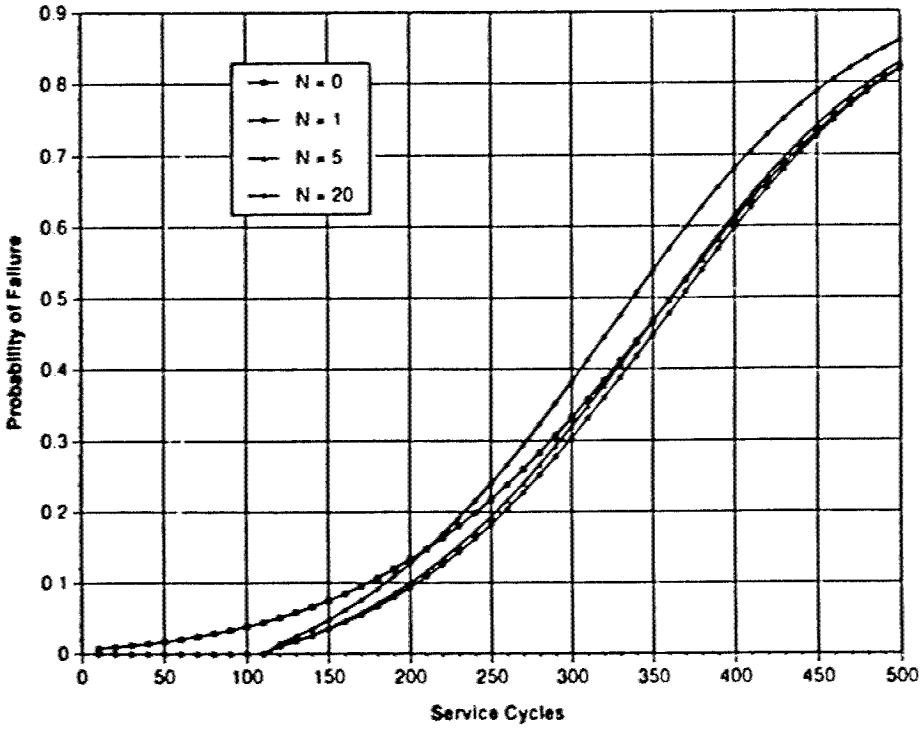

Figure 4.18. CDF of in-service failure probability after different numbers of proof cycles; notched geometry, 100 ksi proof stress, a_i = exp[.05]

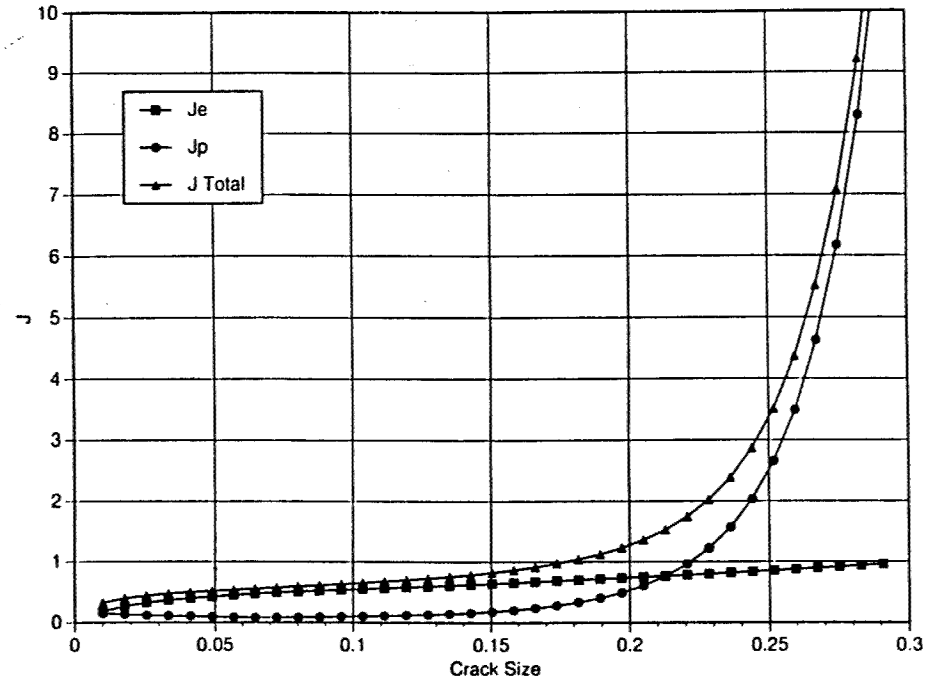

Figure 4.19. Total, elastic, and plastic J values for cracks emanating from double edge notches with 100 ksi nominal stress

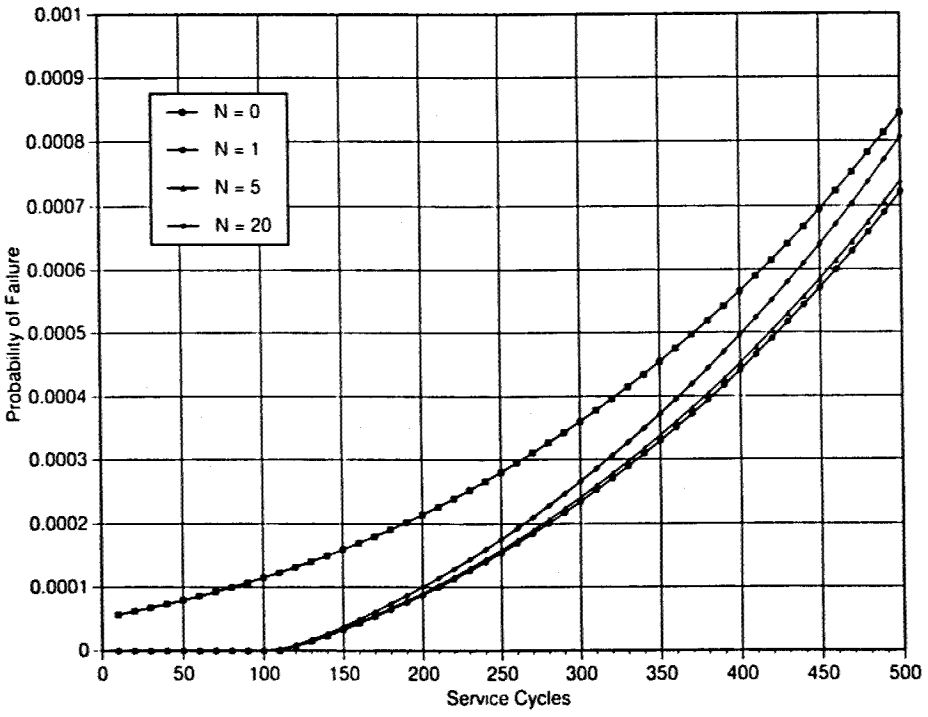

Figure 4.20. CDF of in-service failure probability after different numbers of proof cycles; notched geometry, 50 ksi proof stress, a_i = exp[.05]

been validated for several materials, including IN-718, under conditions in which dJ_{max}/dN increases on each cycle or remains approximately constant with cycling. In short, tear-fatigue theory requires that once tearing has initiated, additional ductile tearing does not occur on subsequent fatigue cycles until J_{max} increases beyond its previous maximum value.

Tear-fatigue behavior following step changes in applied load, such as the step decrease which occurs between proof loading and subsequent service cycling, has not been studied to the same extent. One key question is whether fatigue (service) cycling at the lower load level must continue until the previous J_{max} value (from the proof testing at the higher load level) is exceeded before tearing continues. This would be consistent with the general tear-fatigue rules, which effectively assume that the ductile fracture process zone at the crack tip advances with the crack as it extends by fatigue. This implies that the crack retains full "memory" of its previous history. On the other hand, it is possible that ductile tearing (and subsequent tear-fatigue) during service cycling will re-initiate somewhat independently of the previous proof test response (in other words, when J_{max} from the fatigue cycling exceeds the initiation toughness, even if the previous J_{max} from the proof testing was higher). This approach implies a "loss of memory" of previous crack growth events.

It is simple to envision contrasting scenarios in which each behavior might be observed. Consider one situation where proof testing initiates significant tearing; the subsequent decrease in applied load is relatively small; and the subsequent increase in J_{max} with crack growth is relatively rapid, so that J_{max} exceeds its previous maximum value before the crack tip has moved far beyond its position at the end of the proof cycle. In this case it is reasonable to assume that the ductile fracture process zone does in fact advance with the crack tip as it grows in fatigue. On the other hand, consider a situation where the subsequent decrease in applied (service) loading is sufficiently appreciable that J_{max} decreases considerably, and extensive crack growth is required before J_{max} again increases to proof test levels. In this case, it is more likely that the fatigue crack will simply grow through the previous ductile fracture process zone. Once this has occurred, material memory of the previous ductile tearing event is largely forgotten, and tearing will re-initiate during service cycling when the usual conditions for tearing are satisfied (J_{max} first exceeds the initiation toughness).

In practice, actual material response is likely to lie somewhere between these two extremes: rigorous tear-fatigue rules on the one hand, and a complete loss of material memory (resetting of the resistance curve) on the other hand. Experimental and analytical characterization of the exact response is beyond the scope of the present effort. However, it is important to assess if this ambiguity has a significant effect on the assessment of the relative merits of single and multiple cycle proof testing. If it does not, then it is not so important to understand the behavior completely at this time.

The MCPT/NESSUS computer code was modified to make crack growth predictions based on either the full "memory" or full "loss of memory" theories at the end of proof cycling, and the code was then exercised with various parameter choices to determine what difference it would make. The results show that, in terms of total probability of failure for a fleet of components

containing an assumed distribution of flaw sizes, the assumption about memory makes relatively little difference. For selected individual analyses, when cracks are very near failure following the proof test, the assumption may be of greater consequence. In terms of the overall fleet reliability, however, the differences are not significant.

Sample results for fleet reliability are shown in Figure 4.21. These analyses employed the "baseline" parameter choices for material properties, component and flaw geometry, and applied loading. Similar results were observed for numerous other parameter choices besides the "baseline" configuration. Plotted here is the probability of failure in service for a fleet of components without proof testing or following proof testing with 1, 5, or 20 proof cycles. The "memory" cases assume that the resistance curve is not reset immediately following the proof cycling, while the "loss of memory" cases assume that the resistance curve is reset when the applied loads decrease at the end of the proof cycling. In both cases, the standard "memory" tear-fatigue model is followed during the proof cycling (at constant maximum load) and during the service cycling (also a constant maximum load). The results show that the absolute values of computed failure probability change only slightly, and the comparative trends between different numbers of proof cycles are essentially unchanged. The differences that do exist are greatest for relatively small numbers of service cycles; this coincides, as expected, with cracks which are very near failure during the proof loading. Also as expected, the total probabilities of failure are predicted to be slightly lower for the "memory" assumption, which can predict a brief retardation of fatigue crack growth rates immediately following the proof cycling.

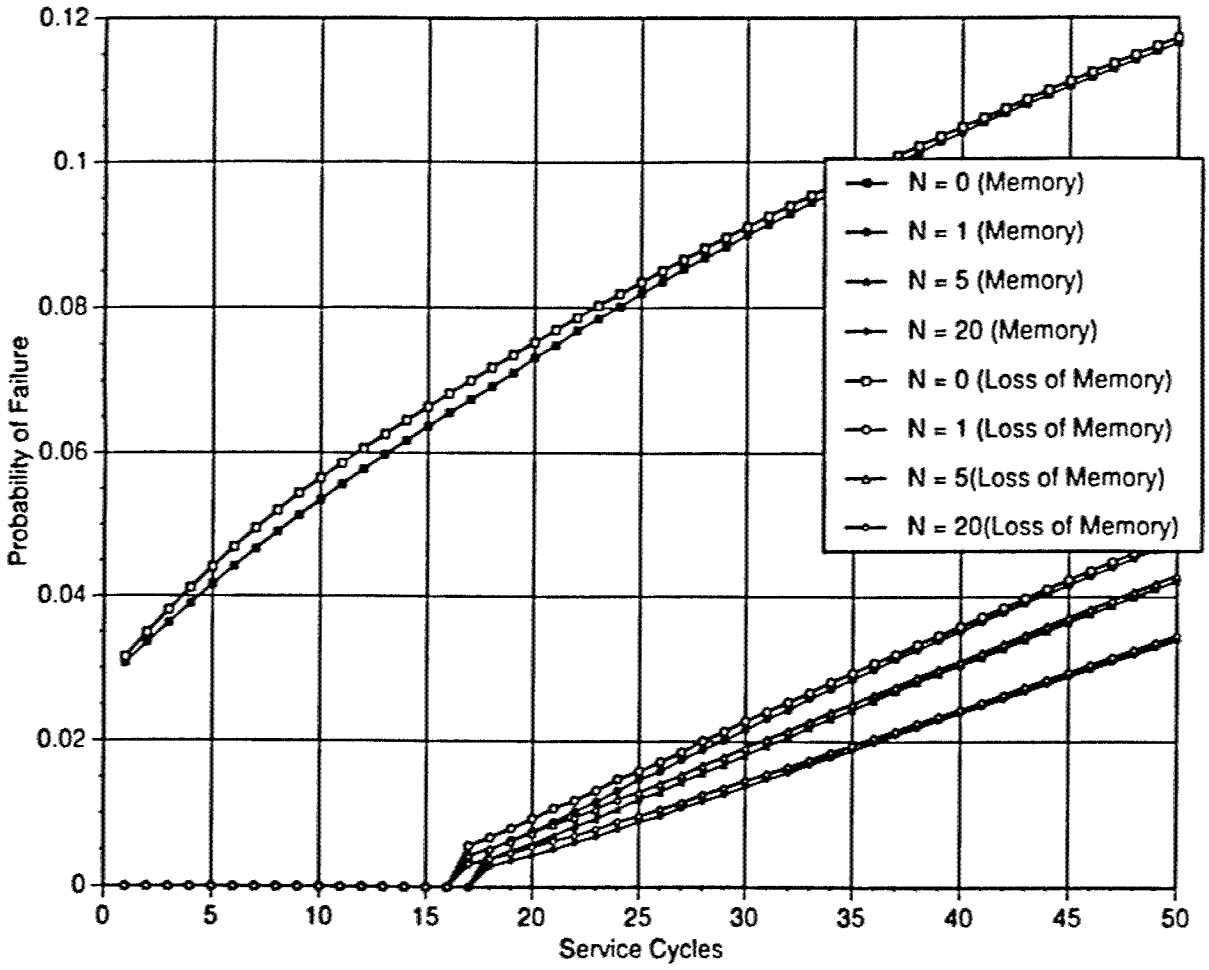

Figure 4.21. Computed in-service failure probability for different numbers of proof cycles and different assumptions about material memory following the proof overload

5. DISCUSSION

5.1 Other Proof Testing Issues

Proof testing is a complex subject. A large number of structural, material, and loading variables can influence the response of a (potentially) flawed component during a proof test and subsequent service cycling. Therefore, in principle, many variables can influence the relative merits of single cycle and multiple cycle proof testing. The current research study, on the other hand, has been necessarily limited in scope. Not all proof test variables have been evaluated quantitatively, and not all potential modes of proof test or in-service failure have been considered. The investigators have attempted to focus on the most significant proof test variables, and they have emphasized the most significant mode of structural failure: the growth of a pre-existing crack as characterized by the established principles of fracture mechanics. Before closing, it is useful to discuss briefly some other proof test variables and some other potential modes of proof test failure. Some of these issues are being treated in more depth under another research contract [41].

5.1.1. Hold Times and Time-Dependent Fracture Behavior

Most proof test loading includes some hold time at a steady maximum load. This hold time may be as short as a few seconds merely to insure that the steady state maximum load has been achieved, or as long as many hours to permit inspection of the component or structure under maximum load. The current Rocketdyne MCPT protocol stipulates hold times of 30 seconds at maximum load on each cycle.

Hold times at maximum load can influence fracture behavior. In general, a component that can withstand a certain maximum critical load for a few seconds may not be able to withstand the same load without failure if held at that level for a longer period of time. This phenomenon occurs because of time-dependent fracture behavior: cracks can grow slowly at a fixed load (or exhibit accelerated growth under cyclic loading when the loading frequency is slower). This crack growth phenomenon can ultimately be linked to time-dependent mechanical deformation or, in some situations, to time-dependent environmental damage in the material. Although a detailed review of the hold time effect in proof testing is beyond the scope of this contract, some brief observations are useful.

Tiffany [48] and Schliessmann [3] were among the first to address hold time effects in proof testing. They both observed that in relatively inert environments, sustained stress crack growth was only significant when the applied stress intensity factor was a large fraction of the critical (time-independent) K value for failure, usually 80 to 90 percent. If the applied K was less than some "threshold" value, as Tiffany termed it, then sustained stress effects were negligible. However, Tiffany noted that this threshold stress could decrease dramatically when environmental factors were introduced, such as high pressure hydrogen gas with Inconel 718. Johnson and Paris [49] subsequently reviewed several more detailed investigations (included their own) of sustained

stress crack growth and noted several characteristic trends in the subcritical crack growth behavior. Typically, the crack growth rate under sustained load initially decreased, and the crack could halt if the stress intensity factor was low enough. At higher stress intensities, the crack growth rate was observed to pass through a minimum and then increase steadily as unstable fracture approached.

These phenomena were all observed in the simulated MCPT surface crack growth experiments (all with 30-second hold times) conducted under the current contract, and summarized in Section 3.5. In particular, substantial time-dependent crack growth was observed only at applied loads very close to the ultimate failure load. The crack growth rate generally decreased to zero after a brief period of growth, except when failure was imminent. In this case, the crack growth rate decreased to a minimum and then increased steadily to instability.

The proper analytical treatment of time-dependent crack growth is not yet entirely clear. Landes and Wei [50] published one of the first significant studies linking subcritical crack growth in an inert environment to creep deformation at the crack tip. More recently Brust and Leis [51-52] have forwarded an analytical method that characterizes time dependent crack growth due to an increase in the elastic-plastic crack driving force that results, not from an increase in load, but from a reduction in the yield properties of the material around the crack tip due to time-dependent creep deformation. Their formulation, however, is currently limited to certain classes of materials in which the local stresses at the crack tip increase with time. It remains possible that some forms of sustained stress crack growth are due to time-dependent changes in the crack advance mechanism, not in the near-tip material properties.

Ingham and Morland [53] took a somewhat simpler approach, considering time-dependent crack growth in the context of a simple *J*-resistance curve framework, and generating different resistance curves at different displacement rates. They also concluded that time-dependent crack growth was only significant when the sustained loads were within a few percent of the collapse load and the remaining ligament was fully plastic. Therefore, time-dependent failure would not be significant in structures with contained yielding.

What are the implications of time-dependent crack growth—and therefore hold times—for the comparison between SCPT and MCPT? Time-dependent crack growth can be thought of as another form of subcritical crack growth, analogous to the subcritical *cyclic* crack growth that occurs during multiple proof cycles. This subcritical cyclic crack growth was shown in the current contract to become significant only when failure was relatively imminent, and this is entirely similar to the earlier observation that sustained stress crack growth becomes significant only near instability. Therefore, by analogy, it would appear that hold times would be most beneficial under the same conditions in which multiple cycles are most beneficial, and that the time-dependent and cycle-dependent phenomena would work together to remove additional near-critical flaws from the population. It is even possible that hold times may improve the relative advantages of MCPT under these conditions. In the limited experimental studies of simulated MCPT conducted in the present contract, it appears that if the hold times had been significantly shorter, failure would not have occurred at the proof loads and numbers of cycles applied. Also

by analogy, it is possible that longer hold times, like increasing numbers of cycles, would further improve fleet reliability, albeit with diminishing incremental benefit.

On the other hand, when multiple proof cycles are less beneficial, hold times may also be less beneficial, although (as for multiple cycles) any additional subcritical damage due to time-dependent crack growth would typically be negligible when failure is not imminent. However, it must be emphasized that no rigorous analyses or experimental evaluations of hold time effects on MCPT have been conducted under the current contract, and therefore all of these comments and conclusions must be regarded as speculative rather than definitive.

5.1.2. Cyclic Hardening and Softening

It is well-known that the constitutive properties of some materials can change significantly following relatively severe cyclic elastic-plastic deformation. Hard materials can soften, and soft materials can harden. As noted in Section 3.4, for example, Inconel 718 in the monotonic condition has a relatively high yield strength and relatively low strain hardening, while its cyclically stable properties include a lower yield strength and higher strain hardening.

Is this significant for the evaluation of MCPT? While no detailed studies of this question were conducted in the current contract, the answer appears to be a qualified "no". First of all, limited parameter studies found that changes in the constitutive relationship alone did not lead to significant changes in fleet reliability following SCPT or MCPT. Second, as long as the number of proof cycles is kept relatively low (five, for example), extensive cyclic changes in the constitutive properties of the material are not likely. Cyclic hardening or softening is a gradual, not an instant process, and often requires many cycles to achieve. The common rule of thumb is to determine cyclic properties at the half-life of a fatigue specimen subjected to constant amplitude straining, thereby implying that the stabilization process will occur much more quickly under more severe cyclic straining.

Of course, cyclic hardening or softening (in a suitable material) is always taking place in the crack tip region due to the locally severe deformation occurring there (even if the remote stresses and strains are mild). Therefore, this effect is automatically included in any normal characterization of crack growth rate properties, and should require no explicit treatment.

On the other hand, cyclic hardening or softening may need to be considered explicitly in the evaluation of SCPT or MCPT when both the proof test deformation and the in-service cyclic deformation are relatively severe. In this case, the assessment of in-service crack growth may need to employ cyclic stress-strain properties (for example, in the computation of ΔJ_{eff}) when those provide a more conservative answer than monotonic properties. However, it may be prudent to retain monotonic properties in the analysis of the proof test itself.

Another possible exception involves proof testing of materials with a pronounced yield point, such as certain steels. These materials can exhibit a more pronounced and rapid change

in the stress-strain relationship following only a few load excursions near or above the yield point, and so a more detailed assessment may be required.

5.1.3. Weldments

Weldments can introduce a new set of complex issues into any fracture analysis. Although nominally the weld metal often retains the same properties as the base metal, and the weldment as a whole can often be treated as a homogenous component, other complications are also possible. Weldments can introduce significant residual stresses, for example. The weld metal and/or the heat affected zone can exhibit different material properties, and sometimes the weld metal properties are intentionally chosen higher or lower than the base metal in order to achieve a certain structural performance. Weldments are also a prime location for initial or service-induced crack-like defects, of course, due to potential inhomogeneities in the weldment itself or to irregularities in the surface or weldment interface.

Although none of these issues have been addressed directly in the current contract, a few speculative observations are useful. Residual stresses can relax somewhat under severe cyclic loading, and so multiple cycle proof testing could cause some additional relaxation. If the residual stresses were previously beneficial for service loading, then MCPT could slightly degrade the in-service performance; the reverse might then be true if the residual stresses were originally detrimental to in-service performance.

Significant variations of local material properties in a weldment, whether intentional or unintentional, could introduce new complications to a tear-fatigue analysis. Due to this complexity, no speculation about SCPT or MCPT outcomes is offered here. Additional analysis would be required to assess these issues.

Another set of potential issues introduced by weldments relates to unusual defect shapes. Actual weldment defects, of course, do not typically take a uniform elliptical or semi-elliptical shape. The study of many such actual weldment defects during Phase I did find that the semi-circular surface crack was a reasonable representative on average, but that same study documented the wide variety of actual shapes, including many irregular shapes that are quite unlike any normal idealized geometry. Furthermore, these irregular weldment defects can occur in local clusters, with small ligaments between them.

Growth of these flaws during proof testing may not follow the customary form of idealized fracture mechanics equations. Early growth may be dedicated to the transformation of irregular shapes (where the crack driving force varies widely around the perimeter of the flaw) into more regular shapes (where the crack driving force is more uniform around the perimeter). Local ligaments between neighboring flaws may fail due to plastic collapse to form new, coalesced cracks. Failure of local ligaments due to severe low cycle fatigue or localized ductile tearing could lead to the sharpening and, effectively, the formation of cracks where blunter voids once existed. Again, these complex crack growth phenomena were not addressed in the current contract, and no damage growth phenomena were considered that were not explicitly fracture

mechanics events. In general, however, additional proof cycles would likely be helpful in the formation and failure (and therefore the detection) of these weldment defects. Of course, it remains possible that additional proof cycles could make a local defect worse without causing it to fail, thereby reducing the in-service reliability, but as noted earlier, the MCPT problem must always be treated from the standpoint of the total fleet population. More definitive answers about the problem of irregular or unusual weld defects would require further analysis.

5.2 The Generality of the Results

The investigations conducted in the current contract have necessarily been limited in scope. Only a small number of crack geometries, crack sizes, resistance curves, etc. have been studied, and only a limited number of combinations of different variables could be considered. Although the parameter studies were intended to exercise several key variables over a wide range or values, and although those parameter studies were interpreted and extended in terms of fundamental understandings about the fundamental crack growth phenomena involved, it must be emphasized most strongly that many practical combinations of parameters remain unexamined. And, of course, the experimental studies under this contract were necessarily limited to a single material and a narrow range of geometries.

In contrast, the real world of reusable aerospace propulsion system components is filled with many different materials, many different geometries, and many different potential hardware defects. Even a single component or proof tested assembly may contain several different critical locations, each with a unique geometrical configuration, local level of constraint, etc. And therein lies a paradox of sorts. On the one hand, as noted in the conclusions to the Phase I report, and confirmed quantitatively in the Phase II work, the selection of an optimum proof test protocol depends on many different variables and may be component-specific. On the other hand, what is needed is a set of general guidelines about the relative merits of SCPT and MCPT that will provide useful engineering guidance for a wide range of real hardware.

This contract has always pursued these general goals, and in fact is concluding now by proposing a general set of practical engineering guidelines for the selection of an optimum proof test protocol (see Sections 6 and 7). However, the complete generality of these guidelines cannot be absolutely guaranteed, in view of the many complex variables involved. And it is exactly this complexity that prevents the formulation of specific, quantitative rules-of-thumb to guide the design of an optimum proof test for every single component. Instead, the guidelines must be more qualitative in nature.

The solution to this dilemma, for the practicing engineer who must confidently design a specific proof test protocol for a specific component, is to perform a specific quantitative analysis of that specific problem. One set of tools that would facilitate this job would be (1) a general-purpose crack growth computer code that provides acceptably accurate predictions of elastic-plastic crack growth due to fatigue, tearing, and their interaction for a variety of practical crack geometries; and (2) a simple probabilistic driver to evaluate the impact on in-service reliability for a given proof test protocol, given some assumed distribution of initial defects. This is a

similar approach to the analysis performed in the current contract, although the research software used in the performance of this contract had limited generality and a cumbersome user interface. But if software of this type was available, the engineer could identify critical locations on his hardware (locations with high stress and/or increased likelihood of initial defects), choose a representative flaw geometry, and choose a representative initial defect distribution, and let the software evaluate changes in reliability for different combinations of proof factor and number of cycles. Software of this type would also be useful in conducting additional research studies of MCPT, including some of the unaddressed issues cited above.

6. SUMMARY AND CONCLUSIONS

1. Multiple cycle proof testing can be effective in removing some of the largest flaws from the population that would not have been removed by conventional single cycle proof testing at the same proof loads. This conclusion is clearly supported both by fracture mechanics theory and by validating experimental observations. Hence, MCPT can be an effective means of identifying and removing defective hardware that could go undetected by conventional SCPT.

2. Multiple cycle proof testing can also cause additional subcritical crack growth to occur in components that do not fail during the proof test. Unfailed cracks can grow more during a multiple cycle proof test than during a single cycle proof test. Therefore, in general, a cracked component that survives a multiple cycle proof test has a slightly shorter remaining service life than if the component had been subjected to a single cycle proof test at the same load. However, this service life difference is negligibly small in most cases. The difference will be significant only in those cases where cracks are relatively large and failure is relatively imminent following the proof test.

3 Probabilistic studies have shown that, in general, when MCPT is consistently applied to a fleet of components containing a distribution of initial flaws, the overall fleet reliability will be higher for a population of components that have been subjected to MCPT than for a population of components that have been subjected to SCPT at the same proof load. From the standpoint of in-service reliability, more good is done by removing a few additional large flaws from the population than harm is done by incremental growth of many small flaws in the population. This benefit generally increases with increasing numbers of proof cycles, although the incremental benefit of additional proof cycles decreases with increasing numbers of cycles. Three possible exceptions to this general principle are addressed in the following three conclusions.

4. From the standpoint of in-service fleet reliability, MCPT can be inferior to SCPT (albeit negligibly so) when the probability of failure due to any proof loading is itself negligibly small. This situation may arise, for example, when the proof loads are relatively small, the possible crack sizes are relatively small, and the material is relatively tough, so that the driving force for crack extension is substantially lower than the material toughness. In this situation, the potential benefit to be gained by adding proof cycles to remove additional large flaws from the population is negligibly small. Therefore, the additional subcritical crack growth caused by the additional proof cycles will reduce net in-service reliability. However, in most cases, this decrease in reliability will also be negligibly small. Therefore, while MCPT is of no additional benefit in this situation compared to SCPT, it can be regarded as being of no substantial detriment, either.

5. When the crack driving force decreases with increasing crack size, failure during proof testing is highly unlikely, although subcritical crack growth can occur for even the largest flaws. Proof testing to any number of cycles (one cycle or many cycles) will be

detrimental under these conditions and should be avoided unless supported by a detailed fracture mechanics analysis. This situation can occur for displacement-controlled configurations, or for configurations in which crack growth in one member merely causes load shedding to an alternative structural member due to the increased compliance of the cracked member, or if the crack resides in a steeply falling stress field due, for example, to residual welding strains. If proof testing cannot be avoided under these conditions, the number of proof cycles should be kept to a minimum, and a comprehensive proof test analysis should be performed based on fracture mechanics.

6. When cracks are located at notch roots and the crack lengths of concern are comparable to the plastic notch field or smaller, and when the stresses and strains in the notch root are severe, then MCPT may not provide additional benefit compared to SCPT. In these situations, additional proof cycles can degrade in-service fleet reliability, although typically by small amounts. This behavior occurs due to the local control condition in the notch root, which causes J values to be relatively high but to increase only slightly with increasing crack length. Therefore, although additional subcritical crack growth occurs relatively easily, failure is unlikely. When the crack lengths are large compared to the notch field, or when local stresses and strains are less severe, the notch is less of a problem for MCPT.

7. The specific benefit or detriment associated with MCPT will depend on a number of different factors, including the proof load factor, the number of proof cycles, the toughness and tearing resistance of the material, the geometric configuration of the crack, the level of structural constraint in the vicinity of the crack, and the distribution of potential crack sizes and crack shapes. Because of these many complex factors, it is not possible to provide a simple set of universal formulas or graphs to select the mathematically optimum proof test protocol and quantify the incremental benefit of that protocol.

8. Individual fracture mechanics analyses of critical component locations are recommended to determine the most appropriate proof test protocol for specific proof testing problems. These analyses would be facilitated by the availability of a general-purpose computer code for crack growth analysis that includes a variety of elastic-plastic fracture mechanics solutions for common crack geometries (especially surface cracks) based on the J-integral parameter, along with practical crack growth algorithms based on J to address monotonic and cyclic crack growth processes and the tear-fatigue interaction between these two mechanisms. Also of benefit would be a simple probabilistic analysis routine to evaluate the changes in fleet reliability for a population of components containing a distribution of initial crack sizes.

9. The parameter studies conducted under the current contract indicate that for wide ranges of variation in many of the important factors, the overall performance of MCPT in comparison to SCPT is relatively consistent. MCPT appears to be either beneficial or benign in comparison to SCPT, and any benefit generally continues to increase with

increasing numbers of proof cycles. In situations where component failure risk is relatively high, MCPT can be a useful means of obtaining additional reliability. In situations where component failure risk is relatively low, MCPT itself offers no additional benefit. However, if multiple proof cycles are desirable or required for other (non-fracture mechanics) reasons, then these multiple cycles will not generally cause any significant deterioration of fleet reliability. Some additional recommendations for selecting an appropriate proof test protocol are contained in the Engineering Guidelines, which follow these conclusions.

10. MCPT can be preferable to SCPT only when viewed from the perspective of component reliability; i.e., a *probabilistic* assessment of structural integrity. From a purely deterministic standpoint, the potential advantages of MCPT cannot be recognized or documented. In particular, if proof testing is being used for the specific purpose of establishing a guaranteed maximum size for any flaw remaining in the component following the proof test (e.g., a quantitative flaw screening in conjunction with a deterministic fatigue crack growth analysis to guarantee a minimum safe remaining life in service), then MCPT offers no apparent additional benefit. The maximum flaw size (based on a deterministic analysis) that could theoretically remain in the component following a proof test to a certain fixed proof load does not change if single or multiple proof cycles are performed; MCPT does not increase or decrease this maximum flaw size relative to SCPT. The potential advantage of MCPT over SCPT is that the frequency of flaws that are slightly smaller than this critical (deterministic) maximum flaw size may be decreased, thereby improving component reliability from a probabilistic perspective.

11. Proof testing to typical proof factors for advanced reusable propulsion systems (factors of 1.2 and less) does not appear to cause significant retardation of fatigue crack growth at service load levels. The overload retardation phenomenon becomes significant only at higher overload ratios.

12. Acoustic emission (AE) shows some promise as a means of detecting significant subcritical crack growth during proof testing. While proof testing and associated flaw behaviors can generate a variety of detectable AE activity, the most substantial AE signals appear to be associated with crack extension as instability is approached. If it were possible to use AE monitoring to detect this damaging subcritical growth, then it could be possible to eliminate the single greatest risk associated with MCPT—substantial subcritical growth of large flaws that are not quite large enough to cause failure—while further improving the ability of the MCPT process to screen potentially dangerous flaws (down to even slightly smaller flaw sizes). AE monitoring would potentially be aided by multiple proof cycles (rather than a single cycle) because the multiple cycles would provide more opportunities for monitoring. However, these conclusions are based on controlled laboratory experiments in which isolation and filtering of extraneous background noise was relatively simple to accomplish, and in which the number of potential AE sources was relatively small. Further studies would be required to evaluate

the feasibility of employing such an AE approach during proof testing of actual hardware in a production environment.

13. Estimates of the J-integral based on modified reference stress formulations are acceptably accurate for many engineering applications. This approach was specifically validated in this study for two important classes of cracked geometries, the semi-elliptical surface crack in a finite thickness plate, and the edge crack growing at a notch root. The modified reference stress estimates are most accurate when they can be guided by limited finite element results. These numerical results provide important assistance in identifying an optimum yield load and/or structural parameter for the reference stress formula, which can then be used to generate J solutions for a much wider range of geometries than can be addressed by the available finite element solutions.

14. Crack growth and instability in tough, ductile materials during single cycle and multiple cycle proof testing is satisfactorily described by elastic-plastic fracture mechanics based on a J-integral characterization. The behavior of cracks during cyclic loading is satisfactorily described by a ΔJ_{eff} approach that accounts for crack closure, while crack behavior during monotonic loading approaching instability is satisfactorily addressed by a J-resistance curve approach. The interactions between monotonic and fatigue crack growth as cycling occurs near instability are satisfactorily described by tear-fatigue theory. These conclusions have been validated by critical experiments with Inconel 718. The broad outlines of these elastic-plastic fracture mechanics approaches are described in the main body of this report. Detailed engineering methodologies for carrying out the computations are being developed and fully documented in two companion contract efforts.

7. ENGINEERING GUIDELINES

7.1 General Background

A series of general conclusions about the comparison between MCPT and SCPT was provided in the Summary and Conclusions section that immediately precedes these Engineering Guidelines. It was concluded that, in general, when MCPT is consistently applied to a fleet of components containing a distribution of initial flaws, the overall fleet reliability will be higher for a population of components that have been subjected to MCPT than for a population of components that have been subjected to SCPT at the same proof load. This conclusion was found to be generally true for relatively wide variations in a number of different material, crack, and proof test parameters, although some exceptions were identified.

The Summary and Conclusions section also noted that, due to the large number of different factors influencing proof test performance, it was not possible to provide a simple set of formulas or graphs to select the mathematically optimum proof test protocol and quantify the incremental benefit of that protocol. Instead, individual fracture mechanics analyses of critical component locations, based on the engineering methodology developed under the current contract and two other contracts, were recommended to determine the most appropriate proof test protocol for specific proof testing problems. As noted, these analyses must be probabilistic to determine properly the relative advantages or disadvantages of MCPT.

Nevertheless, it is useful to summarize some of the lessons learned from the analytical and experimental investigations in this contract in a manner that provides some additional engineering guidance for the selection of a proof test protocol. It will undoubtedly remain a source of some frustration that, due to the complexity of the problem, these guidelines cannot provide simple quantitative rules that unambiguously specify all of the relevant proof test parameters for a given piece of hardware. However, some additional guidance about specific proof testing issues and parameters should be useful to NASA staff and contractors as they approach new proof testing problems.

It must also be emphasized that these engineering guidelines are necessarily based primarily on the analytical and experimental investigations conducted under the current contract, aided by the broader engineering experience and judgement of the investigators. The investigations under the current contract were particularly focused on Inconel 718, an alloy of particular relevance to the SSME and representative of a broader class of tough, ductile superalloys. Therefore, it must be recognized that the generality of the guidelines is necessarily somewhat limited. Further experience with the analysis of proof testing following the general approach described in this report may lead to some revisions in these guidelines. However, the investigators have made every reasonable effort possible within the scope of the contract to develop a fracture mechanics methodology with sufficient generality, and to exercise that methodology over a sufficient range of parameters, to ensure the overall robustness of these guidelines.

It should also be noted that an independent contract effort [41] being conducted for NASA by the same contractor team is producing a much more comprehensive proof test guidelines document that is addressing a wider range of major proof test variables and issues. The current contract effort has a much more limited scope, focusing on the comparison between single cycle and multiple cycle proof testing, although this selection is necessarily influenced to some degree by the other proof test variables. Therefore, the guidelines presented below will focus on the implications of different variables and issues for the selection of single or multiple proof cycles.

7.2 Introduction to Flow Chart Format and Decision Process

For convenience, these engineering guidelines are organized into a simple flow chart format. The flow chart is summarized visually in Figure 7.1. The backbone of the flow chart is a series of key questions and decisions organized into six major steps, each involving a major subject area. For convenience, these key questions are given in shortened form in the flow chart diagram, but the complete questions are given in the text of the guidelines. The answers to each set of questions are interpreted to indicate a strong or weak preference for either SCPT or MCPT, and ultimately to lead to the selection of SCPT or MCPT.

Each series of key questions is prefaced by a brief description of any "Supporting Data" that must be collected and evaluated in order to answer the questions that follow. Also included in the guidelines are some brief explanations to provide background information about the individual technical issues behind the recommendations.

The answer to each individual question typically leads to one of four topical conclusions about the relative desirability or undesirability of MCPT. These four types of topical conclusions can be broadly categorized into four "Codes" as follows:

Code 1. MCPT is clearly indicated to be **potentially damaging**, provides no potential advantages from a fracture mechanics standpoint, and should be avoided if at all possible. SCPT is **recommended**. If MCPT is unavoidable, then the number of proof cycles should be minimized, and the test should be supported by a detailed fracture mechanics analysis.

Code 2. MCPT offers **no potential benefit** from a fracture mechanics standpoint, but is likely to cause little additional damage to the component. SCPT is **recommended**, but if MCPT is necessary or desirable for other reasons, then MCPT is **acceptable**.

Code 3. MCPT offers a **limited potential benefit**, but perhaps only a small benefit relative to the additional cost incurred. MCPT is **recommended**, but SCPT is **acceptable**, and SCPT may be preferable if other factors, such as cost, so indicate.

Code 4. MCPT offers **some meaningful potential benefit** and is therefore **recommended**. SCPT may be **acceptable**, but may offer less benefit than MCPT.

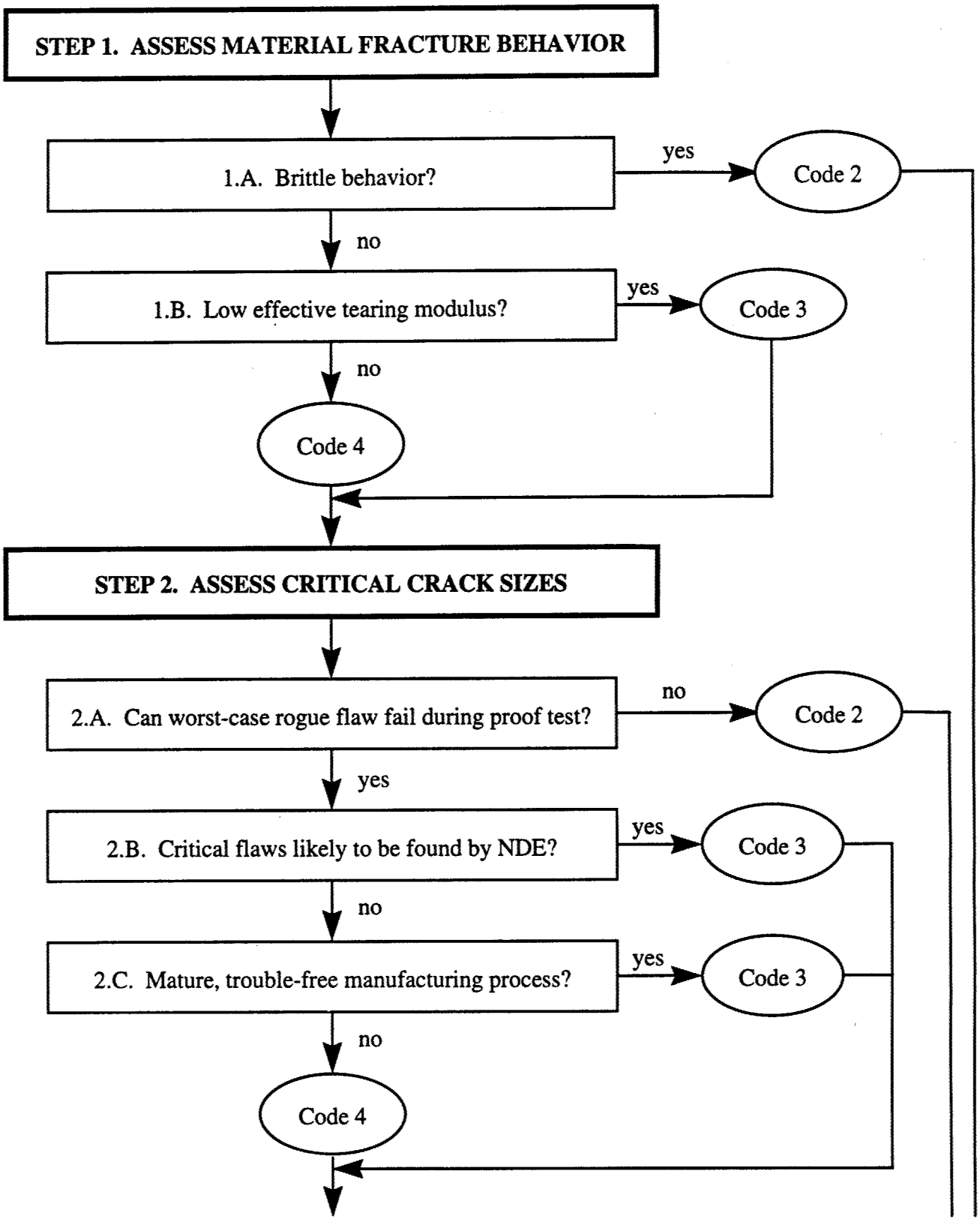

Figure 7.1 Flow chart for Engineering Guidelines

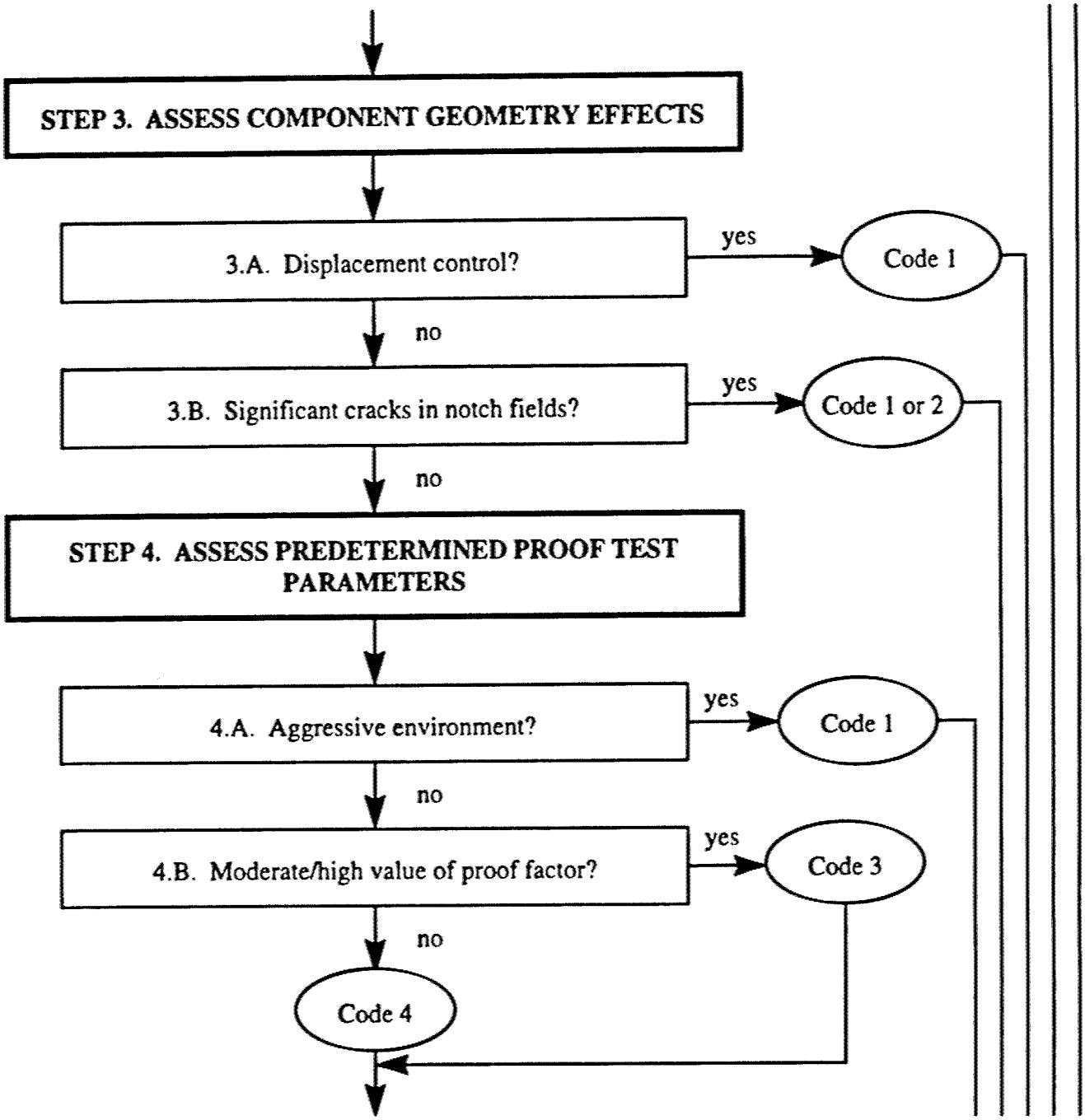

Figure 7.1 Flow chart for Engineering Guidelines (Cont.)

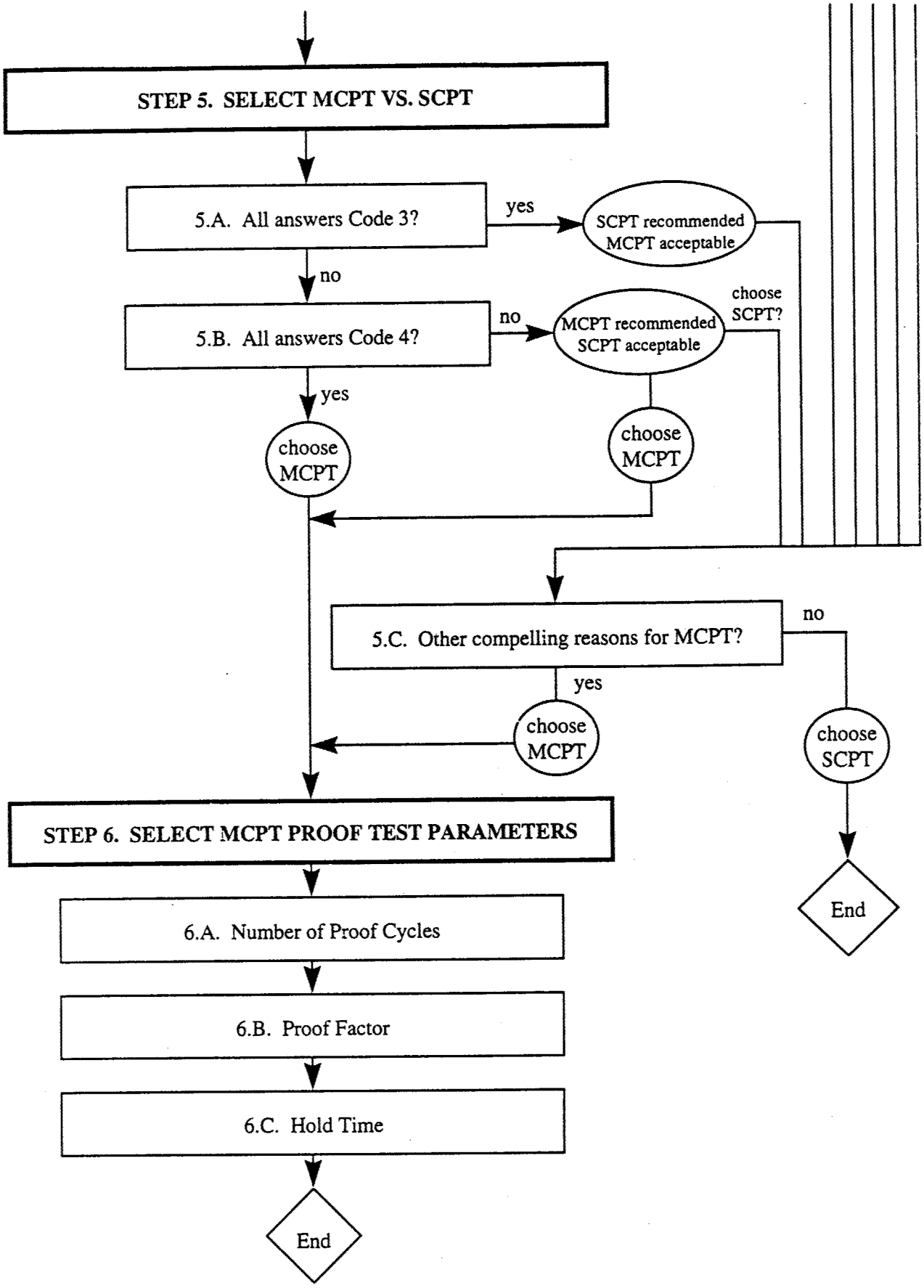

Figure 7.1 Flow chart for Engineering Guidelines (Cont.)

The overall evaluation process to select MCPT or SCPT is integrated in Step 5. If this evaluation process leads to a decision to implement MCPT, the remaining decisions are the selection of the specific number of proof cycles, the proof factor, and the hold time. Some brief guidance on these decisions is available under Step 6 in the flow chart.

Note that any answer yielding a Code 1 or Code 2 automatically short-circuits the decision process to Step 5. Under these circumstances, MCPT is recommended only if there are compelling reasons for multiple proof cycles other than fracture control. If there are no other compelling reasons, then SCPT is selected.

Because of this short-circuit, it may be efficient to begin the flow chart process by considering only those questions that can potentially yield a Code 1 or Code 2. These are questions 1.A, 2.A, 3.A, 3.B, and 4.A. If none of the answers to these questions yields a Code 1 or Code 2, then MCPT may provide some increased benefit relative to SCPT. The user can then work through the entire flow chart to make a final decision about MCPT vs. SCPT.

7.3 Engineering Guidelines: Detailed Description

STEP 1. ASSESS MATERIAL FRACTURE BEHAVIOR

The toughness and tearing resistance of a material is perhaps the issue with the most significance for the efficacy of a proof test. The ability of the material to resist fracture determines the flaw sizes that will be screened at a given proof load. The tendency of the material to exhibit significant subcritical crack extension from ductile tearing and/or fatigue prior to fracture is perhaps the issue with the most significance for the efficacy of multiple cycle proof testing. This crack growth prior to failure is essential to any incremental benefit of additional proof cycles, because it permits some additional flaws to grow to critical size. Ironically, subcritical crack growth also provides the potential for incremental damage during additional proof cycles.

Supporting Data Required:

An experimental measure of the material resistance to fracture, including a description of subcritical crack growth prior to catastrophic separation, must be available. The preferred characterization of toughness for ductile materials is a crack growth resistance curve based on the J-integral, the most commonly used parameter for elastic-plastic fracture mechanics. The J-resistance curve provides an indication of the toughness level at which ductile tearing is initiated, usually denoted by J_{Ic}. The resistance curve also provides an indication of the increasing resistance to additional crack growth, described by the slope of the J vs. Δa curve beyond J_{Ic}, and often denoted as the tearing modulus.

This resistance curve may have been generated according to standard test methods, such as ASTM standards. However, these standard test results may be inadequate for an accurate assessment of the fracture behavior of the component. Most standard fracture tests are designed

to maintain a high level of structural constraint, which yields a lower bound value of toughness and tearing resistance. Many component structural configurations exhibit a lower level of structural constraint.

The influence of local structural constraint on fracture behavior has been widely studied in the international fracture community for the past ten years. Configurations in which high hydrostatic constraint is maintained (e.g., contained plasticity, plane strain, etc.) generally exhibit lower apparent toughness and/or tearing resistance than configurations in which hydrostatic constraint is low (uncontained plasticity, plane stress, etc.). Different crack geometries are also associated with different levels of constraint. Constraint is typically lower for tension loading in comparison to bend geometries, or for cracks that are particularly shallow (or in some cases, very deep). Highly loaded surface cracked structures exhibit substantially less structural constraint than laboratory test specimens subjected predominantly to bending, such as compact tension specimens.

It is now believed that the effect of structural constraint on fracture behavior is more properly described by a change in the crack driving force, as *J*-dominance is lost at the crack tip and higher-order terms become more significant for the description of the crack tip field. Practical applications of this fracture mechanics theory, however, are still in their infancy. Therefore, from a pragmatic standpoint, it is often useful to associate low constraint with high apparent toughness and high constraint with low apparent toughness, especially in the tearing regime.

A material that exhibits relatively low toughness in a thick compact tension or bend specimen, which is designed for high constraint, may exhibit relatively high effective toughness in a structural geometry involving (for example) tension-loaded surface cracks in thin sections. Therefore, any assessment of material fracture behavior must also take into account any significant differences between the constraint levels for the laboratory data and the structural application.

In order to assess the level of local structural constraint, the nature of the stress fields (tension vs. bending) and the characteristic component dimensions at any fracture-critical locations should be determined. One simple measure of crack-tip constraint is to compute the approximate size of the crack-tip plastic zone and to compare this dimension with the characteristic specimen thickness or remaining ligament. If the plastic zone is small compared to the characteristic specimen dimension, then high constraint (approaching plane strain) is likely. If the plastic zone is on the same order as the characteristic specimen dimension, then lower constraint is likely.

If the structural configuration at any fracture-critical location is characterized by moderate to low constraint, then the standard fracture test results may be inappropriate. A better experimental characterization of ductile fracture in this case would be a crack growth resistance curve based on tests employing a specimen and crack geometry and applied stress level that are representative of the actual structural configuration. If a structurally-relevant measure of material

fracture behavior is not available, then available data must be interpreted in the light of engineering experience.

Key Questions:

1.A. *Does the material behavior in a brittle manner in this structural configuration? Does the material fracture catastrophically with little or no prior subcritical crack extension?*

"YES" $\Longrightarrow$ Code 2

Materials that are relatively brittle and that exhibit little or no stable crack extension before failure are poor candidates for MCPT, since the potential advantages of MCPT are based on the potential for stable growth of cracks leading to failure on a subsequent proof cycle. If, however, MCPT is required or desirable for other reasons, relatively little subcritical damage should be done to the component by a limited number of proof cycles.

Note that materials which behave in a brittle manner in a highly constrained laboratory test do not always behave in a brittle manner in a low constraint structural geometry.

1.B. *Does the material behave in a ductile manner in this structural configuration, such that some subcritical crack extension can occur prior to failure, but does the fracture resistance curve exhibit relatively little increase in toughness as the crack tears? In other words, does the material exhibit a relatively flat tearing resistance curve with a relatively low tearing modulus?*

"YES" $\Longrightarrow$ Code 3

"NO" $\Longrightarrow$ Code 4

Materials with a low tearing modulus are also relatively poor candidates for realizing significant benefits from MCPT, because the sharp knee in the *J*-resistance curve means that little tear-fatigue extension is likely. However, some incremental benefit is possible, and relatively little subcritical damage is likely, if MCPT is required or desirable for other reasons.

Materials that exhibit moderate to high toughness, some subcritical crack growth before failure, and some significant increase in toughness as the crack tears, are ideally suited to realize the benefits of MCPT. In this case, MCPT will generally provide some improvement in reliability over SCPT.

However, if the material exhibits extremely high toughness and/or tearing resistance, another practical issue can become dominant. If the toughness and tearing resistance are sufficiently high, and the applied loads are sufficiently low, it may be impossible to cause

failure during the proof test due to any flaws except those that are exceptionally large (and hence detectable by other means). This possibility is addressed in Step 2.

Again, note that materials that exhibit low tearing resistance in a highly constrained laboratory test do not always exhibit low tearing resistance in a low constraint structural geometry. Structural geometries with low constraint are more likely to exhibit high apparent tearing resistance and hence to be more suitable candidates for MCPT. High constraint geometries are most likely to exhibit low apparent tearing resistance and hence to be more suited for SCPT.

STEP 2: ASSESS CRITICAL CRACK SIZES

Specific information about the sizes and shapes of flaws in a component of interest is, in general, not known prior to performing a proof test, unless detailed NDE has been performed. The proof test itself provides only limited information about the presence or absence of relatively large flaws. Nevertheless, the probable range of sizes and shapes of flaws that may be present is an important variable to consider when designing a proof test and choosing the number of proof cycles.

Supporting Data Required:

Simple scoping calculations based on elastic-plastic fracture mechanics principles must be conducted to estimate the critical crack size during the proof test and/or to determine if rogue flaws of practical significance would fail during a proof test. This calculation requires:

(a) A structurally relevant measure of the material fracture behavior, as discussed in Step 1. A complete J-resistance curve is ideal. For the purposes of some scoping calculations below, a simple J_{Ic} value can be adequate.

(b) An estimate of the proof load or proof stress. Although the proof factor itself may not have been formally defined yet, it should be possible to identify a typical or bounding value (e.g., a minimum proof factor from the fracture control requirements) for the purposes of this scoping calculation.

(c) An estimate of the size and shape of a worst-case rogue flaw that might potentially be present at a critical location in the component. This estimate may be based on historical information about defect distributions and engineering judgment about the component itself. If a defect distribution is available, then the rogue flaw size might be chosen to correspond to an extreme value in the right tail of the distribution (for example, the mean value plus three to five times the standard deviation, depending on the level of reliability desired).

(d) An elastic-plastic fracture mechanics methodology for calculating the elastic-plastic crack driving force for the rogue flaw (c) in the component under a single cycle of proof loading (b) and the comparison of this driving force with the material resistance to fracture (a). This methodology should also permit the computation of the critical crack size for the estimated proof loading.

Information should be obtained about the NDE inspections, if any, to be conducted on the component prior to proof test or following the proof test. This NDE information should include some measure of the detectability limits for the given inspection techniques on the given component; i.e., how small of a flaw can be reliability detected?

Finally, information should obtained about the maturity of the specific manufacturing process used to produce the specific component, including historical information about defective components that have been produced previously.

Key Questions:

2.A. *Will the largest rogue flaw size reasonably possible in the component in its current condition cause the failure of the component under anticipated proof loads?*

"NO" $\Longrightarrow$ Code 2

This evaluation is actually fundamental to the decision to perform any sort of proof test at all. If there is no chance that the largest rogue flaw that could be expected to be present in the component would cause failure under the expected proof loads, then there is no reason to perform the proof test from a fracture mechanics standpoint. On the other hand, if proof testing of such a component is required for other (non-fracture mechanics) reasons, then the application of a small number of proof cycles should cause no significant damage to the component.

This calculation should ideally be performed with the complete structurally-relevant resistance curve, accounting for the effects of ductile tearing. For the purposes of evaluating MCPT vs. SCPT in this particular context, it is conservatively adequate to compare the elastic-plastic crack driving force with the initiation toughness value (e.g., J_{Ic}), and neglect the more complicated assessment of crack growth and failure during tearing. [In contrast, note that the use of J_{Ic} alone to estimate critical crack sizes in a conventional proof test flaw screening calculation is non-conservative].

If the postulated worst-case rogue flaw only marginally initiates tearing in a ductile material, but the material exhibits such appreciable toughening with crack advance (a large value of the tearing modulus) that failure of this worst-case flaw is not predicted under the expected proof load, then a worst-case scenario is possible. MCPT has the potential to cause serious subcritical damage to the component without screening defective flaws from the component. In this case, MCPT should be avoided if at all possible.

2.B. *Has the component received prior nondestructive evaluation, or will the component receive post-test NDE, that would be highly likely to detect flaws of critical size in the component?*

"YES" $\Longrightarrow$ Code 3

Here "flaws of critical size" are identified based on a scoping calculation performed with the data collected at the beginning of Step 2. This question and answer are related to 2.A, because NDE can be used as a flaw screening tool to remove critically cracked components from the population. If NDE were 100% reliable, then question 2.B would become the same as 2.A. However, since NDE is not 100% reliable, some potential benefit may remain for proof testing, and hence for MCPT, as a flaw screening method.

2.C. *Is the specific manufacturing process used to produce this particular component a mature and trouble-free process, such that a relatively large number of non-rejectable parts (and a negligible number of defective or rejectable parts) have been produced?*

"YES" $\Longrightarrow$ Code 3

"NO" $\Longrightarrow$ Code 4

The relative maturity of the manufacturing process can impact component integrity. Early in the development cycle of a component, the probability of finding a large rogue defect is usually higher, when all of the potential "bugs" have not yet been identified and eliminated from the production process. In this situation, MCPT can provide greater potential value. On the other hand, when the component design and manufacturing process has improved and stabilized, the chances of finding a large rogue defect may be generally much smaller, and in this situation, SCPT may be preferable to MCPT. In fact, this example is consistent with Rocketdyne MCPT experience. Most Rocketdyne MCPT failures have occurred in the early stages of the hardware development process. Once that development process has matured, no additional MCPT failures have occurred.

Additional Background:

The primary issue relative to crack geometry (depth, length, and shape) is the resulting magnitude of the crack driving force (J or K), in comparison to the material resistance. Larger cracks generate a larger driving force and hence an enhanced probability of failure during the proof test, while smaller cracks generate a smaller driving force and hence a decreased probability of failure during the proof test. MCPT provides a greater benefit relative to SCPT when the probability of failure during the proof test is higher. Therefore, if it is more probable that some large flaws are present in the hardware prior to the proof test, then MCPT is of greater benefit. On the other hand, if it can be established prior to the proof test that relatively large flaws are highly unlikely, then MCPT may result only in subcritical growth in the remaining population of small flaws. In this case, SCPT would be preferred, although MCPT would not

likely cause significant degradation of component remaining life if multiple proof cycles were required for other reasons.

It must be recognized that the shape of a flaw may be a more important factor than its depth. In particular, the aspect ratio of a surface flaw can have a dramatic impact on the crack driving force. A 10:1 aspect ratio flaw has a dramatically higher J value than does a semi-circular flaw of the same depth. It is possible that in a high toughness material, a semi-circular surface flaw of substantial depth could experience no crack extension during a proof test, while a 10:1 flaw could fail. Parameter studies conducted in the current program showed that these high aspect ratio cracks could easily motivate a preference for MCPT, while low aspect ratio cracks of comparable depth (which are generally more common in hardware) generally exhibited a slight preference for SCPT. Again, these observations are consistent with Rocketdyne experience. The majority of MCPT failures in which a specific initiating defect could be identified were associated with high aspect ratio surface flaws. Therefore, if the nature of the component geometry or manufacturing process provides some advance indication of the probable range of crack shapes, then this should be considered when performing the scoping calculations.

STEP 3: ASSESS COMPONENT GEOMETRY EFFECTS

Independent of crack geometry, the geometrical configuration of the component itself can play an important role in planning a proof test. Significant issues include the control mode, any prominent stress concentrations, and the general level of local structural constraint.

Supporting Data Required:

The engineer needs to understand how any fracture-critical location is loaded or strained, and how the crack driving force changes (increase or decrease?) with crack advance. If fracture-critical locations include significant stress concentrations from which cracks might form and grow, then the root radius of the stress concentration should be determined.

Key Questions:

3.A. *Are fracture-critical locations in the component in displacement control, such that the crack driving force decreases with increasing crack length? Or does crack growth at fracture-critical locations cause load shedding to alternate structural members, so that the crack driving force decreases with increasing crack length?*

"YES" $\Longrightarrow$ Code 1

As noted earlier in the Summary and Conclusions, proof testing to any number of cycles should be avoided for displacement-controlled configurations, in which the crack driving force decreases with increasing crack length. If proof testing is unavoidable, the number

of proof cycles should be minimized, and the test should be supported by a detailed fracture mechanics analysis based on accurate structural modeling of the hardware.

Fortunately, most proof tests are conducted under simple pressure loading or simple centrifugal loading (e.g., spin pit testing). Both of these are usually classic load control configurations, in which the crack driving force increases with increasing crack length.

The primary exception of potential concern here is a load-driven configuration with enough redundancy to permit load-shedding to an alternative structural member due to compliance changes in a cracked member. Proof testing should again be avoided altogether in this situation.

Displacement control configurations, when they occur, are also less likely to be fracture-critical locations, so this problem should arise only rarely.

3.B. *Are significant cracks located at the roots of moderate/severe notches or other stress concentrations?*

"YES" $\Longrightarrow$ Code 1 or 2 (see below)

Multiple cycle proof testing is not recommended for certain classes of components potentially containing significant cracks at heavily stressed notches or other stress concentrations. In particular, if initial crack sizes of significance for in-service reliability are small compared to the notch field dimensions (typically, less than 30 to 50 percent of the notch root radius), and if the notch is also severely stressed so that the crack dimensions are comparable to the plastic enclave at the uncracked notch root (but elastic constraint is maintained farther away from the notch), then MCPT should generally be avoided if possible.

If the critical crack size for failure during proof loading is also on the order of the notch field or only slightly larger, then the probability of damaging subcritical crack growth (crack advance without failure) during multiple proof cycles is enhanced. In this case, MCPT is strongly discouraged and must be supported by detailed fracture mechanics analysis if required by other considerations. (Code 1).

If the critical crack sizes for failure due to proof loading are large compared to the initial crack sizes, then proof testing of any type may be of limited value. Subcritical crack growth near the notch root, however, is unlikely to cause significant damage, and so a limited number of proof cycles is acceptable if necessary (Code 2).

In general, in some cases, the initial crack sizes will be sufficiently small that any subcritical crack growth during MCPT will be inconsequential for remaining service life. Here, again, MCPT is acceptable, although of limited value (Code 2).

If the initial crack size is large compared to the notch root radius, or if the plastic enclave at the (uncracked) notch root is small compared to the crack size, then the notch will not have a deleterious effect on the MCPT vs. SCPT comparison, and the proof testing protocol should be evaluated without any explicit consideration of the notch effect (i.e., neglect the notch for the purposes of the proof test analysis).

STEP 4. ASSESS PREDETERMINED PROOF TEST PARAMETERS

In some cases, some proof test parameters may have already been fixed prior to, and independent of, the selection of the number of proof cycles. For example, design considerations related to component static yielding or failure may limit the proof factor to some relatively small ratio. Alternatively, critical crack size considerations may have imposed a relatively large proof factor. The test environment may introduce the potential for environmental influences on crack growth or fracture. Under Step 4, the question is how these predetermined proof test parameters influence the decision between SCPT and MCPT. If these proof test parameters have not been predetermined, then go directly to Step 5.

Key Questions:

4.A. *Will the proof test be conducted in an environment which is known or suspected to act aggressively to promote crack growth or fracture?*

"YES" $\Longrightarrow$ Code 1

Certain environments can act aggressively on certain materials to enhance crack tip damage, leading to accelerated subcritical crack growth and/or a decrease in the effective fracture toughness of the material. In general, these time-assisted processes are not well-characterized, and therefore it is difficult, if not impossible, to incorporate their effects in a proof test analysis. On the other hand, these aggressive environments clearly provide the opportunity for enhanced subcritical damage: damage which decreases the integrity and reliability of the component without being detected. Therefore, the total time of exposure to these environments during the proof test should be minimized. One way of minimizing exposure time is to limit the number of proof cycles to a single cycle. If possible, proof testing should be avoided altogether in aggressive environments.

4.B. *Is the predetermined proof factor a moderate to high value?*

"YES" $\Longrightarrow$ Code 3

"NO" $\Longrightarrow$ Code 4

Parameter studies conducted under the current contract indicate that the incremental benefit of multiple cycles is relatively smaller when the proof factor is greater (and,

hence, when the benefit of the first cycle itself is greater). Therefore, multiple proof cycles may be of more value when the proof factor is limited by other considerations to a relatively smaller number.

It may be possible in some situations to "trade" numbers of proof cycles for a different proof factor. Due to the many complex issues involved, however, it is not possible to provide any simple rules-of-thumb for this trade-off. Here, a detailed probabilistic fracture mechanics analysis should be performed to estimate the effect on fleet reliability of various combinations of proof factor and numbers of cycles.

STEP 5. SELECT SCPT OR MCPT

Step 5 addresses directly the fundamental question about the relative desirability of single-cycle versus multiple-cycle proof testing.

Supporting Data Required:

The input to Step 5 is all the answers to the key questions in Steps 1 through 4. Those answers should be collected and integrated as described in the key questions that follow. Note that if **any** previous questions in Steps 1 through 4 resulted in a Code 1 or Code 2, the flow chart goes directly to question 5.C.

Key Questions:

5.A. *Are all answers "Code 3" ?*

"YES" $\Longrightarrow$ **SCPT is recommended, but MCPT is acceptable and could be beneficial**

In general, as noted in the Introduction to the flow chart, Code 3 indicates a slight potential preference for MCPT over SCPT. However, in the unlikely event that MCPT has at most a marginal potential benefit from *all* perspectives simultaneously (a low effective tearing modulus, a low probability of critical flaws in the hardware, *and* a moderate to high value of the proof factor), the expected overall benefit from MCPT may be negligible at best. In this situation, the slight increase in subcritical damage for all potential smaller flaws may outweigh the slight increase in flaw screening capability. Therefore, SCPT is recommended, but MCPT is still acceptable if other considerations so warrant.

5.B. *Are all answers "Code 4" ?*

"YES" $\Longrightarrow$**MCPT is recommended, but SCPT may be acceptable**

"NO" $\Longrightarrow$ **MCPT is recommended, but SCPT is acceptable**

If all answers are Code 4, then the component is likely an ideal candidate for MCPT. SCPT may still give an acceptable assurance of structural reliability, but may provide measurably less benefit than MCPT.

If a mixture of Code 3 and Code 4 answers have been obtained, then MCPT will likely provide some marginal benefit and is therefore recommended. However, SCPT is acceptable, and may be the preferred choice based on other considerations such as cost. The final selection here should be based on engineering judgement about the relative significance of the various answers in Steps 1 through 4, along with other considerations such as cost and historical precedent.

5.C. *Are there other compelling reasons to perform multiple proof cycles?*

"YES" $\Rightarrow$**MCPT will be performed**

This question is asked only if the prior evaluation process has indicated a preference for SCPT over MCPT. However, in some situations, multiple proof cycles will be desired or required for reasons other than a fracture-mechanics based assessment of component integrity. For example, an assembly sequence may require proof testing at different times during the assembly, such that some components added early in the assembly are tested more than once. Or repeated proof testing may be needed to confirm general workmanship quality not necessarily related to structural integrity (e.g., leak checks).

If Code 2 has been indicated, then it is prudent to go back and review all questions in the flow chart that can potentially yield a Code 1. The short-circuiting nature of the flow chart whenever a Code 1 or Code 2 is indicated means that some of the Code 1 questions may not have been considered previously. It is important to identify if any feature of the problem would indicate a Code 1 condition, because under Code 1 MCPT is potentially damaging.

If Code 1 has been indicated anywhere on the flow chart, then it is most desirable to avoid multiple proof cycles altogether. The other "compelling reasons" should be reviewed to determine if they can be overruled in favor of SCPT.

If MCPT has been judged "acceptable," (Code 2 or Code 3) then it may be implemented with confidence. However, it may be prudent (and cost-efficient) to limit the number of multiple cycles, especially if Code 2 has been indicated.

STEP 6: SELECT OTHER PROOF TEST PARAMETERS FOR MCPT

All questions under Step 6 are based on the assumption that MCPT has been selected from the decision process in Step 5. If SCPT has been selected, then no guidance is available in this document to choose other proof test parameters.

6.A. *How many proof cycles should be selected?*

The guidelines proposed above and below all address the relative merits of MCPT vs. SCPT, without specifying the optimum number of proof cycles. What is the optimum number of proof cycles?

The parameter studies conducted in the current research program generally indicate that if two proof cycles are shown to be better than one proof cycle for a given proof testing problem, then three will be better than two, four will be better than three, and so on *without limit*. In other words, from a strict reliability standpoint, if MCPT is better than SCPT, then more cycles is always better. There is no single optimum number of cycles that can be calculated mathematically in most cases.

However, this observation must be immediately tempered by two additional observations. First of all, the incremental benefit of each additional cycle continuously decreases. The additional benefit accrued by cycle four is generally less than the additional benefit accrued by cycle three. The principle of diminishing returns holds true, and frequently the returns diminish dramatically. The incremental benefit obtained by hypothetical cycles 15 through 20 might be less than the incremental benefit of cycle 2. And in most cases, even when MCPT leads to a perceptible increase in service reliability, the benefit of the first proof cycle is substantially greater than the benefit of any subsequent cycle—perhaps even greater than the summed incremental benefit of all subsequent proof cycles put together.

The second tempering observation is that proof testing is not free. Each additional cycle costs some additional time and manpower. In the extreme case, a large number of proof cycles could cause enough subcritical damage to produce an unnecessarily high proof test mortality rate, or to cause the premature retirement of the remaining unfailed components from service, and hence to incur unnecessary replacement costs.

Therefore, a balanced approach to the selection of the optimum number of proof cycles should be taken. In situations where MCPT is preferable to SCPT (Code 3 and Code 4), a significant but still relatively small number of cycles appears reasonable. The five-cycle protocol currently used by Rocketdyne appears to be a reasonable choice, but from a fleet reliability standpoint there will not be a substantial difference if four cycles, or six cycles, or even ten cycles are adopted. Other considerations, such as experience, convenience, cost, and other reasons for proof testing may legitimately come into play.

In view of these considerations, for convenience, and for the purposes of establishing and maintaining historical precedent, five proof cycles are recommended (but not mandated) whenever MCPT is indicated as being desirable (Code 3 or Code 4).

If Code 1 or Code 2 were previously indicated, then MCPT is of no benefit from a fracture mechanics standpoint. In this case, the number of proof cycles should be limited to the minimum number possible.

If Code 1 was previously indicated, then every effort should be made to limit the number of proof cycles, and to avoid multiple cycles if at all possible. Furthermore, the test should be supported by a detailed fracture mechanics analysis.

6.B. *What should be the proof factor?*

The proof factor is a particularly important parameter for proof test efficacy, and the specification of the proof factor itself is a complex and crucial issue for the optimum design of the proof test. That detailed specification is outside the scope of this particular contract and these guidelines. Detailed guidance on the selection of the proof factor will be provided in the comprehensive guidelines being developed under the Proof Test Philosophy contract.

However, as noted above under Step 4, it may be possible in some situations to "trade" numbers of proof cycles for a different proof factor. Due to the many complex issues involved, however, it is not possible to provide any simple rules-of-thumb for this trade-off. Here, a detailed probabilistic fracture mechanics analysis should be performed to estimate the effect on fleet reliability of various combinations of proof factor and numbers of cycles.

It is not recommended to decrease the proof factor only because additional proof cycles could be imposed. The proof factor should be chosen as high as is reasonably prudent for the component at hand, in order to maximum the flaw-screening capability without unnecessarily deforming otherwise safe components.

6.C. *What should be the proof test hold time?*

Hold time issues were discussed in more detail in Section 5. Longer hold times provide additional opportunities for subcritical crack growth, and this subcritical crack growth will be most substantial for cracks that are near criticality. Small cracks that are far below criticality will generally exhibit no additional subcritical growth during hold times. Due to the limited nature of the investigations of hold time under the current contract, it is not possible to make definitive recommendations for the influence of the hold time on the selection of the number of cycles.

In general, it appears that proof tests with longer hold times increase the benefits of MCPT compared to SCPT. Therefore, if multiple proof cycles have been selected, then consideration should be given to implementing or maintaining nonnegligible hold times during the proof test. However, on the other hand, the nature and extent of time-dependent crack growth is not well-understood or well-characterized. Hold times

introduce an additional element of uncertainty into the interpretation of the proof test. Therefore, long hold times are not recommended.

If multiple cycle testing is unavoidable in aggressive environments, hold times should be minimized or, if possible, eliminated altogether.

8. REFERENCES

1. A. L. Hallden, Rockwell International Internal Letter 9114-8062, 28 September 1979.

2. C. E. Hartblower and P. P. Crimmins, "Fracture of Structural Metals as Related to Pressure-Vessel Integrity and In-Service Monitoring," ASME Paper 71-PVP-60, February 1971.

3. J. A. Schliessmann, "Pressure Vessel Proof Test Variables and Flaw Growth," *Journal of Materials*, Vol. 7, No. 4, December 1972, pp. 465-469.

4. J. F. Kiefner, W. A. Maxey, and R. J. Eiber, "A Study of the Causes of Failures of Defects That Have Survived a Prior Hydrostatic Test," NG-18, Report No. 111 to Pipeline Research Committee, American Gas Association, AGA Catalog No. L51398, November 1980.

5. E. F. Tiffany and E. J. Masters, "Applied Fracture Mechanics," *Fracture Toughness Testing, ASTM STP 381*, 1965, pp. 249-277.

6. S. J. Hudak, Jr., R. C. McClung, M. L. Bartlett, J. H. FitzGerald, and D. A. Russell, "A Comparison of Single-Cycle Versus Multiple-Cycle Proof Testing Strategies," NASA Contractor Report 4318, Aug. 1990.

7. V. Kumar, M. D. German, and C. F. Shih, "An Engineering Approach for Elastic-Plastic Fracture Analysis," Report NP-1931, Electric Power Research Institute, July 1981.

8. R. A. Ainsworth, "The Assessment of Defects in Structures of Strain Hardening Material," *Engineering Fracture Mechanics*, Vol. 19, 1984, pp. 633-642.

9. N. E. Dowling, "*J*-Integral Estimates for Cracks in Infinite Bodies," *Engineering Fracture Mechanics*, Vol. 18, 1983, pp. 925-938.

10. Y.-Y. Wang, "Analysis of Fracture Initiation in Surface-Cracked Plates," M.S. Thesis, Massachusetts Institute of Technology, 1988. See also D. M. Parks and Y.-Y. Wang, "Elastic-Plastic Analysis of Part-Through Surface Cracks," *Analytical, Numerical, and Experimental Aspects of Three Dimensional Fracture Processes, AMD-Vol. 91*, ASME, 1988, pp. 19-32.

11. Y.-Y. Wang, "A Two-Parameter Characterization of Elastic-Plastic Crack Tip Fields and Applications to Cleavage Fracture," Ph.D. Thesis, Massachusetts Institute of Technology, 1991.

12. M. T. Kirk and R. H. Dodds, Jr., "Approximate Techniques of *J* Estimation Applicable to Part-Through Surface Cracks," *Engineering Fracture Mechanics*, Vol. 43, 1992, pp. 123-136.

13. R. H. Dodds, Jr., C. F. Shih, and T. L. Anderson, "Continuum and Micromechanics Treatment of Constraint in Fracture," Structural Research Series Report No. 573, Department of Civil Engineering, University of Illinois at Urbana-Champaign, November 1992.

14. G. Yagawa, Y. Kitajima, and H. Ueda, "Three-Dimensional Fully Plastic Solutions for Semi-elliptical Surface Cracks," *International Journal of Pressure Vessels and Piping*, Vol. 53, 1993, pp. 457-510.

15. A. G. Miller, "*J* Estimation for Surface Defects," Report TPRD/B/0811/R86, Central Electricity Generating Board, 1986.

16. G. G. Chell, "Application of the CEGB Failure Assessment Procedure, R6, to Surface Flaws," *Fracture Mechanics: Twenty-First Symposium, ASTM STP 1074*, 1990, pp. 525-544.

17. J. C. Newman, Jr., and I. S. Raju, "Analyses of Surface Cracks in Finite Plates under Tension or Bending Loads," NASA TP-1578, 1979.

18. "Elastic-Plastic and Fully Plastic Fatigue Crack Growth," Contract NAS8-37828, NASA George C. Marshall Space Flight Center, Southwest Research Institute Project 06-5013, 1992-present.

19. G. G. Chell, "A *J* Estimation Scheme for Cracks at Notches," Appendix to Monthly Technical Progress Report No. 48, NASA-MSFC Contract No. NAS8-37828, January 25, 1996.

20. A. Zahoor, *Ductile Fracture Handbook*, NP-6301-D, Vols. 1-3, EPRI, 1989-1991.

21. R. C. McClung and H. Sehitoglu, "Characterization of Fatigue Crack Growth in Intermediate and Large Scale Yielding," *ASME Journal of Engineering Materials and Technology*, Vol. 113, 1991, pp. 15-22.

22. K. S. Kim and T. W. Orange, "A Review of Path-Independent Integrals in Elastic-Plastic Fracture Mechanics," *Fracture Mechanics: Eighteenth Symposium, ASTM STP 945*, 1988, pp. 713-729.

23. H. S. Lamba, "The *J*-Integral Applied to Cyclic Loading," *Engineering Fracture Mechanics*, Vol. 7, 1975, pp. 693-703.

24. C. Wuthrich, "The Extension of the *J*-Integral Concept to Fatigue Cracks," *International Journal of Fracture*, Vol. 20, 1982, pp. R35-R37.

25. K. Tanaka, "The Cyclic *J*-Integral as a Criterion for Fatigue Crack Growth," *International Journal of Fracture*, Vol. 22, 1983, pp. 91-104.

26. S. Kubo, T. Yafuso, M. Nohara, T. Ishimaru, and K. Ohji, "Investigation on Path-Integral Expression of the *J*-Integral Range Using Numerical Simulations of Fatigue Crack Growth," *JSME International Journal*, Series I, Vol. 32, 1989, pp. 237-244.

27. R. C. McClung, "Finite Element Modeling of Fatigue Crack Growth," *Theoretical Concepts and Numerical Analysis of Fatigue*, Engineering Materials Advisory Services, 1992, pp. 153-172.

28. J. C. Newman, Jr., "A Crack Opening Stress Equation for Fatigue Crack Growth," *International Journal of Fracture*, Vol. 24, 1984, pp. R131-R135.

29. R. C. McClung, G. G. Chell, D. A. Russell, and G. E. Orient, "Development of a Practical Methodology for Elastic-Plastic Fatigue Crack Growth," *Advanced Earth-to-Orbit Propulsion Technology - 1994*, NASA CP 3282, NASA George C. Marshall Space Flight Center, 1994, Vol. II, pp. 248-257.

30. R. C. McClung, G. G. Chell, D. A. Russell, and G. E. Orient, "A Practical Methodology for Elastic-Plastic Fatigue Crack Growth," *Fatigue and Fracture Mechanics: 27th Volume, ASTM STP 1296*, R. S. Piascik, J. C. Newman, Jr., and N. E. Dowling, Eds., American Society for Testing and Materials, in press.

31. K. J. Nix, N. Knee, T. C. Lindley, and G. G. Chell, "An Investigation of Fatigue Crack Growth in a Ductile Material at High Growth Rates," *Fatigue and Fracture of Engineering Materials and Structures*, Vol. 11, 1988, pp. 205-220.

32. K. J. Nix, G. G. Chell, N. Knee, and T. C. Lindley, "An Investigation of the Interaction Between Ductile Tearing and Fatigue in a Low Alloy Steel," *Advances in Fracture and Fatigue for the 1990's, Vol. I: Load History Effects of Fracture Resistance*, PVP - Vol. 166, ASME, 1989, pp. 33-39.

33. R. C. McClung, B. H. Thacker, and S. Roy, "Finite Element Visualization of Fatigue Crack Closure in Plane Stress and Plane Strain," *International Journal of Fracture*, Vol. 50, 1991, pp. 27-49.

34. N. E. Dowling, "Geometry Effects and the *J*-Integral Approach to Elastic-Plastic Fatigue Crack Growth," *Cracks and Fracture*, ASTM STP 601, 1976, pp. 19-32.

35. J. R. Rice, "Elastic-Plastic Fracture Mechanics," *The Mechanics of Fracture*, AMD - Vol. 19, ASME, 1976, pp. 23-53.

36. C. Laird, "The Influence of Metallurgical Structure on the Mechanisms of Fatigue Crack Propagation," *Fatigue Crack Propagation, ASTM STP 415*, 1967, pp. 131-168.

37. D. P. Wilhem and M. M. Ratwani, "Application of the R-Curve Concept to Fatigue Crack Growth," *Journal of Engineering Materials and Technology, Trans. ASME*, Vol. 100, 1978, pp. 416-420.

38. R. C. McClung, "Crack Closure and Plastic Zone Sizes in Fatigue," *Fatigue and Fracture of Engineering Materials and Structures*, Vol. 14, No. 4, 1991, pp. 455-468.

39. H. Kobayashi, T. Kusumoto, and H. Nakazawa, "Cyclic J-R Curve and Upper Limit Characteristic of Fatigue Crack Growth in 2-½Cr-Mo Steel," *Advances in Fracture and Fatigue for the 1990's, Vol. I:Load History Effects of Fracture Resistance,* PVP-Vol. 166, American Society of Mechanical Engineers, 1989, pp. 55-63.

40. T. W. Orange, "Methods and Models for R-Curve Instability Calculations," *Fracture Mechanics: Twenty-First Symposium, ASTM STP 1074*, 1990, pp. 545-559.

41. "Proof Test Philosphy to State-of-the-Art Technology," Contract NAS8-39380, NASA George C. Marshall Space Flight Center, Southwest Research Institute Project 06-5088, 1992-present.

42. D. E. Matejczyk, "Retardation Analytical Model to Extend Service Life," RI/RD86-217, Final Report to NASA Marshall Space Flight Center on Contract NAS8-35507, July 1986.

43. H.-M. Bauschke, D. T. Read, and K.-H. Schwalbe, "Crack Growth Resistance at Surface Cracks in Three Aluminium Alloys," *Defect Assessment in Components - Fundamentals and Applications, ESIS/EGF 9*, Mechanical Engineering Publications, London, 1991, pp. 749-764.

44. "Probabilistic Structural Analysis Methods for Select Space Propulsion System Components," Final Report to NASA Lewis Research Center, Contract NAS3-24389, Southwest Research Institute, September 1995.

45. P. E. Becher and A. Pedersen, "Application of Statistical Linear Elastic Fracture Mechanics to Pressure Vessel Reliability Analysis," *Nuclear Engineering and Design*, Vol. 27, 1974, pp. 413-425.

46. A. Bruckner and D. Munz, "A Statistical Model of Crack Formation in Welds," *Engineering Fracture Mechanics*, Vol. 19, 1984, pp. 287-294.

47. A. B. Lidiard and M. Williams, "A Simplified Analysis of Pressure Vessel Reliability," *Journal of the British Nuclear Energy Society*, Vol. 16, 1977, pp. 207-223.

48. C. F. Tiffany, "On the Prevention of Delayed Time Failures of Aerospace Pressure Vessels," *Journal of the Franklin Institute*, Vol. 290, December 1970, pp. 567-582.

49. H. H. Johnson and P. C. Paris, "Sub-critical Flaw Growth," *Engineering Fracture Mechanics*, Vol. 1, 1968, pp. 3-45.

50. J. D. Landes and R. P. Wei, "Kinetics of Subcritical Crack Growth and Deformation in a High Strength Steel," *Journal of Engineering Materials and Technology, Trans. ASME*, Vol. XX, 1973, pp. 2-9.

51. F. W. Brust and B. N. Leis, "A Model for Predicting Primary Creep Damage in Axially Cracked Cylinders—I. Theory," *Engineering Fracture Mechanics*, Vol. 43, 1992, pp. 615-627.

52. F. W. Brust and B. N. Leis, "A Model for Predicting Primary Creep Damage in Axially Cracked Cylinders—II. Applications," *Engineering Fracture Mechanics*, Vol. 43, 1992, pp. 629-639.

53. T. Ingham and E. Morland, "Influence of Time-Dependent Plasticity on Elastic-Plastic Fracture Toughness," *Elastic-Plastic Fracture: Second Symposium, Volume I—Inelastic Crack Analysis, ASTM STP 803*, 1983, pp. I-721–I-746.

APPENDIX A. Further Documentation of Improved *J* Solutions for Surface Flaws

In Section 2.1 of the main body of this report, a short synopsis was provided of an improved reference stress technique for estimating J for surface cracks in finite thickness geometries. The development of the improved technique was guided by several recently published sets of finite element (FE) J solutions, and these same FE solutions were used to demonstrate the performance of the general solution technique in its final form. In this appendix, further documentation is provided for the FE solutions, the derivation of the modified reference stress technique, and the final comparisons of the FE and reference stress solutions.

Finite Element Solutions

Several finite element solutions for surface cracks in finite bodies were available at the time of this study [A1, A2, A3, A4, A5]. These efforts included a variety of plate and flaw geometries and constitutive relationships, as summarized in Table A1. The geometric nomenclature is illustrated in Figure A1.

Comparison of various numerical results with each other and with simple analytical formulas requires a suitable mathematical framework. Following the EPRI handbook approach, a general form for J in a Ramberg-Osgood material can be postulated according to

$$J_{total} = \frac{K^2}{E'}\left\{1 + \frac{F^2}{C_2}\left(\frac{n-1}{n+1}\right)\left[\frac{(\sigma_\infty/\sigma_0)^2}{1+(\sigma_\infty/\sigma_0)^2}\right]\right\} + \alpha\,\sigma_0\,\varepsilon_0\,th_1\left(\frac{\sigma_\infty}{\sigma_0}\right)^{n+1} \qquad \text{(A.1)}$$

The last (plastic) term contains a non-dimensional factor h_1 that changes with both geometry and strain hardening exponent but not with applied stress. It is this h_1 which is tabulated in the elastic-plastic fracture handbooks, and it is this h_1 (or its equivalent) which any simple estimation technique must compute accurately.

The analysis of Yagawa *et al.* [A5] was based on a fully plastic FE solution, and so the results are already expressed in terms of h_1 (Yagawa *et al.* call it $f(\varphi)$). On the other hand, the early analysis of Wang [A1] and the work of Dodds *et al.* [A4] both employed a Ramberg-Osgood total strain constitutive relationship, and the results were expressed in terms of total J at different applied stresses. In order to compare these results more directly with Yagawa *et al.* and with simple estimation schemes, it would be preferable to extract an estimate of h_1. This extraction can be carried out based on Eqn. A1: the published FE value of total J is set equal to the left hand side of the equation; the elastic term (including the effective crack length correction) is estimated from the Newman-Raju K solution and then subtracted off to leave only the plastic term; and the plastic term is then normalized to solve for h_1. If this process is successful, then the computed h_1 should be approximately the same at all applied stresses. This

TABLE A1
Summary of geometries and constitutive laws for finite element J solutions

Author	Ref.	a/t	a/c	b/c	h/t	Constitutive Law
Wang (1988)	[A1]	0.5 0.6	1.0 0.24	16 3.2	16 16	Ramberg-Osgood (n = 5, 10)
Wang (1991)	[A2]	0.15 0.60	0.24 0.24	16 3.2	16 16	fully elastic/ fully power-law (n = 10)
Kirk (1992)	[A3]	0.13 0.25 0.25	0.763 0.769 0.333	11.77 6.15 2.67	2.85 2.85 2.85	bilinear (plastic slope = E/84)
Dodds (1992)	[A4]	0.25	0.333	2.67	2.85	Ramberg-Osgood (n = 4, 10)
Yagawa (1993)	[A5]	0.2 0.2 0.2 0.5 0.5 0.5 0.8 0.8 0.8	0.2 0.6 1.0 0.2 0.6 1.0 0.2 0.6 1.0	4 4 4 4 4 4 4 4 4	4 1.33 0.8 10 3.33 2 16 5.33 3.2	power-law fully plastic (n = 1, 2, 3, 5, 7, 10)

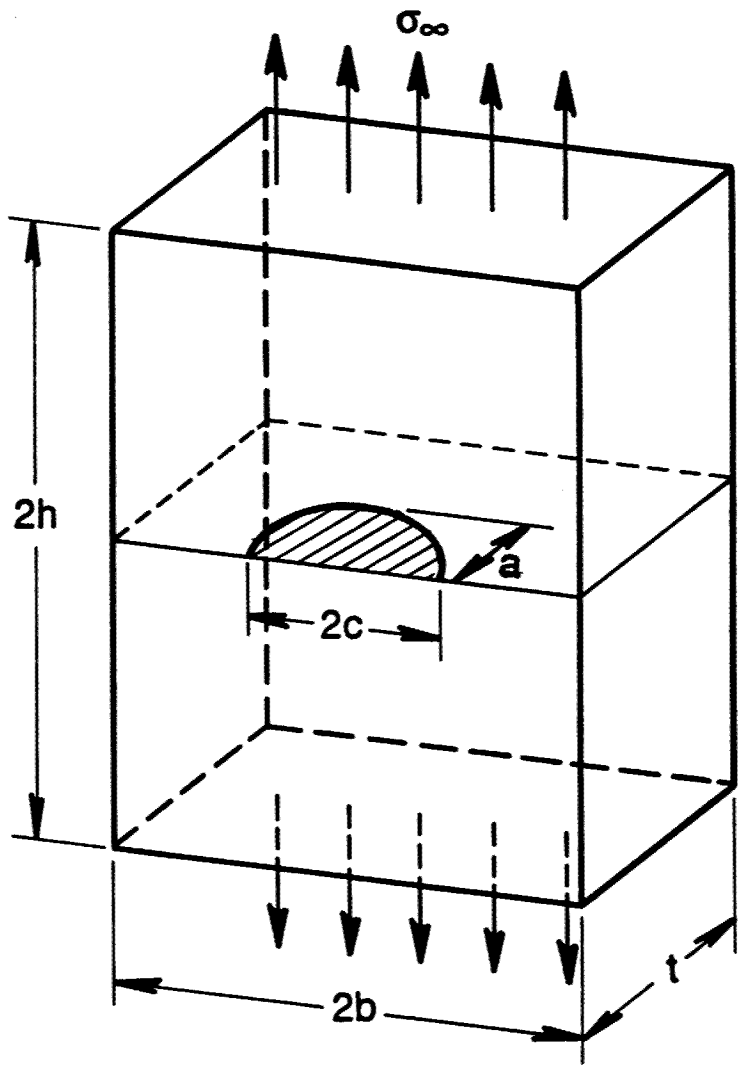

Figure A1. Geometric nomenclature for semi-elliptical surface crack in finite plate

successful result would also serve as an indirect confirmation of the process by which J_{total} can be accurately estimated by summing independent elastic and plastic components.

Graphs of h_1 as a function of applied stress are given for the four earlier Wang analyses in Fig. A2 and the two Dodds *et al.* analyses in Fig. A3. In all cases, h_1 is remarkably constant. Apparent variations in h_1 at lower applied stresses occur because the plastic term itself is very small and small inaccuracies in any variable cause large errors in h_1.

These derived values of h_1 are compared with the published h_1 values of Yagawa in Fig. A4 for $n = 10$. The Wang calculation for $a/t = 0.5$, $a/c = 1.0$ agrees closely with the corresponding Yagawa value ($h_1 = 2.4$ vs. 2.57). The Dodds result for $a/t = 0.25$, $a/c = 0.333$, and the Wang result for $a/t = 0.6$, $a/c = 0.24$, appear to be too high in comparison to neighboring Yagawa results. This disagreement may be partially attributable to small values of b/c for Dodds and Wang, but it may also indicate some inaccuracies in the FE results. These issues will be investigated in more depth below. Similar results were obtained at $n = 5$, where the Wang and Yagawa calculations of h_1 for $a/t = 0.5$, $a/c = 1.0$, were identical, but the Yagawa computations seem low in comparison to the Wang $a/t = 0.6$, $a/c = 0.24$ values.

It is not possible to compare the later results of Wang [A2] or the solutions of Kirk [A3] with the other three sets of results on this same h_1 basis, because different constitutive relationships were employed. The later Wang analysis used a stress-strain law which was perfectly elastic below the yield stress and simple power-law fully plastic above the yield stress. The Kirk analysis was based on a bilinear stress-strain curve. An alternative means of comparing these two solution sets will be developed below.

Reference Stress Estimates

A brief outline of the reference stress method and the key equations for J estimation were provided in Section 2.1. Identification of a suitable form for the yield function f was identified as a key step in the method.

The simplest choice of yield function f for the surface flaw is that based on the reduction in load bearing area due to the presence of the defect. This gives the global yield function,

$$f = 1 - \frac{\pi\, a\, c}{4\, b\, t} \qquad \text{(A.2)}$$

This was the form used in the Phase I estimation technique. As noted in the main body of the report, this form can give f estimates too large for wide plates (large b/c ratios).

An alternative approach is to define some effective plate dimension (in the width direction) that characterizes collapse. One such construction was shown in Fig. 2.1, where the effective width is given as $(2\xi + 2c)$. When stresses in this enclosed region are in yield, collapse

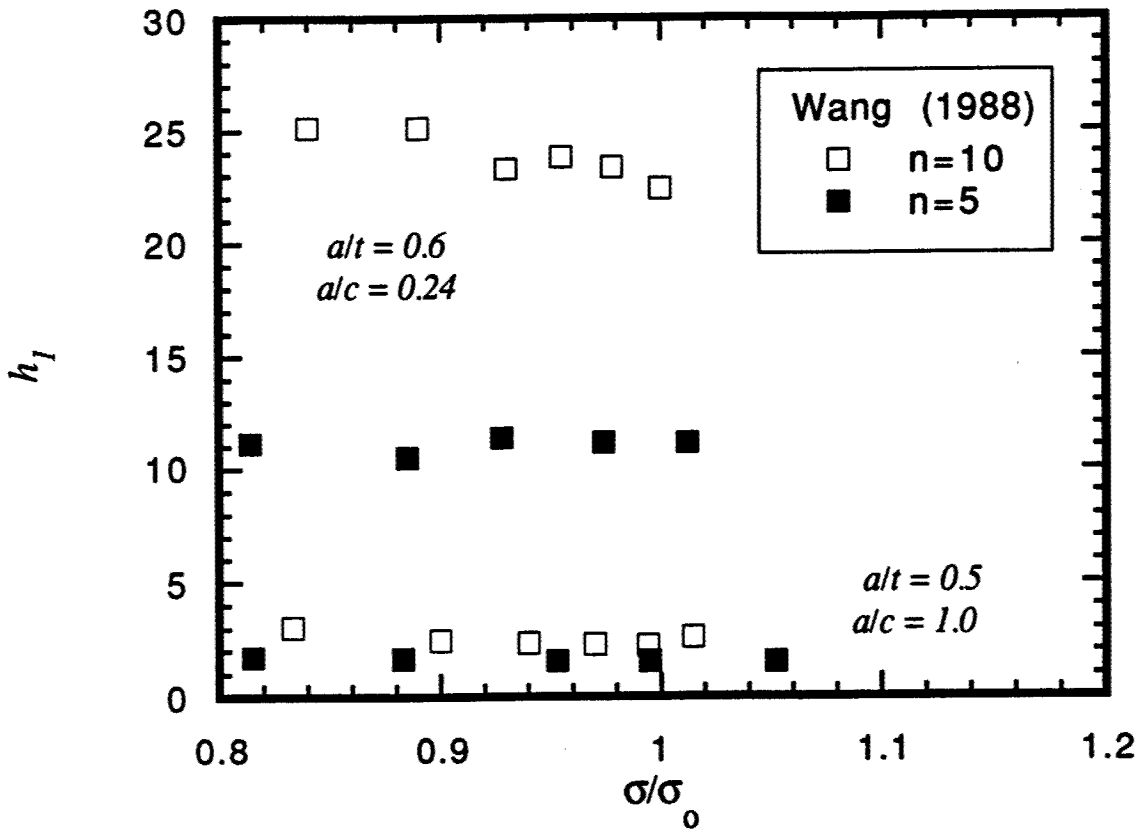

Figure A2. Variation in extracted h_1 with applied stress from Wang (1988) analyses

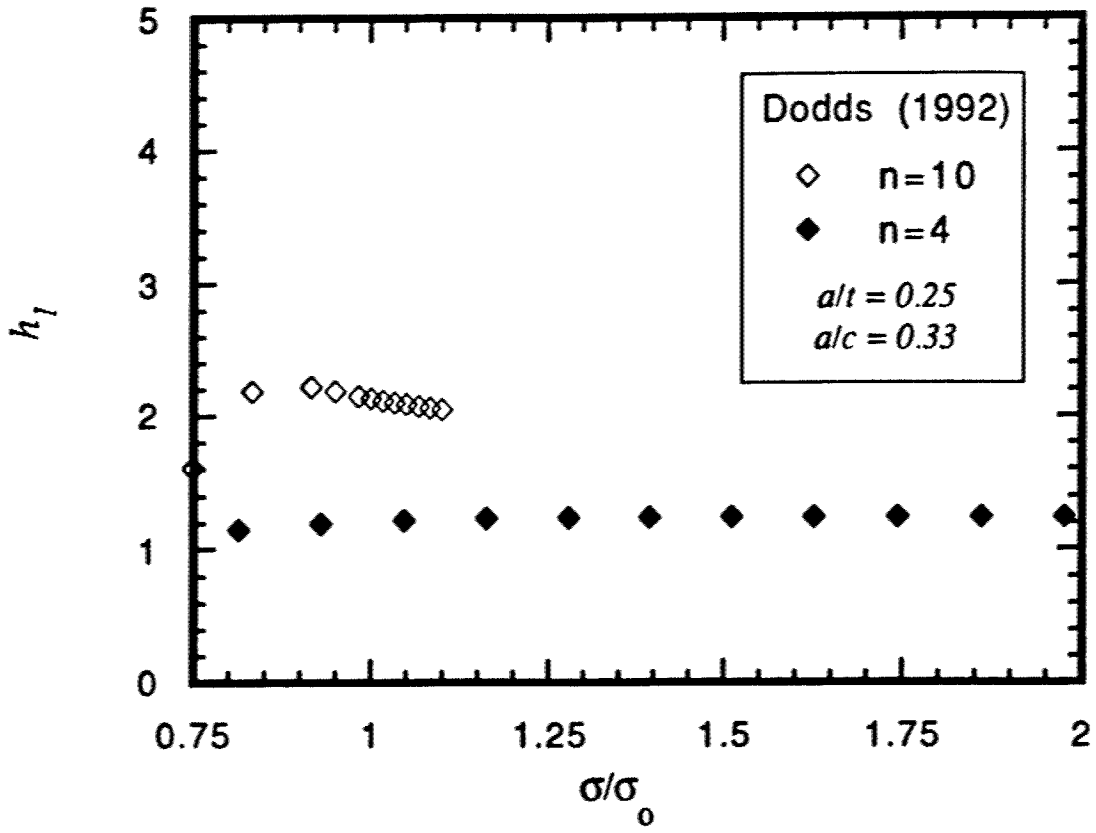

Figure A3. Variation in extracted h_1 with applied stress from Dodds (1992) analyses

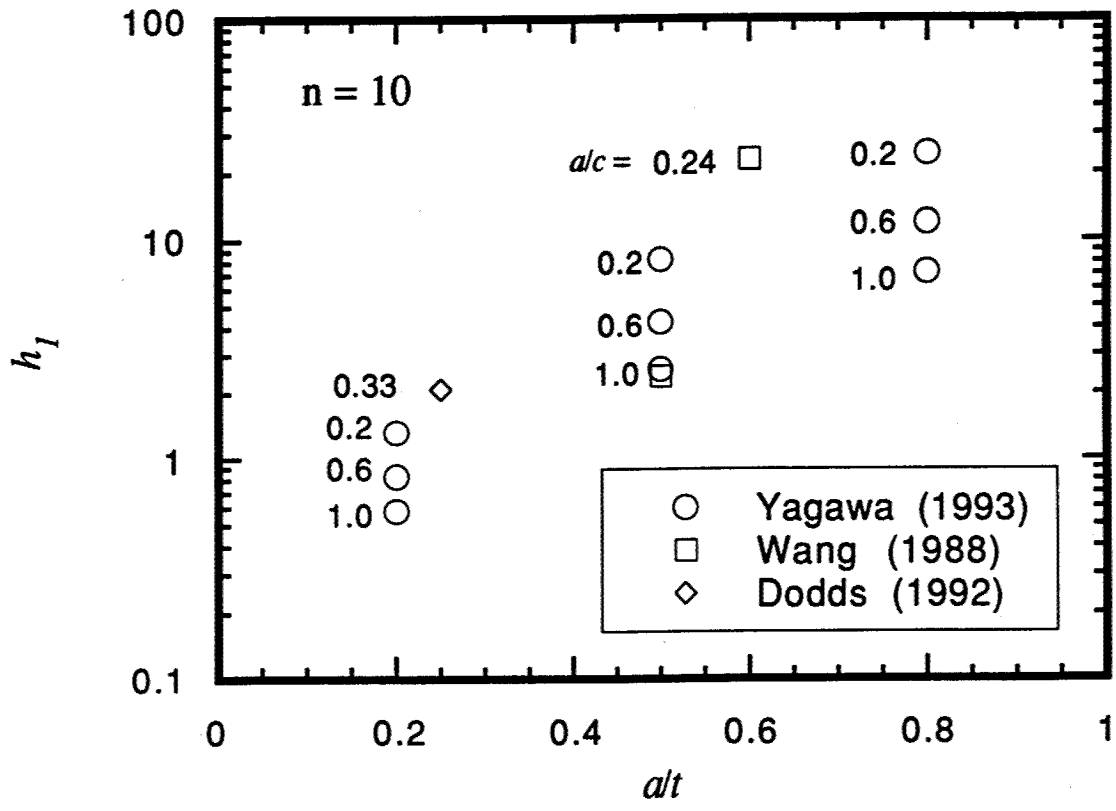

Figure A4. Comparison of h_1 values from various authors

is assumed to occur. The remaining problem now is to select the proper value of ξ. Remembering that the optimum choice of a limit load can be driven by optimum agreement with FE solutions, it is possible to work backwards from available numerical solutions to evaluate different means of defining ξ.

The collapse function for the geometrical construction of Fig. 2.1 can be written as

$$f = \frac{\xi + c\left(1 - \frac{a'}{t}\right)}{\xi + c} \qquad \text{(A.3)}$$

Here the actual semi-elliptical cracked area has been represented by the equivalent rectangular area a' x $2c$, where $a' = \pi a/4$. Other constructions of the effective plate width and equivalent rectangular area are possible and may give slightly different results, especially in various limiting configurations, but the current approach appears reasonable for most practical geometries. Inverting Eqn. A8 and solving for ξ, we obtain the result

$$\xi = \frac{c\,a'}{t(1-f)} - c \qquad \text{(A.4)}$$

There are several possible ways that ξ might be related to the plate geometry. If the h_1 formulation in Eqn. 2.8 and the nominal net section area criterion (Eqn. A.2) are both correct, then $\xi = (b\text{-}c)$ and the non-dimensional quantity $\xi/(b\text{-}c)$ will be equal to 1. Alternatively, it is possible that ξ is related to the plate thickness t, so that the ratio ξ/t will be approximately constant. Another characteristic dimension of the cracked geometry is the crack width $2c$, so the nondimensional ratio ξ/c may be significant.

Collapse functions f have been computed and listed in Table A2 for the five sets of FE solutions summarized in Table A1. Here f has been computed for the Ramberg-Osgood or fully-plastic power law materials according to

$$f = \left\{\frac{h_1}{F^2\,\pi\,(a/t)}\right\}^{\frac{1}{1-n}} \qquad \text{(A.5)}$$

Calculation of f for other constitutive relationships were carried out by algebraically inverting the basic reference stress equation for J, Eqn. 2.4, remembering that $\sigma_{ref} = \sigma\sqrt{f}$, and inserting the appropriate expression for ε_{ref} as a function of σ_{ref}. It should be noted, however, that the calculated f values from the Kirk [A3] results (bilinear stress-strain law) were not independent of applied stress, but steadily decreased with increasing applied stress. The values listed in Table A2 are averages at the highest applied stresses reported by Kirk. Insufficient data were

TABLE A2

Summary of reference stress parameters calculated from finite element solutions

Author	*a/t*	*a/c*	h_1	*f*	$\xi / (b-c)$	ξ / t	ξ / c
Wang (1988)	0.5	1.00	2.40	0.879	0.15	1.12	2.25
n=10	0.6	0.24	23.25	0.830	0.81	4.43	1.77
n=5	0.5	1.00	1.59	0.833	0.09	0.68	1.35
	0.6	0.24	11.09	0.792	0.58	3.16	1.27
Wang (1991)	0.15	0.24		0.971	0.26	1.91	3.06
	0.6	0.24		0.883	1.38	7.57	3.03
Kirk (1992)	0.13	0.76		0.970	0.22	0.41	2.40
bilinear	0.25	0.77		0.937	0.41	0.69	2.12
	0.25	0.33		0.937	1.27	1.59	2.12
Dodds (1992)							
n=4	0.25	0.33	1.24	0.900	0.58	0.72	0.96
n=10	0.25	0.33	2.09	0.911	0.72	0.91	1.21
Yagawa (1993)	0.2	0.2	1.33	0.945	0.62	1.86	1.86
n=10	0.2	0.6	0.83	0.939	0.53	0.53	1.58
	0.2	1.0	0.58	0.923	0.35	0.21	1.04
	0.5	0.2	8.24	0.904	1.03	7.73	3.09
	0.5	0.6	4.26	0.887	0.83	2.06	2.48
	0.5	1.0	2.57	0.876	0.72	1.08	2.16
	0.8	0.2	24.56	0.895	1.66	19.94	4.98
	0.8	0.6	12.06	0.852	1.08	4.33	3.25
	0.8	1.0	7.20	0.832	0.91	2.19	2.74
n=5	0.2	0.2	1.07	0.930	0.42	1.24	1.24
	0.2	0.6	0.66	0.921	0.33	0.33	0.99
	0.2	1.0	0.45	0.893	0.15	0.09	0.46
	0.5	0.2	5.58	0.877	0.73	5.48	2.19
	0.5	0.6	2.66	0.858	0.59	1.47	1.77
	0.5	1.0	1.56	0.841	0.49	0.73	1.46
	0.8	0.2	12.67	0.922	2.34	28.04	7.01
	0.8	0.6	5.45	0.851	1.07	4.29	3.22
	0.8	1.0	3.20	0.810	0.77	1.85	2.31

available from the 1991 Wang [A2] results with a nontraditional constitutive relationship to evaluate the consistency of f.

Calculated values of the three normalized ξ functions are shown in Table A2 and in Figures A5, A6, and A7 as functions of the normalized crack depth a/t. Note that different authors and strain hardening exponents (or constitutive relationships) are distinguished by symbol. Open symbols denote n = 10, filled symbols represent n = 5 or 4 (Dodds), and the crossed squares identify the Kirk bilinear results. Variations in a/c are not specified in these figures.

Figure A5 shows that ξ was, in general, considerably smaller than the remaining plate width (b-c), especially for large b/c ratios. Note in Table A2, for example, the Wang [A1] results for a semi-circular crack with b/c =16, when the cracked area is only 2.5 percent of the total gross section area. Therefore, the nominal net section area criterion (Eqn. A.2) often gave limit load estimates much too high and reference stress J estimates too low. This was precisely the finding in Phase I, where the nominal net section area approach to defining a limit stress was employed. The agreement appeared to worsen gradually for shallower cracks.

Figure A6 shows that ξ was not well correlated with the plate thickness t. A constant ξ/t criterion would tend to give reference stress estimates of J much too high (collapse functions f much too low) for deeper cracks, especially for small a/c values (see also Table A2). At the same time, a constant ξ/t could give very nonconservatively low J estimates (f too high) for shallower cracks and larger a/c values.

A better correlation was exhibited in Fig. A7 between ξ and the crack half-width c. The ratio ξ/c was approximately bounded by 1 and 3 for most of the geometries considered, although some apparent dependence on a/t, a/c, and perhaps n remained. The only prominent outliers in the data were the results of Yagawa *et al.* [A5] for one shallow semicircular flaw and one deep, elongated flaw. These exceptions will be discussed further below.

Several approaches can be taken to the selection of an optimum ξ/c value. One approach, which might be more appropriate in the development of global analysis rules for practical safety assessments, would be to choose a constant value for ξ/c which would apply uniformly to all crack shapes and constitutive relationships. If a best estimate of J is desired, then an intermediate value of perhaps ξ/c = 1.5 - 2.0 may be a good choice. This selection gave predictions of the plastic J term (as represented by the plastic factor h_1) which were usually within ±15 percent of the published FE results, never more than 20 percent low, and only occasionally excessively conservative. Some of the larger disagreements may have been due to inaccuracies in the FE solutions, as discussed later. And, as also discussed further below, note that the accuracy of the total J estimate will often be much better than the accuracy of the plastic J estimate. If a more universally conservative fracture assessment is desired for all crack shapes, then a smaller ξ/c value, perhaps 1.0, may be appropriate (at the expense of greater conservatism for the deepest cracks).

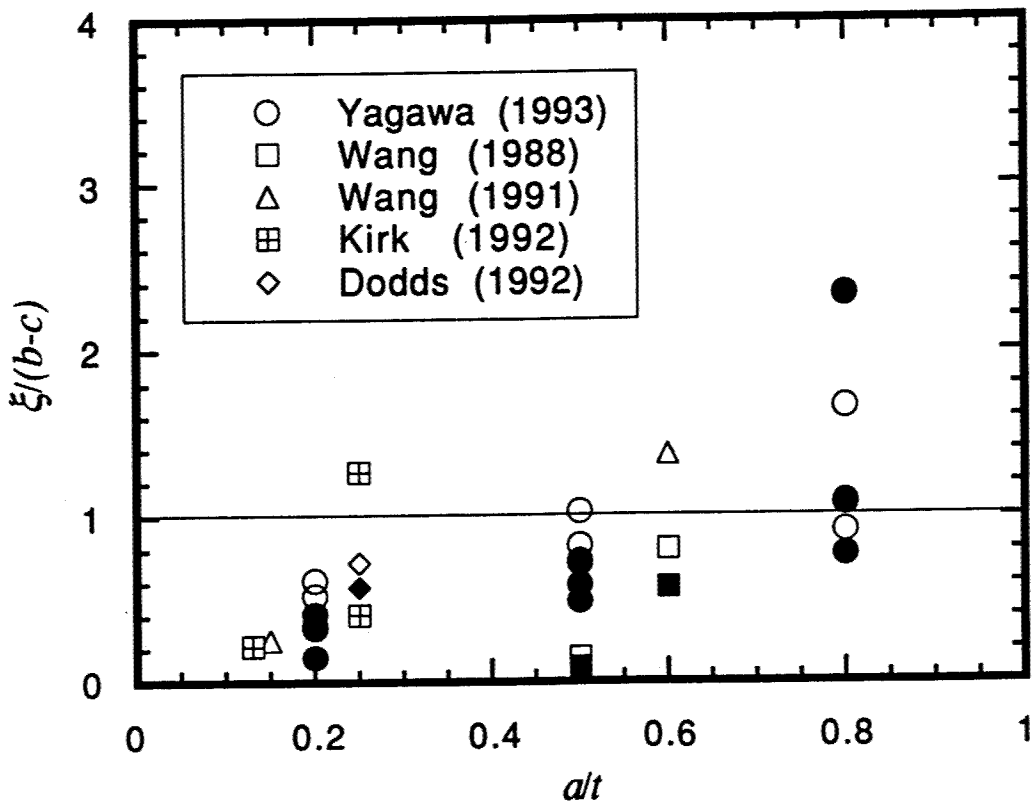

Figure A5. Normalized representative plate width ξ/(b-c) as function of *a/t*

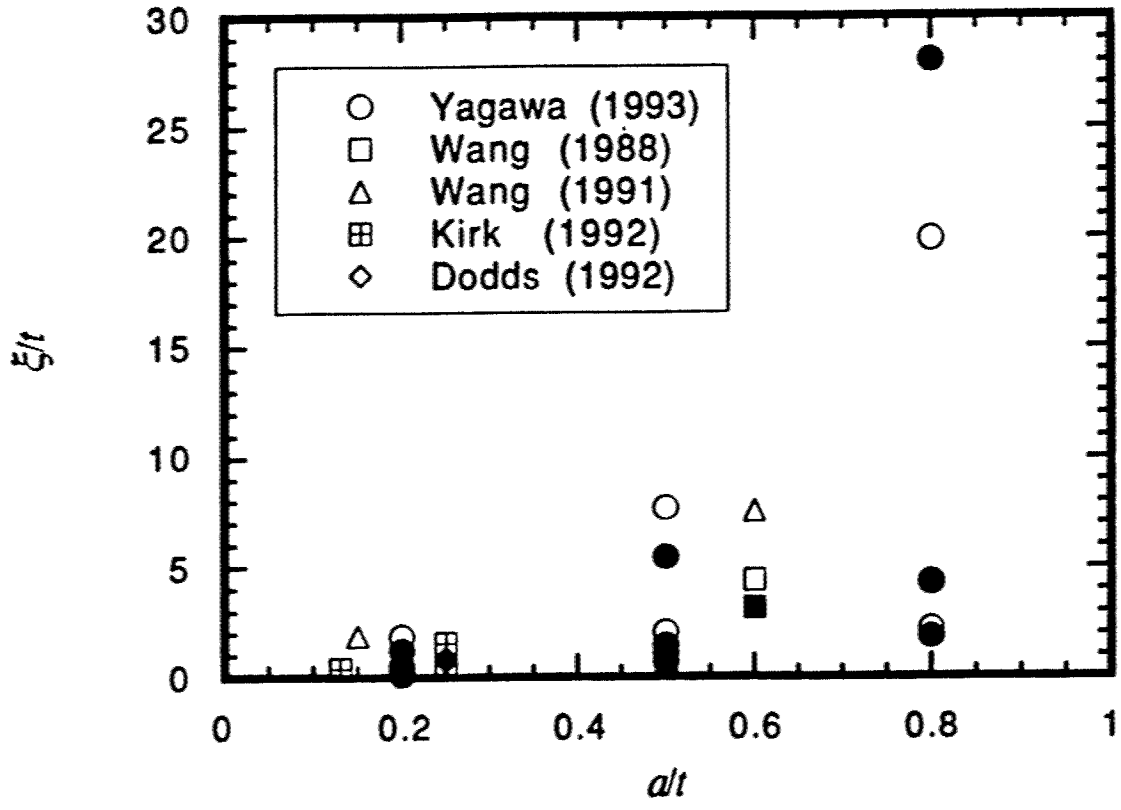

Figure A6. Normalized representative plate width ξ/t as function of a/t

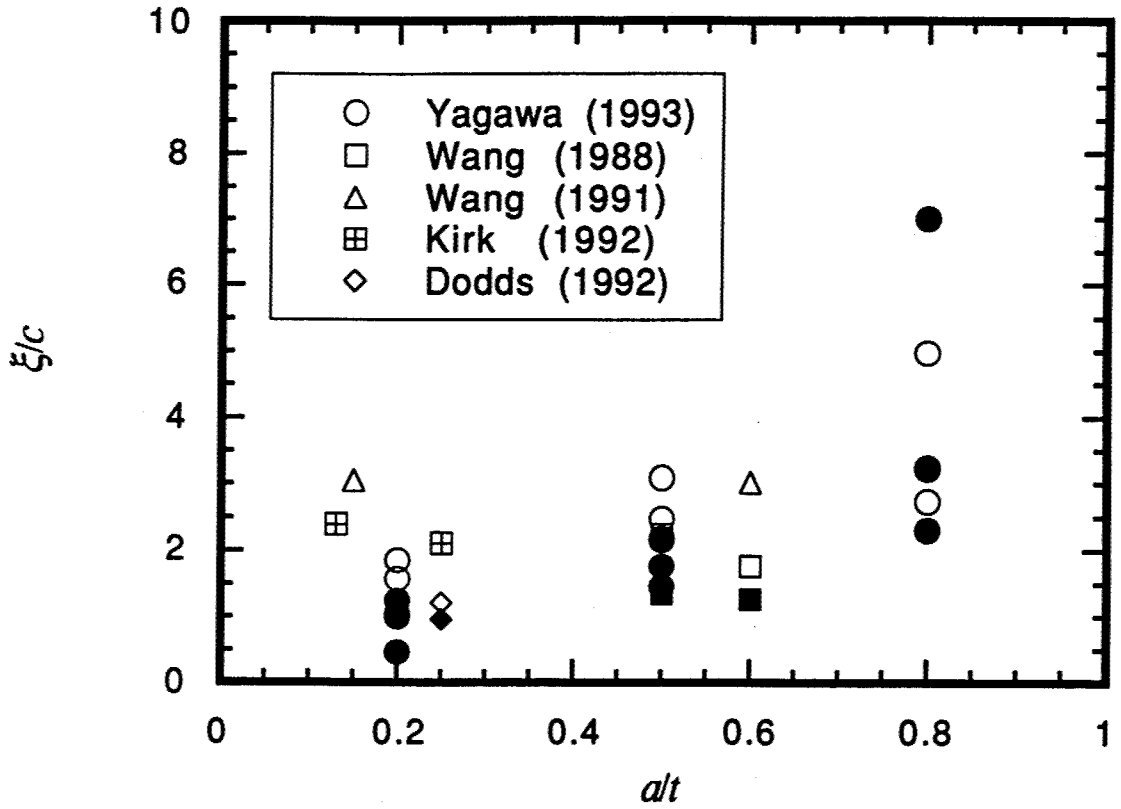

Figure A7. Normalized representative plate width ξ/c as function of a/t

Comparisons of Reference Stress and Finite Element Results

Comparisons of predicted and published FE h_1 values for several different choices of ξ/c are summarized in Table A3. These comparisons suggest that the engineering analyst may wish to fine tune his selection of ξ/c depending on the general nature of his applications problem: perhaps choosing ξ/c slightly smaller for shallower flaws or higher strain hardening (smaller n), or ξ/c slightly larger for deeper flaws or lower strain hardening. Note that the h_1 predictions were slightly less sensitive to ξ/c for shallower flaws and smaller strain hardening exponents. It may also be useful to develop a more complex expression which gives a more accurate ξ/c as a function of other geometry parameters, such as a/t and a/c, and perhaps also as a function of constitutive variables, such as n. It should be emphasized, however, that a single intermediate value of ξ/c will give remarkably good estimates of J for a wide range of crack shapes and sizes and strain hardening behavior. This simplicity and universality is one of the strengths of the general reference stress approach.

Predictions of total J based on the reference stress approach (Eqn. 2.7) with a constant $\xi/c = 1.75$ are compared with the original FE results of Wang, Dodds, and Kirk in Figures A8 - A12. Note that if ξ was calculated to be greater than the remaining plate width (b-c), then ξ was set equal to (b-c), because the theoretical area defined by the larger ξ was not actually available to carry load. Reference stress predictions of h_1 for a fully plastic material are compared with the Yagawa results in Fig. A13 for $n = 5$ and 10.

Wang (1988), Wang (1991), and Dodds (1992)

Figures A8 and A9 show excellent agreement (±12 percent) between the reference stress predictions of total J and the FE results of Wang [A1] and Dodds [A4] for different crack shapes, crack depths, and strain hardening exponents. All these analyses were based on the standard Ramberg-Osgood constitutive model. The reference stress estimates for the later Wang [A3] results based on a more complex stress-strain law (fully elastic below the yield stress, fully power law above the yield stress) were more conservative, especially for the deeper crack, although very limited FE results were available. The excellent agreement between the reference stress and earlier Wang results for the exact same geometry (but a Ramberg-Osgood constitutive relationship) suggests that this later disagreement was related to the nature of the stress-strain relationship, which contained a sharp discontinuity in the rate of increase of plastic strain at the yield stress. A similar conservatism in reference stress estimates was also observed for another set of FE results based on a stress-strain curve with a sharp corner, the Kirk analyses discussed below.

Kirk (1992)

The reference stress estimates of total J are compared with the Kirk [A3] finite element results based on a bilinear stress-strain law in Figures A11 and A12. The comparisons expressed in terms of normalized applied stress, Fig. A11, showed that the reference stress estimates were somewhat conservative at applied stresses very near the yield stress, but generally did a good job of following the very severe upturn in J with increasing load. These changes in J are depicted more clearly in Fig. A12, which emulates the original figures of Kirk by representing J as a

TABLE A3
Ratio of predicted to published h_1 for different ξ/c values

			Ratio of predicted/published h_1		
Author	***a/t***	***a/c***	**ξ/c = 1.0**	**ξ/c = 1.75**	**ξ/c = 2.5**
Wang (1988)	0.5	1.00	2.24	1.25	0.91
n=10	0.6	0.24	2.10	1.02	*0.78
n=5	0.5	1.00	1.15	0.89	0.78
	0.6	0.24	1.15	0.84	*0.74
Dodds (1992)					
n=10	0.25	0.33	1.10	*0.86	*0.86
n=4	0.25	0.33	0.99	*0.92	*0.92
Yagawa (1993)	0.2	0.2	1.26	1.02	0.91
n=10	0.2	0.6	1.19	0.94	0.86
	0.2	1.0	1.02	0.83	0.74
	0.5	0.2	2.88	1.61	1.18
	0.5	0.6	2.43	1.36	0.99
	0.5	1.0	2.16	1.21	0.88
	0.8	0.2	10.98	3.80	2.19
	0.8	0.6	7.05	2.42	1.40
	0.8	1.0	5.69	1.97	1.13
n=5	0.2	0.2	1.04	0.95	0.90
	0.2	0.6	1.00	0.91	0.87
	0.2	1.0	0.88	0.80	0.76
	0.5	0.2	1.42	1.10	0.95
	0.5	0.6	1.30	1.00	0.87
	0.5	1.0	1.20	0.93	0.80
	0.8	0.2	3.26	2.04	1.59
	0.8	0.6	2.37	1.48	1.16
	0.8	1.0	1.95	1.22	0.95

* denotes $(b\text{-}c) < \xi$, so ξ set equal to $(b\text{-}c)$

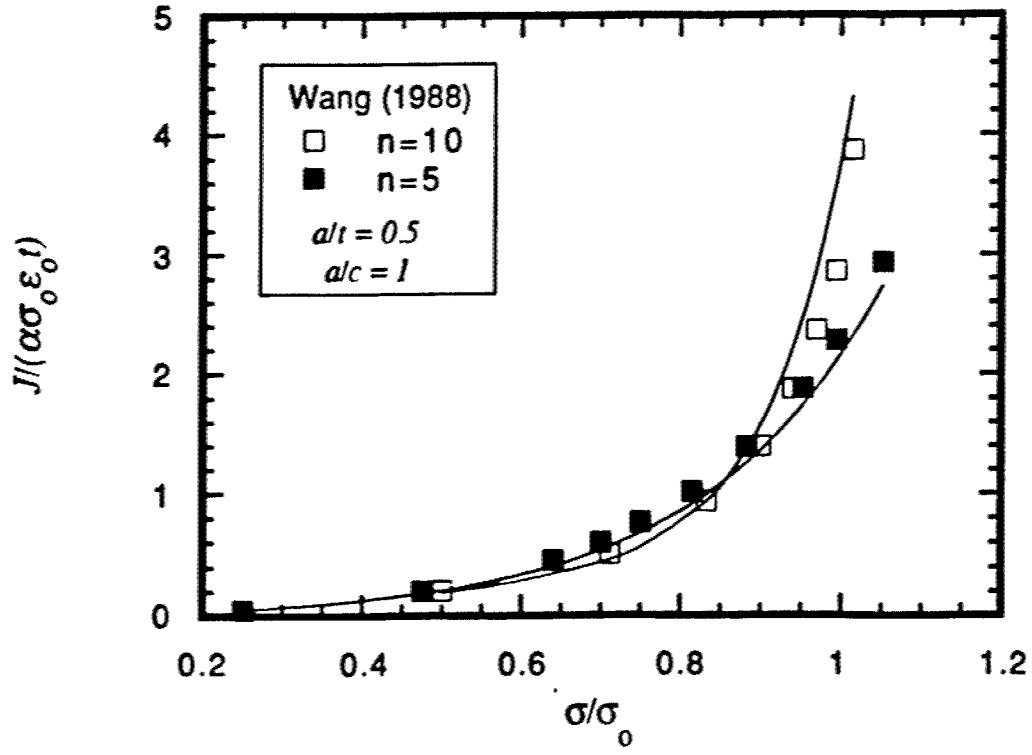

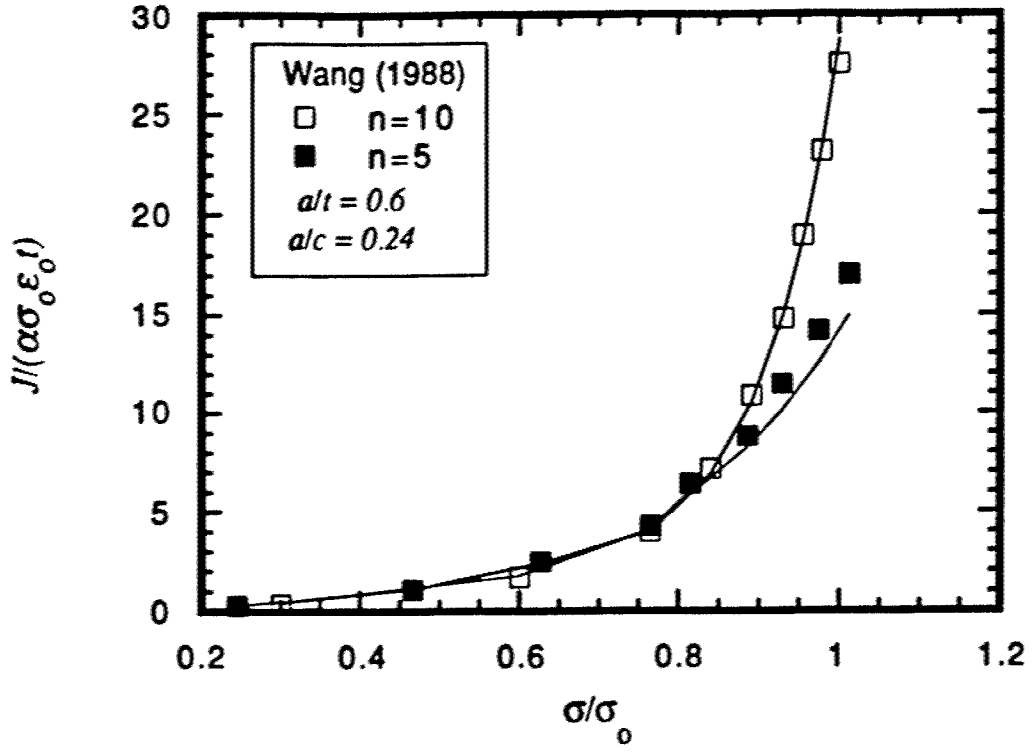

Figure A8. Comparison of reference stress J predictions with Wang (1988) finite element results

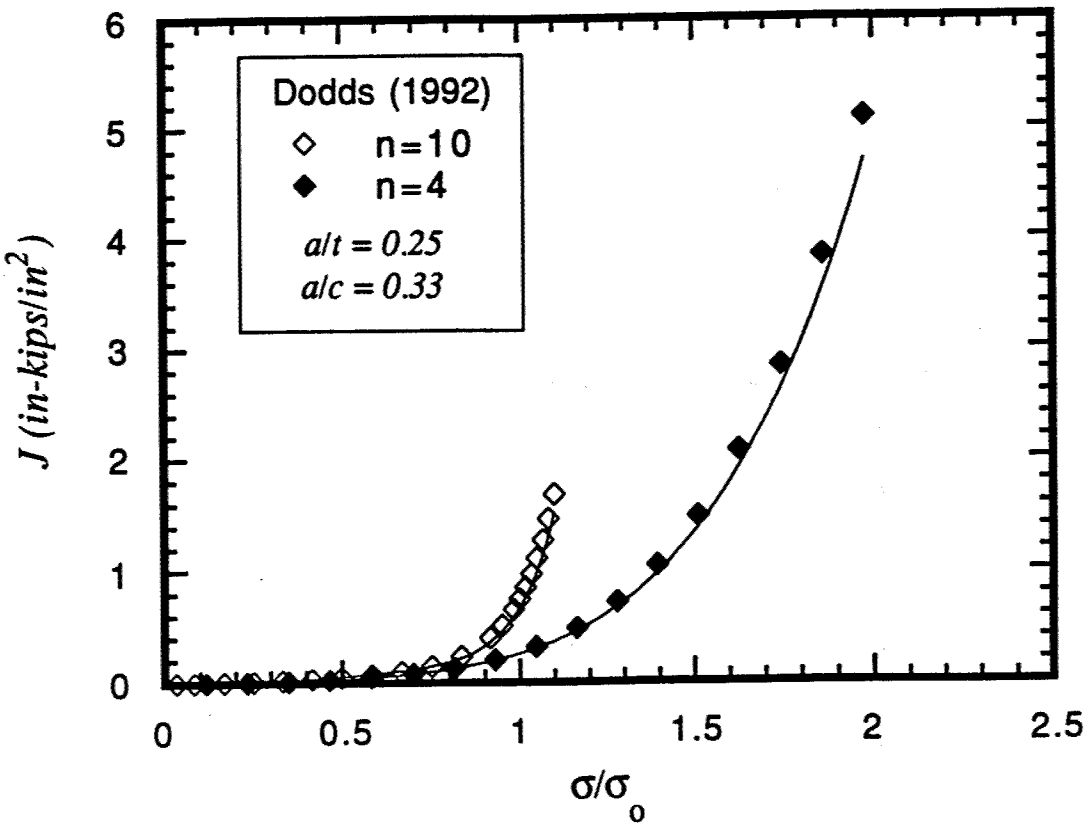

Figure A9. Comparison of reference stress J predictions with Dodds (1992) finite element results

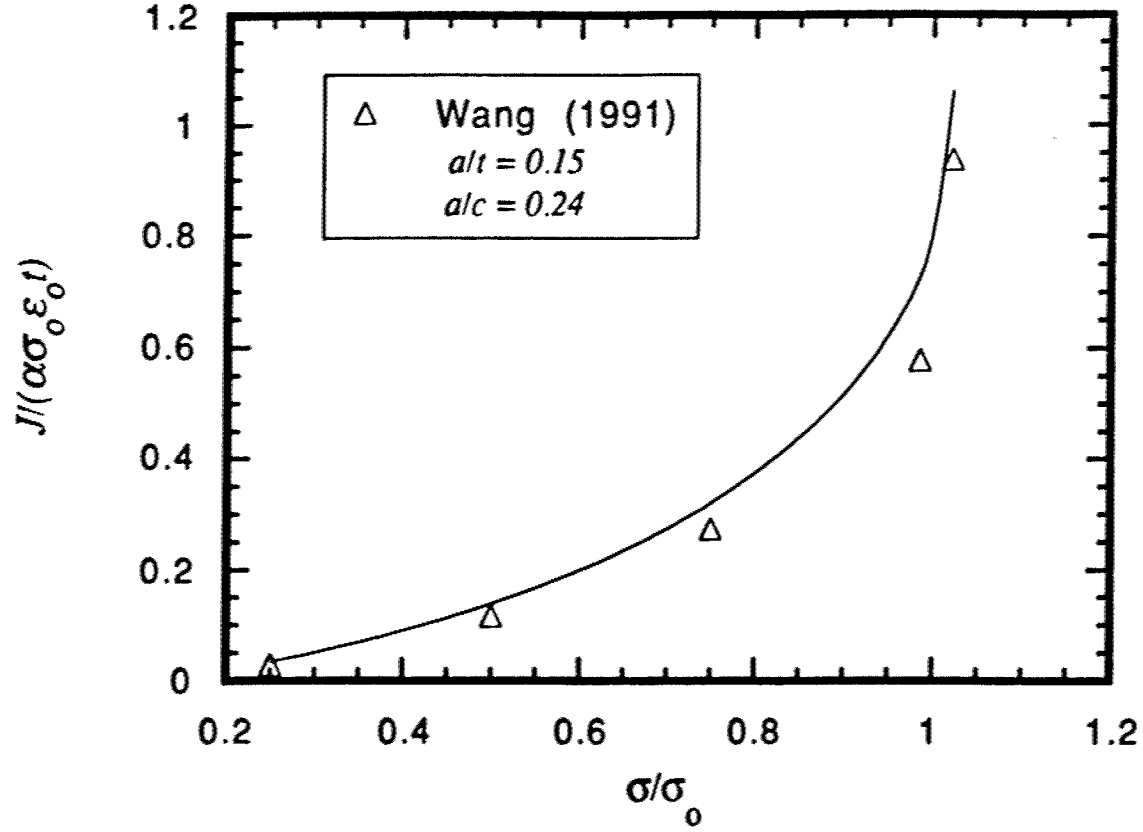

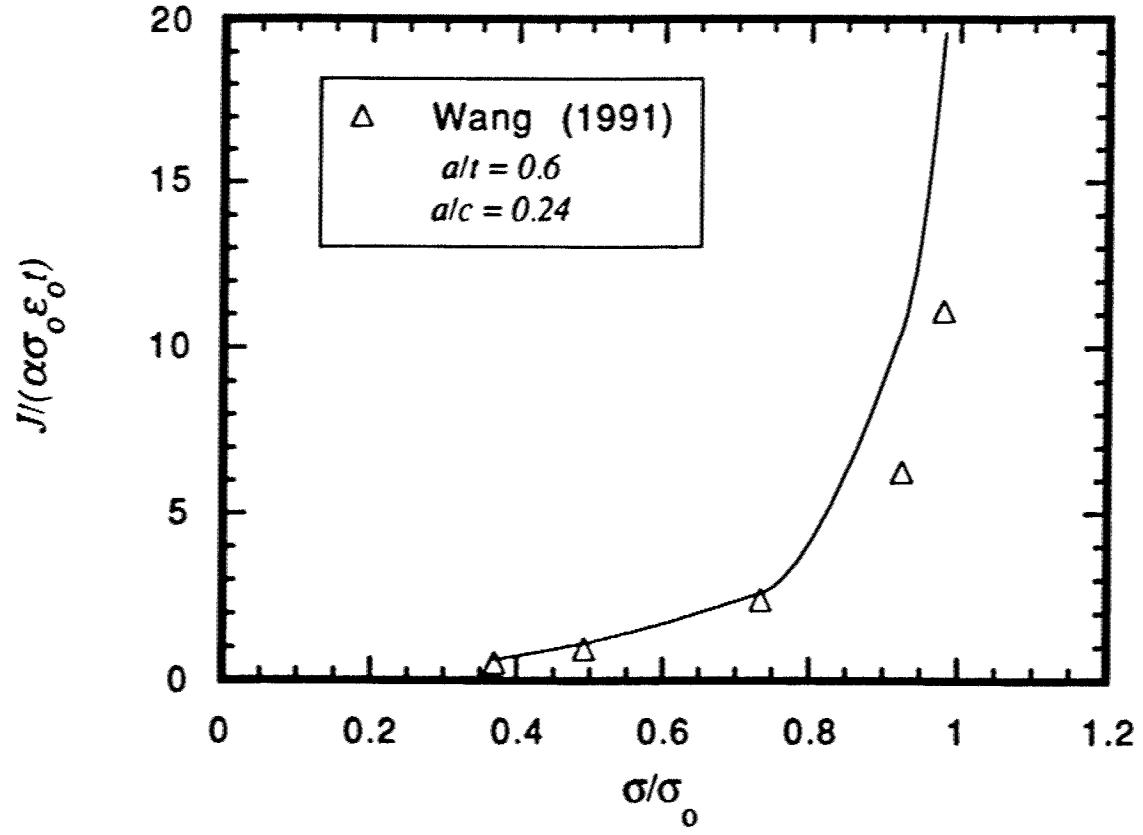

Figure A10. Comparison of reference stress J predictions with Wang (1991) finite element results

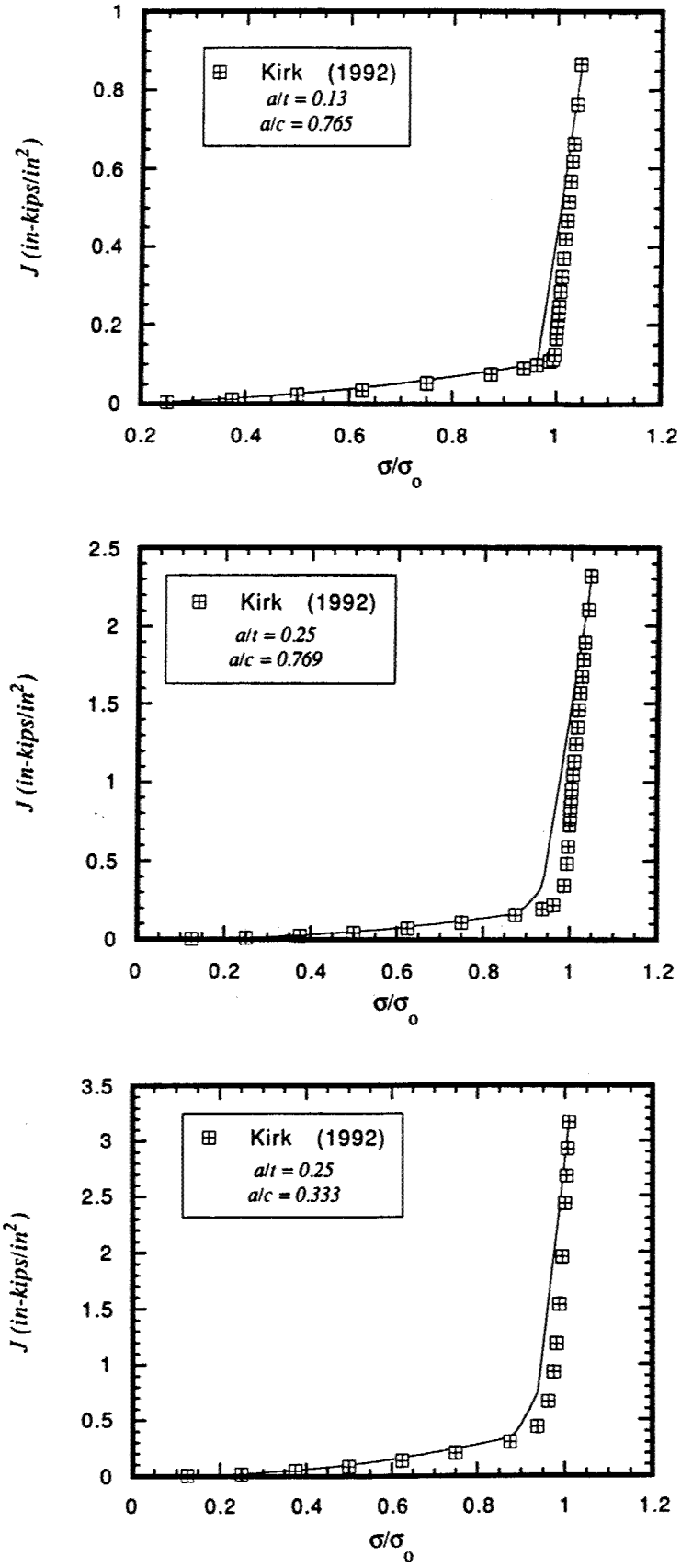

Figure A11. Comparison of reference stress J predictions with Kirk (1992) finite element results in terms of normalized applied stress

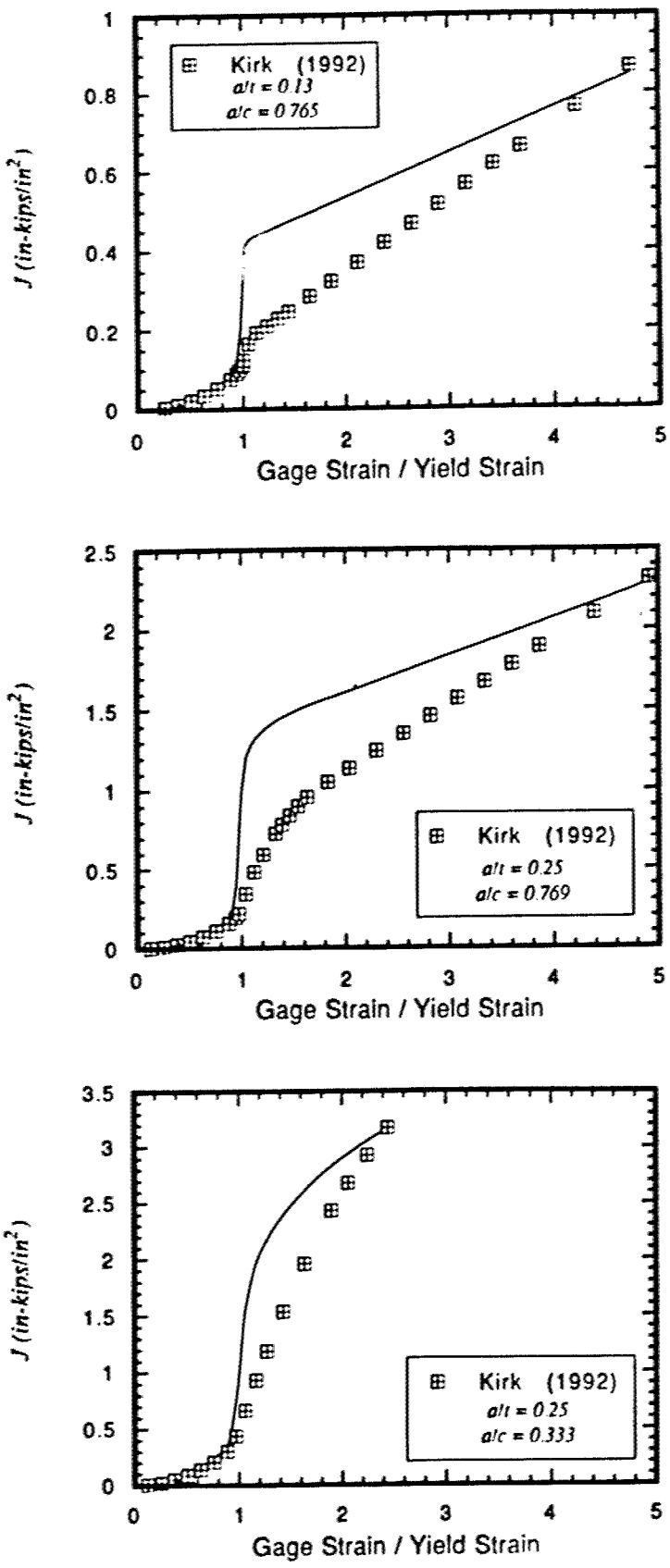

Figure A12. Comparison of reference stress J predictions with Kirk (1992) finite element results in terms of normalized applied strain

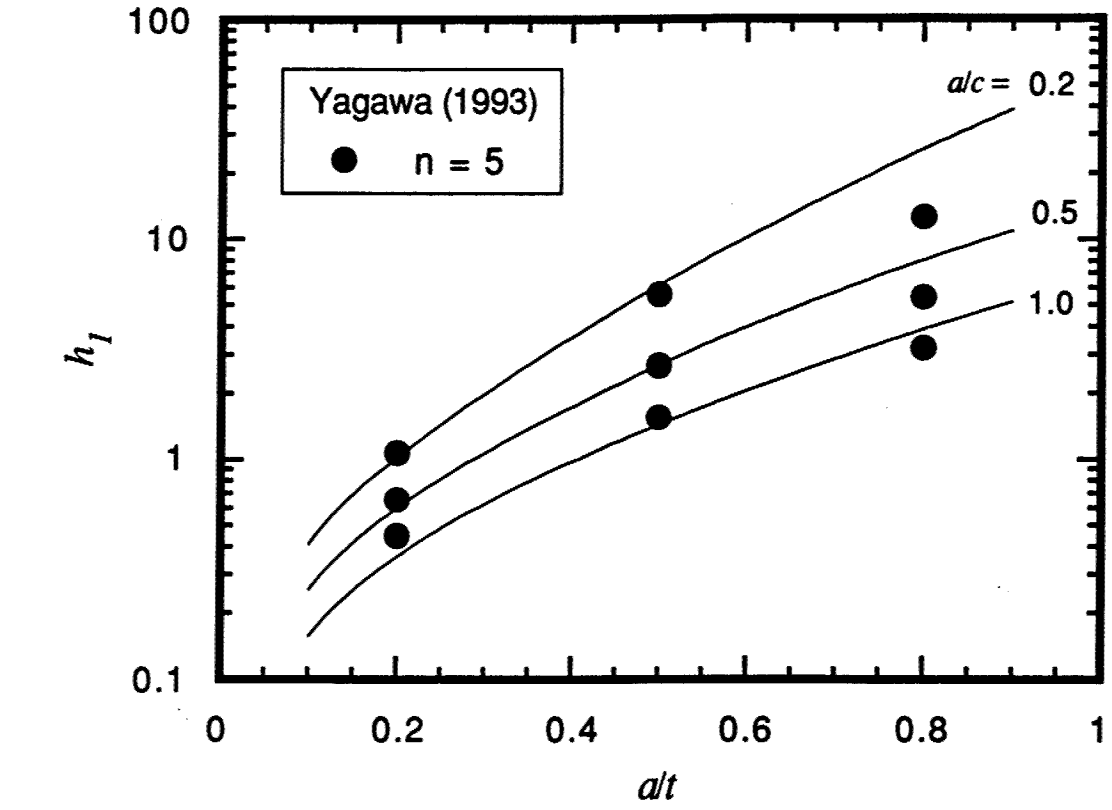

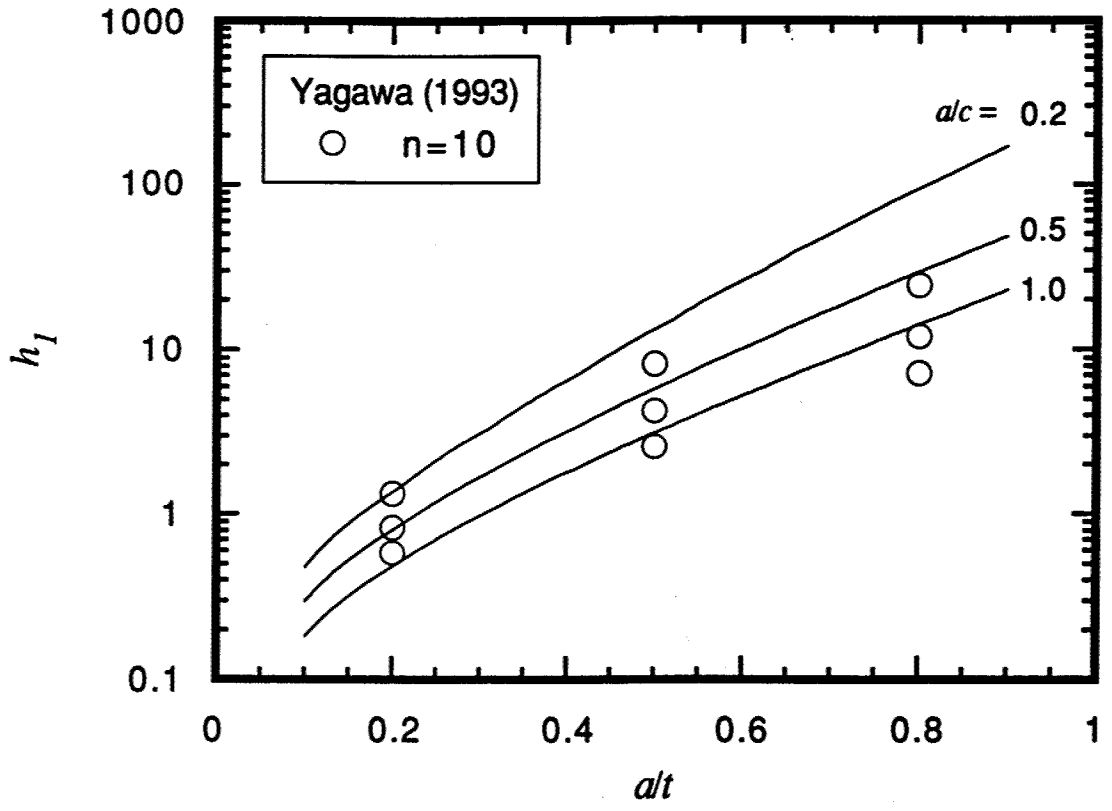

Figure A13. Comparison of reference stress h_1 predictions with Yagawa (1993) finite element results

function of normalized applied strain. These graphs show that the reference stress estimates could be quite conservative - as much as a factor of 2x or 3x - at applied stresses within a few percent of the yield stress, but that the reference stress estimates were increasingly accurate at higher and lower applied stresses.

This large change in accuracy with changes in applied stress, which was not observed in any of the estimates for power law hardening materials, was consistent with the earlier observation that the derived value of the collapse function, f, changed significantly with applied stress. The derived values of f at applied stresses very near yield were generally significantly higher (closer to $f = 1$), which implies a larger value of ξ/c and (ultimately) a smaller J value. Improvements in J estimates would require some means of predicting this change in collapse function or characteristic plate length. Remember that a similar conservatism in J was observed for the Wang (1991) FE analysis with a similar two-stage constitutive relationship. It appears, therefore, that this particular reference stress formulation may have difficulty in handling the sharp discontinuity in the rate of plastic strain increase - from zero to a large positive number - at the yield stress. Further studies of the reference stress method for these types of stress-strain curves are required. It is encouraging, however, that the errors in the current reference stress estimates are systematically conservative rather than nonconservative.

Of course, it should be noted that in actual engineering practice, reliable predictions of J for any material with such a sharp knee in the stress-strain curve will be precarious at applied stresses very near the yield stress. Even an "exact" analysis scheme can significantly overestimate or underestimate J if the assumed yield strength is in error by only 1 or 2 percent. Actual safety assessments must pay close attention to appropriate conservative bounds on both σ_{ys} and J.

Comments on two observations by Kirk [A3] about the reference stress method in general are also in order here. He concluded from comparison of his own reference stress J estimates with his FE results that the reference stress estimates always significantly underestimated J. He also remarked that the reference stress method was unable to model correctly the general trends in the J vs. strain relationship in tension because it failed to distinguish the different regimes of post-yield behavior, including the distinction between net-section and gross-section yielding. These two statements may have been true at least in part, however, because Kirk chose to neglect the influence of the crack on the limit load calculation; i.e., he chose $f = 1$ for all geometries, so that $\sigma_{ref} = \sigma_{\infty}$ everywhere. The reference stress estimates in Figure A12 appear to demonstrate two distinct regimes of post-yield behavior: a change from small-scale yielding to net ligament or net section yielding when $\sigma_{ref} > \sigma_{ys}$, transitioning to gross section yielding (with a corresponding decrease in the J vs. strain slope) when $\sigma_{\infty} > \sigma_{ys}$. However, additional study is needed to evaluate further the accuracy of reference stress estimates based on a global collapse function for characterization of the elastic-plastic fracture mechanics response of a part-through crack exhibiting net section yield in the remaining ligament.

Yagawa (1993)

Comparisons of the reference stress estimates of h_1 for $\xi/c = 1.75$ with the calculations of Yagawa *et al.*, Figure A13, indicated general agreement for most geometries but significant disagreement in a few cases. Reference stress and FE results for the plastic J term agreed within ±20 percent in almost two-thirds of the cases considered, and reference stress estimates were never more than 20 percent low. Some apparent dependence of prediction quality on both a/c and a/t was observed. This may indicate that a more exact form of ξ/c should have some functional dependence on the crack shape and depth. A brief numerical investigation of all Yagawa results for $n = 5$, 7, and 10 found that an improved ξ/c estimate of the form

$$\frac{\xi}{c} = 3.4\left(\frac{a}{t}\right)\sqrt{\frac{c}{a}} \qquad \textbf{(A.6)}$$

gave reference stress predictions of h_1 within -20 to +25 percent of FE values for all 27 combinations of crack shape, crack depth, and strain hardening exponent. However, Eqn. A.6 gave surprisingly inferior predictions of h_1 or J for some of the Wang, Dodds, and Kirk results, which prompted a closer look at the original Yagawa *et al.* analysis.

Yagawa *et al.* [A5] systematically compared their elastic calculations of K for their nine crack geometries with the original Newman-Raju finite element results [A6] for the same configurations. Agreement was good (within a few percent) in some cases and poor in others. In the worst case, the Yagawa linear elastic solution for $a/t = 0.8$, $a/c = 0.2$ was over 20 percent lower than the respective Newman-Raju solution. This is precisely the crack geometry for which the reference stress estimate gave the worst agreement with the Yagawa results, significantly overestimating the Yagawa h_1. Agreement between Yagawa and Newman-Raju was also particularly poor (Yagawa 10 to 15 percent lower) for $a/t = 0.8$, $a/c = 0.6$, and for $a/t = 0.5$, $a/c = 0.2$, both of which also showed some significant disagreement between reference stress and Yagawa calculations of h_1. If it is assumed that the Newman-Raju solution is "exact," then the Yagawa errors in computing K may indicate some fundamental modeling difficulties which would almost certainly be amplified when solving the more complex fully-plastic problem. Of course, it is also possible that the Newman-Raju solution is somewhat in error for these geometries. If so, then those errors would have been propagated in the reference stress calculations, since the reference stress estimate depends on the closed-form representation of the Newman-Raju K solution.

In view of these comparisons, and in view of the disagreements in h_1 noted earlier in Fig. A4 between Yagawa and Wang-Dodds (Yagawa always apparently lower), it appears reasonable to conclude that the Yagawa values of h_1 are likely too low for some geometries. The simple reference stress estimates are perhaps not so excessively conservative for those geometries as was originally indicated. It remains likely that ξ/c does have some systematic dependence on a/c and a/t, but neglecting this dependence should not preclude acceptably accurate estimation

of J for many crack shapes and sizes. As additional FE results become available, it should be possible to refine these observations about ξ/c and draw firmer conclusions.

Discussion: Accuracy of J Solutions

Any discussion of solution accuracy must begin with consideration of the accuracy of the original FE J solutions. Numerical analysis of such complex elastic-plastic problems is not a trivial exercise, and the results cannot be automatically assumed to be infallible. Round-robin analysis exercises have found a disturbingly large scatter in results for J on even simple two-dimensional geometries [A7]. Improved understandings of numerical modeling issues should prompt improved solution accuracy, but error will not be eradicated. It is instructive to note that several of the numerical solutions investigated in this report disagreed with the "benchmark" Newman-Raju solution in the elastic regime by as much as 10 percent in K -- and sometimes much more, as noted above in discussion of the Yagawa *et al.* results. Of course, the Newman-Raju solution is not infallible, either. Remember that a large number of different elastic K solutions were proposed for the semi-elliptical surface crack geometry before Newman-Raju emerged and was accepted as an informal standard. Therefore, it is probably not possible to claim better than about 10 to 20 percent accuracy in J for any of the FE results considered in this report, and much worse accuracy appears likely for a few FE results.

Furthermore, this accuracy is conditional on a reasonably exact representation of the material constitutive relationship and the actual crack shape. Differences between the actual stress-strain response of the material and the idealized Ramberg-Osgood (or other constitutive) relationship which has been assumed, including the effects of cyclic softening or hardening, can introduce significant errors in the calculated J, especially at large n. The implications of even small errors in estimating the yield strength were highlighted above in discussions of the Kirk predictions for materials with a bilinear stress-strain curve.

A reference stress J estimate which is good to within 20 or even 30 percent, then, may be about as accurate as can be expected or required in practice. Even larger errors in the estimation of the plastic J term (which is the real focus of the reference stress approach, since the elastic term follows directly from the K solution alone) may not be particularly troublesome. For a Ramberg-Osgood material, the relative magnitude of the elastic and plastic J terms in a reference stress formulation is given approximately by

$$\frac{J_p}{J_e} = \left(\frac{\sigma_{-}/\sigma_0}{f} \right)^{n-1} \qquad \text{(A.7)}$$

The plastic term will only become dominant when σ_{-}/σ_0 is greater than f, and this dominance will be particularly intense only for larger n. For many problems, however, the elastic and plastic terms in J will be of similar magnitude. In this case, even a 50 percent error in estimating J_p

would cause only about a 25 percent error in calculating total J (and less than a 15 percent error in calculating the equivalent K value), assuming that the elastic solution is known accurately.

In view of these observations about solution accuracy, we conclude that the proposed reference stress estimate of J will be entirely acceptable for many engineering applications. Furthermore, the reference stress approach is particularly attractive in view of its successful application to not only a wide range of crack shapes and sizes but also a variety of constitutive relationships. This simplicity and robustness suggest that the reference stress method might be preferred over a more "rigorous" finite element approach for some applications.

Acknowledgements

Prof. G. Yagawa, Prof. R. H. Dodds, Jr., Dr. M. T. Kirk, and Dr. Y.-Y. Wang are thanked for promptly providing their numerical results in various forms.

References

A1. Y.-Y. Wang, "Analysis of Fracture Initiation in Surface-Cracked Plates," M.S. Thesis, Massachusetts Institute of Technology, 1988. See also D. M. Parks and Y.-Y. Wang, "Elastic-Plastic Analysis of Part-Through Surface Cracks," *Analytical, Numerical, and Experimental Aspects of Three Dimensional Fracture Processes, AMD-Vol. 91*, ASME, 1988, pp. 19-32.

A2. Y.-Y. Wang, "A Two-Parameter Characterization of Elastic-Plastic Crack Tip Fields and Applications to Cleavage Fracture," Ph.D. Thesis, Massachusetts Institute of Technology, 1991.

A3. M. T. Kirk and R. H. Dodds, Jr., "Approximate Techniques of J Estimation Applicable to Part-Through Surface Cracks," *Engineering Fracture Mechanics*, Vol. 43, 1992, pp. 123-136.

A4. R. H. Dodds, Jr., C. F. Shih, and T. L. Anderson, "Continuum and Micromechanics Treatment of Constraint in Fracture," Structural Research Series Report No. 573, Department of Civil Engineering, University of Illinois at Urbana-Champaign, November 1992.

A5. G. Yagawa, Y. Kitajima, and H. Ueda, "Three-Dimensional Fully Plastic Solutions for Semi-elliptical Surface Cracks," *International Journal of Pressure Vessels and Piping*, Vol. 53, 1993, pp. 457-510.

A6. J. C. Newman, Jr., and I. S. Raju, "Analyses of Surface Cracks in Finite Plates under Tension or Bending Loads," NASA TP-1578, 1979.

A7. L. H. Larsson, "The EGF Round Robin on Numerical EPFM," Proc. 5th European Conference on Fracture (ECF5), September 1984, pp. 425-445.

REPORT DOCUMENTATION PAGE

Form Approved
OMB No. 0704-0188

Public reporting burden for this collection of information is estimated to average 1 hour per response, including the time for reviewing instructions, searching existing data sources, gathering and maintaining the data needed, and completing and reviewing the collection of information. Send comments regarding this burden estimate or any other aspect of this collection of information, including suggestions for reducing this burden, to Washington Headquarters Services, Directorate for Information Operation and Reports, 1215 Jefferson Davis Highway, Suite 1204, Arlington, VA 22202-4302, and to the Office of Management and Budget, Paperwork Reduction Project (0704-0188), Washington, DC 20503.

1. AGENCY USE ONLY *(Leave Blank)*	2. REPORT DATE	3. REPORT TYPE AND DATES COVERED
	July 1999	Contractor Report (Final)

4. TITLE AND SUBTITLE

A Comparison of Single-Cycle Versus Multiple-Cycle Proof Testing Strategies

5. FUNDING NUMBERS

NAS8-37451

6. AUTHORS

R.C. McClung, G.G. Chell, H.R. Millwater, D.A. Russell,* and G.E. Orient*

7. PERFORMING ORGANIZATION NAMES(S) AND ADDRESS(ES)

Southwest Research Institute
P.O. Drawer 28510
San Antonio, TX 78228-0510

8. PERFORMING ORGANIZATION REPORT NUMBER

M-931

9. SPONSORING/MONITORING AGENCY NAME(S) AND ADDRESS(ES)

George C. Marshall Space Flight Center
Marshall Space Flight Center, Alabama 35812

10. SPONSORING/MONITORING AGENCY REPORT NUMBER

NASA/CR—1999-209426

11. SUPPLEMENTARY NOTES

Prepared for Structures and Dynamics Laboratory, Science and Engineering Directorate.
Technical Monitor: Henry M. Lee
*Subcontract Support from Rocketdyne Division, Rockwell International Corporation, 6633 Canoga Ave., Canoga Park, CA 91303

12a. DISTRIBUTION/AVAILABILITY STATEMENT

Unclassified-Unlimited
Subject Category 39
Standard Distribution

12b. DISTRIBUTION CODE

13. ABSTRACT *(Maximum 200 words)*

Single-cycle and multiple-cycle proof testing (SCPT and MCPT) strategies for reusable aerospace propulsion system components are critically evaluated and compared from a rigorous elastic-plastic fracture mechanics perspective. Earlier MCPT studies are briefly reviewed. New *J*-integral estimation methods for semielliptical surface cracks and cracks at notches are derived and validated. Engineering methods are developed to characterize crack growth rates during elastic-plastic fatigue crack growth (FCG) and the tear-fatigue interaction near instability. Surface crack growth experiments are conducted with Inconel 718 to characterize tearing resistance, FCG under small-scale yielding and elastic-plastic conditions, and crack growth during simulated MCPT. Fractography and acoustic emission studies provide additional insight. The relative merits of SCPT and MCPT are directly compared using a probabilistic analysis linked with an elastic-plastic crack growth compute code. The conditional probability of failure in service is computed for a population of components that have survived a previous proof test, based on an assumed distribution of initial crack depths. Parameter studies investigate the influence of proof factor, tearing resistance, crack shape, initial crack depth distribution, and notches on the MCPT versus SCPT comparison. The parameter studies provide a rational basis to formulate conclusions about the relative advantages and disadvantages of SCPT and MCPT. Practical engineering guidelines are proposed to help select the optimum proof test protocol in a given application.

14. SUBJECT TERMS

multiple-cycle proof testing, elastic-plastic fracture mechanics, resistance curves, elastic-plastic fatigue crack growth, tear-fatigue, surface cracks, notches, *J*-integral, reference stress method, probabilistic analysis, Inconel 718, acoustic emission, fractography

15. NUMBER OF PAGES

187

16. PRICE CODE

A09

17. SECURITY CLASSIFICATION OF REPORT	18. SECURITY CLASSIFICATION OF THIS PAGE	19. SECURITY CLASSIFICATION OF ABSTRACT	20. LIMITATION OF ABSTRACT
Unclassified	Unclassified	Unclassified	Unlimited

National Aeronautics and
Space Administration
AD33
George C. Marshall Space Flight Center
Marshall Space Flight Center, Alabama
35812